

**UNCLASSIFIED**

---

**AD 260 274**

---

*Reproduced  
by the*

**ARMED SERVICES TECHNICAL INFORMATION AGENCY  
ARLINGTON HALL STATION  
ARLINGTON 12, VIRGINIA**

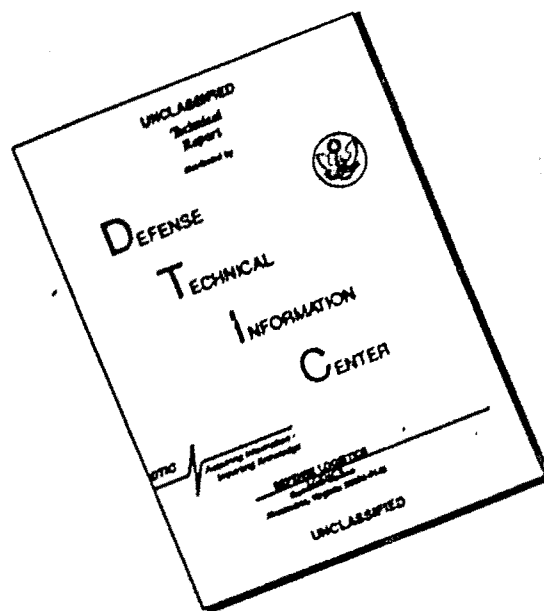


---

**UNCLASSIFIED**

NOTICE: When government or other drawings, specifications or other data are used for any purpose other than in connection with a definitely related government procurement operation, the U. S. Government thereby incurs no responsibility, nor any obligation whatsoever; and the fact that the Government may have formulated, furnished, or in any way supplied the said drawings, specifications, or other data is not to be regarded by implication or otherwise as in any manner licensing the holder or any other person or corporation, or conveying any rights or permission to manufacture, use or sell any patented invention that may in any way be related thereto.

# DISCLAIMER NOTICE



THIS DOCUMENT IS BEST QUALITY AVAILABLE. THE COPY FURNISHED TO DTIC CONTAINED A SIGNIFICANT NUMBER OF PAGES WHICH DO NOT REPRODUCE LEGIBLY.

CATALOGED BY ASTIA  
AS AD No. \_\_\_\_\_

260274

# BOEING



NOX  
61-8-1



TRANSPORT DIVISION



D6-7190

DESIGN STUDY FOR EXPERIMENTAL AIRBORNE

ANTENNA FOR KC-135 AIRCRAFT

Final Engineering Report

By

A. Andermann, Luis L. Oh and C. D. Lunden  
Boeing Airplane Company  
Transport Division  
Renton, Washington

Air Force Contract No. AF19(604)-7373  
February 14, 1961

Issue No. \_\_\_\_\_

Issue to \_\_\_\_\_

Approved By J. R. Utterstrom  
J. R. Utterstrom

Prepared for

ELECTRONICS RESEARCH DIRECTORATE  
AIR FORCE CAMBRIDGE RESEARCH LABORATORIES  
OFFICE OF AEROSPACE RESEARCH  
UNITED STATES AIR FORCE  
BEDFORD, MASSACHUSETTS

LIST OF THE ENGINEERS WHO CONTRIBUTED TO THE  
WORK REPORTED

Alfred Andermann	Ph. D. Cand.
Bjorn DeBough	B.S.M.E.
John Fan	B.S.E.E.
John A. Hockenson	B.S.M.E.
Donald A. Houck	B.S.E.E.
Gene A. Kemper	M.S. Math.
Clarence D. Lunden	B.A. Physics
Larry T. Norin	B.S.E.E.
Luis L. Oh	M.S.E.E.
James E. Schuler	B.S. Arch.
Charles Su	M.S.E.E.
Joe B. Weatherhead	B.S.M.E.

Requests for Additional Copies by Agencies of the  
Department of Defense, their Contractors, and other  
Government Agencies should be directed to the:

ARMED SERVICES TECHNICAL INFORMATION AGENCY  
ARLINGTON HALL STATION  
ARLINGTON 12, VIRGINIA

All other Persons and Organizations should apply to:

U. S. DEPARTMENT OF COMMERCE  
OFFICE OF TECHNICAL SERVICES  
WASHINGTON 25, D. C.

## CONTRACT FULFILLMENT STATEMENT

This is the Final Engineering Report submitted in fulfillment of Air Force Contract AF 19(604)-7373 covering the period from June 1, 1960 to February 14, 1961.

The work was performed under Boeing Engineering Authorization No. 037, W. O. 69326, following Boeing Document No. D6-5596 "Program Plan and Requirements" for this contract.



## ABSTRACT

The result of a design study of a microwave antenna system for the Boeing KC-135 aircraft is presented. The antenna is an upward-looking, steerable, high-gain antenna for very-long-range, two-way communications, using signals relayed by satellites (active or passive) or scattered by belts of orbiting chaff. Critical antenna design problems connected with the very-high average transmitter power and the very-low receiver noise figure are considered in detail.

The bulk of the effort reported herein has been devoted to:

- 1) A rigorous analysis of the microwave antenna noise temperature at altitude.
- 2) The design of a low-noise, low-loss antenna receiving system and of a high-power transmitting system.
- 3) The design of an antenna-pointing system with an accuracy commensurate with the antenna half-beamwidth of 2.5 degrees
- 4) A site survey of the KC-135 for the best location for the antenna and a study to determine structural requirements created by the new antenna installation.
- 5) The design of an optimum radome based on a compromise between electrical and aerodynamic considerations.
- 6) The design of a three-axis antenna mount and tracking drive system.
- 7) The installation design of the maser receiver and the high-power transmitter unit.
- 8) The design of electrical and equipment cooling systems.
- 9) High-power testing of microwave components.

## TABLE OF CONTENTS

	<u>Page</u>
ABSTRACT	2
LIST OF ILLUSTRATIONS	6
LIST OF TABLES	8
 I. INTRODUCTION	 9
1.0 <u>Purpose</u>	9
2.0 <u>History</u>	9
 II DISCUSSION	 11
1.0 <u>System Concept</u>	11
2.0 <u>Antenna System</u>	16
2.1 <u>Antenna Design</u>	16
2.2    Equivalent-Antenna and Feed Noise Temperature	19
2.2.1    Sources of Noise	19
2.2.2    System Losses	21
2.2.3    Total Noise Temperature	21
2.2.4    Assumptions used in the Noise Calculation	23
2.2.5    Conclusion	23
2.3    High-Power Components	24
2.3.1    Transmit-Receive Waveguide Switch	24
2.3.2    Waveguide Rotary Joints	25
2.3.3    Waveguide Flanges	26
2.3.4    Pressurizing Windows and Caps	26
3.0 <u>Antenna Mount and Servo Drive System</u>	31
3.1 <u>Requirements and Design Criteria</u>	31
3.1.1    Criteria for Drive System Rating	31
3.1.2    System Selection (Azimuth and Elevation Channels)	34
3.1.3    Torque and Speed Calculation	35
3.1.4    Time Constants and Transfer Functions (Azimuth and Elevation Channels)	38
3.1.5    Antenna Angular Position Feedback Transducer	39
3.1.6    Remote Control and Indication of Antenna Polarization	42
3.2    Description of Mounting Frame and Drive System	45
4.0 <u>Computer and Pointing System</u>	47
4.1 <u>Requirements and Design Criteria</u>	47
4.1.1    Accuracy Requirements	47
4.1.2    Computation Requirements	54
4.2    Computer Selection	64
4.3    Operators Console	67

## TABLE OF CONTENTS (con't)

	<u>Page</u>
5.0 <u>Radome Design</u>	70
5.1 <u>Radome Dimensions</u>	70
5.2 <u>Radome Thickness</u>	70
5.3 <u>Radome Material</u>	71
5.4 <u>Radome Power Transmission</u>	71
5.5 <u>Radome Attachment</u>	71
6.0 <u>Site Survey</u>	74
7.0 <u>Electrical System</u>	76
7.1 <u>General</u>	76
7.2 <u>Specific Airplane Configuration</u>	76
7.3 <u>Airplane Modifications</u>	76
7.4 <u>Ground Checkout</u>	79
7.5 <u>Limitations</u>	79
8.0 <u>Equipment Cooling System</u>	81
8.1 <u>Liquid Cooling</u>	81
8.2 <u>Forced-Air Cooling</u>	81
9.0 <u>Aircraft Modification</u>	82
III SUMMARY AND CONCLUSION	83
IV BIBLIOGRAPHY	85
V APPENDICES	89
A. Antenna Design	90
B. Calculation of Solar Noise Temperature	103
C. Calculation of Noise Temperature Due to Oxygen and Water Vapor in the Atmosphere	105
D. Calculation of Total Equivalent Antenna Temperature	118
E. High-Power Testing of Microwave Components	134
F. Summary of "Project Needles" Techniques	144
G. Satellite Orbit Computations	146
1. Orbital Elements	
2. Secular and Periodic Motions of the Node of an Artificial Earth Satellite	150
H. Computer Subsystem: Comparison between Analog and Arithmetic or Incremental Digital Computers.	154
I. Antenna Drive Control System	154
1. Z-Transform Method	
2. Error Compensation by Digital Programming	
3. Generalized Digital Compensation	
J. Summary of Characteristics of Hughes M-252 Computer	167

# TABLE OF CONTENTS (con't)

	<u>Page</u>
K. Digital Pointing Computer. (Sections 3.2.4 through 3.4.5.2 of Source Control Drawing D10-60603)	168
L. Site Survey Profiles	174
M. Power Requirements for Microwave Communication System	177
N. Drawing Index - Microwave Antenna Installation	183
O. Peripheral Microwave Investigations	187



## LIST OF ILLUSTRATIONS

<u>Figure</u>	Page
1.1 Schematic diagram of the airborne microwave antenna system	12
1.2 1/3-scale mock-up of receiver and antenna system (front view)	14
1.3 1/3-scale mock-up of receiver and antenna system (rear view)	15
2.1.1 Sketch of the Paraboloid Antenna	18
2.3.1 VSWR vs Thickness of dielectric windows	28
2.3.2 Pressurizing teflon cap and mount assembly	29
2.3.3 T-R waveguide switch	30
3.1 Gust probability of KC-135 airplane	32
3.2 Angular rates and displacements due to turbulence for straight and level flight of KC-135 airplane at 35,000 ft.	33
3.3 Block diagram of antenna drive system	36
3.4 Wiring diagram of lear type 3055 dry powder magnetic clutch servo unit with optional amplifier	40
3.5 Antenna angular position feedback transducer	41
3.6 Remote control and indication of antenna polarization	43
3.7 Upper antenna platform	46
4.1 View of terrestrial sphere (azimuth computation)	55
4.2 Sectional view of earth (elevation computation)	55
4.3 Schematic diagram of antenna drive system	66
4.4 Operator's console	68
5.1 Power density vs distance along antenna axis	72
5.2 Calculated radome power transmission efficiency	73
6.1 Radome location on KC-135 aircraft	75
7.1 KC-135 airplane electrical system	77
7.2 Proposed klystron beam-power multiple-feeder system	78
7.3 Microwave communication electrical power	80
A-1 Coordinate system for determination of the reflector surfaces	91
A-2 Circular aperture distribution for 30 db sidelobe	94
A-3 Transition from rectangular to cylindrical waveguide antenna feed	97
A-4 Antenna-feed tuner	100
A-5 Photograph of antenna feed assembly	101
A-6 Measured input VSWR of the antenna feed assembly	102

# LIST OF ILLUSTRATIONS (con't)

<u>Figure</u>		<u>Page</u>
C-1	Variation of atmospheric temperature with altitude	106
C-2	Variation of atmospheric density with altitude	107
C-3	Noise temperature, $T_n$ , due to oxygen and water vapor in the atmosphere	117
D-1	2-foot cassegrain paraboloid antenna pattern	119
E-1	Block diagram of high-power test set-up	137
E-2	Photograph of high-power test set-up	138
E-3	Photograph of teflon-support TE-TEM-TE rotary joint after breakdown	139
E-4a	Photograph of TE-TM-TE rotary joint (for RG-52/U)	140
E-4b	Photograph of TE-TM-TE rotary joint (for RG-51/U)	141
E-5	Photograph of high-power test results of teflon windows	142
E-6	Photograph of pressurizing teflon cap	143
G-1	Coordinate reference system	147
H-1	General system configuration using an arithmetic digital computer	151
H-2	General system configuration using an incremental digital computer	151
I-1	Digital control system	155
I-2	Properties of an ideal sampler	155
I-3	Comparison of continuous and sampled-data system	155
I-4	Program controlled digital computer	156
I-5	Block diagram of open loop digital computer control system	156
I-6	Block diagram of digital feedback control system channel	157
I-7	Generalized digital compensation	157
I-8	Single channel of antenna drive system (simplified)	157
K-1	Desk height cabinet rack	171
K-2	Sloping front console	171
L-1	Beam obscuration as a function of antenna site at various bank angles	175
L-2	Beam-body obscuration at various stations for 30° bank angle	176

# List of Tables

<u>Table</u>		<u>Page</u>
2.2.1	Noise temperature due to oxygen and water vapor in the atmosphere	22
2.2.2	Total antenna and system noise temperature at 8 kmc	22
4.1.1	Error breakdown of tracking system	49
4.1.2	Analog inputs available to digital pointing computer on KC-135 aircraft	51
C-1	Noise Temperature difference, $\Delta T$ , between sea level and different altitudes for several antenna look angles	116
C-2	Noise temperature, $T_a$ , due to oxygen and water vapor in the atmosphere	116
D-1	Power distribution of the antenna beam in Fig. D-1	120
D-2	Antenna temperature at 40,000 ft. when the beam is pointing at zero degree (zenith)	121
D-3	Antenna temperature at 40,000 ft. when the beam is pointing at 85 degrees	122
D-4	Antenna temperature at 40,000 ft. when the beam is pointing at 90 degrees	124
D-5	Antenna temperature at 20,000 ft. when the beam is pointing at zero degree (zenith)	125
D-6	Antenna temperature at 20,000 ft. when the beam is pointing at 85 degrees	126
D-7	Antenna temperature at 20,000 ft. when the beam is pointing at 90 degrees	128
D-8	Antenna temperature at sea level when the beam is pointing at zero degree (zenith)	129
D-9	Antenna temperature at sea level when the beam is pointing at 85 degrees	130
D-10	Antenna temperature at sea level when the beam is pointing at 90 degrees	132
D-11	Summary of antenna temperature due to atmospheric and ground emissions	133
M-1	Power requirements for microwave communication system (115/200 volt 400 cycle AC loads)	178
M-2	Power requirements for microwave communication system (28 volt DC loads)	179
M-3	Power requirements for microwave communication system (28 volt AC loads)	180
M-4	Graph-AC electrical load analysis	181
M-5	Graph-DC electrical load analysis	182

# I INTRODUCTION

## 1.0 Purpose

The design study conducted for an airborne high-gain antenna mounting-and-control system which can be used for tracking a fixed object located in the hemisphere above the local aircraft horizontal is described in this report. The antenna is to be directed at the object throughout all conditions of the flight, including those induced by pitch, roll and yaw. The positioning of the antenna is to be derived from aircraft navigation and stabilization equipment as well as from accurate knowledge of the position of the object. The minimum height of the object is assumed to be 1500 miles. System requirements and suggested approaches are stated in the original Request for Proposal 26, and in the responding Proposal 24.

Contractually, the work was divided into two phases:

- Phase I: Conduct a study to define a design approach and determine what system capability can be accomplished and report the results of this study to the Communication Sciences Laboratory, AFRD, for approval.
- Phase II: Upon approval of Phase I, prepare a complete set of drawings and specifications sufficient to effect procurement of the system components and to install the system on a KC-135 airplane.

The transmitter, a 10-kw cw klystron power amplifier operated at  $8350 \pm 50$  mc, is being developed by Varian Associates, Palo Alto, California. The first stage of the receiver, a helium-cooled, closed-loop, maser amplifier operated at  $7750 \pm 50$  mc, is being developed by Hughes Research Laboratory, Malibu Beach, California. The receiver noise temperature is expected to be near  $20^\circ\text{K}$ . Because of the requirements imposed by the very-high transmitter power and the very-low receiver noise figure, few existing components and no subsystems are suitable for use in the system.

## 2.0 History

The past decade has seen long forward strides in long-haul radio communications: tropospheric scatter, ionospheric-meteor scatter, and satellite (active and passive) communications. With each of these steps, the question arises, "Will it work on aircraft?" and each time the answer is found by exhaustive field tests---tests instrumented by equipment designed for the propagation mode of interest, within the limits of present knowledge.

---

Superscripts refer to listed references in the bibliography (Section IV) of this report.

A number of modes of point-to-point communication via satellite have been conceived; each have their advocates:

Active satellite	(Courier)
Passive satellite	(Echo)
Dipole belt	(Needles)

For instantaneous communications, sender and receiver both focus energy on a common relay point above their own local horizons. Optimum frequency for satellite relay is near the atmospheric "window" at 5 kmc; in this band high-gain antennas are required to offset path losses. When one terminal is aboard on aircraft, complications arise due to the instability and mobility of the platform and the problem becomes one of achieving sufficient gain, yet pointing the antenna accurately enough in flight to realize the design antenna gain.

Conventional microwave installations on aircraft are now mainly limited to radar—search, fire-control, weather—with low-average power (50-500 watts) and receiver noise temperatures of 500-2000°K. Novel problems connected with the high average transmitter power and low receiver noise are thermal in character; thermal breakdown of components by the transmitter, thermal noise in the receiver. These demand careful attention in the antenna system design.

## II DISCUSSION

### 1.0 System Concept

The basic elements of the airborne antenna system are the radome, antenna and antenna feed, antenna mount and servo system, computer and pointing system, electrical system, and cooling system. Most steerable microwave antenna systems employ altazimuth mounts in which the antenna is fed through rotary joints at the motion axes. A search has revealed neither a suitable mount system nor a waveguide rotary joint that will handle 10 kw cw power and have a bandwidth of from 7.7 to 8.4 kmc. Proposals from several electronic firms have indicated the feasibility of developing a 10-kw rotary joint but with bandwidth of only 1 percent.

To minimize the noise within the antenna system, the maser receiver should be located as close as possible to the antenna feed. Since a rotary joint will increase the noise temperature of the receiving system and since the development of such a joint to operate at both the transmit and receive frequencies is difficult, the antenna feed system should be designed so that no rotary joints are necessary at the front end of the receiver. Several antenna system configurations were considered:

- 1) Receiver attaches to and moves with the antenna, the transmitter unit is stationary and located in the aircraft cabin (needs three high-power rotary joints).
- 2) Receiver and transmitter tube attach to and move with the antenna; power supply and cooling unit are stationary (eliminates rotary joints but needs high-power DC slip rings and flexible cables).
- 3) Receiver and transmitter tube attach to and move with the antenna; power supply rotates with the antenna platform along the vertical axis (eliminates high-power DC slip rings but needs slip rings for primary AC power).

The feasibility of each configuration was discussed with Hughes Research Laboratory (receiver contractor), Varian Associates (transmitter contractor) and the ARDC contracting officers.

System configuration No. 1 was chosen because the last two configuration have the following disadvantages: (Fig. 1.1)

- 1) The radome must be either pressurized or pressure containers provided for the transmitter tube.
- 2) A mass many times that of the antenna must be moved.
- 3) The equipment placed in the radome is inaccessible for servicing and maintenance in flight.

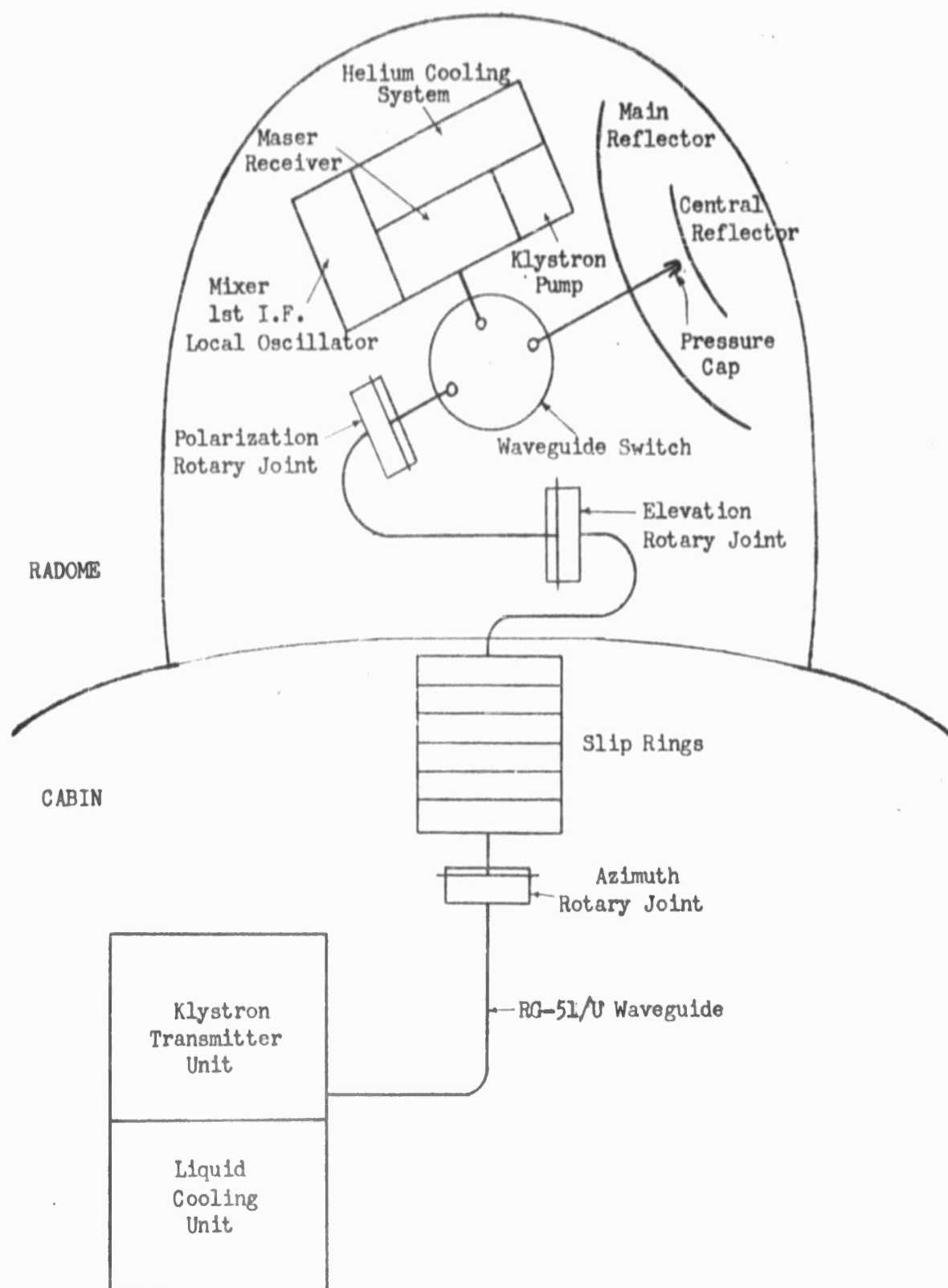


Fig. 1.1 Schematic Diagram of the Airborne Microwave Antenna System

Since substantially hemispheric coverage is required, the antenna must be located on the top centerline of the aircraft. Studies have shown the optimum location to be station 670. This choice is a compromise between aerodynamic consideration, and minimum airframe-beam interference.

The shape of the radome was chosen as a compromise between good electrical characteristics (hemispheric) and minimum effect on aircraft performance (long and low). A length-to-height ratio of 3 to 1 was chosen (39"H x 53"W x 114"L). Such a shape and size will reduce the aircraft range by 10 percent but will have an overall average power transmission of about 96 percent. The maximum boresight error will be less than one-half degree for any antenna look angle. A single sandwich wall with honeycomb core construction was chosen for the radome design. To reduce dielectric heating of the radome by the 10-kw power output from the antenna, Emerson and Cuming ECCO-L-65 low-loss laminating resin was used for radome material. A sample of a laminate using this resin was tested and found to exhibit satisfactory electrical properties up to 300°F. It was determined that a sandwich wall construction using ECCO-L-65 resin with a rain erosion coating could handle a maximum power density of 90 watts per square inch. Maximum calculated power density at the radome is 70 watt/inch<sup>2</sup> (Fig. 5.1).

No stabilized platform was used. The drive mechanism has the following motion capability: continuous 360° in azimuth, minus 25° to plus 120° (30° past vertical) in elevation, and a 180° change in antenna polarization. Antenna pointing commands are supplied to the drive servo-motors by a digital computer which computes the desired antenna angle from stored data on the "satellite or orbiting belt" position and attitude sensed from existing aircraft systems.

A transmit-receive waveguide switch located at the back of the parabolic dish connects the antenna to the transmitter or receiver as selected by the operator; switching time is approximately 50 milliseconds. The maser amplifier, the local oscillator and the first IF stage are mounted on a gimbal supporting the antenna to avoid any rotary joints between the antenna and this stage of the receiver. Conventional rigid waveguide with rotary joints at the motion axes connects the TR switch to the transmitter unit in the aircraft cabin.

The maser receiver power supply, the first IF signal, the elevation and polarization pointing command are channeled through a multi-terminal, slip-ring assembly located along the vertical shaft within the cabin. The maser compressor is cooled by the transmitter cooling unit through a specially designed doughnut liquid rotary joint and tubing.

A 1/3 scale mock-up of the antenna and maser receiver arrangement is shown on Figures 1.2 and 1.3. However, this is not the final configuration.







D6-7190

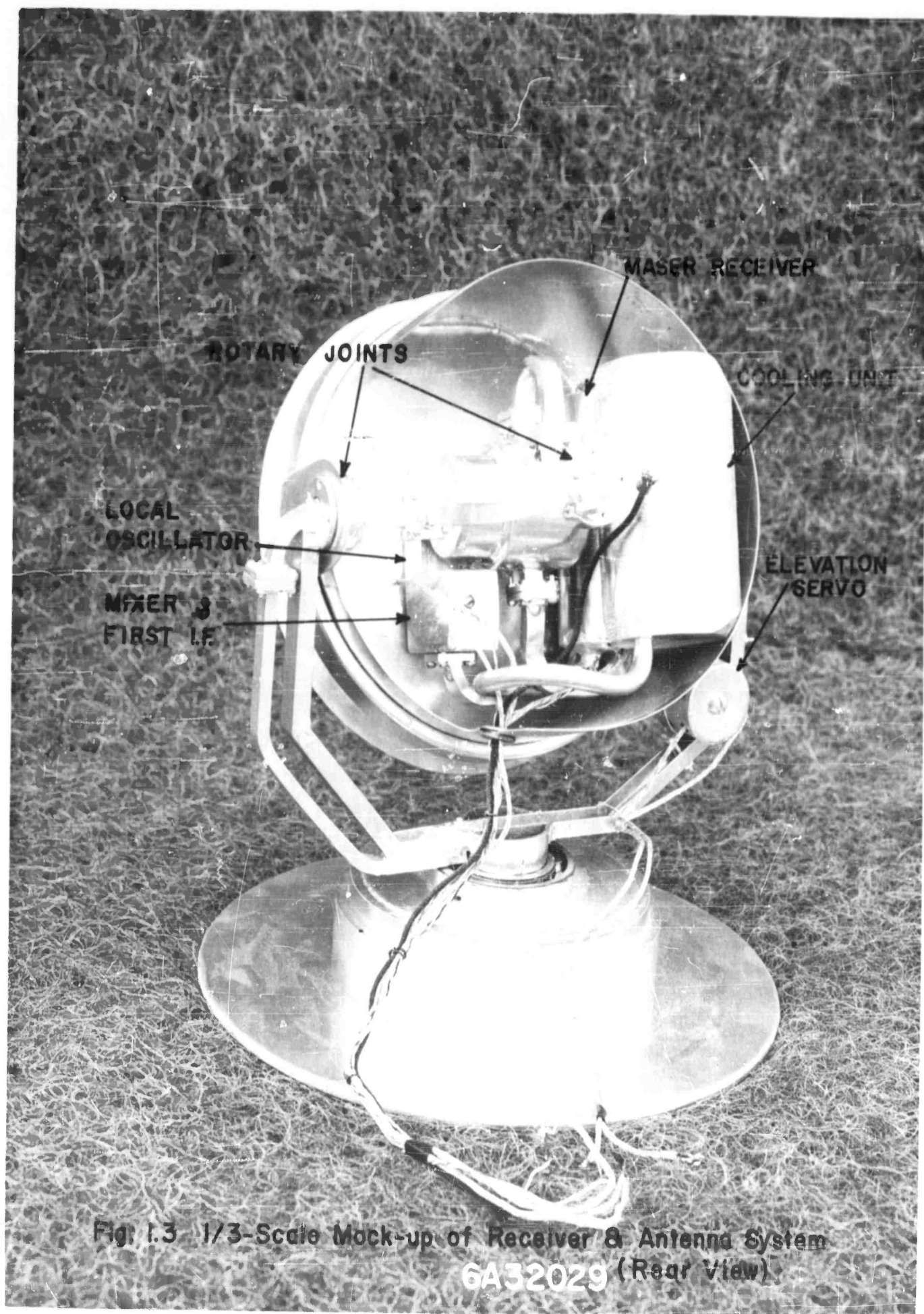


Fig. 1.3 1/3-Scale Mock-up of Receiver & Antenna System  
6A32029 (Rear View)

## 2.0 Antenna System

### 2.1 Antenna Design

Antenna configurations such as luneberg lens, linear arrays, parabolic dishes were investigated. The requirements of a complete upper hemisphere coverage necessitates the use of either a paraboloid antenna or a two-dimensional linear array. However, for simplicity in the feed system, a paraboloid antenna was chosen. The following antenna specifications were selected as a result of the antenna noise-temperature study and are compatible with the condition of the contract:

- |  |                          |
|--|--------------------------|
| 1) Frequency of operation                              | 7.7 to 8.4 kmc           |
| 2) Minimum gain  | 30 db                    |
| 3) Minimum sidelobe                                    | -25 db                   |
| 4) Power handling capacity                             | 10 kw cw 100% duty cycle |
| 5) Antenna polarization                                | linear, adjustable       |
| 6) Waveguide   | RG-51/U                  |
| 7) Antenna feed as short as possible for minimum loss. |                          |

inquiries to leading microwave antenna manufacturers such as Dalmo-Victor, Melpar Inc., Diamond Antenna and Microwave Corporations, Technical Application Corporation, Hughes Aircraft Company, and others have indicated that no off-the-shelf antennas can meet the above specifications and that a developmental program will be required to produce such an antenna.

Several low-sidelobe antenna-feed techniques were investigated. An existing Boeing chlain-feed paraboloid antenna has -28 to -30 db side-lobes, but the tapering section of the feed cannot withstand 10 kw cw power. The same is true for Dalmo-Victor back-to-back feed paraboloid antenna for search-and-track radar. A type of cassegrain paraboloid antenna which evolved from the low-noise hoghorn antenna can be designed for better than -25 db sidelobe and better than 50 db front-to-back ratio. The feed is a circular waveguide which is capable of handling 10 kw cw power, operating on a TE<sub>11</sub> mode. This type of antenna was developed at the RCA Victor Co. Ltd.,<sup>1</sup> Montreal, Quebec and found to be a wide-band, low-reflection coefficient antenna. A similar antenna is currently being used in the Bell Telephones' TJ Relay Radio System.<sup>2</sup>

For low sidelobe, a 2-foot parabolic dish is needed for an antenna with a minimum of 30 db gain and  $5^\circ \times 5^\circ$  beam at 7.7 kmc. However, to decrease spill-over a 26-inch dish was used. Using the design in reference (1) with a 30-db Taylor aperture distribution (Ref. 3), a coscagram-type paraboloid antenna was designed. Because of the aperture blocking effect of the central reflector the sidelobe level is expected to increase from -30 db to -26 db.

The antenna feed is a straight section of circular waveguide which supports a  $TE_{11}$  mode. A transition section is used to connect the circular waveguide feed to the rectangular RG-51/U waveguide. Two capacitive screws located near the circular-to-rectangular transition section are used for antenna tuning. Additional tuning can be accomplished by adjusting a movable slug of the central reflector. A 0.03-inch thick teflon pressurizing cap is located at the feed aperture.

Figure 2.1.1 is a sketch of the antenna with the dimensions labeled. The design details of the antenna reflectors and the antenna feed are shown in Appendix A.

$\psi$ (degrees)	$\rho$ (inches)
0	7.350
20	7.579
30	7.878
40	8.324
50	8.948
60	9.800
70	10.954
80	12.526
82	12.904
84	13.309

-X	y
0.40	1.888
0.42	1.802
0.44	1.715
0.46	1.628
0.48	1.539
0.50	1.449
0.52	1.358
0.54	1.264
0.56	1.168
0.58	1.069
0.60	0.952
0.62	0.856
0.64	0.739
0.66	0.610
0.68	0.457
0.70	0.240
0.708	0.000

$$\rho \cos^2 \psi/2 = 7.350242$$

( $\rho$  in inches)

12"

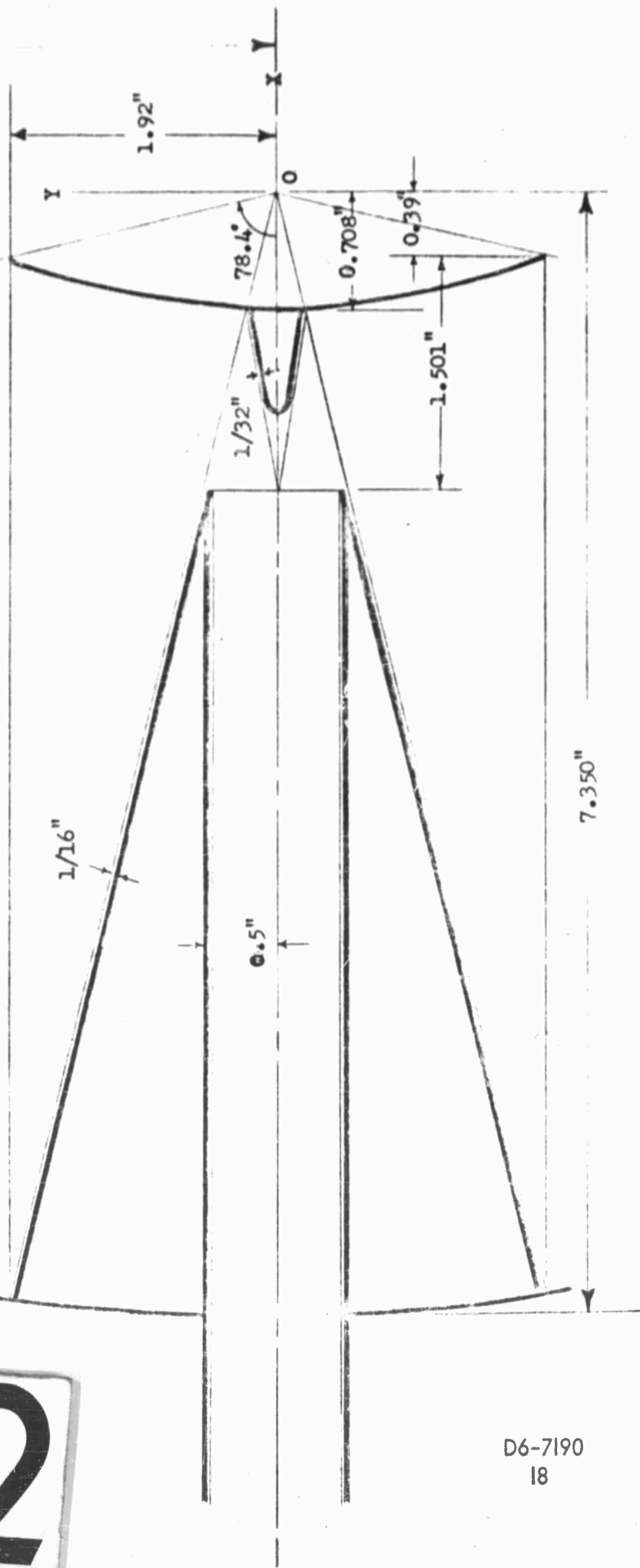


0.58 ..... 1.007  
 0.60 ..... 0.952  
 0.62 ..... 0.856  
 0.64 ..... 0.739  
 0.66 ..... 0.610  
 0.68 ..... 0.457  
 0.70 ..... 0.240  
 0.708 ..... 0.000

2

$$14.718 \ x^2 - 27.8416 \ x + 12.3576 = y^2$$

(x, y in inches)



D6-7190  
18

## 2.2 Equivalent-Antenna and Feed-System Noise Temperature

The sensitivity of an antenna system is determined by the noise power received by the antenna from its surroundings and by the noise of the receiver connected to it. The noise in an ordinary microwave receiver is much higher than the noise received by the antenna. Consequently, receiver noise becomes a dominant factor in determining system sensitivity. However, with the advent of low-noise receivers such as maser and reactance amplifier, antenna noise becomes comparable to or lower than receiver noise. Therefore, an exact knowledge of the antenna noise is vital since it may determine the overall sensitivity of the system.

The antenna noise temperature at microwave frequencies is caused almost exclusively by thermal energy originating from an exchange of radiation with the medium in which the antenna is embedded. If the antenna is in thermal equilibrium with its surroundings, its equivalent temperature can be expressed as:

$$T_A = \frac{1}{4\pi} \int G(\theta, \phi) T(\theta, \phi) d\Omega$$

where  $G(\theta, \phi)$  is the directional-antenna gain function and  $T(\theta, \phi)$  is the directional effective temperature. The three-dimensional integral of Equation (1) can be replaced by a two-dimensional sum of the following form:

$$T_A = \sum_i \bar{T}_i \bar{G}_i \frac{\Delta\theta_i}{2\pi}$$

where  $\bar{G}_i = \frac{\Delta\theta_i}{2\pi}$  and  $\bar{T}_i$  are average gain figures and temperature in the direction of interval angle  $\Delta\theta_i$ .

In order to evaluate the equivalent antenna temperature,  $T_A$ , it is necessary to determine the values of  $T_i$  contributed by radiation from sources outside and within the atmosphere.

### 2.2.1 Sources of Noise

The noise in a high-gain antenna oriented skyward can be classified into two sources: that from outside the atmosphere and that from within the atmosphere. The sun, the moon, the planets, the stars, the interstellar hydrogen and the center of the galaxy are the sources of noise from outside the atmosphere. The oxygen and water vapor that attenuate microwaves are sources of noise within the atmosphere. With the exception of the sun and the moon, noise from extraterrestrial bodies is negligible at centimeter wavelengths.

#### 1) Noise from the Sun:

The variability of solar noise depends strongly on the radio wavelength.<sup>7</sup> For waves shorter than 2 to 3 cm, the intensity is steady and undisturbed; for waves between 3 and 60 cm, often called the decimeter range, disturbances occur frequently and are more intensive near sunspot maximum. At optical and millimeter wavelengths, the radiation follows closely that expected from a black body at 6000°K.<sup>8</sup> At 8 kmc, however, the radiation from the sun is that expected from a body at 30,000°K (Appendix B).



## 2) Noise from the Moon and Planets:

Estimates or measurements of lunar noise temperature vary from a value of  $150^{\circ}\text{K}$  at  $400\text{ mc}$ <sup>9</sup> to about  $200^{\circ}\text{K}$ – $280^{\circ}\text{K}$  at  $24\text{ kmc}$ <sup>10</sup> and  $35\text{ kmc}$ .<sup>11</sup>

The noise temperature of planets Venus, Jupiter and Mars at 3 and 9 cm wavelengths is on the order of  $1^{\circ}\text{K}$  or less<sup>12</sup> and that of Saturn is less than  $0.1^{\circ}\text{K}$ <sup>13</sup>

## 3) Noise from the Stars

Noise from the stars can be grouped into two classes: (1) that from discrete sources such as Cassiopeia A, Cygnus A, Taurus A, Virgo A, and (2) that from a generally diffuse background in which a maximum occurs along the galactic plane and a minimum towards the galactic poles.<sup>14</sup> The noise from the galaxy decreases markedly with increasing frequency; on long wavelengths, the maximum emissions correspond to an enclosure at  $100,000^{\circ}\text{K}$ , but at centimeter wavelengths, it falls below measurable limits. The maximum galactic noise temperature at  $1\text{ kmc}$  is about  $38^{\circ}\text{K}$ , and is less than  $1^{\circ}\text{K}$  above  $5\text{ kmc}$ .<sup>15</sup>

## 4) Noise from Interstellar Hydrogen

Hydrogen radiation is limited to a single wavelength of 21-cm and is unimportant as a source of interference at other wavelengths.

## 5) Noise Due to Oxygen and Water Vapor in the Atmosphere

At microwavelengths, the noise from within the atmosphere is due to absorption by oxygen and water molecules, and is greatly dependent on the elevation angle of the antenna beam. Both noise and attenuation are minimum when the antenna is pointing at the zenith and increase as the beam drops toward the horizon. The water vapor density is about  $10\text{ gr/m}^3$  at sea level and decreases to a negligible amount at altitudes greater than 5 km or 16,500 feet.<sup>16</sup>

At ground level, the antenna noise temperature due to oxygen and water vapor varies from  $5^{\circ}\text{K}$  to  $165^{\circ}\text{K}$  as the zenith angle increases from  $0^{\circ}$  to  $90^{\circ}$ . At 40,000 ft, the noise temperature varies from  $1^{\circ}\text{K}$  to  $34^{\circ}\text{K}$  as the antenna scans from  $0^{\circ}$  to  $90^{\circ}$  (Appendix C).





## 6) Noise from Other Sources:

The extreme short-wave end of the radio spectrum below about 30 cm is relatively free from man-made interference, and lightning-discharge noise does not present a significant problem at wavelengths shorter than 2 or 3 meters. The earth is a hot body of 288°K, its temperature is higher than that of the sky. However, if the antenna main beam is not directed toward the earth and if the fuselage or the wing of an aircraft is used as a shielding for an air-borne antenna, the noise from the direction of the earth is greatly reduced.

### 2.2.2 System Losses

To minimize the noise within the antenna system, the maser receiver is located as close as possible to the antenna feed. An estimate of the antenna noise temperature due to internal losses follows:

<u>Component</u>	<u>Loss in Percent of 290° K</u>	<u>Equivalent Noise Temperature</u>
Radome	5%	14.5°K
Antenna dish	1%	2.9
Antenna feed loss	2%	5.8
TR Switch	1%	2.9
Total		26.1°K

### 2.2.3 Total Noise Temperature

For a high-gain antenna at 8 kmc, the noise temperature due to radiation from extraterrestrial bodies such as the stars, the planets, and the galaxy is negligible. The noise from the sun and the moon may be a source of trouble, but is of a limited nuisance type, occurring only when the main antenna beam is pointed in the direction of the offending body. Since the sun and the moon as observed at the earth have an angular diameter of about 0.5 degrees, the noise rise is of a temporary or transient nature in satellite communications. Calculations of solar noise temperature are presented in Appendix B.

Noise due to oxygen and water vapor in the atmosphere is greatly dependent on the elevation angle of the antenna beam and on the altitude of the airborne antenna. A rigorous analysis of the noise temperature at sea level and at altitudes up to 50 kilometers is presented in Appendix C. The results at 40,000 feet, at 20,000 feet and at sea level are presented in Table 2.2.1.

Table 2.2.1

NOISE TEMPERATURE DUE TO OXYGEN AND  
WATER VAPOR IN THE ATMOSPHERE

ALTITUDE	ANTENNA ZENITH ANGLE				
	0°	60°	80°	85°	90°
Sea Level	5.07°K	10.26	28.6	53.3	165.7
20,000 ft.	2.53	5.27	14.21	25.8	72.25
40,000 ft.	1.13	2.49	6.7	11.5	34.1

The antenna-noise temperature contributed by the atmosphere, by the hot earth and by the sun is evaluated in Appendix D. The results of a typical -25 db sidelobe 2-foot paraboloid antenna at 8 kmc are tabulated in Table 2.2.2.

Table 2.2.2

TOTAL ANTENNA AND SYSTEM NOISE  
TEMPERATURE AT 8 KMC

ALTITUDE	40,000 ft.			20,000 ft.			Sea Level		
	0°	85°	90°	0°	85°	90°	0°	35°	90°
<u>NOISE SOURCE</u>									
1. Atmospheric and Ground Emission	1.2°K	14.6	32.9	2.7	35.3	60.6	5.3	73.6	116.6
2. Solar Radiation *	4.0	4.0	4.0	4.0	4.0	4.0	4.0	4.0	4.0
3. System loss	26.1	26.1	26.1	26.1	26.1	26.1	26.1	26.1	26.1
Total noise temperature	31.3	44.7	63.0	32.8	65.4	90.7	35.4	103.7	146.7°K

\* The solar noise is the radiation intercepted by the first -25 db sidelobe.

#### 2.2.4 Assumptions used in the Noise Calculation

##### 1) Noise Temperature Due to Solar Radiation (Appendix B)

At 8 kmc and from a disturbed sun, the solar noise-power density on the earth was estimated at five times that of a black-body at  $6000^{\circ}\text{K}$ .

Because of the excessive temperature increase when the main lobe is directed toward the sun, only the solar noise that is intercepted by the first -25 db sidelobe was considered.

##### 2) Noise Temperature Due to Atmospheric and Ground Emission (Appendix C)

At 8 kmc, the noise temperature from atmospheric emission is mainly due to oxygen and water vapor. The first 50 kilometers of the atmosphere were considered in the calculation. Beyond this altitude, the temperature contribution is negligible; and beyond 5 kilometers, almost no water vapor exists. For noise-temperature calculation at high altitudes, the power absorption coefficient was assumed to be directly proportional to the atmospheric density.

##### 3) Total Equivalent Antenna Noise Temperature (Appendix D)

The antenna noise temperature due to atmospheric and ground emission was evaluated by determining the average temperature of the medium in which the beam is pointing, the average is weighted by the gain function of the antenna. The airframe acts as a shield for the antenna from the ground emission. The airframe reflectivity is assumed to be 90%. The temperature contribution was evaluated at each 5-degree interval.

#### 2.2.5 Conclusion

It is concluded that the increase of antenna noise temperature at 8 kmc is almost entirely due to oxygen and water vapor in the atmosphere and to radiation from the hot earth. Extra-terrestrial noise from discrete sources such as the sun, the moon, and the stars will generally be only a limited nuisance type. Since the satellite is orbiting the earth at a very high speed, the time when trouble may be experienced should be small. The sun will be the worst offender, however, the computer should be able to determine the exact time when trouble may be expected, so that allowances may be made.

Because of the high noise temperature when the antenna is pointing close to the horizon it would be more difficult to communicate with the satellite at an angle greater than  $85^{\circ}$  from the zenith. At 40,000 feet, the antenna system noise temperature is  $31.3^{\circ}\text{K}$  when the antenna is pointing at the zenith and is  $44.7^{\circ}\text{K}$  when it is pointing at an angle approximately  $5^{\circ}$  from the horizon.



The system losses on the transmitter side is not a critical factor because sufficient transmitter power is available. However, components of minimum loss are considered in the design to save power and reduce heating.

## 2.3 High-Power Components

One of the major problems in the Experimental Airborne Antenna System is the availability of system components that can withstand 10 kw cw power. RG-51/U liquid-cooled waveguide was proven capable of handling more than 10 kw cw power, and is used in the entire system. Other high-power components that are needed are waveguide switches, waveguide rotary joints, waveguide flanges, pressurizing windows, and antenna feed.

### 2.3.1 Transmit-Receive Waveguide Switches

Several commercial high-power waveguide switches have been investigated. Some of them show capability of handling 10 kw power, however, only two switches were tested by Varian Associates, Palo Alto, California. One of the switches was manufactured by Bogart Mfg. Corp., Brooklyn, New York and the other by Sivers Lab, Stockholm, Sweden. Both switches can withstand as much as 20 kw cw power. Bogart's switch was chosen for this system because its temperature rise is not as fast as Sivers' switch under the same operating condition. The specifications of the Bogart waveguide switch follows: (Fig. 2.3.3)

#### Electrical Specifications:

Frequency Range	7.05 to 10.00 kmc
VSWR	1.10 maximum
Insertion Loss	Less than 0.1 db
Ave. Power	25kw
Isolation	60 db min.
Switching Time	0.05 seconds

#### Mechanical Specifications:

Weight	4 pounds (approx.)
Safe Pressure	35 P.S.I.G.

Other switching schemes such as ferrite switches or diplexers are either too lossy or incapable of handling 10-kw cw-power.

### 2.3.2 Waveguide Rotary Joints

Intensive investigation was conducted to establish that design and manufacturer of a high-power, low loss rotary joint is within the present state-of-the-art. Several electronic companies have shown their capability of designing a high-power rotary joint that will meet Boeing specifications. Most conventional waveguide-rotary joints fall under two types:

1. TE-TEM-TE Coaxial Transition - A common coaxial probe transition is used to transfer power between two rectangular waveguide sections by means of symmetrical TEM mode. Because of the small diameter of the center conductor and the presence of dielectric support in the transition section, this type of joint has a low cw power rating. Its bandwidth, however, is very wide.
2. TE-TM-TE Circular Cavity Transition - A circular TM mode cavity is used as a transition. The joint uses no dielectrics and therefore has a much higher cw power rating than the coaxial type. However, the transition section has a very narrow bandwidth.

High-power test of the two types of rotary joint at Boeing, proves that only the second type (TE-TM-TE) can withstand high cw power with an insertion loss of less than 0.2 db. However the narrow bandwidth characteristics of its transition precludes the use of the joint at both the receive and transmit frequencies. Consequently, rotary joints are employed only on the transmitter side of the antenna system. The test result of both types of rotary joint at 9500 mc is compiled in Appendix E.

Demornay-Bonardi and the Diamond Antenna and Microwave Corporations have indicated that one of their coaxial-type rotary joints can be modified to meet Boeing's specifications, but that no X-band high power is available to them for testing. Demornay Bonardi sent a coaxial-type 7.05-10.00 kmc rotary joint to Boeing for testing. Upon application of one kilowatt cw power at 9500 mc for a duration of three minutes, the center conductor of the joint melted and the teflon support charred.

Associated Industries, Airtron, Kearfott, Thorson, Technicraft and Raytheon companies have submitted proposals for developing a TE-TM-TE mode type, 10-kw rotary joint for use with RG-51/U. The quoted maximum VSWR and the maximum insertion loss are about 1.15:1 and 0.2 db at 8350 mc with 1 to 2% bandwidth. The developmental cost ranges from \$4,000.00 to \$20,000.00.

A TE-TM-TE mode, aluminum, rotary joint to be used with RG-51/U was received from Premier Microwave Corporation, Port Chester, New York. This joint is designed to operate at 9300 mc. Measurements at Boeing showed that the dissipative loss (scattering-coefficient method) is about 0.1 db. The joint was subjected to about 10-kw cw-power at 9500 mc for a period of 30 minutes. The temperature rise of the joint was maintained at 120°F with an air blower directed at the joint. No effect on the electrical or physical characteristics of the joint was observed after the test. (Appendix E). Premier has assured Boeing that similar type of joint can be

designed to operate at  $8350 \pm 50$  mc. For this frequency range, the diameter of the circular transition section will be increased by 10 to 12%. For pressurization, a high temperature seal can be inserted.

In view of extensive contacts with leading microwave manufacturers, and of high-power tests at Boeing, it is concluded that rotary joints suitable for this system can be supplied by industry at reasonable time and cost.

### 2.3.3 Waveguide Flanges

Varian Associates has designed and tested a waveguide flange successfully up to 20 kw cw power. This flange is essentially a standard UG-51/U cover flange with an O-ring groove similar to the O-ring groove used on UG-52A/U choke flange. The area outside the O-ring groove was undercut to insure contact at the desired surfaces. This flange will be used throughout the system.

### 2.3.4 Pressurizing Windows and Caps

Pressurizing windows are needed in the antenna system. The window located in the circular antenna feed must pass both the transmit and receive frequencies therefore, a non-resonant window must be used. In addition, it must withstand 10-kw cw power without dielectric thermal breakdown or voltage breakdown at an altitude of 40,000 feet. For high cw power applications, high-density ceramic bodies such as pure beryllium oxide are suitable for window materials, and are so used in power klystrons. Because of the high dielectric constant of ceramics, a non-resonant X-band window would have to be in the order of 0.01 in -thick<sup>25</sup> (Fig. 2.3.1). Ceramics at this thickness are fragile and may rupture at relatively low pressure. In addition, a thin window inside the guide would leave the mouth of feed horn unpressurized and subject to voltage breakdown at altitude. A second choice of window material is low-loss teflon dielectric. However, a high-power test at Boeing showed that a piece of 0.06 inch thick teflon window placed inside a RG-52/U waveguide started to melt when subjected to approximately 10-kw cw power at 9500 mc. The melting of the teflon is due to dielectric heating and is concentrated in the central region of the waveguide where the electric field is maximum. Test results are shown in Appendix E.

Varian Associates has operated a half-wave resonant ceramic window in a 1.25-inch circular waveguide at 20 kw cw power with 15 psig of dry nitrogen on one side and sea level air pressure on the other side. The window material was high-purity alumina AL-300, made by Western Gold and Platinum Company, Belmont, California. However, Varian advised that this window will not withstand voltage breakdown at pressure equivalent to 40,000 feet altitude.

As an alternative, a 0.03-inch thick hemispherical teflon cap placed at the aperture of the circular antenna feed will be used instead of a conventional window. As the cap is located outside the feed, the power incident on it will be more evenly distributed and any heat generated in the cap can be dissipated into space. The cap was tested for voltage breakdown with sea level pressure on one side and 90,000 feet altitude air pressure on the other side. No breakdown occurred at a power level of about 50-kw (0.002 duty-cycle). The VSWR introduced by the cap is 1.13 (Fig. 2.3.1).

No 10-kw cw-power was available for testing the dielectric heating of the teflon cap. To simulate these heating conditions, a 0.03 in.-thick Tenite cap was subjected to 90 watts average power at 8100 mc for a duration of one hour. Tenite was selected because it has the same softening temperature as teflon but 200 times as lossy ( $\tan \delta = 0.03$ ). No deformation of the cap was observed. There was a slight increase in temperature in the Tenite, however, the heat generated can be readily dissipated by the air cooling system in the radome. The degree of dielectric heating generated in the Tenite material is approximately that of teflon of same thickness if subjected to 18-kw power. The validity of this simulation test must be verified by actual testing of the teflon cap at 10-kw cw power.

Figure 2.3.2 is a sketch of the pressurizing teflon cap and mount assembly. The mount is also a part of the circular feed and is screwed into the rest of the feed. This arrangement facilitates replacement of the teflon cap in case of damage. This cap can be machined easily and requires no special tooling.

Some of the peripheral investigations related to this project is listed in Appendix O.

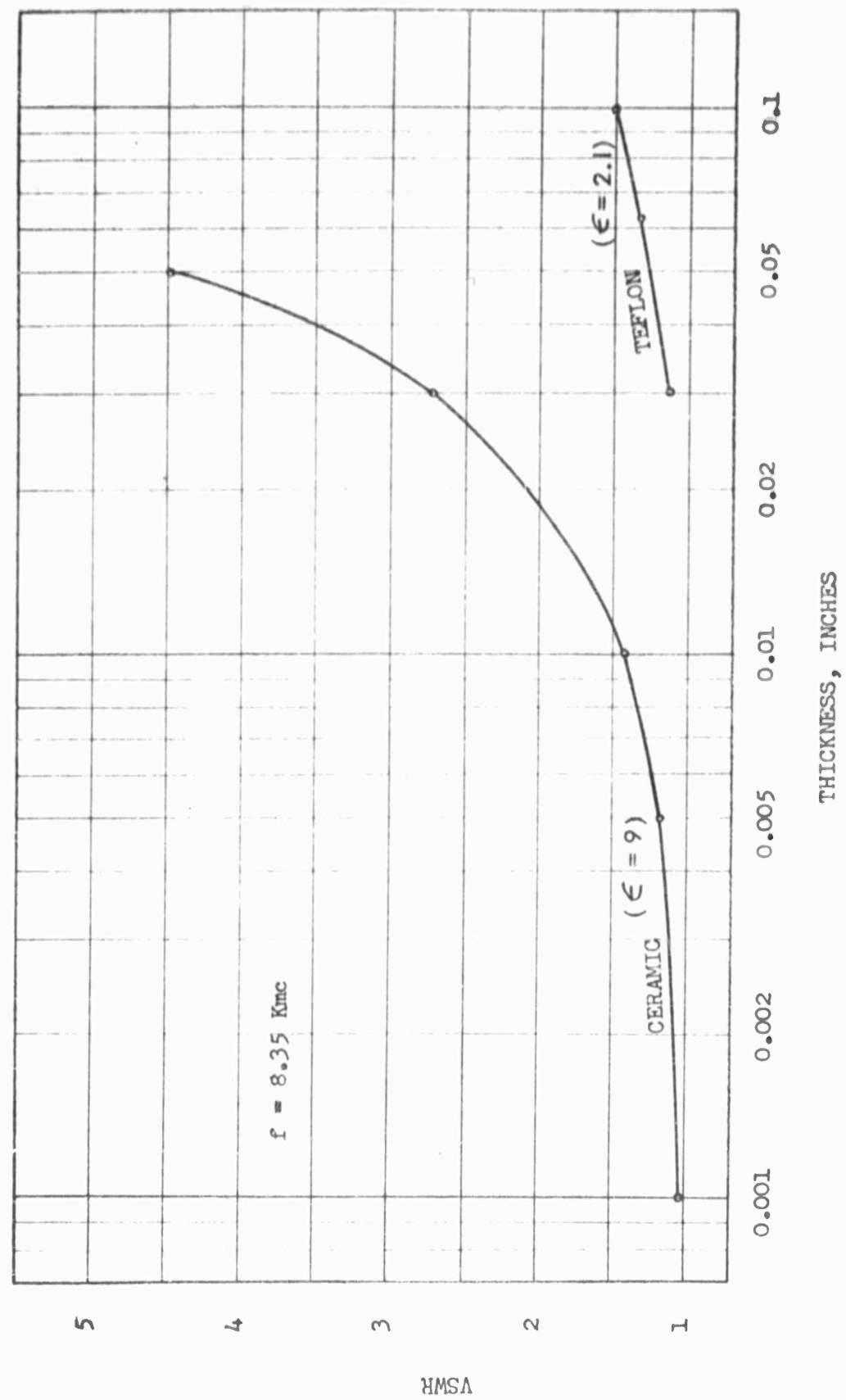


Fig. 2.3.1 VSWR VS THICKNESS OF DIELECTRIC WINDOWS



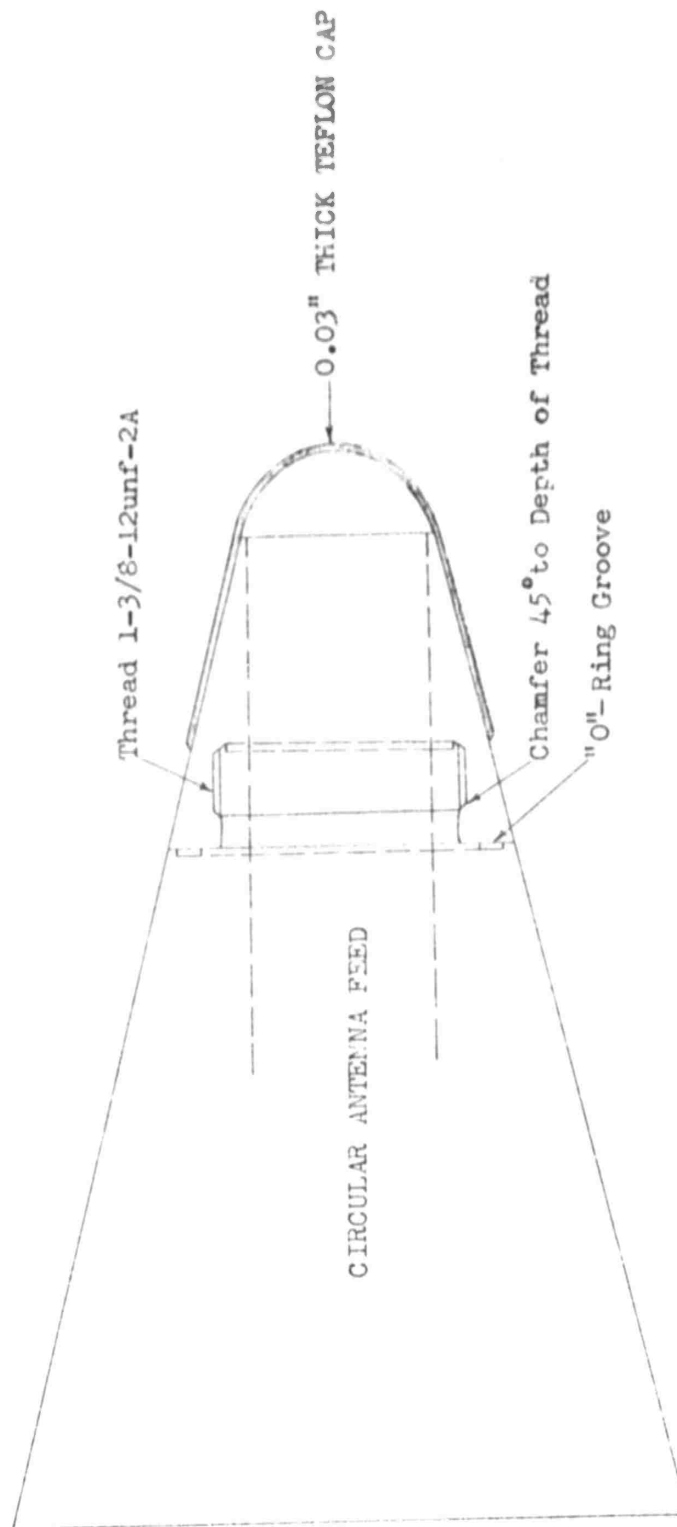
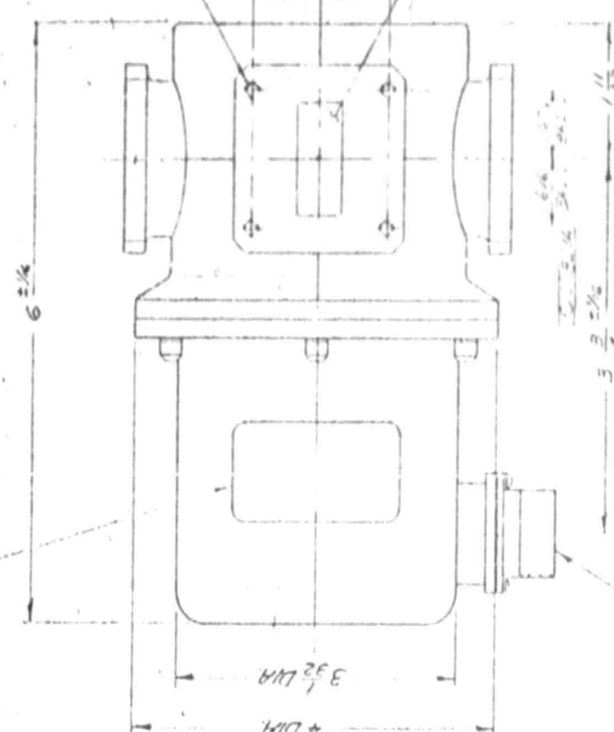
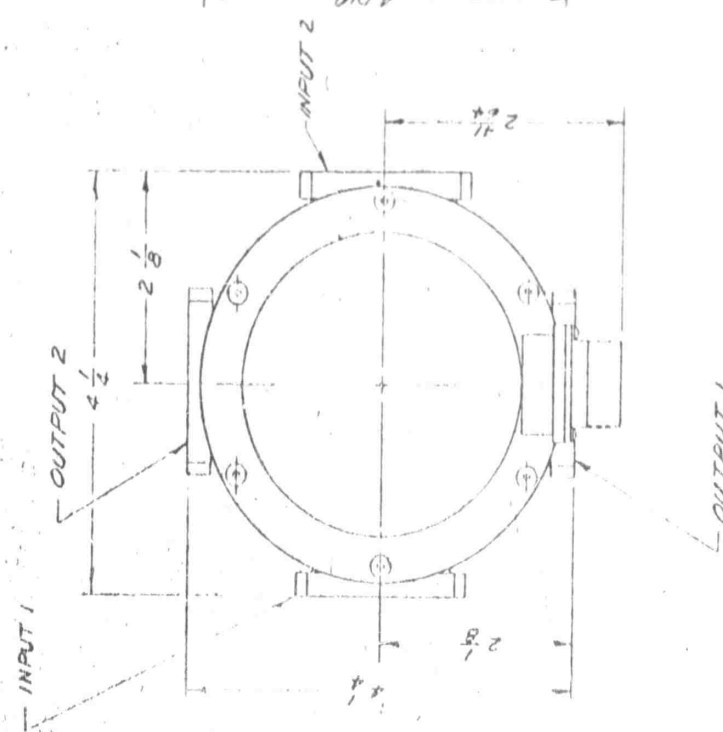


Fig. 2.3.2 PRESSURIZING TEFLON CAP AND MOUNT ASSEMBLY

RECEIPTABLE NO. 10333-1759

STANDARD "BOGART" NAMEPLATE  
Dwg. NO. C10333-1759



8-32 TAP HOLES, 4 FLANGES

1.122 ± .004  
RECT OPENING

NOTE:

- 1- PAINT HEAT-RESISTING GLYCERYL-PHTHALATE BLACK ENAMEL TYPE II PER SPEC. MIL-E-5557 MASK FLANGE FACES, HOLES & THREADS OF THE RECEIPTABLE.
- 2- WHEN SWITCH IS DE-ENERGIZED INPUT 2 IS CONNECTED TO OUTPUT 1 & INPUT 1 IS CONNECTED TO OUTPUT 2.
- 3- WHEN SWITCH IS ENERGIZED INPUT 2 IS CONNECTED TO OUTPUT 2 & INPUT 1 IS CONNECTED TO OUTPUT 1.

ELECTRO-MECHANICAL SPECIFICATIONS

FREQUENCY RANGE	705 to 10 KHz
VSWR	1.10 MAX.
AVG. POWER	25 KW CW
ISOLATION	60 DB MIN.
SWITCHING TIME	0.05 SECONDS
INTERLOCKING	1.5
WEIGHT	4 POUNDS APPROX.
SAFE PRESSURE	35 PSIG. DRY NITROGEN
RECEIPTABLE	3 MIL-E-5557 BLACK ENAMEL ENAMEL
RECEIPTABLE	2 C10333-1759 BOGART STD. NAMEPLATE
RECEIPTABLE	1 C1255-1 ASSEMBLY

RECEIPTABLE SOLENOID



WIRING DIAGRAM

FIG. 2.3.3 T-R WAVEGUIDE SWITCH

RECEIPT NO. 10333-1759

DATE: OCT 4 1959

91759

"B" BAND "X" SWITCH  
OUTLINE

SEE NOTE 1

FINAL 17-1

ALUMINUM

RECEIPT NO. 10333-1759

DATE: OCT 4 1959

91759

"B" BAND "X" SWITCH  
OUTLINE

SEE NOTE 1

FINAL 17-1

ALUMINUM

RECEIPT NO. 10333-1759

DATE: OCT 4 1959

91759

"B" BAND "X" SWITCH  
OUTLINE

SEE NOTE 1

FINAL 17-1

ALUMINUM

### 3.0 Antenna Mount and Servo Drive System.

#### 3.1 Requirements and Design Criteria

The KC-135 microwave communication antenna covered by this contract has a  $5^\circ \times 5^\circ$  half-power beamwidth and requires a pointing computer and servo drive system for accurate tracking of the orbiting satellite or "needles belt". The satellite or "needles belt" will be used as the microwave scatterer for long range communication. A summary of "Project Needles" techniques is given in Appendix F. It is important to achieve and maintain antenna-pointing and stabilization errors that are sufficiently small to realize full antenna gain. The antenna mount and drive system must enable the antenna to be directed at the object throughout all conditions of the flight, including those induced by roll, pitch and yaw. The minimum height of the object is assumed to be 1500 miles. The frequency response of the servo drive system must therefore be adequate to cope with the random yaw, pitch and roll perturbations of the aircraft, with the relative satellite movement and with suddenly applied bank angles.

##### 3.1.1 Criteria for Drive System Rating

- a. Random yaw, pitch and roll perturbations of the aircraft. The antenna will be directed at the object throughout all conditions of the flight, including those induced by roll, pitch and yaw. Gust-probability data from reference (22) indicate that 99.8% of the time a 10-ft/sec root-mean-square gust velocity, described as "severe turbulence approaching thunderstorm activity", will not be exceeded (Fig. 3.1). A 10 ft/sec RMS gust velocity corresponds to the following aircraft angular motions (Fig. 3.2):

<u>Plane</u>	<u>RMS Displacement</u>	<u>RMS Velocity</u>	<u>Frequency</u>
Roll	1.45 deg.	0.95 deg/sec	0.105 c.p.s.
Pitch	0.87	0.85	0.156
Yaw	0.5	0.65	0.208

All data are valid only at the center of gravity (cg) of the airplane, because at other locations additional vibrations due to airplane flexibility exist. However, the platform will be installed on top of the fuselage near the cg, and these vibrations will therefore be negligible.

During a more recent flight survey on the effect of gust and clear turbulence conditions on the aircraft structure, the KC-135 31-18 model was exposed to extreme conditions of 30 ft/sec vertical, and 20 ft/sec lateral gusts. Pitch-and yaw-rate meters were installed, and at peak pitch-and yaw-rates of comparable peak amplitudes these rates would correspond to pitch and yaw frequencies of 0.3 and 1.0 c.p.s. respectively.

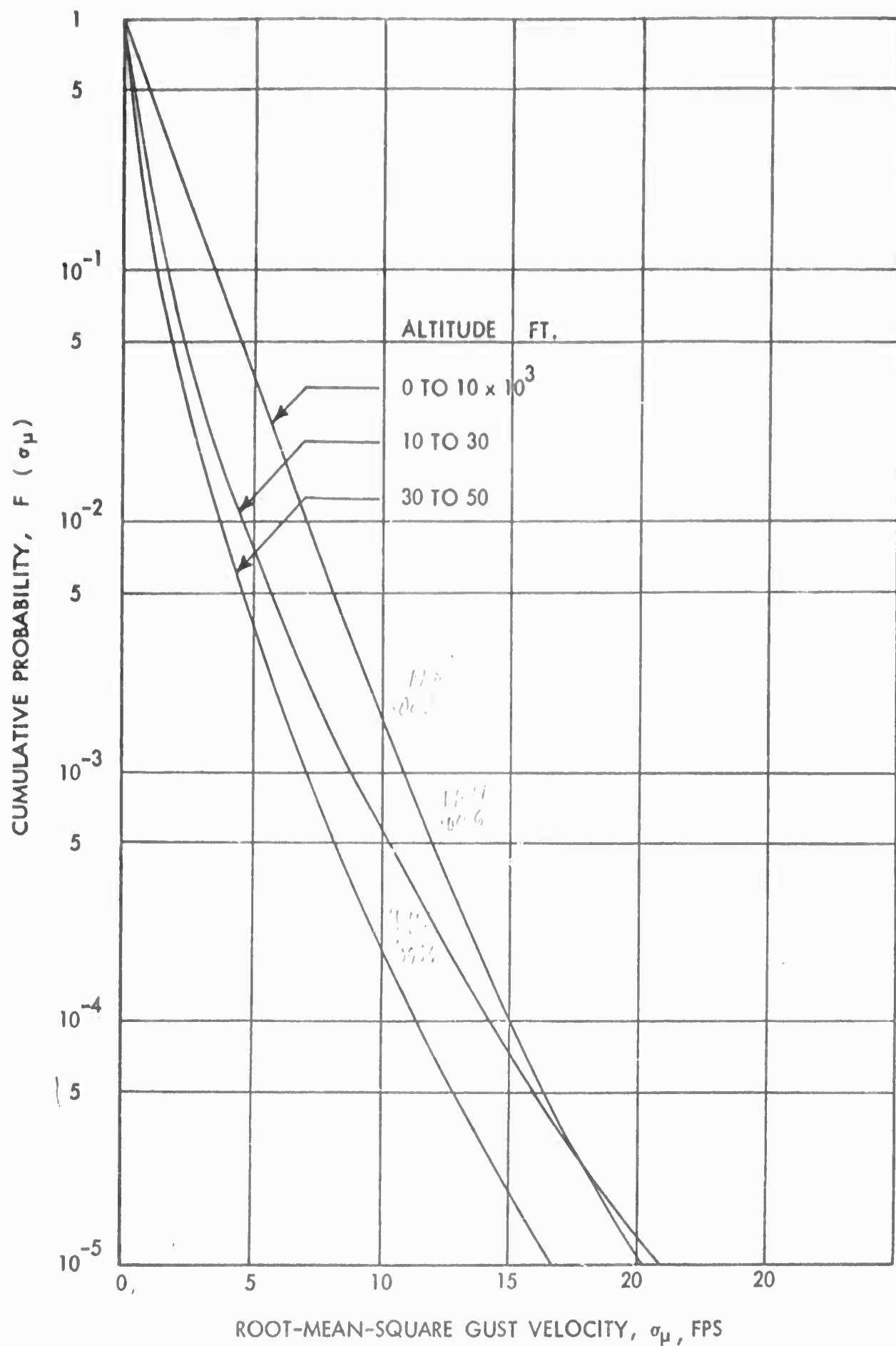


Fig. 3.1 GUST PROBABILITY  
of KC-135 AIRPLANE

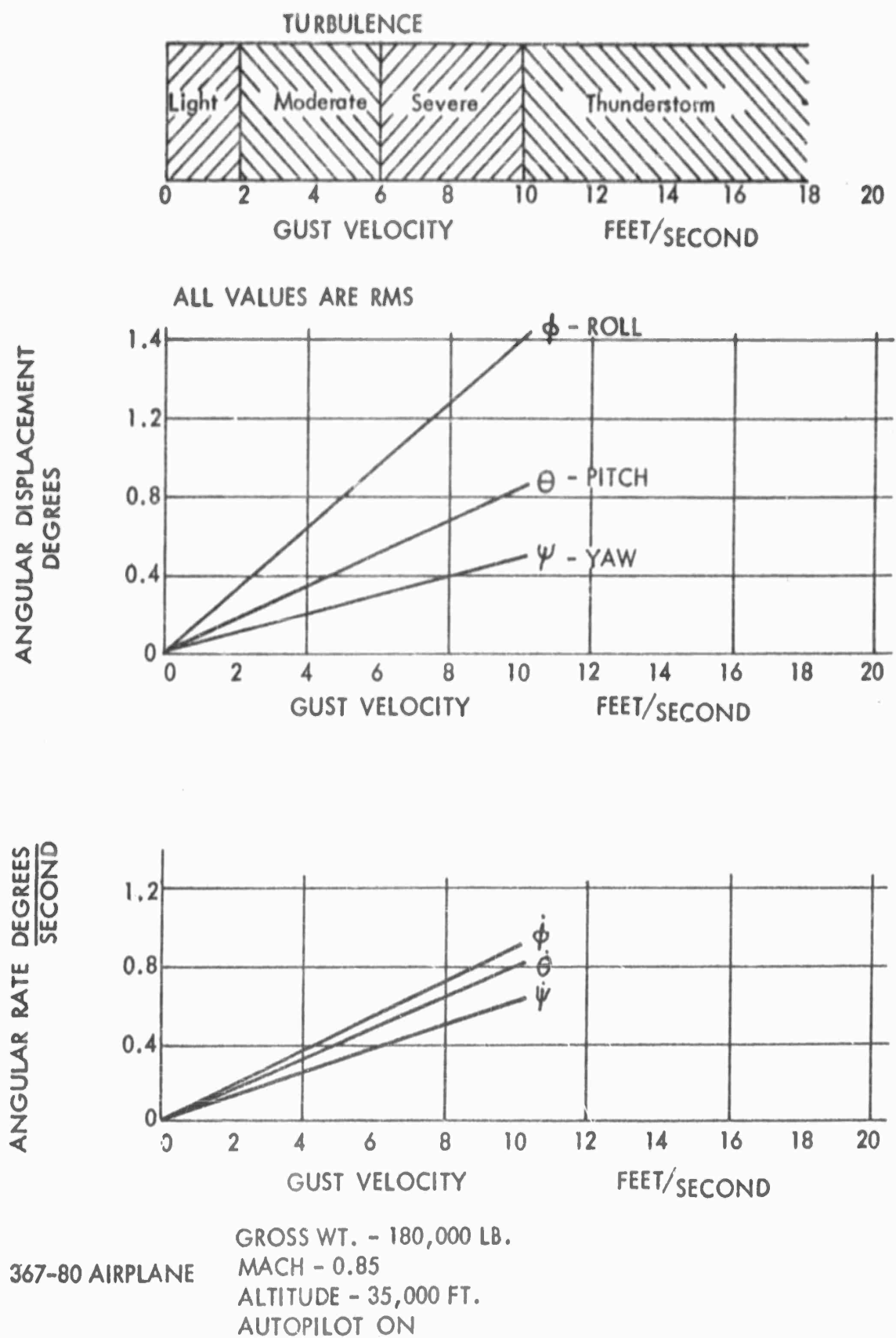


Fig. 3.2

ANGULAR RATES AND DISPLACEMENTS DUE TO  
TURBULENCE FOR STRAIGHT AND LEVEL FLIGHT  
OF KC-135 AIRPLANE AT 35,000 FT.

- b. Satellite movement. The maximum rate of movement of the pointing vector tracking a satellite in free orbit at a minimum height of 1500 miles, for an orbit velocity of 20 kfps.
- c. Suddenly applied bank angles. Bank angles will in general not exceed 30 degrees, and the rate of application will not exceed 10 degrees per second in coordinated turns.

Clearly, the criterion for the antenna drive system power rating is determined by the random yaw, pitch and roll perturbations of the aircraft. A minimum speed of about 2 rpm is required to enable the antenna to be directed at a satellite whilst the aircraft is being banked.

### 3.1.2 System Selection (Azimuth and Elevation Channels)

Existing off-the-shelf hardware, requiring a minimum amount of modification, was to be used in this contract wherever possible. Two systems were found to be compatible with the contract requirements.

- a. The antenna and servo drive assembly (AF designation: AS-1058 (XY-1)/APW-23) of the Sperry-built Microwave Command Guidance (MCG) Airborne Director (USAF designation of complete equipment: AN/APW-13) has an almost flat frequency response up to 3.5 cycles per second, which is more than adequate for compensating the random motion of the KC-135 airplane in atmospheric turbulence. This system was built to integrate tracking, command and telemetry functions for any surveillance drone aircraft; the prototype was installed in a B-50 airplane. The final version is on a GC-135 airplane, and it is suitable for operation in an airborne environment.

Modifications required to adapt the antenna and drive assembly to this project will consist of replacing the microwave plumbing by components of higher power handling capacity, replacing the antenna nutation drive by a polarization drive, and modifying the antenna elevation look angle from "35° down to 90° up" to "25° down to 120° up," measured from the horizontal plane. The 120° figure will make it possible to point the antenna at a satellite near the zenith when a 30° bank angle is applied to the aircraft.

b. The alternative was to design and build the platform at Boeing using Lear-type 3055 Dry powder Magnetic Clutch Servo drives which are already in use on the KC-135 as part of the Lear MC I Autopilot (ref. 23). The system has a linear response up to about 1 cps which will also be adequate for compensating the random motion of the KC-135 airplane in atmospheric turbulence. The Lear Type 3055 Servo Unit consists of: -

- (1) A three-phase AC drive motor energized at 102 to 124 volts (100 volts nominal) line to neutral, and at a frequency of 380 to 420 cycles per second (400 cps nominal), drawing maximum full load current (160 in-lbs. output shaft torque at 29-38 rpm) not exceeding 1.50 amperes per phase at a minimum power factor of 0.40. The drive motor is the prime torque developing unit and runs at approximately constant speed.
- (2) A pair of dry powder magnetic clutches. The torque developed by the drive motor is transmitted to the output shaft by energizing the control winding of the powdered clutch. Each clutch will be energized from a direct current power source of 24 to 29 volts. Each clutch circuit will have a DC resistance of not less than 190 ohms at 25°C, and the maximum current drawn by either clutch will not exceed 200 milliamperes.
- (3) A reach gear (output shaft) which mechanically ties the two clutches together.

Both the Sperry MCG antenna and servo drive assembly and the Lear-type 3055 Dry Powder Magnetic Clutch Servo are suitable for operation in an airborne environment, and can be incorporated into the azimuth and elevation channels of the antenna servo drive system (Fig. 3.3) so that error detection, and system compensation can be achieved with a suitable computer program. Although the Sperry unit has superior frequency response, and is potentially capable of superior overall control system performance, the other system was selected for two reasons: firstly because of the major modifications required to adapt the Sperry unit, and secondly because the Boeing-built platform will require a smaller fuselage cut-out for the radome installation, maintaining the integrity of the fuselage structure.

### 3.1.3 Torque and Speed Calculation

The Lear type 3055 dry powder magnetic clutch servo supplies a maximum output shaft torque of 260 lb. in. at a speed of 29 to 38 rpm (32 rpm nominal) when the differential clutch current is 135 milliamperes. Two separate units will be geared down 10:1 to the azimuth and elevation drives respectively, the mechanical efficiency of the gearing being conservatively estimated at 80%.

The actuator gain then becomes 
$$\frac{0.80 \times 10 \times 260}{12 \times 135} = 1280 \text{ ft lb per ampere.}$$

The overall gear ratio from the 7300 rpm drive motor will then be  $10 \times 227 = 2270$ , giving a peak nominal speed of 3.2 rpm. The nominal torque of the clutch servo in normal operation is 45 lb. in. which is equivalent to

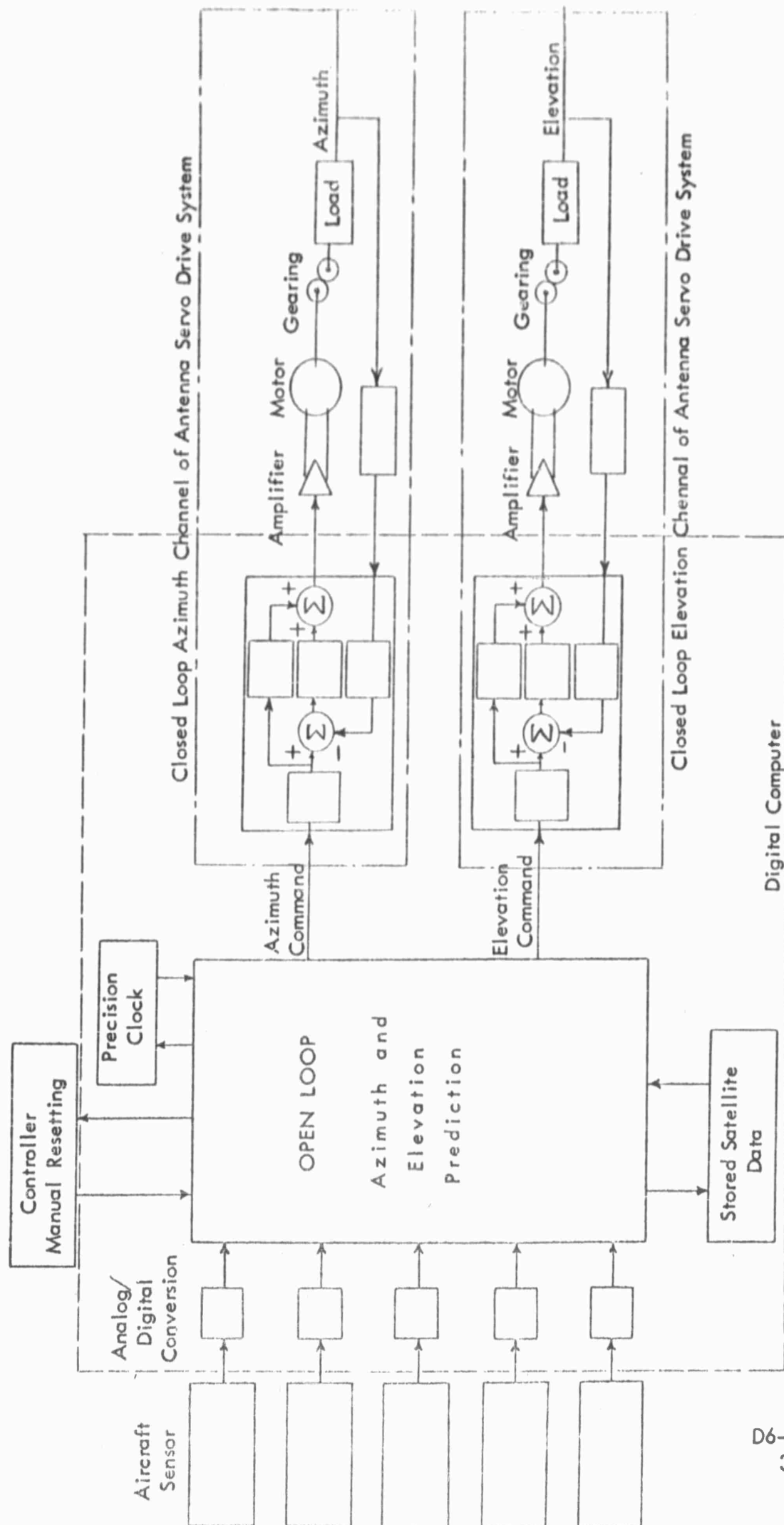


Fig. 3.3 Block Diagram of Antenna Drive System

Note: Error Detection, System Compensation and Improvement of Stability and Accuracy of the Control System can be achieved by a suitable computer program



$$\frac{.80 \times 10 \times 45}{12} = 30 \text{ lb. ft. available for the antenna drive.}$$

If a system having a moment of Inertia  $J \text{ lb-ft}^2$  must respond to a peak amplitude of  $\hat{\Theta}$  radians at a frequency of  $f$  cycles per second, then the instantaneous amplitude, velocity and acceleration, respectively, are given by:

$$\Theta = \hat{\Theta} \sin 2 \pi f t. \quad \text{rads}$$

$$\dot{\Theta} = \hat{\Theta} (2 \pi f) \cos 2 \pi f t \quad \text{rads/sec}$$

$$\ddot{\Theta} = -\hat{\Theta} (4 \pi^2 f^2) \sin 2 \pi f t \quad \text{rad/sec}^2$$

The major part of the instantaneous torque required will be the accelerating torque, and if the friction in the system is negligible, then these quantities may be considered equal.

$$\text{Then, Torque } T = J \ddot{\Theta} = - J \hat{\Theta} (4 \pi^2 f^2) \sin 2 \pi f t \quad \frac{\text{lb-ft}^2}{\text{sec}^2}$$

$$\begin{aligned} \text{Peak Torque } \hat{T} &= J \hat{\Theta} (4 \pi^2 f^2) \frac{\text{lb-ft}^2}{\text{sec}^2} \times \frac{1}{g} \frac{\text{sec}^2}{\text{ft}} \\ &= \frac{4 \pi^2}{32.2} J \hat{\Theta} f^2 \text{ lb-ft} \end{aligned}$$

To estimate the peak torque required, the moment of inertia  $J$  will be taken as  $40 \text{ lb-ft}^2$ , and the maximum frequency and amplitude figures derived in para. 3.1.1 will be approximated as below: -

$$\begin{array}{ll} \text{perturbation frequency} & f = 1 \text{ cps} \\ \text{peak amplitude} & \hat{\Theta} = \frac{1}{40} \text{ radian} = 1.44 \text{ degrees} \end{array}$$

$$\text{then the peak velocity } \hat{\dot{\Theta}} = \frac{2 \pi}{40} = .157 \text{ rad/sec} = 9 \text{ deg/sec} = 1.5 \text{ rpm}$$

$$\begin{aligned} \text{the peak acceleration } \hat{\ddot{\Theta}} &= \frac{4 \pi^2}{40} = 1.0 \text{ rad/sec}^2 = 57.3 \text{ deg/sec}^2 = 0.15 \\ &\text{rev/sec}^2 \end{aligned}$$

$$\begin{aligned} \text{and the peak torque } \hat{T} &= \frac{4 \pi^2}{32.2} 40 \times \frac{1}{40} \times 1^2 \text{ lb-ft} = 1.25 \text{ lb-ft} = \\ &15 \text{ lb-ins} \end{aligned}$$

The estimated friction torque of the rotary joint transmitting the microwave power

$$T_f = 8 \text{ oz-ins} = 0.5 \text{ lb-ins} \approx 0.04 \text{ lb-ft.}$$

This is only about 3% of the accelerating torque considered above, and the assumption of a system with negligible friction is therefore clearly justified.

The above figures show that the Lear type 3055 servo will have considerable margin beyond the anticipated torque requirements.

#### 3.1.4 Time Constants and Transfer Functions (Azimuth and Elevation Channels)

##### Description

The Lear type 3055 magnetic particle clutch servo uses a continuously-rotating prime mover geared to two counter-rotating clutches. The clutch output members are then geared to a common output.

The clutch consists of an electrical coil, a magnetic core structure, and a low inertia drive disc centrally located in an annular air gap filled with a finely-divided magnetic powder. Upon excitation of the clutch coil, this powder locks the drive disk to the rotating core structure and applies an output torque directly proportional to the clutch excitation.

The clutch output torque is essentially independent of speed and there is very little inherent damping in the system, and therefore, stabilization must be obtained by means of compensation. In conventional servo loops good results are obtainable using either a tachometer generator to provide velocity damping or by using current feedback in the form of error rate damping.

##### Transfer Function

The open loop transfer function for this type of servo actuator with an inertia load is as follows:

$$\frac{\theta_o}{i_{in}} = \frac{K}{JN} \frac{1}{s^2 (T_e s + 1) (T_m s + 1)}$$

where: -

- $\theta_o$  = output shaft position
- $i_{in}$  = differential clutch current (amperes)
- $N$  = gear ratio between servo actuator and inertia load output shaft
- $K$  = actuator gain-inch pounds per ampere
- $J$  = inertia at output shaft, total of internal and external
- $T_e$  = electrical time constant
- $T_m$  = mechanical time constant

Approximate values of the parameters are: -

$K = 1280 \text{ lb-ft per ampere}$   
 $J = 40 \text{ lb-ft}^2$   
 $T_o = 45 \text{ milliseconds}$   
 $T_m = 5 \text{ milliseconds}$   
 $N = 2270/l.$

The clutch currents will either be supplied directly from the pointing computer, or a Lear type 133081-01 amplifier as used in the LI02 autopilot in the Caravelle aircraft, having linear response, will be inserted between the pointing computer and the servo unit. (Fig. 3.4).

### 3.1.5 Angular Position Feedback Transducers (Azimuth and Elevation)

Position feedback devices of high accuracy and resolution are required in the closed-loop servo drive channels in order to achieve and maintain small antenna pointing and stabilization errors and to realize the full antenna gain.

The system error analysis (section 4.1) indicated the need for error detection and system compensation to be carried out within the digital pointing computer as part of the computer program. All types of position feedback devices forming suitable inputs to a digital computer, either directly or indirectly, were considered for this application. Digital shaft encoders, both of the optical and electro-mechanical type, and potentiometers were eliminated from consideration due to their doubtful reliability. Digital shaft encoders of the electromechanical type and potentiometers employ rubbing contacts which are subject to wear and vibration and are avoided in synchros. Digital shaft encoders of the optical type are basically rather delicate components of which ruggedized designs suitable to the airborne environment have recently been constructed but have not yet proved themselves in actual airborne operation. The selection therefore was narrowed down to one of the following components (Fig. 3.5):

- (1) Austin Shaft Position Quantizer. This unit generates pulses proportional to angular shaft position. It consists of a metal housing containing a synchronous motor that drives two rigidly coupled, engraved pulse generating discs at 3600 rpm speed of the motor. Each disc has 499 pulse generating positions and a gap. A magnetic pickup head is mounted adjacent to each pulse generating disc. One head is fixed and the other is coupled to the input shaft. When employed with suitable electronic equipment its accuracy is one part in 4096. The price of this quantizer is \$985 each in lots of 1 to 3, and delivery runs 90 to 120 days.

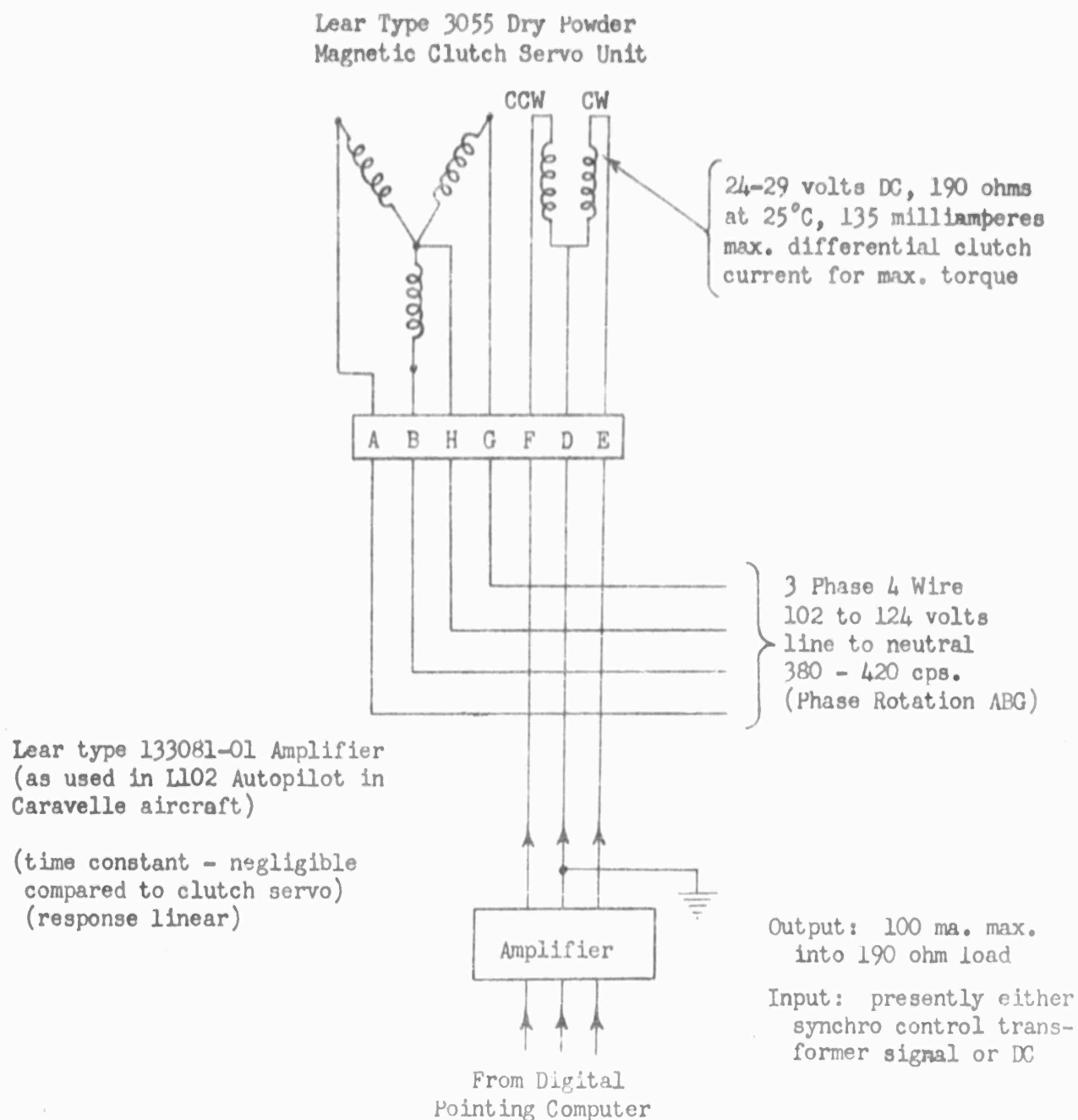
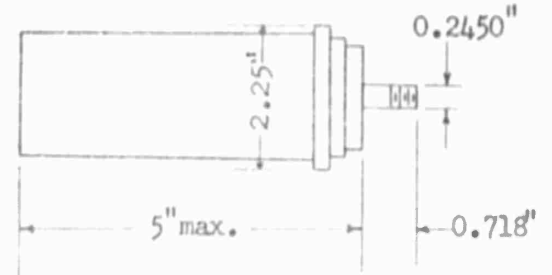
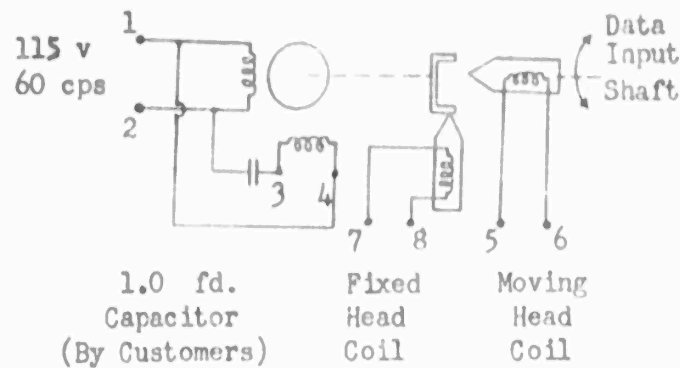


Fig. 3.4 WIRING DIAGRAM OF LEAR TYPE 3055 DRY POWDER MAGNETIC CLUTCH SERVO UNIT WITH OPTIONAL AMPLIFIER

# WIRING DIAGRAM

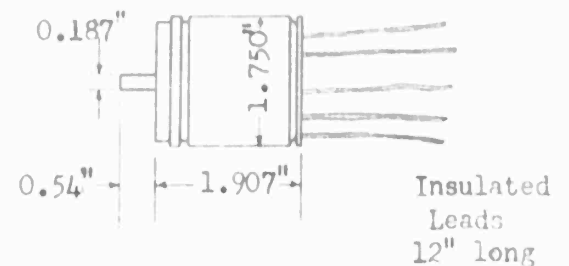
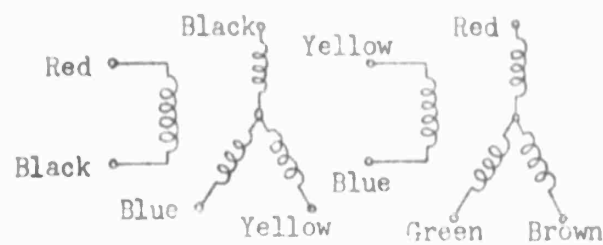
# OUTLINE DIAGRAM

1. AUSTIN SHAFT POSITION QUANTIZER  
Model 8-5 Accuracy =  $360^\circ/4096$



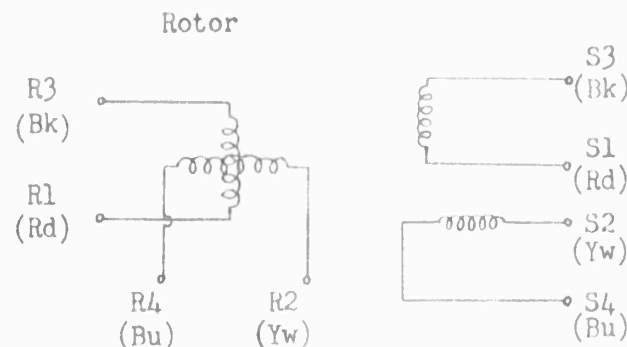
2. BENDIX ELECTRICAL TWO-SPEED AUTOSYN SYNCHROS  
Eclipse-Pioneer Type No. AY-996-A1

Single Speed Dual Speed (11:1)



Input to rotor: 26 v 400~S.P.  
Accuracy: 1.0 minute max.

3. KEARFOTT SIZE 11 SYNCHRO RESOLVER  
Type: R982-004 Transmitter



(This winding will  
not be used)

Input to rotor: 26v 400 ~  
Maximum Error from Electrical  
Zero = 3 minutes

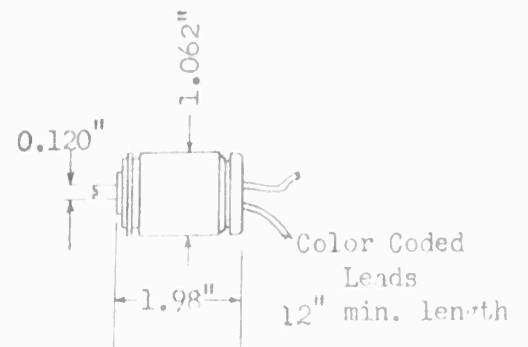


Fig. 3.5 ANTENNA ANGULAR POSITION FEEDBACK TRANSDUCER

D6-7190

- (2) Bendix Two-Speed Autosyn Synchro Transmitter (Size 15). This synchro has single speed and dual speed (11:1) windings and the accuracy is one minute of arc (1 part in 21,600); present price is about \$1200 each.
- (3) Kearfott Size 11 Three-Minute Synchro Resolver. This resolver has sine and cosine outputs with maximum errors of three minutes of arc (1 part in 7200), and is available as an "off-the-shelf" item for about \$108.

The Kearfott resolver was selected for this application because of the advantages of small size and weight, simplicity as compared with the Austin unit which requires a special 60 cycle supply, and the Bendix unit requiring ten leads, which must be brought through slip rings in the case of the elevation channel. An additional advantage of the Kearfott over the Bendix unit is the reduced computer work load involved in obtaining the closest estimate of an angle in terms of two resolver voltages as compared with six two-speed synchro transmitter voltages.

### 3.1.6 Remote Control and Indication of Antenna Polarization

A survey of the operational requirements of this experimental communication system indicated the need for the remote control and indication of the antenna polarization. This was agreed to by Messrs. L. Ames and A. Orange of AFCRL on September 13, 1960, during their visit to Seattle. Given, say vertical polarization of the signal transmitted from the ground, it will be part of the proposed airborne research program, to determine whether the received signal, after scattering by a satellite, or needles belt, has a preferred direction of polarization.

Existing off-the-shelf hardware, requiring a minimum amount of modification, was to be used in this contract wherever possible, and the Lear type 3055 dry powder magnetic clutch servo was therefore selected for the drive in the polarization plane. This servo motor is already in use on the KC-135, forming part of the automatic pilot trim stabilizer, and also of the azimuth and elevation channels of the microwave antenna servo drive system, and can supply 160 in-lbs. output shaft torque at 29 to 38 rpm. The only additional parts required on the antenna platform will be suitable gearing to drive the rotatable portion of the antenna system and a size 11 synchro transmitter (Fig. 3.6). With a phase rotation of the power source of ABC applied to motor terminals ABG, energizing pin E will engage one clutch causing clockwise rotation of the output shaft when the unit is viewed from the output shaft end. With a phase rotation of the power source of ABC applied to motor terminals ABG, energizing pin F will engage the other clutch causing counterclockwise rotation of the output shaft end. (Fig. 3.6 is reproduced from Specification Control Drawing 10-2710).

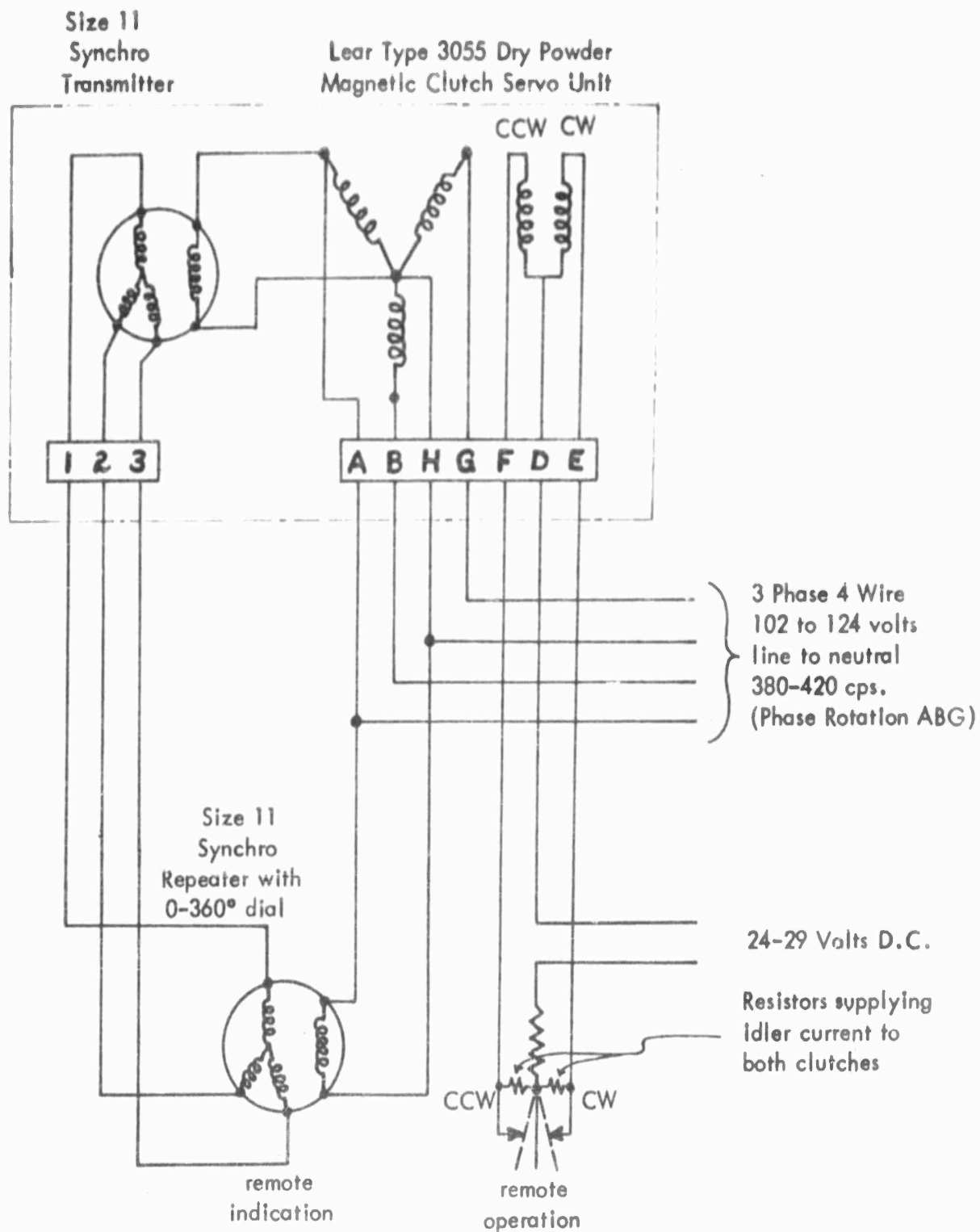


Fig. 3.6 Remote Control and Indication of Antenna Polarization

To eliminate drift of the output shaft in the unenergized condition, W. K. Sturges of Lear Engineering Dept. recommended the use of adjustable series resistors for supplying quiescent currents of about 5% of full load value to both clutches, with a range of adjustment from 3% to 7%.

From Technical Data Sheet for Model 3055C-3: -

Clutch d.c. resistance = 190 ohms

Current at max, torque = 135 milliamperes

d.c. voltage = 24-29

Resistance required for 3% current at 29V input

$$= \frac{29}{.03 \times .135} - 190 = 7160 - 190 \approx 7000 \text{ ohms}$$

Current rating at 7% of 0.135<sup>A</sup> = 9.5 milliamperes

Power rating = .0095<sup>2</sup> x 7000 = 0.63 watts

Nominal resistance for 5% current at 27V

$$= \frac{27}{.05 \times .135} - 190 = 4000 - 190 \approx 3800 \text{ ohms}$$

Resistor selected: - Daystrom Type 313 - 64H-752, 1.5 watts  
(BAC: -R14 WX-752)(7500 ohms)

These resistors will be installed initially set at 3800 ohms. Slight adjustment to one or both units may then be required to eliminate any tendency for the output shaft to drift in either CW or CCW direction.



### 3.2 MOUNTING FRAME AND DRIVE SYSTEM

To simplify installation and to reduce the amount of rework to airplane structure, the antenna mount assembly was designed in two sections, the upper platform and the lower platform. In addition to providing a support for the antenna dish and the drive system, the mounting frame also supports the receiver components. As discussed in Section 11-1.0, it was desirable to locate these components adjacent to the dish.

The upper platform is a gimbal assembly consisting of a yoke, an elevation frame and a polarization frame. The elevation frame and polarization frame are positioned by separate Lear servo motors Part No. 300445-02. This is a constant-running motor with dry magnetic clutches for clockwise or counterclockwise directional control of the output shaft. A Kearfott synchro resolver is used on the elevation shaft to furnish position indication to the computer. A synchro is used on the elevation shaft and one on the polarization shaft to transmit signals to remote indicators for visual indication of elevation and polarization positions. (Fig. 3.7)

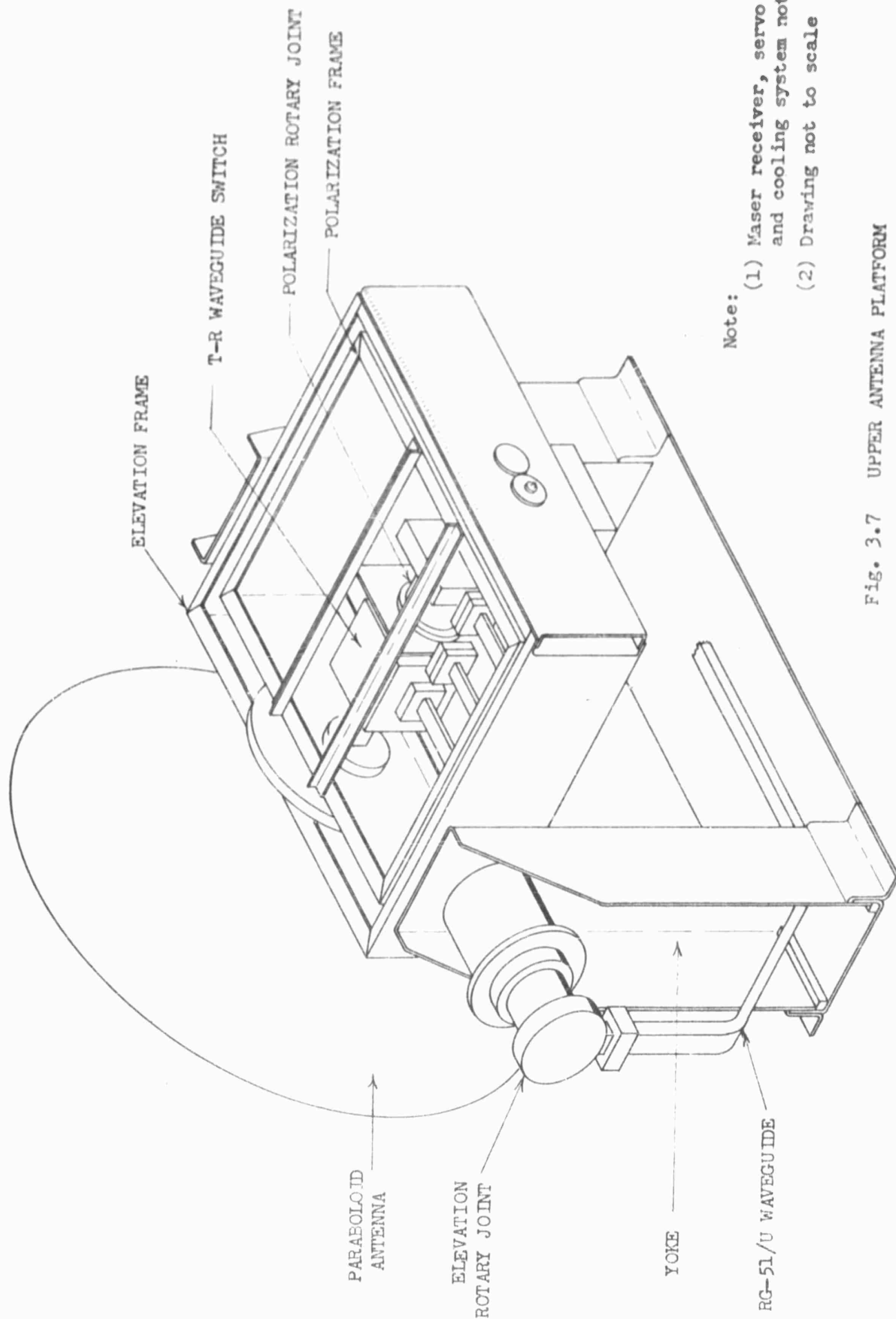
The lower platform assembly located in the airplane cabin contains the azimuth drive mechanism. This mechanism consists of a housing which mounts to aircraft structure, an azimuth drive shaft which rotates on anti-friction bearings, and a Lear servo motor Part No. 30445-02 which drives the azimuth drive shaft through a gear box. Additional equipment included in the lower platform assembly is an electrical slip ring assembly to transmit power, a waveguide, a rotary waveguide joint and a rotating joint to transmit liquid coolant.

The azimuth, elevation, and polarization servo motors provide the following operating speeds:

Azimuth	3 RPM
Elevation	3 RPM
Polarization	6 RPM

The following are limits of travel of these assemblies:

Azimuth	Continuous motion clockwise or counterclockwise 25° below the horizontal with respect to the airplane to 30° past the zenith with respect to the airplane.
Polarization	90° clockwise from normal to 90° counterclockwise from normal-total travel to be 180°.



Note:

- (1) Maser receiver, servo motors and cooling system not shown.
- (2) Drawing not to scale

Fig. 3.7 UPPER ANTENNA PLATFORM

#### 4.0 Computer and Pointing System

##### 4.1 Requirements and Design Criteria

The KC-135 microwave communication antenna covered by this contract has a  $5^\circ \times 5^\circ$  half-power beamwidth and requires a pointing computer and servo drive system for accurate tracking of the orbiting satellite or "needles belt". The satellite or "needles belt" will be used as the microwave scatterer for long range communication. A summary of "Project Needles" techniques is given in Appendix F. It is important to achieve and maintain antenna-pointing and stabilization errors that are sufficiently small to realize full antenna gain. The antenna mount and drive system must enable the antenna to be directed at the object throughout all conditions of the flight, including those induced by roll, pitch and yaw. The minimum height of the object is assumed to be 1500 miles. The frequency response of the pointing system must therefore be adequate to cope with the random yaw, pitch and roll perturbations of the aircraft, with the relative satellite movement and with suddenly applied bank angles. The basic criteria for the pointing computer rating are therefore the same as the "Criteria for Drive System Rating" outlined in Section 3.1.1.

##### 4.1.1 Accuracy Requirements

A  $2\frac{1}{2}^\circ$  error in pointing the antenna at the satellite or needles belt used as the microwave scatterer for long-range communication corresponds to a loss of 3 db compared to the full antenna gain. In assessing the significance of such a potential loss of gain due to pointing and stabilization errors to the overall performance of the communication system it is well to bear in mind that in the receiver the complexities of a maser with a closed cycle liquid helium cooling system were considered worthwhile as compared to a nitrogen system for the sake of an extra 2-3 db gain. Clearly a certain amount of sophistication in the pointing system is therefore justified to keep the overall error to less than about one degree.

The computation of the required azimuth and elevation angles of the antenna system requires a number of steps using input data from existing aircraft sensors and stored satellite data. The cumulative errors of these additive or multiplicative steps must be kept to a minimum, and the angle information must therefore be handled accurate to the nearest minute or fraction of a minute. This corresponds to an accuracy of 1 in 21,600, or better, in azimuth. In the original design proposal (Ref. 24) all possible types of computers, both analog and digital were considered. The above figure immediately eliminates analog computers from consideration, since a computing precision of better than one part in 1,000 is difficult to achieve in analog systems.

The simplest type of digital system will employ a digital computer to predict the required azimuth and elevation angles. After conversion into analog form these computer outputs will actuate conventional analog servo systems for the azimuth and elevation channels respectively. This type of system was considered in detail in the original design proposal (Ref. 24) and the corresponding error analysis, after allowing for additional contingencies, is shown listed in the column "Conventional Servo System" in Table 4.1.1.

The total "Estimate for Middle Latitudes" is a 1.4 degree RMS error in the optimum mode of operation in latitudes where the magnetic compass can be relied upon. This cannot be considered entirely satisfactory, in view of the line of reasoning developed in the first paragraph of this section. In addition the RMS error criterion is not strictly applicable to errors of synchro components which may be additive in particular combinations of angles.

Many methods of obtaining increased pointing accuracy exist; however the replacement of the conventional servo system by a sampled-data servo system will suffice to bring the RMS error below 1 degree in middle latitudes using input data from existing aircraft sensors. Error detection, system compensation, and improvement of stability and accuracy of the control system will then be achieved by means of a suitable computer program. A block diagram of such a system is given in Fig. 3.3 and the revised error estimates in the columns headed "Sampled Data Servo System" in Table 4.1.1.

In polar latitudes the compass system in the KC-135 aircraft goes to the "directional gyro mode", and the azimuthal accuracy of the existing aircraft instrumentation is severely limited by the random drift of about 1 degree per hour of the directional gyro installed (Table 4.1.2). Three methods of improving the directional reference in polar latitudes were considered.

(1) Automatic Astrocompass

The MD-1 Automatic Astrocompass tracks a star or the sun on the basis of best available true heading and longitude and latitude information, and produced a highly refined true heading. Unfortunately this instrument would be of least use when most urgently required, that is during the prolonged periods of arctic (or antarctic) twilight.

(2) Strapdown Rate Gyro

Mr. F. S. Preston, Chief Engineer of the Norden Division of United Aircraft Corporation, claims that a directional reference having less than 0.1 degree drift per hour is easily realized by means of a Norden strapdown rate gyro and a standard method of pulsing it and counting the pulses. This instrument only requires a simple setting-up procedure, either in flight or prior to take-off on the ground to obtain a datum. Unfortunately this simplified application of an inertial-platform component has not been finalized yet and a firm proposal may not be available before the end of the first quarter of 1961.

Table 4.1.1 ERROR BREAKDOWN OF TRACKING SYSTEM

Error Source	Conventional Servo System		Sampled Data Servo System	
	Estimate for Middle Latitudes		Revised Estimate (4) Middle Latitudes	Estimate for (4) Polar Latitudes
Platform stabilization	0.3 deg.		----	----
Aircraft Position (1)	0.15		0.3 deg	0.2H(3) deg
A/D conversion (2) (12 bits)	$0.088 / \sqrt{3}$		$0.088 / \sqrt{3}$	$0.088 / \sqrt{3}$
Computer round-off and truncation	0.176		----	----
D/A conversion (12 bits)	$0.088 / \sqrt{3}$		----	----
Synchro transmitter (cx) accuracy	0.11		0.11	0.11
Synchro differential (cdx) accuracy	0.11		----	----
Magnetic compass accuracy	0.5		0.25 (10)	----
Synchro control transformer (ct) accuracy	0.117		----	----
Servomechanism accuracy	0.5		----	----
Gear backlash	0.5		-----(5)	-----(5)
Radome boresight error	0.5		-----(6)	-----(6)
Roll/Pitch	$0.5(7)(1.0)$		$0.5(7)(1.0)$	0.5 (1.9) (7)
Subsatellite position	0.6 (8)		0.6 (8)	0.6 (8)
Directional gyro accuracy	----		----	1.0 H (9)
TOTAL	1.4 R.M.S.		0.9 R.M.S.	$\sqrt{H^2 + 0.8^2}$ deg R.M.S.

Remarks (1) - (9): see overleaf

BOEING

NO. D6-7190

PAGE 49

2-7000

Remarks (related to Table 4.1.1)

- (1) A four-mile aircraft navigation error causes a satellite 1500 miles distant to appear 0.15 degrees from its actual position.
- (2) The maximum error of 1 bit (0.088 deg.) in the rectangular statistical error distance of A/D and D/A converters results in  $0.088/\sqrt{3}$  deg. RMS error.
- (3) H = number of hours since last fix and gyro drift correction.
- (4) In the revised estimate computation, the conventional servo-system has been replaced by a sampled-data feedback control system, where the system error can be made zero at the sampling instants. Stabilization errors will therefore be negligible, and pointing errors will be limited to the errors of the existing aircraft sensors, and of the orbit computations.
- (5) In the revised system, position feedback will be arranged 1:1 on the output shaft, so backlash will not appear as a position error.
- (6) In the revised system, optical alignment of the mounting will be specified. Any residual error will be measured and can be combined with radome refraction error, if appreciable, and applied as a correction in the computer.
- (7) The accuracy of the attitude-reference system is only about  $1^\circ$  when bank is suddenly applied. Another condition of increased error is on take-off when acceleration forces may cause errors of  $5^\circ - 6^\circ$ , but this case has not been considered.
- (8) The subsatellite position has a velocity of about 5 miles/sec. "Space track" provides data correct to 3 seconds of time, corresponding to an uncertainty of 15 miles of subsatellite position.
- (9) Sperry's plant test spec calls for drift rate less than  $0.2^\circ/\text{hour}$ , but deterioration in shipping and installation generally takes place. Sperry will therefore be able to supply a specially selected gyro, and if handcarried and installed with special care, more than 5-fold improvement in accuracy will be possible. Lear can provide a pitch and roll stabilized azimuth gyro with free drift reduced to  $0.25^\circ/\text{hr}$ , i.e. after H hours, directional gyro accuracy will be within  $0.25 H$ . Similarly Kearfott can provide a directional gyro with friction average bearings having less than 0.25 degree drift per hour. The cost of a precise gyro heading reference will be about \$10,000.
- (10) A compass swing and careful compass compensation prior to the tracking antenna flight test program will enable the N.I. compass to achieve the 0.25 degree accuracy claimed for it. Similarly it is recommended that optical alignment of the doppler radar antennas should be carried out, prior to the tracking antenna flight test program, to attain the full potential accuracy of the doppler radar system.

Table 4.1.2 Analog Inputs Available to Digital Pointing Computer  
on KC-135 Aircraft. (Existing, with exception of items marked (\*).)

Physical Quantity	Source	Electric Analog and Scale	Remarks
<u>Yaw</u>			
Magnetic Heading	Kearfott NI Compass	CX, 115V	+ 1/4° accuracy T° /hour drift
Gyro Heading		also electric signal which tells when the compass goes to the directional gyro mode	
Precise Gyro Heading	Extra Directional Gyro (*)	CX, 115V	0.2°/hour drift or better
Pitch	Lear MC I Autopilot	(Lear or Kearfott or Sperry or Norden)	normally to C.T. with 10k load (6' synchro)
Roll	Lear MC I Autopilot	CX, 115V	normally to C.T. with 10k load (6' synchro)
Yaw Rate	Lear MCI Autopilot	200 mV/deg./sec.	(inductive pick-off)
Pitch Rate	Lear MCI Autopilot	200 mV/deg./sec.	(inductive pick-off)
Roll Rate	Lear MCI Autopilot	200 mV/deg./sec.	(inductive pick-off)
Drift Angle	Doppler APN 8I	CX, 26V	(6' synchro)
Ground Speed	Doppler APN 8I	CX, 26V	(6' synchro)
True Airspeed	Kollsman TAS Unit	36°/100 knots /100 knots	(6' synchro)
Latitude	Ford ASN 6 Computer	coarse 1:1 fine 36:1	(6' synchro) (6' synchro)
Longitude	Ford ASN 6 Computer	coarse 1:1 fine 36:1	(6' synchro) (6' synchro)

Abbreviations

CX = synchro transmitter

C.T. = 2 synchro control transformer

Note

Use pilot's systems. Copilot is on  
isolated power source.

BOEING

NO. D6-7190

PAGE 51



2-7000

Table 4.1.2 Analog Inputs Available to Digital Pointing Computer  
on KC-135 Aircraft. (Existing, with exception of items marked (\*).)

Physical Quantity	Source	Electric Analog and Scale	Remarks
<u>Time</u>	Airborne Quartz Crystal Oscillator (*)	1 megacycle signal at 2.0v RMS level across a 50 ohm resistive load	long term stability at least 1 part in $10^8$
<u>Platform Azimuth</u> <u>Platform Elevation</u>	Antenna System (*) Antenna System (*)	3 minute Synchro Resolver, 26v 1:1 3 minute Synchro Resolver, 26v 1:1	+ .05° accuracy } Position ± .05° accuracy } Feedback } Signals

Abbreviations

CX = synchro transmitter  
C.T. = synchro control transformer

Note

Use pilot's systems. Copilot is on  
isolated power source.





- (3) Specially selected directional gyro, or directional gyro with friction average bearings. About a 5-fold improvement is possible by means of a standard directional gyro specially selected at the vendor's plant, or by means of a directional gyro employing friction average bearings, for an additional expenditure of about \$10,000 (See remark (9) related to Table 4.1.1)

The main source of error using existing instrumentation will be the true heading in polar latitudes when the aircraft compass system is in the directional gyro mode of operation. To minimize pointing errors, the installation of a precise directional reference is recommended. The Norden strapdown rate gyro appears to be the optimum solution if suitable delivery can be arranged. As an alternative, the installation of a directional gyro employing friction average bearings appears advisable. This precise directional gyro should preferably be a Kearfott unit suitable for operating in conjunction with one of the existing N1 and J4 compass systems in the KC-135 aircraft, both of which are made by Kearfott.

Analog/digital and digital/analog conversion errors can be considered negligible in the sampled data servo system if the digital computer can accept synchro transmitter inputs, and provide analog voltage outputs, directly without any intermediate electromechanical conversion stage.

Additional factors entering in the over-all accuracy of the system are:

- 1) Time. In digital computers using a magnetic drum memory, operations are generally synchronized from the drum, the speed of which may only be regulated within 5%. This is inadequate for "real time" computations of subsatellite positions. An airborne quartz crystal oscillator is therefore necessary, and a "clock" signal will be available for computer use from equipment supplied by AFCRL. This signal will be at a frequency of 1 megacycle at 2.0V. RMS level across a 50 ohm resistive load. This will be the same signal used by the AFCRL data acquisition and storage equipment. Long-term stability will be at least 1 part in  $10^8$ .
- 2) Magnetic Variation. To obtain the best estimate of true heading from the magnetic heading, the variation should be either stored in the computer memory for a finite number of increments of geographical area or computed from a power series approximation.

These conditions, essential to the adequate performance of a sampled data servo system, have been incorporated into the computer specification (Ref. 27) and some of the relevant portions not otherwise discussed in this report are contained in Appendix K.

#### 4.1.2 Computation Requirements

##### "Azimuth Command" and "Elevation Command"

The primary function of the computer is the prediction of open-loop "azimuth command" and "elevation command" angles for accurate tracking of the orbiting satellite or "needles belt" by means of the steerable antenna.

In view of the uncertainties of the needles belt orbit, the problem was approached in terms of a number of point satellites any one of which must be kept close to the center of antenna pattern throughout all flight conditions. Since a "needles belt" has one degree of freedom less than a point satellite it is no more difficult to ensure that the antenna is kept pointed at a portion of the needles belt. However, the question as to which portion of the needles belt should be looked at to optimize the overall communication system performance depends on many factors which will not be known until the needles belt has been established, and the additional factors involved will be introduced into the computer program at such time.

The basic problem may be stated: - given the aircraft and satellite positions, the "azimuth command" and "elevation command" angles for the satellite tracking antenna platform are to be obtained. Figures 4.1 and 4.2 illustrate the spherical and plane triangles to be solved in the azimuth and elevation computations respectively.

##### a. Azimuth Command (Spherical Triangle APS in Fig. 4.1)

- (1) Given 2 sides and incl. angle to find 3rd side (Natural Haversine Formula)

$$\text{hav } p = \text{hav } (s-a) + \sin s \sin a \text{ hav } P \quad \text{hav } \Theta = \frac{1}{2}(1 - \cos \Theta)$$

$$= \sin^2 \frac{\Theta}{2}$$

- (2) Given 3 sides to find any angle (Cosecant Formula)

$$\text{hav } \hat{A} = \text{hav } a - \text{hav } (s-p) \cdot \text{cosec } s \cdot \text{cosec } p$$

$$\text{Azimuth Command} = \hat{A} - \text{True Heading} + f_1(\text{roll, pitch})$$

##### b. Elevation Command (Plane Triangle CAS in Fig. 4.2)

$$\hat{A} + \hat{S} = 180^\circ - \hat{O}$$

$$\tan \frac{\hat{A} - \hat{S}}{2} = \frac{a-s}{a+s} \tan \frac{\hat{A} + \hat{S}}{2} \quad \begin{cases} a = R + H \\ b = R + h \end{cases}$$

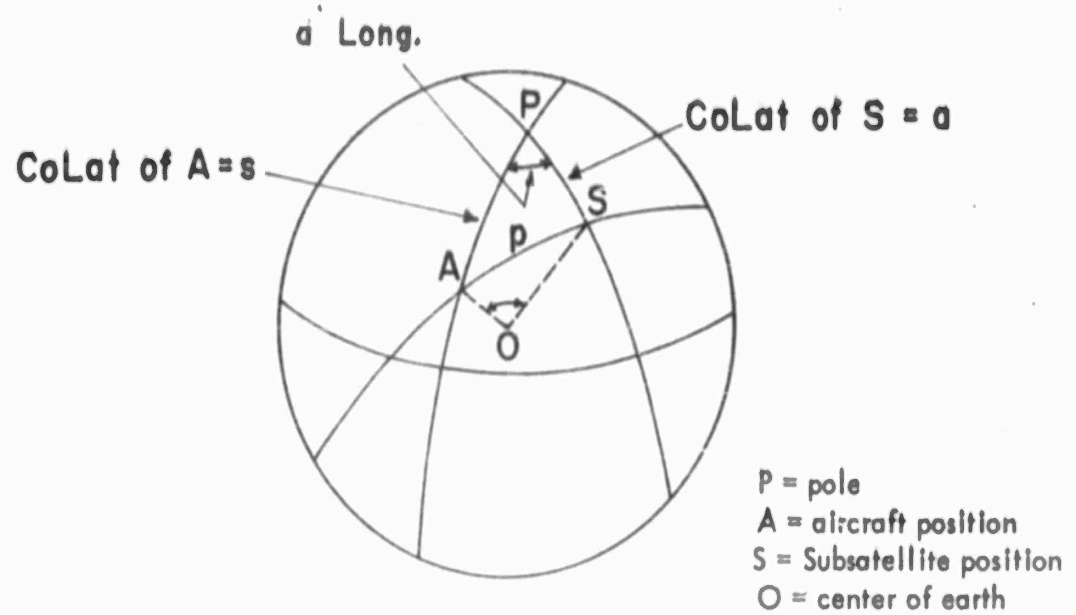


Fig. 4.1 View of Terrestrial Sphere (Azimuth Computation)

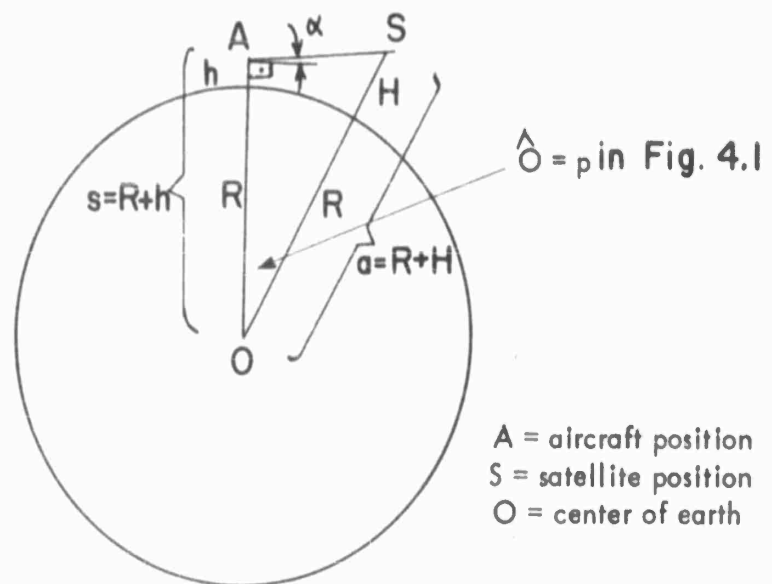


Fig. 4.2 Sectional View of Earth (Elevation Computation)

$$\begin{aligned}
\alpha &= \hat{A} - 90^\circ = \frac{\hat{A} - \hat{S}}{2} + \frac{\hat{A} + \hat{S}}{2} - 90^\circ \\
&= \tan^{-1} \left[ \frac{(R+H) - (R+h)}{(R+H) + (R+h)} \tan \left( 90^\circ - \frac{P}{2} \right) \right] + \left( 90^\circ - \frac{P}{2} \right) - 90^\circ \\
&= \tan^{-1} \left[ \frac{H-h}{2R+H+h} \tan \left( 90^\circ - \frac{P}{2} \right) \right] - \left( \frac{P}{2} \right)
\end{aligned}$$

---

Elevation command =  $k + f_2$  (roll, pitch, yaw)

---

The effect of all conditions of the flight, including those induced by roll, pitch and yaw, on the "azimuth command" and "elevation command" may then be allowed for by means of the above additive terms  $f_1$  and  $f_2$  respectively, which will be functions of roll, pitch and yaw.

The next section shows how part of this problem, in addition to obtaining instantaneous aircraft position, can be solved by means of a digital navigation computer, where the terms "destination" or "target" or "subsattellite position" are interchangeable.

The initial source of heading is magnetic heading from the N-I compass. In the computer, magnetic heading is modified by magnetic variation, determined by longitude and latitude, to develop a true heading (best available true heading).

The AN/APN-89 uses the Doppler principle to provide the computer with groundspeed and drift angle information.

The computer uses all the above information to determine distance travelled and for constant correction of present position.

## Mathematics of Digital Navigation Computer

### SYMBOLS

$\Theta_m$  = Magnetic Compass Heading

$\Theta_G$  = Gyro Heading

$V_A$  = True Airspeed

$\Delta t$  = Cycle Interval

$L$  = Present Latitude

$\lambda$  = Present Longitude

$\tau$  = Fix Interval

$\Theta_d$  = Doppler Drift Bearing

$V_W$  Wind Speed

$V_{W_n}, V_{W_e}$  = North and East Components of Wind Velocity

$\Theta_W$  = Wind Direction

$V_G$  = Ground Speed

$V_e, V_n$  = North and East Components of Ground Velocity

$\Theta_t$  = True Track

$\Theta_H$  = True Heading

$R_o$  = Range to Destination - Measured Along Lesser arc of Great Circle.

$R'_o$  = Range to Destination - Angular Distance

$\Theta_o$  = Bearing to Destination - Measured to the Great Circle Track from True North

$(L', \lambda')$  = Fix Position

$(L_f, \lambda_f)$  = Destination or Target or Subsatellite Position

$(L_e, \lambda_e)$  = Last Computed Position

$R_e$  = Effective Radius from Center of Earth.



### Computer Equations

(1) True heading is computed from magnetic compass heading, and magnetic variation, astrocompass heading, or gyro heading, depending upon the mode of operation

$$\Theta_H = \Theta_m + f(\lambda_e, L_e) \text{ ----- (1)}$$

The  $f(\lambda_e, L_e)$  corrections are either stored for a finite number of increments of geographical area or computed from a power series approximation.

(2) When a directional gyro is used, the gyro heading is continually corrected for precession, convergence and drift (if available).

(3) A more accurate wind velocity may then be obtained if  $V_G$  and  $O_D$  are available from an optional doppler radar input: -

$$\Theta_T = \Theta_H + \Theta_D \text{ -----(a)}$$

$$V_{WE} = V_G \sin \Theta_T - V_A \sin \Theta_H \text{ -----(b)}$$

$$V_{WN} = V_G \cos \Theta_T - V_A \cos \Theta_H \text{ -----(c)}$$

$$V_W = \sqrt{V_{WE}^2 + V_{WN}^2} \text{ -----(d)}$$

$$\Theta_W = \pi + \tan^{-1} \frac{V_{WE}}{V_{WN}} \text{ -----(e)}$$

To get average values, a smoothing computation is used over several program cycles, the radar output being rather noisy.

(4) A major branching in the program then takes place, a special program being used in polar regions to avoid the discontinuities of the geographic coordinates, and the mode of computation is determined by the magnitude of the cosine of the present latitude.

(5) At low and middle latitudes, the computation proceeds in the normal mode: -

$$V_E = V_a \sin \Theta_H + V_W \sin (\Theta_W + \pi) \text{ -----(2)}$$

$$V_n = V_a \cos \Theta_H + V_W \cos (\Theta_W + \pi) \text{ -----(3)}$$

$$\Theta_T = \tan^{-1} \frac{V_E}{V_n} \text{ -----(4)}$$

### Computer Equations (cont'd)

$$V_G = \sqrt{V_E^2 + V_n^2} \quad \text{-----(5)}$$

(6) The sines and cosines will be computed as power series expansions rather than storing a table of constants.

(7) Changes in latitude and longitude are then found: -

$$\Delta L = \int_0^t \frac{V_n dt}{R_e} \quad \text{-----(6)}$$

$$\Delta \lambda = \int_0^t \frac{V_E dt}{R_E \cos L} \quad \text{-----(7)}$$

$$L = \Delta L + L_e \quad \text{-----(8)}$$

$$\lambda = \Delta \lambda + \lambda_e \quad \text{-----(9)}$$

For small changes in position between program cycles, the trapezoidal integration method provides sufficient accuracy.

(8) The effective radius of the earth,  $R_e$  can be either stored as a constant, or computed using various corrections for ellipticity and altitude, depending on the accuracy desired and the types of sensors available.

(9) True bearing and range of a destination (or target position or sub-satellite position), selected by a hand switch are then computed for a great circle course.

$$R'_O = \cos^{-1} \left\{ \cos (L - L_f) - [1 - \cos (\lambda_f - \lambda)] \cos L_f \cos L \right\} \quad \text{----(10)}$$

$$R_O = R_E R'_O \quad \text{----(11)}$$

$$\Theta_O = \cos^{-1} \left\{ 1 + \frac{\sin L_f - \sin (L + R'_O)}{\sin R'_O \cos L} \right\} \quad \text{----(12)}$$

To save computation time and storage space only one destination is computed in every program cycle.

(10) When  $\cos L$  becomes less than some predetermined constant  $K$ , computation will proceed in the polar mode in the next program cycle, with reference to a pseudo-transverse pole located at the equator on the intersection of the true heading great circle arc at the instant of change to the polar mode, or with reference to a transverse pole located at the equator on the intersection of the greenwich meridian. All desired quantities are then transformed back to geographical coordinates.

(11) In the polar mode computation the wind direction is transformed continuously along a great circle path, because in polar regions the wind travels along on essentially straight path while the true north direction changes rapidly.

(12) Before a new computation cycle begins, a check program may be inserted which tests certain circuit properties. If an incorrect answer results, an indication of computer malfunction is given, and the computer switches to a standby mode.

#### Aircraft Attitude

Instantaneous yaw, pitch and roll, also yaw rate, pitch rate and roll rate will be available to the computer from autopilot components (see Table 4.1.2). If all these sensors are sampled periodically, clearly there will be considerable redundancy of information which will improve the overall accuracy and reliability.

#### Satellite Orbit Prediction

The long range prediction of satellite orbital parameters with a high degree of accuracy is a complex problem. The satellite is acted upon by all bodies in the universe. Some of the perturbations are negligible for low altitude satellites while other perturbations are negligible for high altitude satellites. Unfortunately, there is no dividing altitude for determining which perturbations are or are not negligible.

The Systems Research Group conducted an investigation of various methods of accurate satellite orbit prediction applicable to airborne digital computers. It was desired to develop a method which will predict the satellite orbit parameters (see Appendix G for definitions) with a desired accuracy for an extended period of time. The method should not demand an excessive amount of computer complexity.

Three systems were under consideration

1. The satellite orbit would be predicted by a ground computer capable of handling a complex program. The predicted orbital parameters are put on a magnetic tape, drum, or other storage device. This storage device is then sent to the aircraft. This, of course, could eliminate a prediction program in the airborne computer. Aeronutronics was contacted regarding such a program. They claim to have a 5,000 instruction IBM 709 program which computes satellite position 64 times per interval of time. This program was used on Echo I with an accuracy of one tenth of a degree at the end of a week. The program essentially predicts an orbit on the basis of initial conditions, then corrects the orbit on the basis of radar observations taken shortly after the time of the initial conditions. The program is claimed to be quite complex in that it contains some subtle perturbations, as radiation pressure.



It was felt that this program may be too complex for small airborne computers. However, a suggestion has been made by the Physics Technology and Data Processing Programming Group of the Engineering Computing and Analysis Staff which would make use of the ground prediction program. A ground computer would be used to predict the orbit of a satellite (or satellites) for a period of days, possibly a week. This information would be put on tape and installed in the airplane. For any flight the period of time during which communication will be maintained will be known. This information will be used to search the tape for the satellites which will be visible at this time. The orbital parameters for the given period of time will be transferred to a drum prior to the time of communication. This is done to overcome the storage limitations of the computer and the problem of necessary interrogation time of the tape.

2. The airborne computer would be programmed to predict the satellite parameters for an extended period. This, of course, would demand more computer complex than system 1. Also, the inputs to the program must be very accurate.
3. This system is a compromise between systems 1 and 2. A ground computer would predict the satellite orbit. However, the orbital parameters sent to the airborne computer would only be given for large increments of time. For example, the orbital parameters corresponding to the positions of the satellite differing by fifteen minutes of time could be given to the airborne computer. The airborne computer would contain a relatively simple program for orbit prediction. The initial conditions for this program would be updated in increments of fifteen minutes by the store parameters from the ground program.

There are existing orbit prediction programs which are relatively simple. Such programs usually consider a very basic mathematical model. For instance, a spherical earth and Keplerian orbit or a non-spherical earth and Keplerian orbit. Some programs may include perturbations due to drag.

One of the programs considered would use about 700 instructions and 50 storage locations.

The final selection of the method of satellite orbit computation to be used depended on two factors:

1. It was ascertained from AFCRL that a typical flight test program may consist of a 3-legged itinerary such as Hanscomb Field - Thule - Anchorage - Hauscomb Field, the performance of which, including ground servicing en route, may take up to about a week. This period was therefore selected as the minimum prediction period during which no voluminous updated information need be supplied to the aircraft.
2. Lincoln Laboratory have methods available for accurate satellite prediction for at least one week in advance, and can make this information available in the form of IBM cards giving the orbital elements and their first

derivatives predicted for hourly intervals up to one week ahead.

It was therefore decided to make use of this information by transferring it to punched paper tape and feeding it into the memory drum of the airborne digital computer by means of a tape-reader. The data so stored will then be used for periodic interpolation and updating of the satellite data. The computer program will then have provision for reducing these data to the instantaneous altitude, and latitude and longitude of the subsatellite position.

#### Servo System Compensation

The secondary function of the computer is the conversion of "azimuth command" and "elevation command" signals, together with azimuth and elevation feedback signals, into suitable control signals in the form of clutch coil currents to the Lear type 3055 Dry Powder Magnetic Clutch Servo units employed for the antenna system azimuth and elevation drives respectively. There is very little inherent damping in the system (see Section 3.1.4) and stabilization must be obtained by means of compensation achieved in the computer program (Appendix I).

#### Computer Workload

The above survey of some of the mathematical complexities involved follows the approach of the navigator rather than that of the mathematician and is useful in examining the adequacy of existing computers in meeting the requirements of this contract. For instance in Figs. 4.1 and 4.2 a spherical earth approximation was made. However, the approximation involved in equating 1 minute of latitude and a nautical mile = 6080 ft. is only true at 48°N or S and a more exact approximation is

$1' \text{ lat} = 1 \text{ n.m.} = 6077.1 - 30.7 \cos(2 \times \text{lat})$ . The polar radius is 3950.01 s.m. (= 3430.27 n.m.) and the equatorial radius is 3963.35 s.m. (= 3441.86 n.m.), corresponding to an oblate spheroid of compression 1/297.

A detailed rigorous mathematical systems analysis for an airborne antenna control system for communication via a space object was carried out by the Engineering Computing and Analysis Staff as part of this contract (Ref. 29). In this analysis the earth's coordinate system is carried into the aircraft coordinate system. This transformation is accomplished by a translation and five elementary rotations. The translation effectively translates the earth's coordinate system to the aircraft position. The five elementary rotations account for aircraft longitude, latitude, heading, pitch, and roll, in that order.

An inspection of the results of either approach indicates that a major portion of computer time will be taken up in computing and updating trigonometric functions, corresponding to each sampling instant, which probably will occur at 0.1 to 0.5 second intervals. Since each trigonometric ratio is computed as a power series, truncation errors may accumulate unless skillful interpolations and approximations are employed for varying time periods, say up to 60 seconds before recomputing every trigonometric function (Ref. 47). This is one of the reasons why the programming of an airborne digital computer of restricted size and capacity is a specialized art and is generally left to the computer manufacturers to enable them to make the best use of their machine.

#### 4.2 Computer Selection

A digital-computer control system is essentially a type of sampled-data control system in which the signals are in the form of a digital code. The digital computer interacts dynamically with other parts of the system, which will have high accuracy if the system overall transfer function is equal to unity. In conventional continuous-data servo systems this condition cannot be realized; however with a sampled-data feedback control system it is not difficult to make the output equal to the input, and thus, the system error equal to zero, at the sampling instants. This can be done if the over-all pulsed transfer function is made equal to unity by designing a suitable programming function; if the sampling rate is kept high, an almost perfect control system can be obtained.

In this digital computer system open-loop azimuth and elevation command signals will be predicted by the computer, using periodically sampled input data from existing aircraft sensors and periodically updated satellite data. The basic mathematical equations are summarized in Section 4.1.2 and the inputs available in Table 4.1.2.

Satellite data will be available on request from Lincoln Laboratory prior to take-off from Hanscomb Field in the form of IBM cards giving the orbital elements and their first derivatives (See Appendix G for definitions) predicted for hourly intervals up to one week ahead.

These data will be transferred to punched paper tape and fed into the memory drum of the airborne digital computer by means of a tape-reader, to be stored there for periodic interpolation and updating of the satellite data.

The azimuth and elevation command signals will be fed into the respective closed-loop channels of the antenna servo drive system; error detection, system compensation, and optimization of the stability and accuracy of the drive system will be achieved by a suitable computer program.

Existing off-the-shelf hardware, requiring a minimum amount of modification, will be used wherever possible in the performance of the contract.

The following five digital computers have been considered for this project:

- (1) The Librascope CP 209 incremental computer specified for the A3D bombing navigation system, and for the Bendix "Sky Sweeper" missile tracking system. Unfortunately, an incremental computer has too limited capacity where the orbital information of a number of different satellites has to be updated, and an arithmetic digital computer then becomes preferable.

A general comparison between analog, arithmetic and incremental digital computers is given in Appendix H.

- (2) The Librascope ASN-24 transistorized "navigation system building block" computer which has been applied to the Convair Centaur guidance system. Unfortunately, this computer is not capable of directly accepting synchro voltages, but requires a separate synchro-digital conversion module for every input which will degrade the accuracy of each input by about 1/4 degree. In addition it is doubtful whether the capacity of this computer is adequate for maintaining a sufficiently high sampling rate and for coping with a complete servo system compensation program. A theoretical analysis of the system compensation problem is given in Appendix I.
- (3) The digital techniques used by Computer Control Company in their Coordinate Conversion Computer for Project Echo for converting the satellite orbital elements to azimuth and elevation could be adapted to the requirements of this contract. Unfortunately this equipment was not designed for operation in an airborne environment, and existing hardware could not be used without considerable redesign.
- (4) The IBM ASC-15 missileborne digital computer designed for the Titan vehicle guidance system in conjunction with an AC Spark Plug inertial platform. This computer is not too well suited to the computation of trigonometric functions and their inverse, but will have adequate capacity when a special "Divide Unit" is added. Unfortunately, this computer in its existing form can only accept inputs in the form of multiple bit rate pulses, and a "Buffer Storage Unit" would have to be added to enable the computer to accept periodically sampled digital inputs. In addition, one electromechanic analog/digital conversion unit would be required for each channel as under (3) above. Further disadvantages of this computer are:

- (a) The program will not stay indefinitely on the memory drum, and the IBM Consultant suggested that a new program should be fed into the computer before every flight.
  - (b) A manual controller would have to be specially designed as there was no such requirement in the original missile application.
- (5) The Hughes M-252 fully transistorized general-purpose arithmetic digital computer, developed for use in the inertial guidance system of the SD-5 surveillance drone. This computer has sufficient capacity, can accept synchro transmitter voltages directly without deterioration of accuracy, has an associated manual controller, and can be adapted for this project by wiring changes on the input and output channels.

It has been shown that the system stabilization errors will be negligible, and pointing errors will be limited to the errors of the existing aircraft sensors, and of the satellite orbit computations provided that a digital computer is used which can accept synchro transmitter inputs directly and has sufficient capacity for a complete servo system compensation program. The Hughes Type M-252 computer has been designed for operation in an airborne environment, and can be modified to meet the requirements of the referenced contract. It has therefore been selected for this application. A summary of its characteristics is given in Appendix J, and a schematic diagram showing the Hughes M-252 computer incorporated into the antenna drive system in Fig. 4.3.

Hughes can supply a modified computer within 5-8 months after receipt of contract for a basic cost of about \$80,000. However the requirement of 5 months delivery would lead to tight scheduling and would be more expensive than eight months delivery. Auxiliary units, such as a tape reader or an extra drum containing a test program that can be used for trouble shooting with some fault isolation capabilities, are not included in the above price. The design of the optimal program is a specialized technique for which IBM-704-programmers, for instance, are not too well adapted, and programming will be the vendor's responsibility.





### 4.3 Operators Console

A survey of the optimum method of controlling and monitoring this experimental communication system indicated a requirement for an operators console. This was agreed to by Mr. L. A. Ames of AFCRL in a letter dated November 14, 1960 and it is envisioned that two operators will be stationed at the console. Provision will be made for mounting the following components on the console.

- a. Power distribution panel. (The A/C at present has a project power distribution system installed - ref. BAC drawing No. 5-71750, diagrams X22.65, X23.65 and X24.65).
- b. Navigation instruments (G.P.I., compass, clock, etc.).
- c. Maser monitoring instruments.
- d. Receiver monitoring instruments and recorder (about 1 1/2 sq. ft. of panel area, exclusive of recorder).
- e. Transmitter monitoring instruments.
- f. Modulator monitoring instruments and remote control panel (about 1 1/2 sq. ft. of panel).
- g. Computer and antenna monitoring instruments.
- h. Oscilloscope - (rack-mounted Tektronix)
- i. Interphone Jack Boxes for operators.

In addition space will be available for mounting the units making up the complete computer, complete in their cases, within one or more of the modules assembled into the console. The console design shown in Fig. 4.4 has been assembled from modules made by the Stantran Division of Wyco Metal Products. In the standard commercial form these modules will withstand about 7-10g loading, but all the modules can be supplied in a strengthened and braced form to withstand the 20g stressing specified for airborne use.

To avoid duplication of instruments, the two operators' stations have been arranged in line making up an assembly which is over 9 ft. long and will be positioned in the KC-135 in the fore-aft direction.



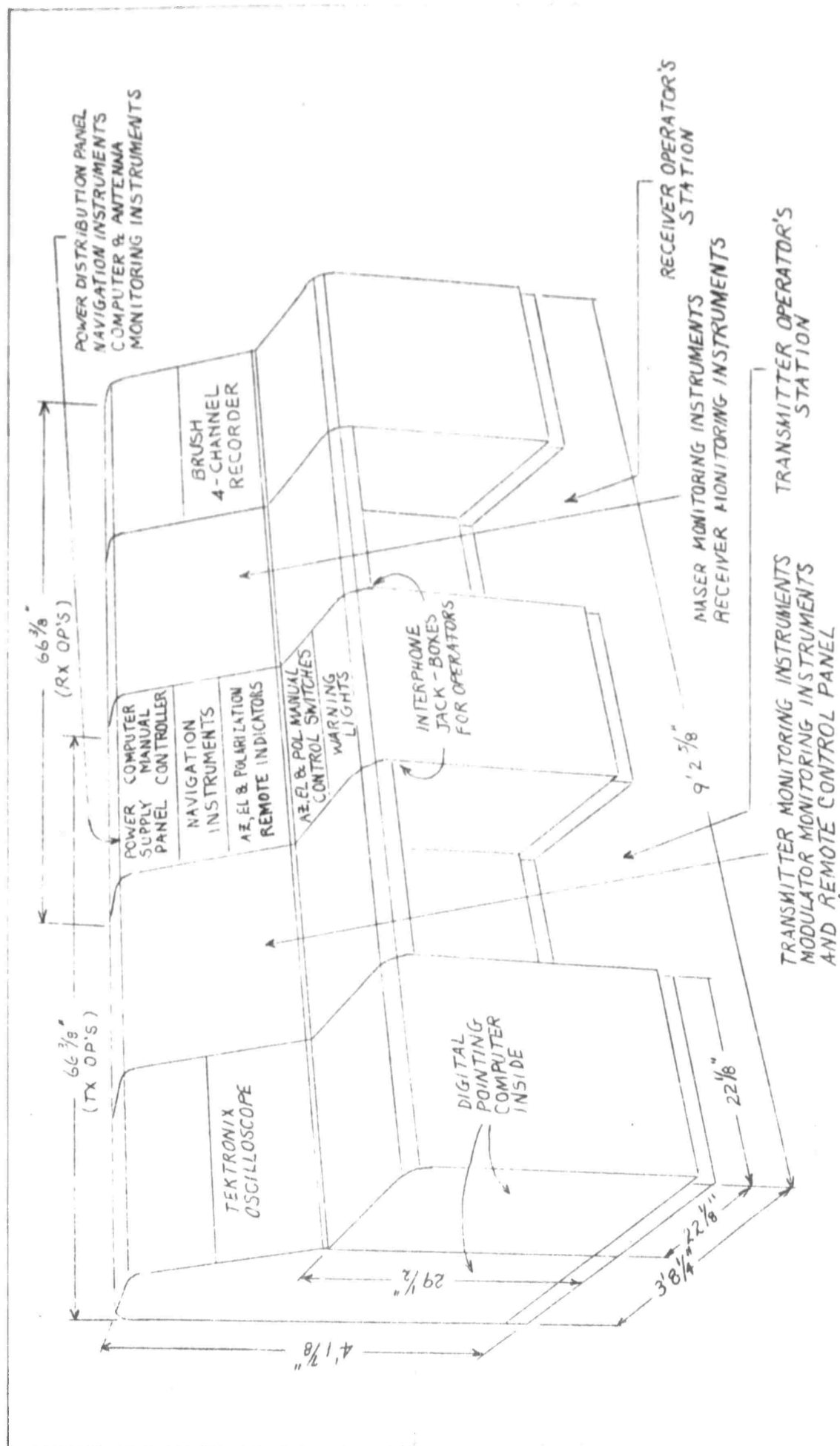


FIG. 4.4 OPERATORS' CONSOLE

Each operator's controls will be spread over 66 3/8" of panel space.

The size of an instrument panel depends primarily upon the normal arm reach of the human operator. In general, convenient arm reach is about 28 inches from the respective shoulder pivot point. This rule is not hard and fast because in most situations the operator has freedom to bend his body and thus extend the useful reaching distance (Ref. 51). The arrangement shown will therefore not lead to excessive operator fatigue.

The station on the left is the transmitter operator's station, and all instruments and controls related to the operation of the system in the transmitting mode are accessible to the operator.

The station on the right is the receiver operator's station, and all instruments and controls related to the operation of the complete system, in the reception mode are accessible to the receiver operator.

All instruments and controls common to them are mounted between them, so that either one or both of the operators at his station can initiate all necessary actions for his part of the system.

#### Recorder System

A permanent record of receiver signal strength and corresponding azimuth elevation and polarization angles, and timing marks, will be available on a Brush 4-Channel Recorder. The recorder pen-motors showing the three angular positions will be driven from the wiper arms of precision potentiometers energized from stabilized power supplies and mounted on Kearfott remote servo assemblies (see Fig. 3.4 for schematic circuit diagram). The remote servo assemblies receive electrical values of azimuth, elevation and polarization angles in the form of synchro signals from the synchro transmitters driven through 1:1 gearing from the corresponding output shafts of the antenna platform. These signals are received on the control transformers in the remote servo assemblies. The control transformer output is amplified to excite a servo motor so that it will drive the control transformer to null. By keeping the output of the control transformer at zero, the shaft position of the motor will continuously represent a mechanical value of the corresponding angle and will, in turn, be represented by the voltage across the potentiometer wiper.

## 5.0 RADOME DESIGN

### 5.1 Radome Dimensions

From an electrical standpoint, a spherical transmitting section is desirable for a fixed radome housing a scanning antenna. However, aerodynamic studies show that a radome of this shape increases the aircraft drag much more than an elliptical or faired shape having the same frontal area. The following tabulation shows the effect of radome shape and size on aircraft performance:

RADOME HEIGHT	RADOME WIDTH	RADOME LENGTH	L/H	RANGE LOSS
30"	30"	30"	1.0	12%
30"	30"	90"	3.0	6%
30"	30"	150"	5.0	3%

The shape was chosen as a compromise between good electrical characteristics and minimum effect on aircraft performance. The final radome has a length-to-height ratio of about 3 to 1 (39" H x 52" W x 114"L), and causes a 10 percent loss in aircraft range.

### 5.2 Radome Thickness

A single sandwich wall radome was chosen as the construction that would best provide good electrical performance consistent with sufficient physical strength. The single sandwich construction consists of a honeycomb core bounded by two thin high-strength skins with a rain erosion coating on the exterior skin. The thickness of the rain erosion coating and the radome skins are 0.01 inch and 0.03 inch respectively. The thickness of the core material is 0.346 inch. These are the optimum dimensions calculated with an existing computer program used for radome design.

Various flat-sides cross-sectional shapes were examined for strength and rigidity in an attempt to keep the aerodynamic drag of the dome as small as possible. To determine if the .03 - .346 - .03 thickness was satisfactory would require tests to determine their stress distribution and deflection characteristics. To avoid this testing, it was decided to use a configuration in which the station plane contours would be circular arcs. This provides a structure closer to one with known characteristics and calculations show the .346 core - .03 face ply combination is acceptable from both a strength and deflection standpoint. A proof pressure test to verify these calculations is specified in the radome specification. However, this does increase the frontal area of the radome and this circular shape causes a 3% additional range loss to the aircraft.

### 5.3 Radome Material

One main problem in the present radome which ordinarily is not encountered in radome design is the dielectric heating of the radome material by the 10-kw cw power output from the antenna. Figure 5.1 shows the approximate power density of the 10-kw cassegrain paraboloid antenna as a function of distance along the antenna axis. This near field calculation is based on a 10-db cosine illumination (ref. 21). A maximum of about 70 watts per square inch is attained at distances of 30, and 70-100 inches.

The radome skin chosen to withstand this high power flux is Emerson and Cuming ECCO-L-65, low-loss laminating resin ( $\epsilon = 4.6$ ,  $\tan \delta = 0.0058$ ). The honeycomb material is glass-laminated polyester having a density of approximately 8lb/cu.ft ( $\epsilon = 1.2$ ,  $\tan \delta = 0.006$ ). A sample of the radome was tested and found to exhibit satisfactory electrical properties up to 300°F. It was determined that a sandwich wall construction using the ECCO-L-65 resin with a rain erosion coating could handle a maximum power density of 90 watts per square inch. If the rain erosion coating is not used, a maximum power density of 180 watts per square inch could exist without exceeding a temperature of 300°F.

### 5.4 Radome Power Transmission

The power transmission efficiency of several radome shapes was calculated. The radome electrical thickness was chosen for maximum transmission at a mean design incidence angle of 60°. Figure 5.2 shows the minimum one-way power transmission that maybe expected. The overall average power transmission that may be expected is about 96 percent. The distances between the antenna aperture and the radome varies from approximately 12 inches to 74 inches depending upon the antenna zenith angle. In any case, the maximum boresight error will not exceed one-half degree.

### 5.5 Radome Attachment

The equipment installed under the radome can only be reached by removing the radome. As this equipment will be used for experiments, a method of attaching the radome which would permit easy and rapid removal was considered a primary design objective. This feature has been incorporated in the design by attaching the radome with ten latches which can be unlatched by the removal of a single screw in each latch. This latch design provides for misalignment when re-attaching the radome. The "snap in" weather seal can be quickly installed and adjusted and it does not interfere with the installation of the radome.

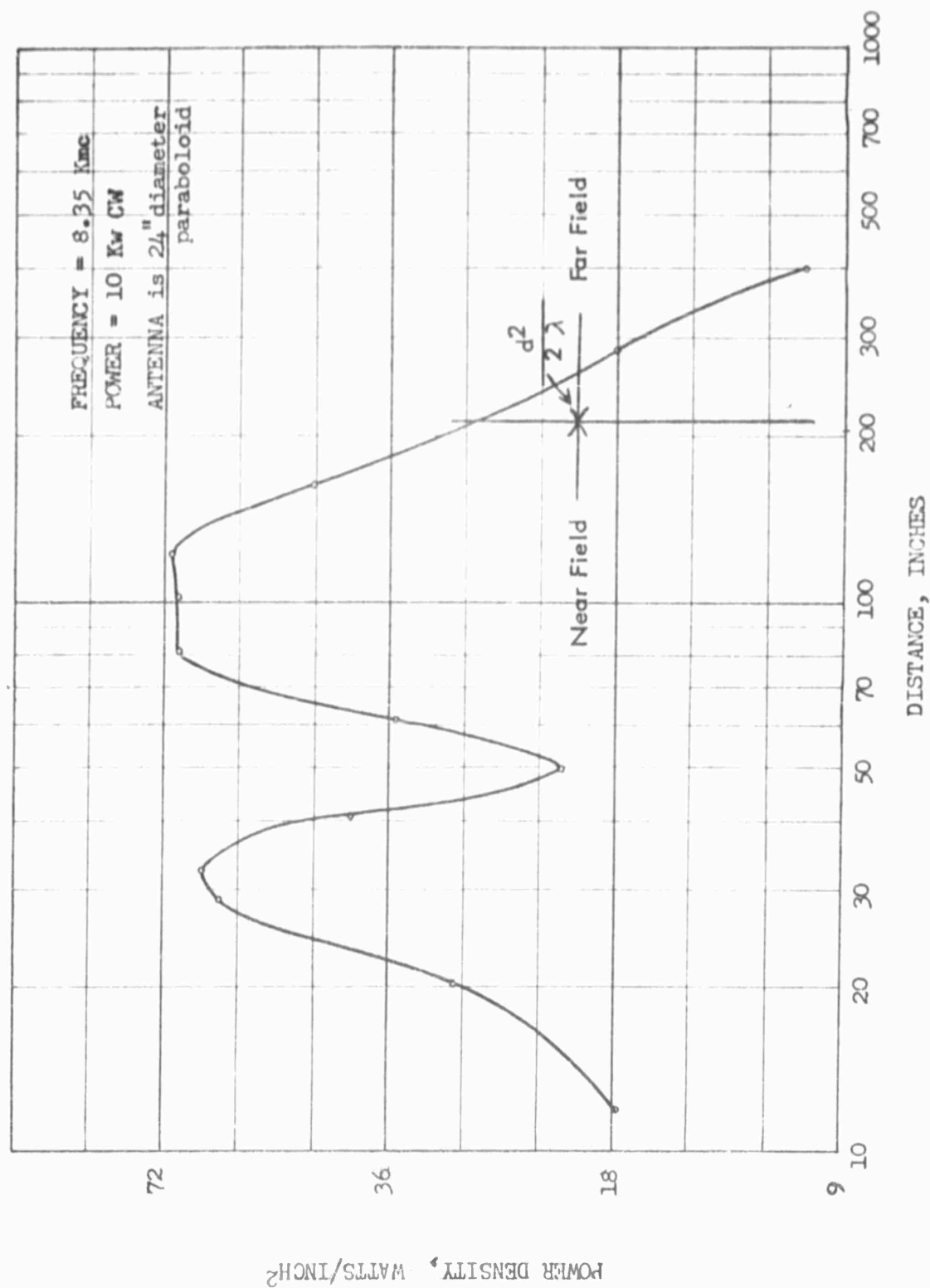


Fig. 5.1 POWER DENSITY VS DISTANCE ALONG ANTENNA AXIS

FREQUENCIES: 7750mc and 8350mc  
 ANTENNA POLARIZATION: Arbitrary

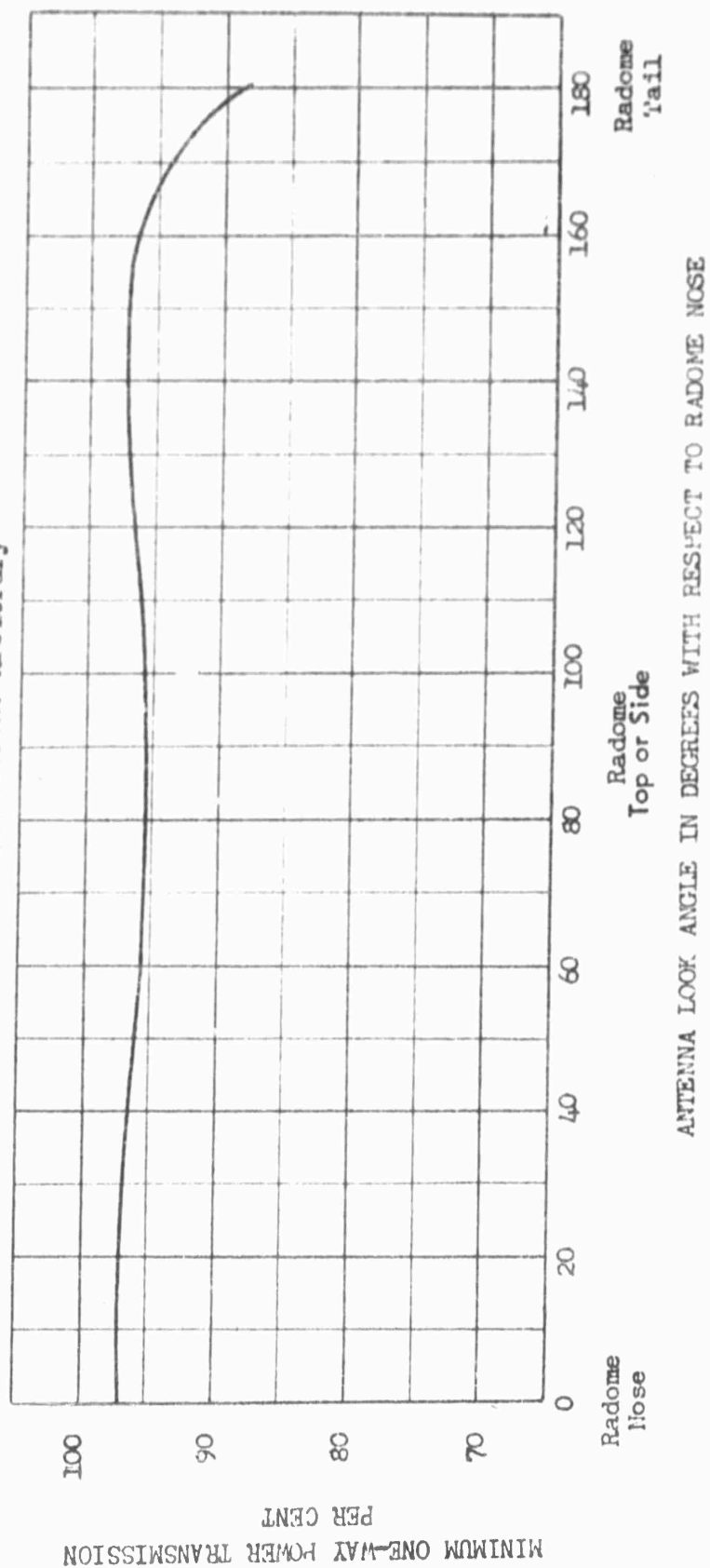


Fig. 5.2 CALCULATED RADOME POWER TRANSMISSION EFFICIENCY

## 6.0 Site Survey

If a single antenna is used and substantially upper-hemispheric coverage is required, the antenna must be located on the top of the aircraft. Locations on the wings or vertical tail were eliminated because the flexibility of these members under flight conditions would cause a variable orientation relation between an antenna mounted on their structure and existing body-mounted attitude sensors. In addition, equipment located near the wing tips or on the vertical tail are subjected to considerably higher accelerations during flight in turbulent air than equipment located near the center of gravity of the aircraft. An antenna at these locations would be considerably removed from the majority of the transmitting and receiving equipment which would be located in the aircraft cabin. A location on the top centerline of the body was therefore chosen.

Aerodynamic studies determined that from a drag standpoint the preferred location was in the vicinity of body stations 550 to 750. Studies showed that the beam obscuration by the wings and tail decreases in forward antenna locations (Appendix L). From a structural standpoint the location was not critical but it is undesirable to have the radome extend across a circumferential skin joint. The antenna support structure is simplified if the area adjacent to the body production joints is avoided. The structure of the area selected will provide maximum rigidity.

Exterior visual inspection of the radome installation is convenient for locations over the wing and such locations provide a platform base for servicing the radome and antenna equipment.

After weighing the above factors - aerodynamics, structural, beam obscuration - the antenna was located with the centerline of the azimuth axis at station 670 (Fig. 6.1).

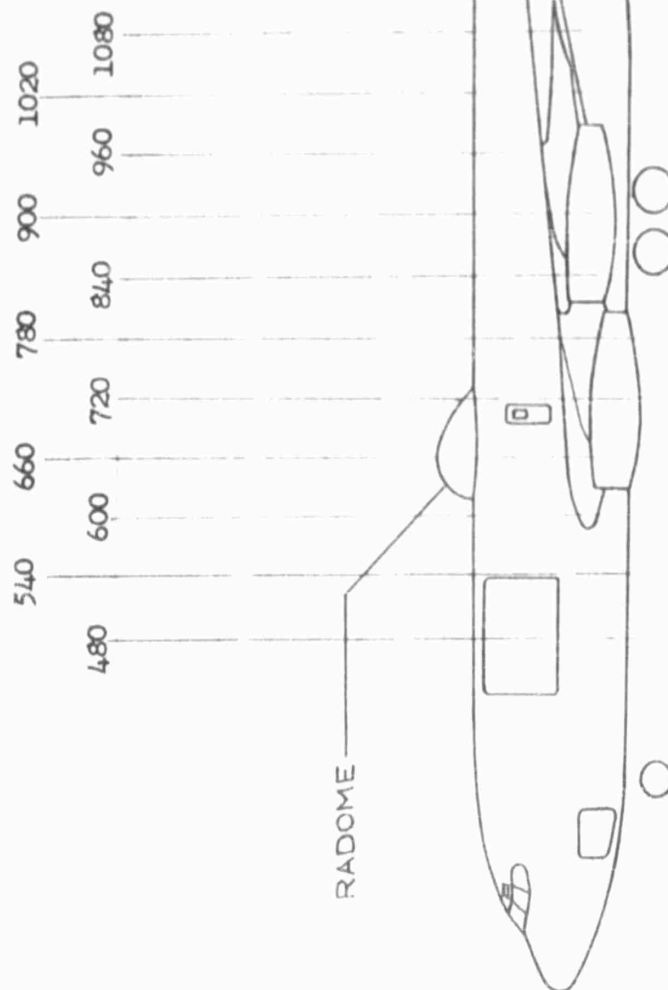


Fig. 6.1 RADOME LOCATION ON KC-135 AIRCRAFT

CALC			REVISED	DATE	D6-7190
CHECK					
APPD					
APPD					
BOEING AIRPLANE COMPANY RENTON, WASHINGTON					PAGE 75



## 7.0 ELECTRICAL SYSTEM

### 7.1 General

The KC-135 airplane basic electrical power system (Fig. 7.1) is capable of furnishing 120 KVA of 400-cycle AC power from alternators located in three of the four engine pods. A portion of this 120 KVA is transformed and rectified to make available 200 amps of 28-volt DC power. Of the total power available, approximately 35 KVA AC and 80 amps DC are required for general airplane systems during cruise. Power from the alternators must be supplied to the experimental microwave communication system, in which the klystron power-amplifier is by far the largest load.

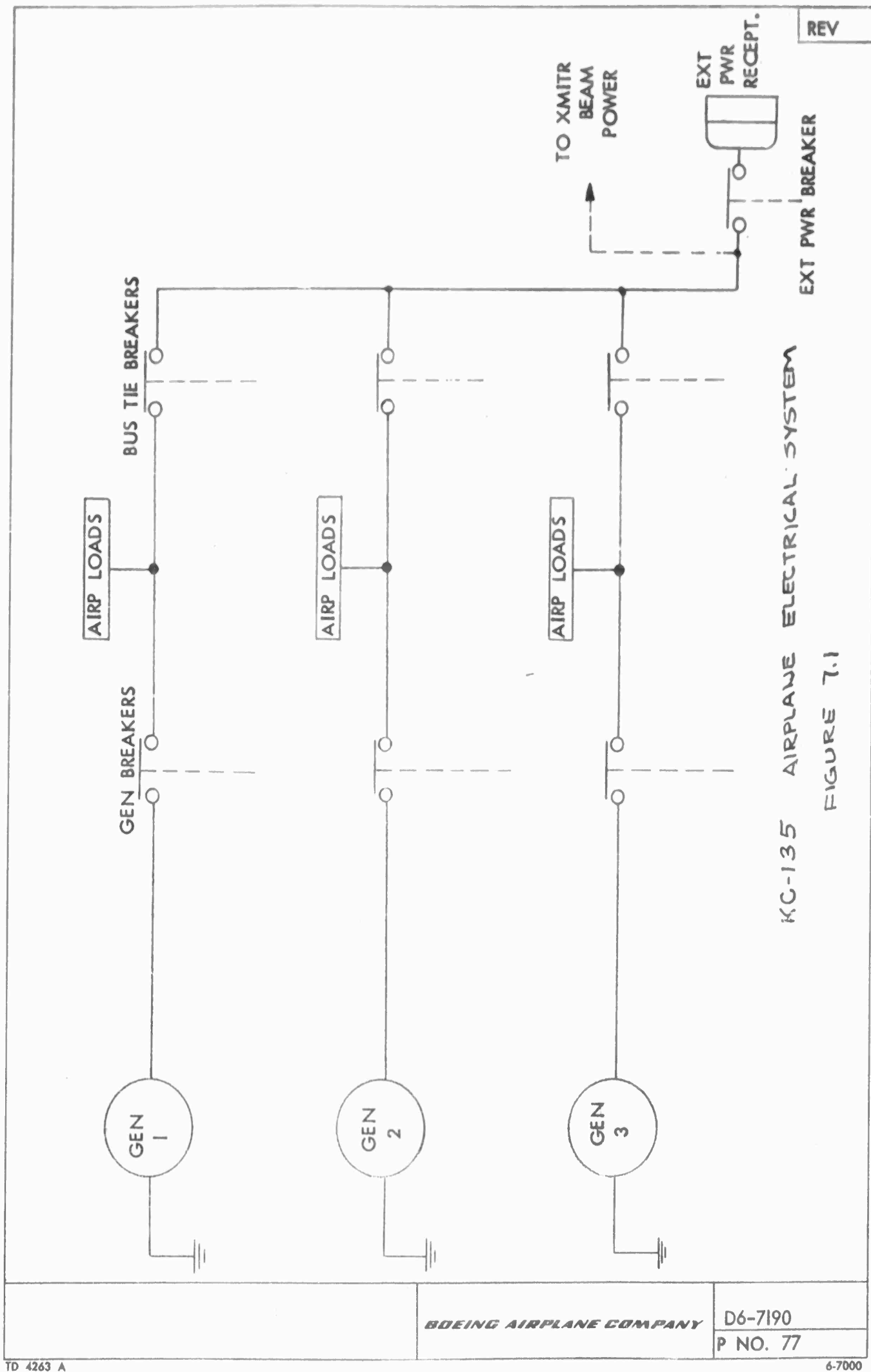
### 7.2 Specific Airplane Configuration

Airplane 55-3120 assigned for this program has been previously modified to provide special power for research electronics installations. Modifications have added additional transformer rectifiers and inverters to provide 5 KVA of 60-cycle power. In addition, receptacles for 400-cycle power have been located in various places in the airplane. The largest block of power available in this distribution system is from a 400 cycle three-phase receptacle, located at Sta. 857, capable of providing 60 amps per line.

### 7.3 Airplane Modifications

It was assumed, early in the program, that the existing power distribution system in airplane 55-3120 could be used to power the communication system. Varian Associates, later informed Boeing that the klystron beam supply would require approximately 40 KVA (approximately 116 amps per line) three-phase power with an additional 10 KVA for control power. Since the existing power distribution system will furnish a maximum of 60 amps per line, a new distribution system capable of 40 KVA minimum must be provided.

Circuit breakers approved for airplane installation and capable of carrying over 60 amps continuously are not available. It was, therefore, decided to provide a multiple feeder network consisting of eight 50 amp circuit breakers and four No. 8 feeders per phase, as shown in Figure 7.2, to furnish the required transmitter beam power. Additional power will be obtained from the existing 60 amp receptacle at Sta 857. The 40 KVA required for the transmitter beam power is equivalent to the total power output of one generator. Since this load plus the basic airplane load would obviously overload one generator, the circuit is interlocked with the generator controls in such a manner that if the generators are not paralleled, power is not available for operation of the communication system.



KC-135 AIRPLANE ELECTRICAL SYSTEM

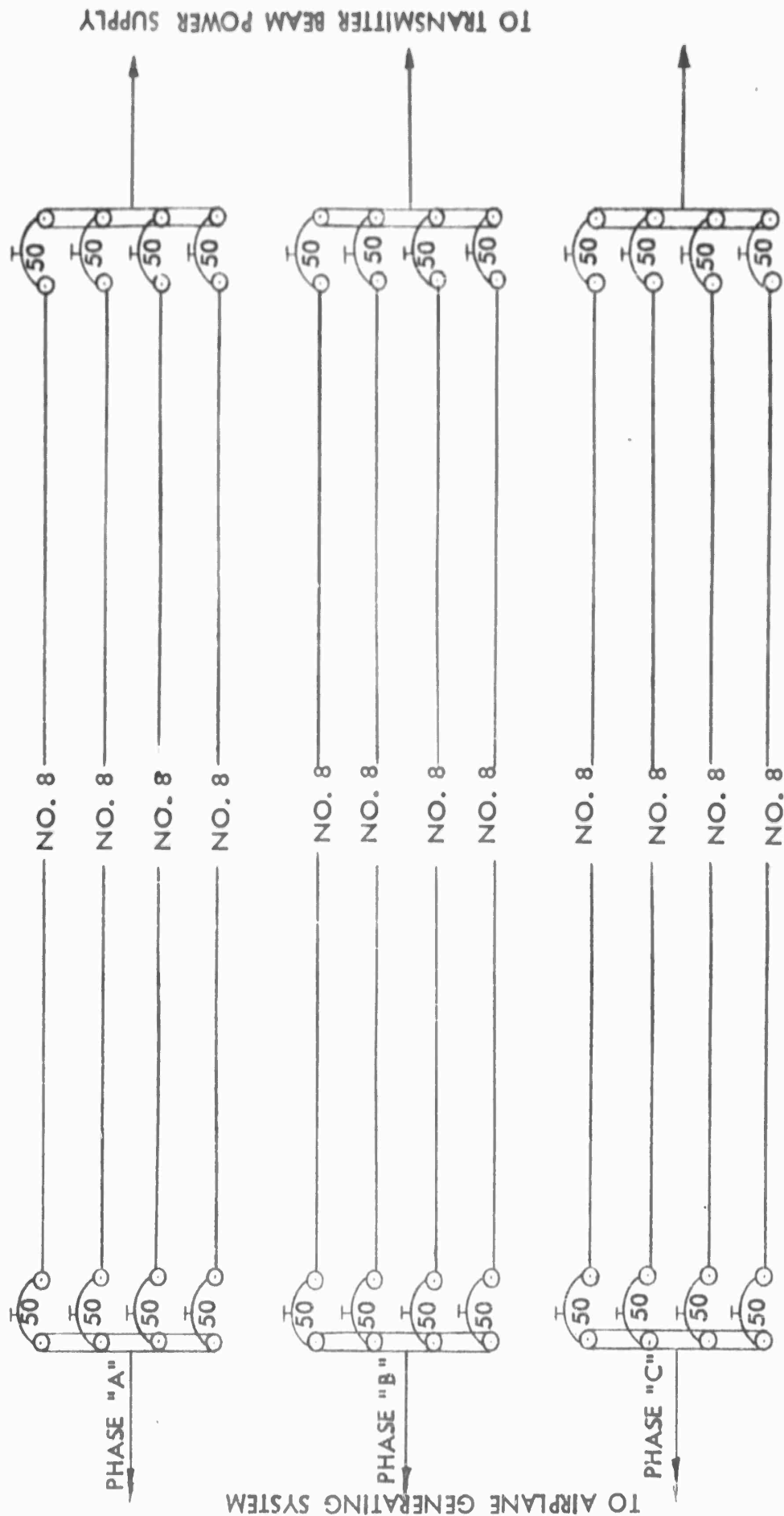
FIGURE 7.1

REV

BOEING AIRPLANE COMPANY

D6-7190

P NO. 77



PROPOSED KLYSTRON BEAM-POWER MULTIPLE-FEEDER SYSTEM  
FIGURE 7.2

BOEING AIRPLANE COMPANY

D6-7190

P NO. 78

A single pole switch located on the pilot's overhead panel to control the research equipment power was changed to a two-pole switch to provide positive pilot control for the existing distribution system as well as the added 40 KVA beam power system. The communication electrical power system then has three points of control (Fig. 7.3).

1. The pilot can turn off the system power by operating a switch on the overhead instrument panel.
2. The system interlocks will turn the system off automatically if a generator fails or the generators become unparallelled.
3. The system operator has a switch which controls all power.

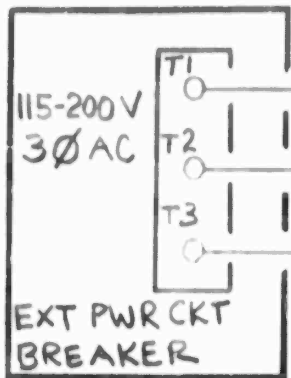
Additional controls for the transmitter are provided by Varian Associates.

#### 7.4 Ground Checkout

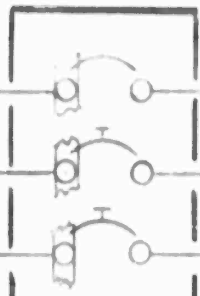
The existing external power configuration is adequate for, and each airplane is tested at, 50 KVA. Since the required power for this system is somewhat above the 50 KVA there is some doubt about the adequacy of the system. To be certain that the external power system is capable of carrying the required power, the existing No. 2 copper wires in the system are replaced with No. 0 copper wire. This insures the adequacy of the electrical system for full power ground testing.

#### 7.5 Limitations

Because of the large total load on the system, the pilot should monitor the generator loads frequently. During a water injection take-off with this communications system operating, the electrical loads very nearly approach the maximum electrical system output ( Appendix M ). The true electrical configuration of airplane 55-3120 is unknown and any additional electrical equipment, other than the basic airplane equipment, will increase the total load further. Because of this, a water injection take-off with this communication system operating should be avoided; otherwise, the electrical system may be operated within the limitations of the Flight Handbook, T. O. IC-135(K)A-1.



P15 MAIN AC PWR  
SHIELD



RECEPTACLE  
STA 857(R)  
(115/200 VOLTS  
3Ø A.C.)

RESEARCH EQUIP.  
POWER CONTROL

RESEARCH  
EQUIP. PWR.



PILOTS PNL

28V DC



P13 SW DC  
CB PNL

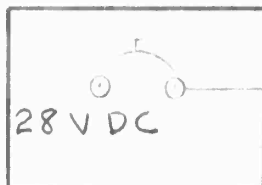
BUS

GENERATORS  
ISOLATED

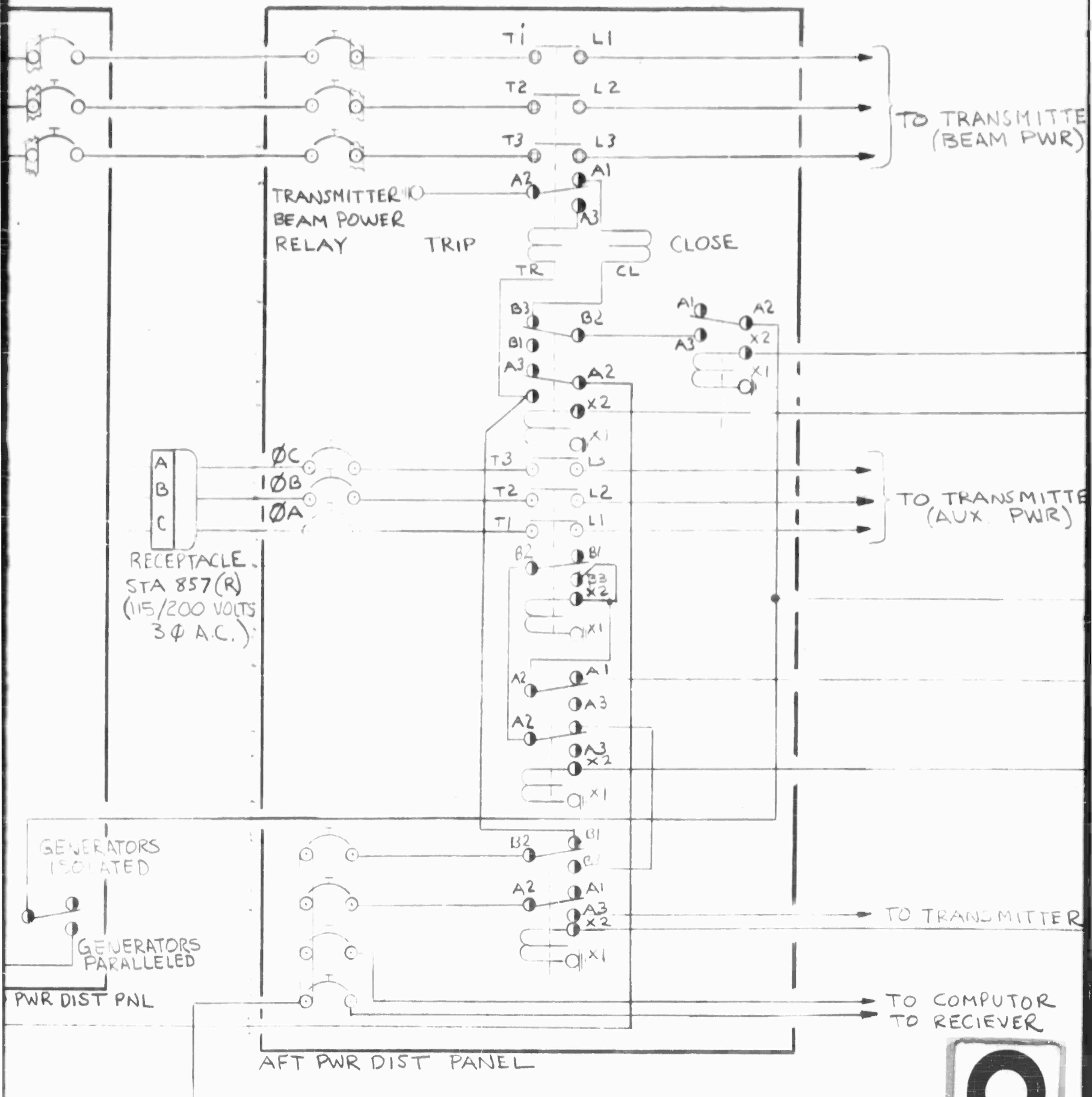


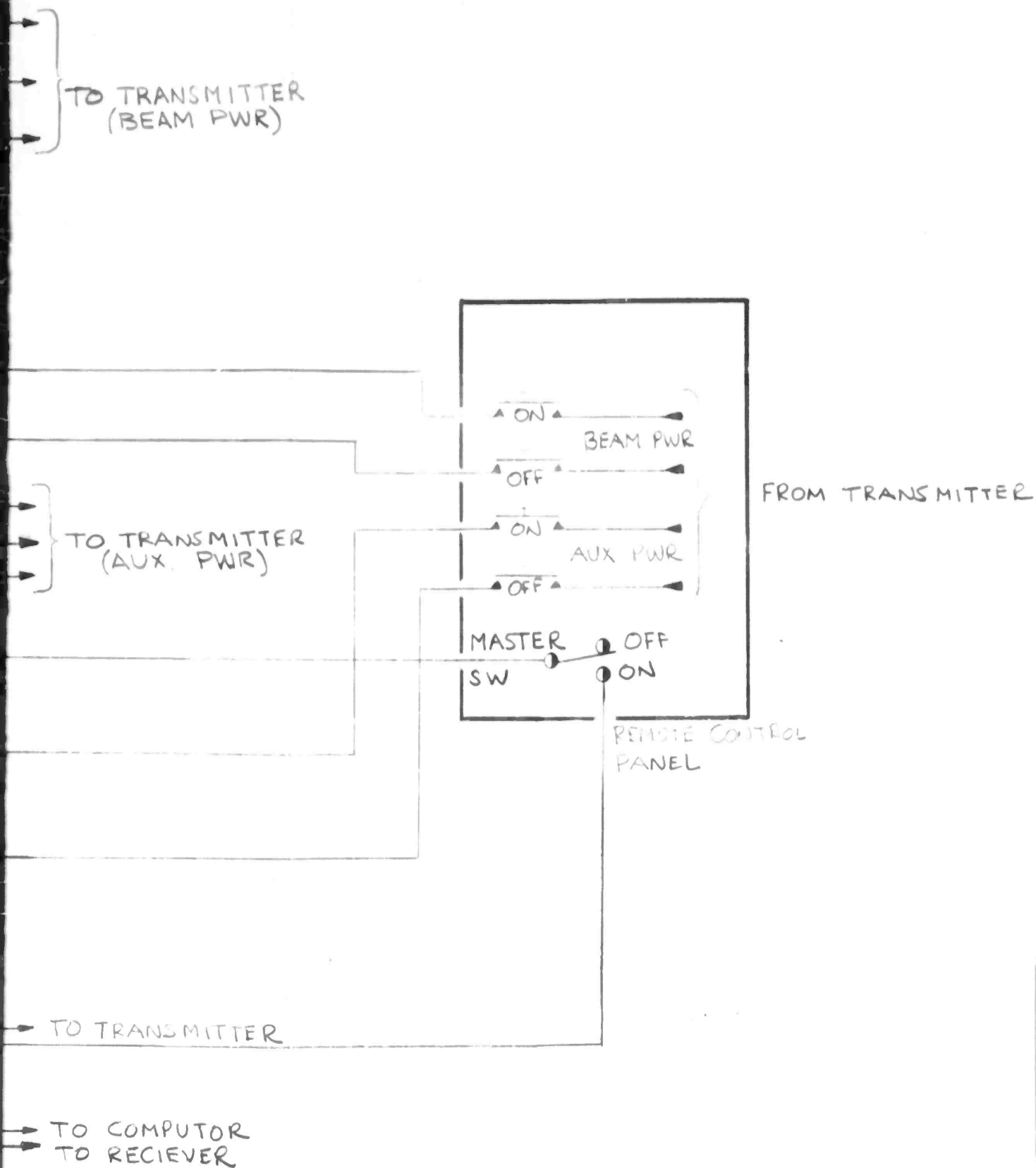
GENERATORS  
PARALLELED

FWD PWR DIST PNL



P8 MAIN CKT  
PRK PANEL





MICROWAVE COMMUNICATION ELECTRICAL POWER

FIGURE 7.3

## 8.0 Equipment Cooling System

Both liquid and air cooling systems are employed in the airborne antenna system. Varian Associates provides a liquid cooling unit for the 10-kw klystron power amplifier. Coolant from this unit is used to cool the maser receiver and the microwave transmission components. Forced air is circulated within the radome to cool components not readily accessible to liquid lines.

### 8.1 Liquid Cooling

The Hughes receiver is a closed-loop helium-cooled maser located for best noise performance on the upper antenna platform. The maser heat-exchanger compressor is liquid-cooled by running a coolant line from the transmitter cooling unit in the cabin. The coolant is transferred through the rotating azimuth drive shaft by means of a sealed liquid rotary joint in the lower platform housing. This line is also used to cool the microwave plumbing and components.

### 8.2 Forced Air Cooling

Air is drawn from outside the aircraft and introduced into the radome by means of a Torrington Mfg. Co. No. MSA-11000 blower and a duct system. Inside the radome the duct encircles the base of the antenna and has nozzles which direct the air flow toward the upper platform assembly. The air is then exhausted overboard through a cutout in the lower aft edge of the radome.

The forced air cooling system requirements were based on maintaining the temperature of the air in the radome below 125°F. Maximum ambient air temperature on the ground was assumed to be 100°F. Radome heat loads were estimated as follows:

#### Maximum Ground Conditions

Solar Load	1.2 KW
Equipment Load	<u>3.0 KW</u>

TOTAL LOAD 4.2 KW

Amount of Air Required 560 CFM

#### Conditions at 40,000 feet altitude

Convective Loss	-1.4 KW
Equipment Load	<u>3.0 KW</u>

TOTAL LOAD 1.6 KW

Amount of Air Required 200 CFM



## 9.0 Aircraft Modification

The design considerations of the installation on the aircraft were flight safety, structural integrity, antenna system performance, ease of modification, and minimum refurbishment. This installation will add drag to the aircraft to the extent of reducing the range and rate of climb by an estimated 10 percent. Such penalties on aircraft performance in experimental missions are tolerable, but would probably be unacceptable on military missions. However, the radome drag will cause a negligible change in the aircraft take-off performance and minimum control speeds and no restrictions need be placed on aircraft speed or altitude due to this installation.

The location chosen for the antenna is near the forward body fuel tank vent outlet. Fuel vapors vented by this outlet either on the ground or in flight could cause an explosive atmosphere to exist around the antenna which contains electrical equipment and wiring carrying a potential high enough to be a possible spark source. To eliminate the chance of an accident from a combination of the above conditions, the fuel tank vent outlet will be relocated aft to the vicinity of the aft fuel tank vent outlet.

The forward coverage of the presently installed upper anti-collision light will be partially obstructed by addition of the radome. An additional anti-collision light will be added forward of the radome to retain complete upper hemispheric coverage after the radome is installed.

The antenna and mount system are designed to be capable of withstanding, without tearing loose, the air loads to which they would be subjected if the radome should fail and be carried away in flight. To minimize the chance of radome failure due to air loads, a structural proof test of the radome is specified. Electrical breakdown strength of the radome will be checked prior to first flight by full-power transmission tests. Approximately 50 drawings of antenna installation and aircraft modification have been prepared. A list of the drawings and their Boeing Index numbers are given in Appendix N.

### III SUMMARY AND CONCLUSION

A design study of an airborne microwave antenna system suitable for radio propagation studies and for communication has been reported. Problems relating to the low receiver noise, to the high transmitter power, and to the instabilities of the KC-135 airplane are considered, and solutions to these appear within the present state of the art.

Microwave noise due to atmospheric absorption is significantly lower at high altitudes, permitting closer approach to the theoretical lower limits of maser noise temperatures. This puts a premium on low-noise antenna design. Ground-based radio telescopes with X-band noise temperatures of  $85^{\circ}$  -  $200^{\circ}$  K (depending on zenith angle) have been reported. (30,31) The antenna temperature in the present system will not exceed  $40^{\circ}$  -  $50^{\circ}$  K; with the Hughes maser the system temperature will be below  $60^{\circ}$  K, except very close to the horizon.

Ten kilowatts cw-power at X-band was unheard-of on the ground five years ago, let alone on aircraft. Problems posed by this high power aloft include: primary ac to drive the transmitter, dielectric heating of radomes;  $I^2R$  heating of rotary joints, waveguide, and flanges; high-altitude voltage breakdown; related heat-flow and cooling problems. The lowest possible losses in design and components have been sought. In general, what was good microwave design for the transmitter was good also for the receiver. All critical microwave components have been subjected to close scrutiny and testing. Devious, but realistic and theoretically defensible, tests have been devised to power-test microwave components despite the non-availability of 10-kilowatt transmitters. This study has left few stones unturned in attempts to achieve a microwave antenna design that is responsive both to the explicit specifications and to the demands implicit in the companion klystron transmitter and maser receiver.

Microwaves are now used extensively on aircraft for gun-laying and fire control radar, employing closed-loop, null-seeking servo systems. Basic differences between radar and communications, plus great disparities in path geometry, have dictated an open-loop antenna pointing system for which existing hardware is poorly suited. In this scheme, faith must reside in the pointing computer and the original inputs, just as in an astronomer's telescope computations; the "object in space" is not usually visible. Considerable effort therefore has gone into devising a realtime computation scheme capable of meeting the demands placed on it by rapidly moving aircraft and satellite(s) and compatible with present aircraft attitude and reference sensors. Hardware suitable (with modification) for the job is believed to be available, lending some hope that the airborne communicator's confidence may approach that of the astronomer.

Modification and loss of performance in the KC-135 resulting from this antenna installation will be nominal. Conversely, the KC-135 should provide a nearly ideal platform — lots of a-c power, smooth fastride, shirtsleeve environment — on which to perform radio propagation and communication research studies.

Research programs have a way of evolving — from the evidence they amass — along lines not readily predicted at the start. An airborne microwave radio telescope endowed with modest resolution, high mobility, and phenomenal sensitivity should be useful for many studies well beyond the scope of satellite communications. These might include:

high-altitude noise profiles

radio ducting and refraction cloud and atmospheric physics

planetary radioastronomy

earth albedo

reentry telemetry

Whether then for research or communications, for science or engineering, a useful tool has been delineated and its technical feasibility established; the next step is to build one.

#### IV . BIBLIOGRAPHY

1. P. Foldes and S. G. Komlos, "Theoretical and Experimental Study of Wideband Paraboloid Antenna with Central-Reflector Feed," RCA Review, Vol 21, No. 1, pp. 94-116, March 1960
2. J. Gammie and S. D. Hathaway, "The TJ Radio Relay System," BSTJ, Vol 34, p. 4, pp. 821-878, July 1960
3. R. C. Hansen, "Tables of Taylor Distribution for Circular Aperture Antennas," Tech. Memo No. 587, Feb. 1959, Hughes Aircraft Company
4. S. Silver, "Microwave Antenna Theory and Design," Vol 12, Rad. Lab. Series, p. 340 McGraw Hill Book Company, New York
5. G. L. Ragan, "Microwave Transmission Circuit" Radiation Lab. Series, Vol 9, pp. 366, McGraw Hill Book Company, New York, 1947
6. P. H. Smith, "The Asymmetrical Waveguide Tuning Plug," BTL Report, MM 44-170-59, December 8, 1944
7. Lovell, B. "Radio Astronomy" Chapman, and Hall, London, p. 145, 1952
8. Smith, Alex G. "Extraterrestrial Noise as a Factor in Space Communication," IRE Proc. p. 596, April 1960
9. N. G. Roman, Yaplee, B. S. "Radio Sources and Milky Way at 440 MC" IRE Proc. Vol 46, pp. 199-204, January 1958
10. Piddington, J. H., Minnet, H. C. "Microwave Thermal Radiation from the Moon," Australian Journal Scientific Research, Vol A2, p. 63, March 1949
11. Gibson, J. E. "Lunar Thermal Radiation at 35 KMC," IRE Proc. Vol 46, pp. 280-286, January 1958
12. Mayer, C. H., McCullough, T. P., Sloanaker, R. M. "Measurements of Planetary Radiation at Centimeter Wavelengths," IRE Proc. Vol 46, pp. 260-266, January 1958
13. Drake, F. D., Ewen, H. I, "A Broad-Band Microwave Source Comparison Radiometer for Advanced Research in Radio Astronomy," IRE Proc Vol 46, pp. 53-60, January 1958

14. Ko, H. C. "The Distribution of Cosmic Radio Background Radiation," IRE Proc. Vol 46, pp. 208-215, January 1958
15. Pierce, J. R. "Satellite System for Commercial Communications," IAS Paper No. 60-40 Presented at the IAS 28th Annual Meeting, New York N.Y. January 25-27, 1960
16. D. C. Hogg "Effective Antenna Temperature Due to Oxygen and Water Vapor in the Atmosphere," Jour. of appl. Phys. Vol 30, No. 9, pp. 1417-1419, September 1959
17. Dicke, R. H., Beringer, R., Kyhl, R. L. and Vane, B. A. "Atmospheric Absorption Measurements with a Microwave Radiometer," Physical Review, Vol 70, p. 340, 1946
18. Minzner, R. A., Champion, K.S.W. and Pond, H. L. "The ARDC Model Atmosphere, 1959," Air Force Survey in Geophysics, No. 115, AFCRC TR-59-267
19. Forward, R. L. Richey, F. "Effect of External Noise on Radar Performance," Research Report No. 126, Nov. 1959, Hughes Research Laboratory
20. Hansen, Robert C. "Low Noise Antennas" The Microwave Journal, Vol 2 pp. 19-24 June 1959
21. Mumford W. W., Ranucci J. "Power Density Along the Axis of A Circular Antenna with Tapered Illumination" Bell Labs Tech. Memo. MM-59-6436-3, March 4, 1959
22. D6-3451, December, 1957 "Study of the Random Motion of the KC-135 Airplane in Atmospheric Turbulence", Boeing Airplane Company
23. D10-2710, March 4, 1960, "Specification for Servomotor Automatic Pilot Stabilizer Trim, (For use on Model KC-135 jet-tanker-transport)", Boeing Airplane Company
24. D6-5272, February 1960, "Airborne Microwave Antenna for Satellite Tracking from a KC-135 Aircraft", Design Proposal, Boeing Airplane Company
25. Zucker H., Knop G. M. and Gutfreund K., "Development of High Altitude Waveguides", WADC Technical Report 59-741, Feb. 1960.
26. AFCRC Purchase Request Number 81280, Dec. 1, 1959, "Design Study for Experimental Airborne Antenna for KC-135 Aircraft"
27. D10-60603, Jan. 16, 1961, "Source Control Drawing for Digital Pointing Computer" (For use on Model KC-135 airplanes), Boeing Airplane Company
28. Klass P. J. "Techniques of 'Project Needles' Detailed", Aviation Week, September 19, 1960, pp. 30-31.

29. D6-5881, Oct. 10, 1961, "Systems Analysis for an Airborne Antenna Control System for Communication via a Space Object", Boeing Airplane Company
30. J. A. Giordmaine, et.al., "A Maser Amplifier for Radio Astronomy at X-Band" IRE Proc. Vol. 47, pp. 1062-1069 June 1959
31. R. W. DeGrosse, et.al., "Ultra-Low-Noise measurements using a Horn Reflector Antenna and a Traveling-wave Maser". Journal Applied Physics, pp. 2013, Dec. 1959
32. L. J. Milosevic, R. Vantey "Traveling-Wave Resonator" IRE Trans. Vol. MTT6, No. 2, pp. 126-143, April 1958.
33. Easton, R. L. Fleming, J. J., "The Navy Space Surveillance System," Proc. IRE, Vol. 48, No. 4, pp. 663-669, April 1960.
34. Moe, M. M. "Solar-Lunar Perturbations of the Orbit of an Earth Satellite", Jour. APS. May 1960, pp. 485-487.
35. Herget, P. and Munsen, P., "A Modified Hansen Lunar Theory for Artificial Satellites," Astronomical Jour., Vol. 63, pp. 430-433, November 1958
36. "The American Ephemeris and Nautical Almanac for the Year 1959," U. S. Naval Observatory, Washington, D.C., 1957
37. Blitzer L., Nature, June 11, 1960, pp. 874-5
38. Jeffreys H., "The Earth", 4th ed<sup>n</sup>, Ch 4, Cambridge University Press, 1959
39. Tou J., "Digital Compensation for Control and Simulation," Proc. IRE, Vol. 45, pp. 1243-1248, September 1957
40. Salzer, J.M., "System Compensation with a Digital Computer," IRE Conv. Record, Part V, March 1954, pp. 179-186
41. Salzer, J. M., "Frequency Analysis of Digital Computers Operating in Real Time" Proc. IRE, Vol 42, No. 2, pp. 457-466, February 1954
42. Linville, W. K. and Salzer, J. M., "Analysis of Control Systems Involving Digital Computers" Proc. IRE Vol 41, pp. 901-906, July 1953
43. Curk, H. M. and Rubinoff, M., "Numerical Solution of Differential Equations" Proc. Eascon. pp. 58-64, December 1954
44. Scarborough, J. B. "Numerical Mathematical Analysis," John Hopkins press; Baltimore, Md., 1950
45. Marden, M. "The Geometry of the Zeros of a Polynomial in a Complex Variable," Amer. Math. Soc., N. Y., Ch. 10 1949

46. Tou, J. "Stability Criterion for Digital Feedback Control System," Proc NEC, Vol. 12 pp. 336-346, October 1956
47. Unpublished Boeing memorandum from J. Alvorez to J. Connell of July 25, 1960
48. T. O. IC-135(K)A-2-II, June 15, 1959, Revised December 15, 1960, "Radio, Communication and Navigation Systems, USAF Series KC-135A Aircraft"
49. Luis Oh, "Effect of KC-135 Airframe on Top-Fuselage-mounted rotating Antenna", Boeing Airplane Company Document, No. D6-3076, January 23, 1959
50. K. Akabane, "A Polarimeter in the Microwave Region" Proc IRE, Vol. 46:1, January 1958, p. 194
51. Woodson W.E., "Human Engineering Guide for Equipment Designers", University of California Press, Berkeley, 1957

V APPENDICES



## APPENDIX A ANTENNA DESIGN

### A. Antenna Reflector Design

The equations for the paraboloid (main reflector) and hyperboloid (central reflector) can be expressed as:

$$\rho \cos^2 \frac{\psi}{2} = f \quad (1)$$

where  $\rho$  and  $\psi$  are polar coordinates and  $f$  is the focal length (Fig. A-1)

and:

$$\alpha x^2 + \beta x + \gamma = y^2 \quad (2)$$

where  $x$  and  $y$  are rectangular coordinates and  $\alpha$ ,  $\beta$  and  $\gamma$  are constants to be determined.

Substituting  $\rho \sin \psi = y$  into equation (1) we obtain,

$$\frac{y}{\sin \psi} (\cos^2 \frac{\psi}{2}) = f \quad (3)$$

or

$$(4f^2 + y^2) \cos^2 \psi + 2y^2 \cos \psi + (y^2 - 4f^2) = 0 \quad (4)$$

therefore

$$\cos \psi = \frac{-y^2 \pm 4f^2}{4f^2 + y^2} \quad (5)$$

Taking the positive sign only, we have,

$$\cos \psi = \frac{f^2 - y^2}{4f^2 + y^2} \quad (6)$$

and

$$\tan \psi = \frac{fy}{4f^2 - y^2} \quad (7)$$

From Figure A-1,

when  $\psi = \psi_2$ ,  $y = b$  and  $\tan \psi_2 = \frac{a}{x_0}$

then,

$$\frac{4fb}{4f^2 - b^2} = \frac{a}{x_0} \quad (8)$$

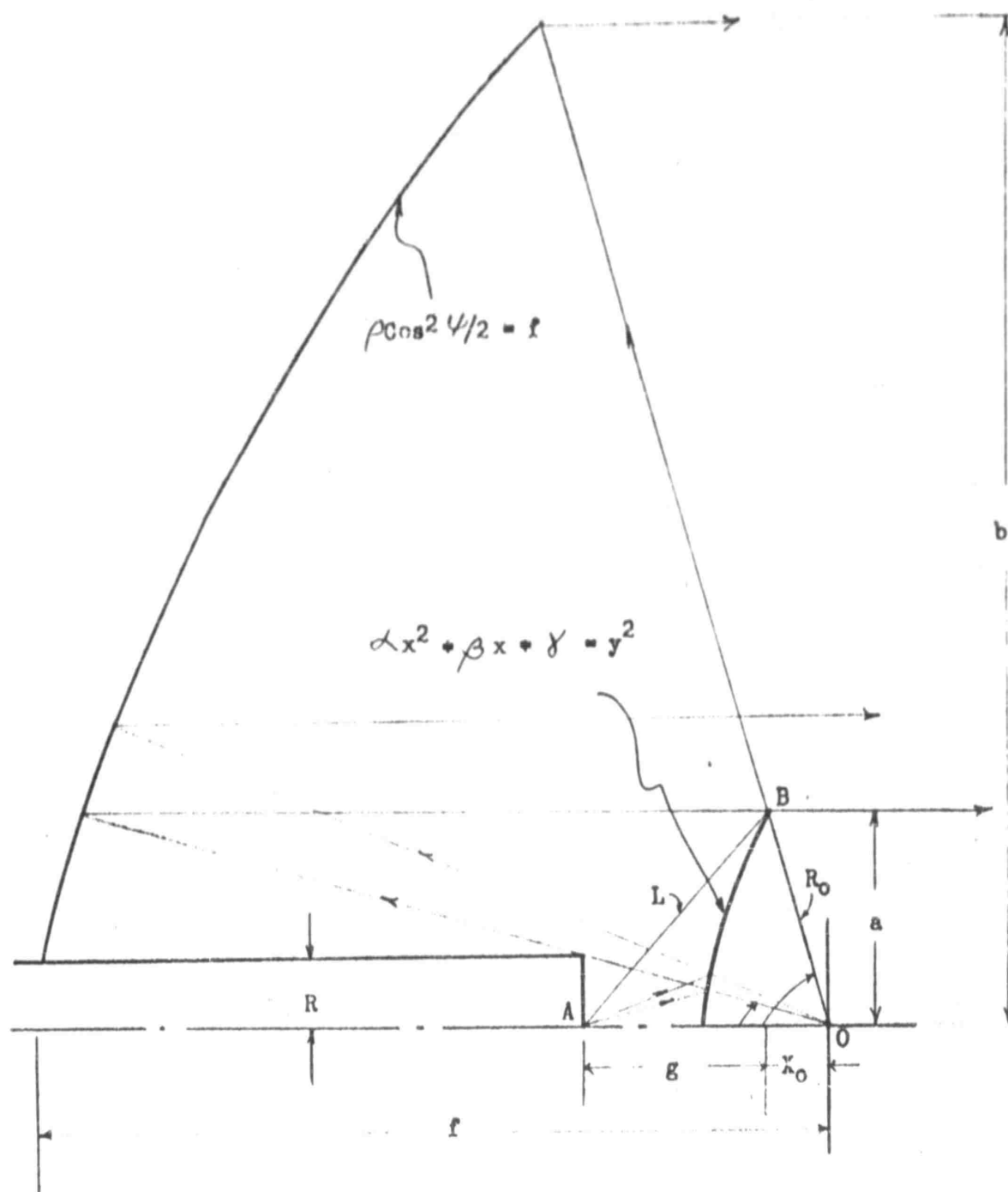


Figure A-1 Coordinate System for Determination of the Reflector Surfaces.

when  $\phi = \phi_1$ ,  $y = a$  and  $\tan \phi_1 = \frac{R}{g + x_0}$

then

$$\frac{4fa}{4f^2 - a^2} = \frac{R}{g + x_0} \quad (9)$$

Solve  $f$  from Eqs. (8) and (9)

$$f = \frac{abg \pm \sqrt{b^2 g^2 - b(a^2 - bR)(R-b)}}{2(bR - a^2)} \quad (10)$$

In order that  $f$  be a real number, it should be such that

$$b^2 g^2 \geq b(a^2 - bR)(R-b) \quad (11)$$

or

$$a^2 \geq \frac{b(bR - R^2 - g^2)}{b - R} \quad (12)$$

To minimize the blocking effect of the central reflector, the smallest  $a$  must be chosen, therefore:

$$a^2 = \frac{b(bR - R^2 - g^2)}{b - R} \quad (13)$$

In this case Equation (10) becomes:

$$f = \frac{abg}{2(bR - a^2)} \quad (14)$$

From Figure A-1 the following equation can be obtained from the geometrical configuration of the central reflector.

$$(g + x_0 - x)^2 + y^2 = [L - (R_0 - r)]^2 = (C + r)^2 \quad (15)$$

where

$$r = (x^2 + y^2)^{\frac{1}{2}} \quad \text{and} \quad C = L - R_0$$

Therefore

$$\frac{(g + x_0)^2 - (L - R_0)^2}{(L - R_0)^2} x^2 - (g + x_0) \frac{(g + x_0)^2 - (L - R_0)^2}{(L - R_0)^2} x$$

$$+ \frac{\left[ (g + x_o)^2 - (L - R_o)^2 \right]^2}{4 (L - R_o)^2} = y^2 \quad (16)$$

Comparing Eq. (16) and Eq. (2), It is evident that

$$\alpha = \frac{(g + x_o)^2 - (L - R_o)^2}{(L - R_o)^2}$$

$$\beta = -(g + x_o) \frac{(g + x_o)^2 - (L - R_o)^2}{(L - R_o)^2} = -(g + x_o) \alpha \quad (17)$$

$$\sigma = \frac{(g + x)^2 - L - R_o)^2}{2 (L - R_o)} = \frac{(L - R_o)^2}{4} \alpha^2$$

Therefore, Equation (2) can be written as:

$$x^2 - (g + x_o) \alpha x + \frac{(L - R_o)^2 \alpha^2}{4} = y^2 \quad (18)$$

From Ref. (3) P. 3, for a 30 db sidelobe Taylor distribution, the ideal beamwidth,  $\theta_o = 60.55^\circ$ , but we want a beamwidth of  $\theta_o = 5^\circ$ ; so

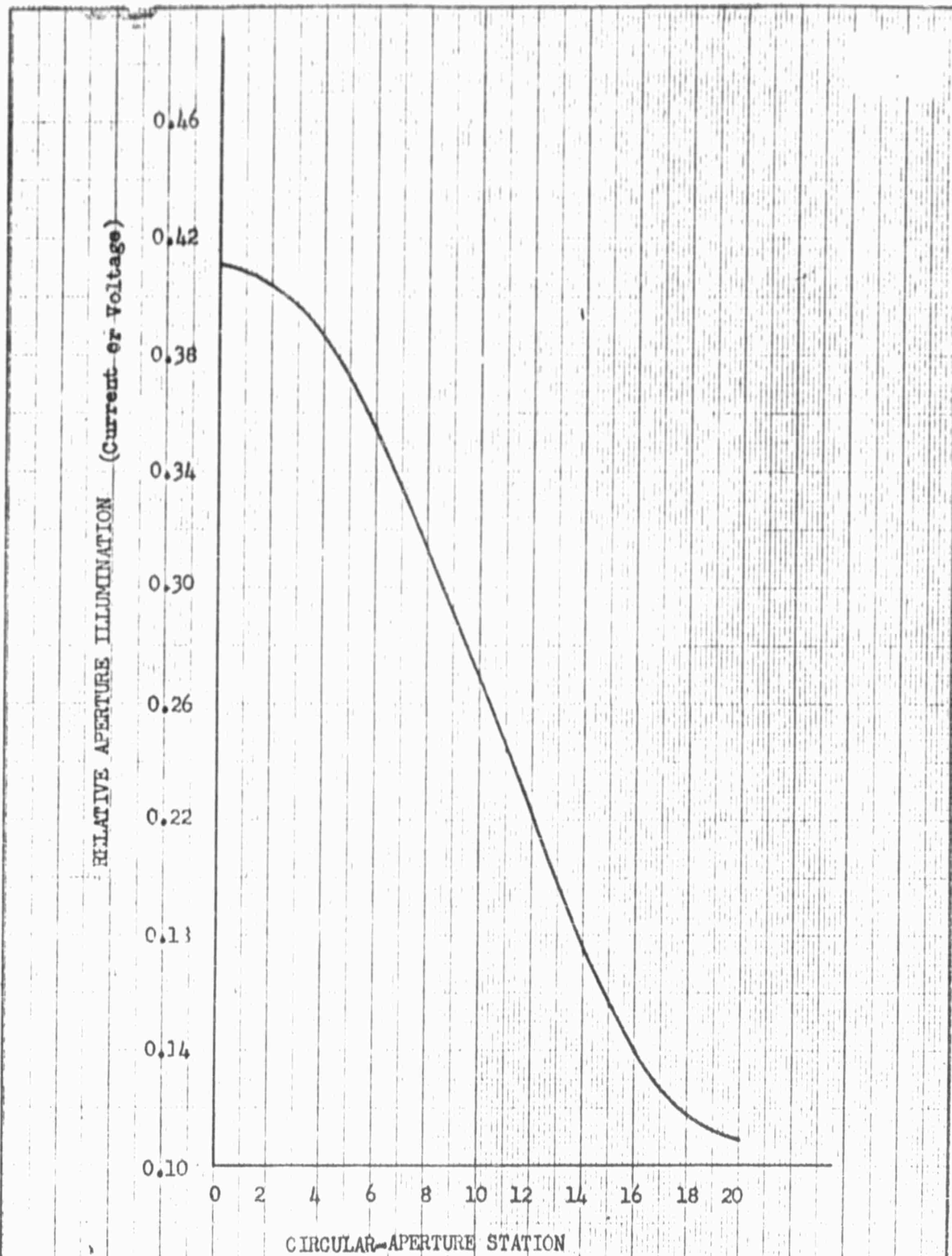
$$\frac{\beta_o}{\theta_o} = \frac{60.55^\circ}{5^\circ} = 12.11 \quad (19)$$

From Ref. (3), P. 6, the above value corresponds closely to  $\bar{n} = 3$  which has an aperture distribution as shown in Figure A-2 and the voltage ratio  $\eta$ , between the center and the edge of the aperture is:

$$\eta = \frac{0.4142}{0.1146} = 3.62 = \frac{1}{0.276} \quad (20)$$

From the radiation pattern of a circular waveguide, It is found that the point with the voltage 0.276 of that of the center makes an angle of  $52^\circ$  with the axis<sup>4</sup>, therefore:

$$g = \frac{a}{\tan 52^\circ} = 0.782 a \quad (21)$$



CALC			REVISED	DATE	CIRCULAR-APERTURE DISTRIBUTION FOR 30 DB SIDELOBES	Fig-A-2
CHECK						D6-7190
APR					BOEING AIRPLANE COMPANY	PAGE 94
APR						

As a rule of thumb, the diameter,  $D$ , of the parabolic antenna with a -30 db sidelobe can be expressed approximately as

$$D = \frac{80 \lambda}{\theta_{(HP)}} = \frac{80 \times 1.54}{5^\circ} = 24.6''$$

where

$\lambda$  = Free space wavelength at 7.7 kmc

$\theta$  = Half power beamwidth

Therefore, the main lobe gain,  $G_m$ , assuming an antenna efficiency,  $\eta$ , of 0.4 is;

$$G_m = \left( \frac{\pi D}{\lambda} \right)^2 \eta = \frac{3.14 \times 24.6^2}{1.54} \times 0.4 = 1000 = 30 \text{ db}$$

For expediency, a 2-foot parabolic disk will be chosen, thus

$$b = \frac{D}{2} = 12''$$

For minimum sidelobe considerations and for a suitable feed dimension, an optimum ratio of  $\frac{a}{b} = 0.16$  was chosen, so

$$a = 0.16 b = 12 \text{ in.} \times 0.16 = 1.92 \text{ in}$$

And the screen coefficient

$$T = 1 - \left( \frac{a}{b} \right)^2 = 1 - 0.256 = 0.9744$$

or 97.44% which will increase the sidelobes from -30 db to -26 db. From Eq. (21) we get

$$g = 0.782a = 1.50144 \text{ in}$$

Substituting the above values into Eq. (13), we can solve for,

$$R = 0.5033 \text{ in}$$

and into Eq. (14), we obtain

$$f = 7.350242 \text{ in}$$

From Eq. (8).

$$x_o = \frac{a(4f^2 - b^2)}{4fb} = 0.392391 \text{ in.}$$

And from Figure A-1 we can solve for the following:

$$R_o = \sqrt{x_o^2 + a^2} = 1.95968 \text{ in.}$$

$$L = \sqrt{g^2 + a^2} = 2.43735 \text{ in.}$$

Substituting the results into Eq. 17, we obtained,

$$\alpha = 14.7184$$

$$\beta = 27.87416$$

$$\gamma = 12.357633$$

Therefore, the equation of the parabola (main reflector) is

$$\rho \cos^2 \frac{\phi}{2} = 7.35024$$

and the equation of the hyperbola (central reflector) is

$$14.7184 x^2 - 27.87416 x + 12.357633 = y^2$$

#### B. Antenna Feed Design

The transition from a rectangular waveguide (RG-51/U) to a cylindrical waveguide antenna feed at 8 kmc can be accomplished by using quarter-wavelength step transformers. As the primary modes in both the circular and the rectangular waveguides are similar (TE-mode), the cylindrical waveguide may be excited directly from the end. However, if the rectangular waveguide is terminated abruptly in the cylindrical waveguide, the VSWR will be high because of the sharp discontinuity at the junction. Therefore, a quarter-wavelength transformer may be used to improve the impedance transformation. Two conducting blocks are used to form the quarter-wavelength step-transformer at the junction of the waveguide (Fig. A-3).

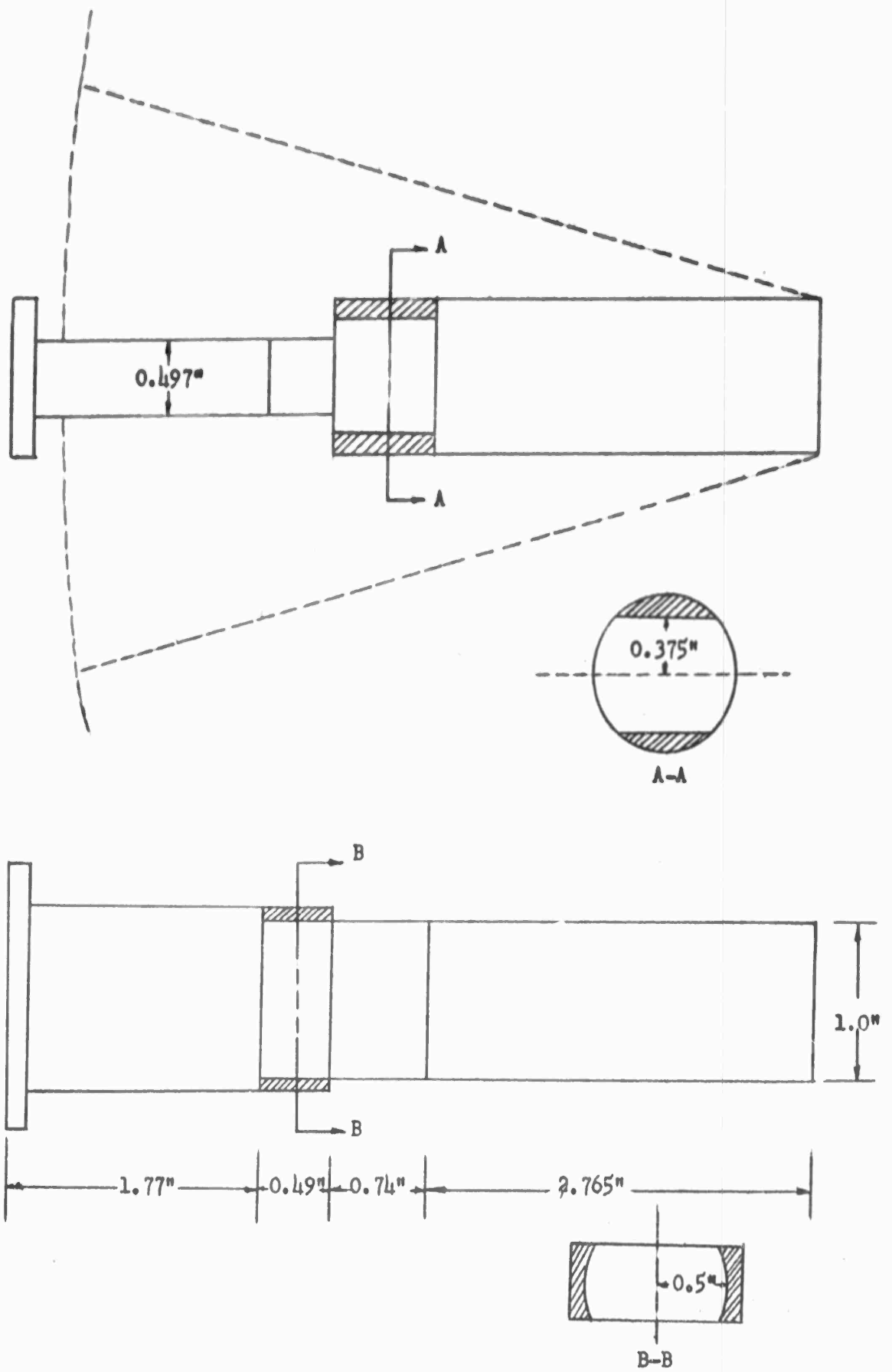


Figure A-3 TRANSITION FROM RECTANGULAR TO CYLINDRICAL  
WAVEGUIDE ANTENNA FEED



### Design Data

#### (1) Rectangular Waveguide - $TE_{10}$ Mode

$$\text{O. D.} \quad a_o = 1.25 \text{ in.}$$

$$b_o = 0.625 \text{ in.}$$

$$\text{I. D.:} \quad a_i = 1.122 \text{ in.}$$

$$b_i = 0.497 \text{ in.}$$

$$\lambda_c = 2a_i = 2.244 \text{ in.}$$

$$f_c = \frac{V_c}{\lambda_c} = 5.263 \text{ kmc}$$

$$\lambda_g = 1.963 \text{ in. (at 8 kmc)}$$

Length of the step transformer,  $L_R$ , is

$$L_R = \frac{\lambda_g}{4} = 0.491 \text{ in.}$$

and the reduced radius,  $R_H$ , in the H-plane is

$$R_H = \frac{1}{2} \left( \frac{a_i}{2} + R \right) = \frac{1}{2} \left( \frac{1.122}{2} + 0.5 \right) = 0.5 \text{ in.}$$

#### (2) Cylindrical Waveguide - $TE_{11}$ Mode

$$\text{I. D.:} \quad R = 0.5 \text{ in.}$$

$$\lambda_c = 3.41 r = 1.705 \text{ in.}$$

$$f_c = 6.928 \text{ kmc}$$

$$\lambda_g = 2.95 \text{ (at 8 kmc)}$$

The length of the step transformer,  $L_c$ , is

$$L_c = \frac{\lambda_g}{4} = 0.74 \text{ in.}$$

and the reduced radius,  $R_E$ , in the E-plane is

$$R_E = \frac{1}{2} \left( \frac{b}{2} + R \right) = \frac{1}{2} \left( \frac{0.497}{2} + 0.5 \right) = 0.375 \text{ in.}$$

### C. Antenna-Feed Tuner

A compound double-screw tuner in the rectangular waveguide is used for antenna impedance tuning. The tuner is a two fixed-position, susceptance-screws spaced one-eighth guide wavelength apart. These screws introduce either inductive or capacitive shunt susceptance at very nearly constant phase. Because of the use of large rounded screws, the depth of insertion for a given reflection is small, thus, the danger of voltage breakdown at the tuner is reduced. To facilitate manual tuning, the tuner section is located close to the back of the paraboloid antenna disk. (Fig. A-4).

### D. VSWR Measurements of the Feed Assembly

The antenna feed assembly consists of a double-screw tuner, a rectangular to circular guide transition, a Teflon pressurizing cap, and an antenna central reflector. (Fig. A-5) The measured input VSWR of the feed assembly without tuning is 1.1 at the design frequency of 8 kmc, but was higher at the transmit (8.35 kmc) and receive (7.75 kmc) frequencies (Fig. A-6a). With proper tuning, using a sweep-frequency reflectometer, the input VSWR was reduced to below 1.1 at both frequencies (Fig. A-6b). The pressurizing cap has negligible effect on the VSWR of the feed.

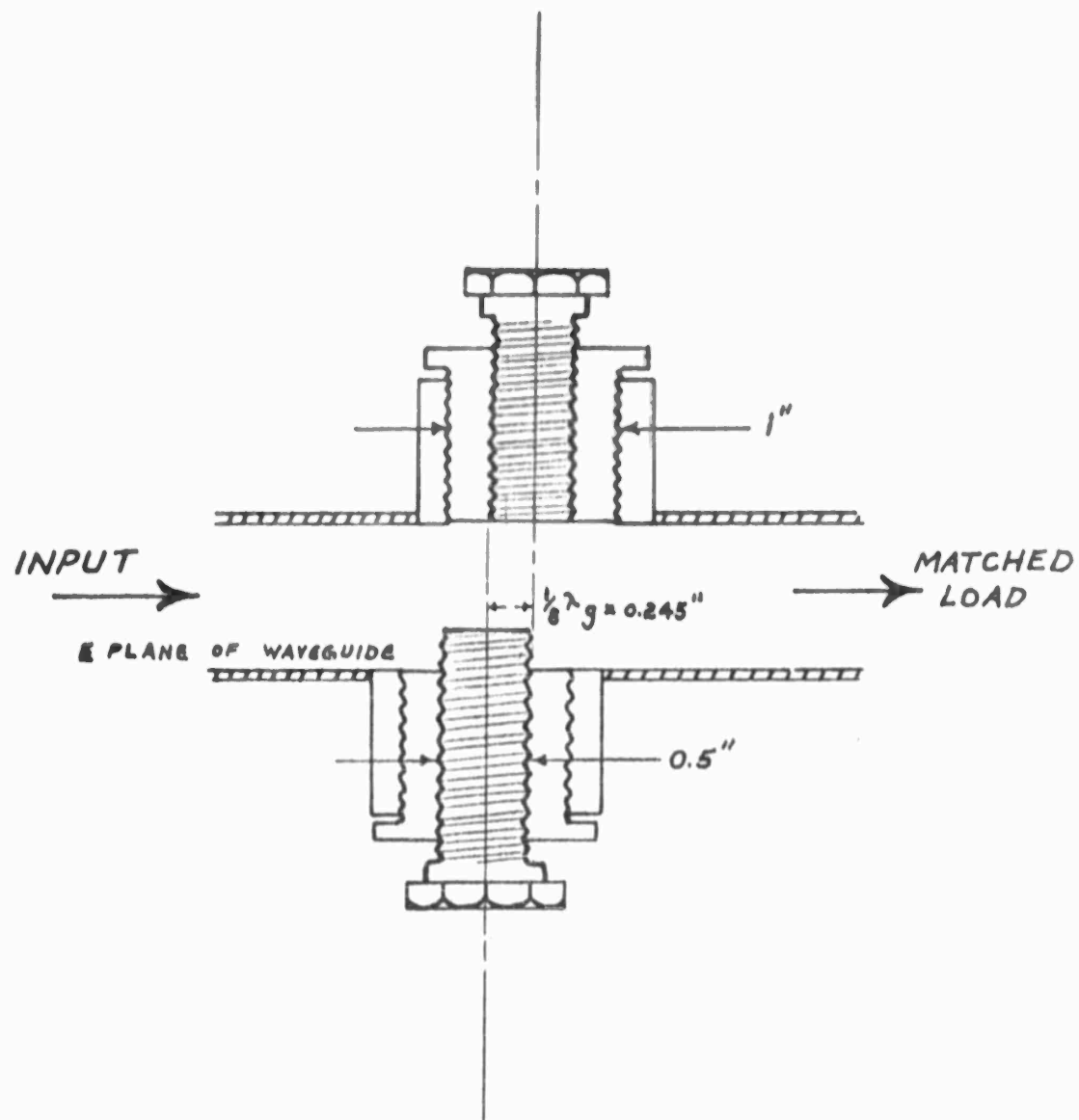
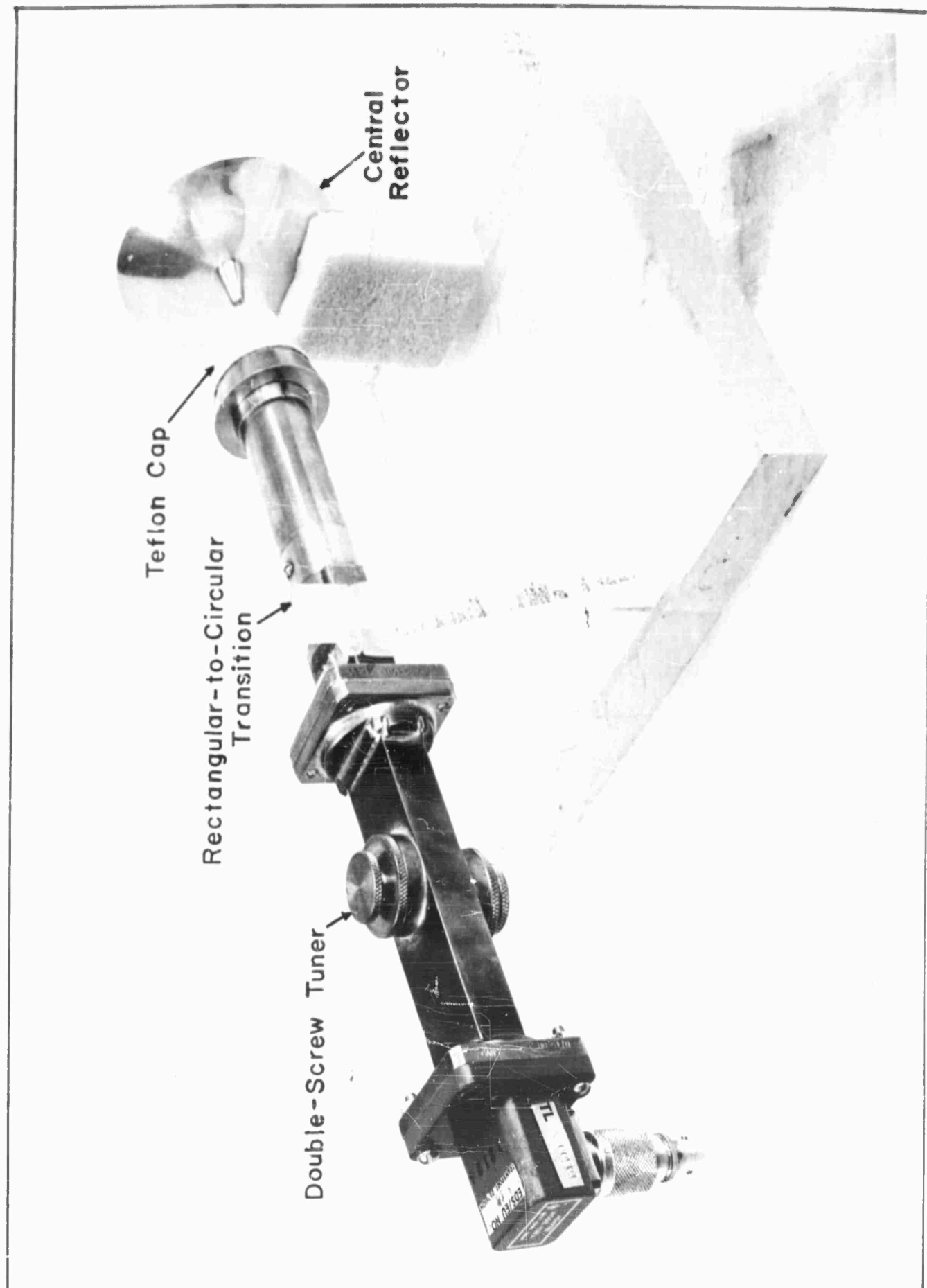
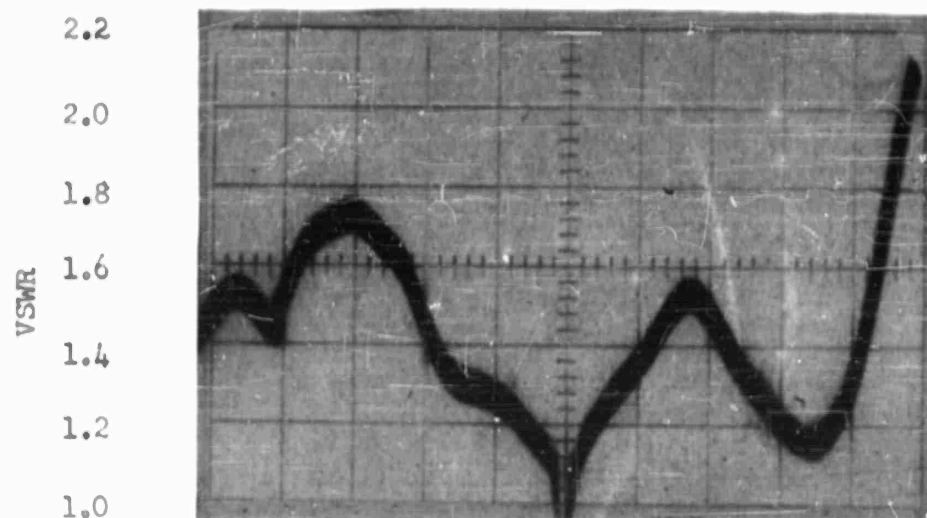


Figure A-4 ANTENNA-FEED TUNER



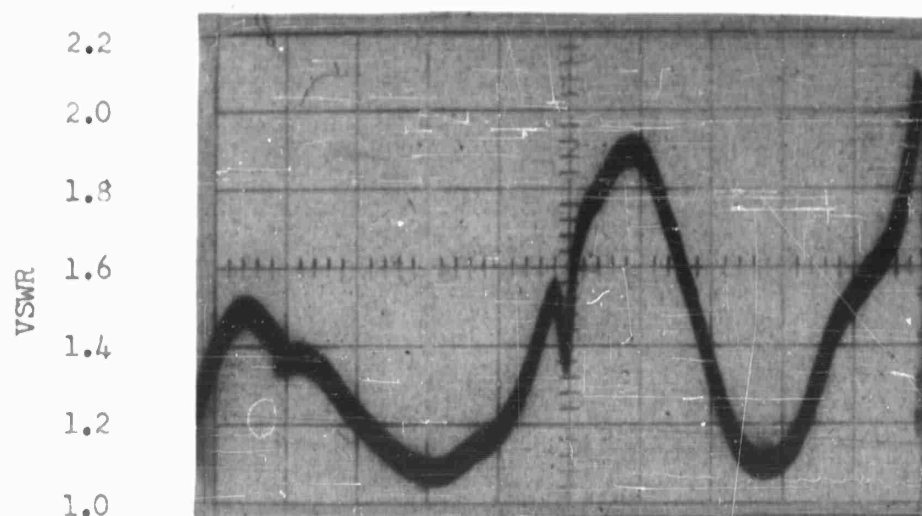
CALC			REVISED	DATE	Antenna Feed Assembly	Fig. A-5
CHECK						D6-7190
APPD						PAGE
APPD						101
					BOEING AIRPLANE COMPANY SEATTLE 24, WASHINGTON	



Note:  
A sharp dip at 8 Kmc  
is due to microswitch  
transient.

7.50 7.75 8.00 8.25 8.50  
Frequency, Kmc

(a) Untuned Antenna Feed Assembly



7.50 7.75 8.00 8.25 8.50  
Frequency, Kmc

(b) Tuned Antenna Feed Assembly

Fig. A-6 MEASURED VSWR OF THE ANTENNA FEED ASSEMBLY

## APPENDIX B

### Calculation of Solar Noise Temperature

The power radiated by a black body of temperature,  $T$ , in a frequency band,  $B$ , can be expressed as<sup>7</sup>

$$P = \frac{2 \pi kTB}{\lambda^2} \text{ watts/m}^2$$

where:

$$\begin{aligned} K &= \text{Boltzmann's constant} = 1.38 \times 10^{-23} \\ \lambda &= \text{wavelength in meter} \\ T &= \text{temperature in Kelvin} \\ B &= \text{bandwidth in cps.} \end{aligned}$$

Therefore, the total power,  $P_s$ , radiated by the sun is:

$$P_s = \frac{2 \pi kTB}{\lambda^2} 4 \pi R^2 \text{ watts} \quad (2)$$

and the solar power density,  $P_r$ , on the earth is:

$$P_r = \frac{2 \pi kTB}{\lambda^2} \left( \frac{R}{D} \right)^2 \text{ watts/m}^2 \quad (3)$$

where:

$$\begin{aligned} R &= \text{radius of the sun} = 8.64 \times 10^5 \text{ miles} \\ D &= \text{sun-to-earth distance} = 93 \times 10^6 \text{ miles.} \end{aligned}$$

For a disturbed sun, the probable maximum noise radiation at 8 kmc is five times that of a black body at 6000°K,<sup>8</sup> thus,  $T$  is 30,000°K. Substituting all numerical values into Equation (3) yields:

$$P_r = 7.45 \times 10^{-27} \frac{30,000}{\lambda^2} B \text{ watts/m}^2 \quad (4)$$

The total noise power intercepted by the antenna beam pointing at the sun can be written as:

$$kT_e B = P_r A = 7.45 \times 10^{-27} \frac{30,000}{\lambda^2} B \frac{g \lambda^2}{4 \pi} \quad (5)$$

where:

$T_e$  = equivalent antenna temperature

$A$  = effective antenna aperture

$g$  = antenna gain.

The equivalent antenna temperature is then reduced to:

$$T_e = 1.3 g^\circ K. \quad (6)$$

If the main beam of the 30-db gain antenna is pointing toward the sun, the antenna temperature will be increased to 1300°K. This would incapacitate the system during the receiving cycle. However, the sun as observed at the earth have an angular diameter of about 0.5 degrees. Consequently, although the black-out is only a temporary or transient nature in satellite communications, it cannot be avoided.

Efforts should be made to minimize the solar noise intercepted by the sidelobe. An increase in the antenna temperature for antennas of various sidelobe level when the sidelobe is pointing toward the sun is tabulated as follows:

<u>Sidelobe Level</u>	<u><math>T_e = 1.3g^\circ K</math></u>
-10 db	130°K
-15	40°
-20	13°
-25	4°
-30	1.3°

## APPENDIX C

### Calculations of Noise Temperature Due to Oxygen and Water Vapor in the Atmosphere

Hogg<sup>16</sup> calculated the effective noise temperature due to atmospheric oxygen and water vapor at the terminal of a high-gain antenna at sea level with a frequency range of 0.5 to 40 kmc. At 8 kmc, the effective temperature increases from about 3° to 120°K as the zenith angle is increased from 0° to 90°. In his calculation, only the first 20 kilometers of the atmosphere were considered.

For airborne antennas at high altitudes, the noise temperature due to oxygen will be much less than that at sea level and that due to water vapor will be negligible since almost no water vapor exist beyond 5 km.

In the following calculations for noise temperature, the first 50 km of the atmosphere will be considered. This will give a truer and a slightly higher temperature than the calculations shown in reference 16. The antenna pattern assumed will be a delta function of response versus angles and therefore, subtends an infinitesimal solid angle. The temperature of such an antenna is given by:<sup>17</sup>

$$T_a = \int_0^{\infty} \alpha_r T_r \exp \left( - \int_0^r \alpha_r dr \right) dr \quad (1)$$

where:

$T_a$  = antenna noise temperature

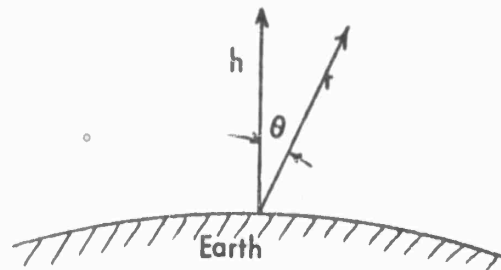
$T$  = temperature at a point  $r$ ,

$\alpha_r$  = power absorption coefficient due to both oxygen and water vapor at a point  $r$ .

For noise temperature calculations at high altitude, the power absorption coefficient,  $\alpha_r$ , will be assumed to be directly proportional to the density,  $\rho_r$ , at that altitude. Figures -1 and -2 are curves of atmosphere temperature and density as a function of altitude plotted from data in the ARDC model atmosphere, 1959.<sup>18</sup> The equation corresponding to each portion of the curve are also shown. The noise temperature,  $T_a$ , can then be calculated by substituting these distribution equations into equation (1).

To evaluate  $T_a$  of an antenna at any altitude,  $h$ , and pointing at any elevation angle,  $\theta$ , Equation (1) can be written as:

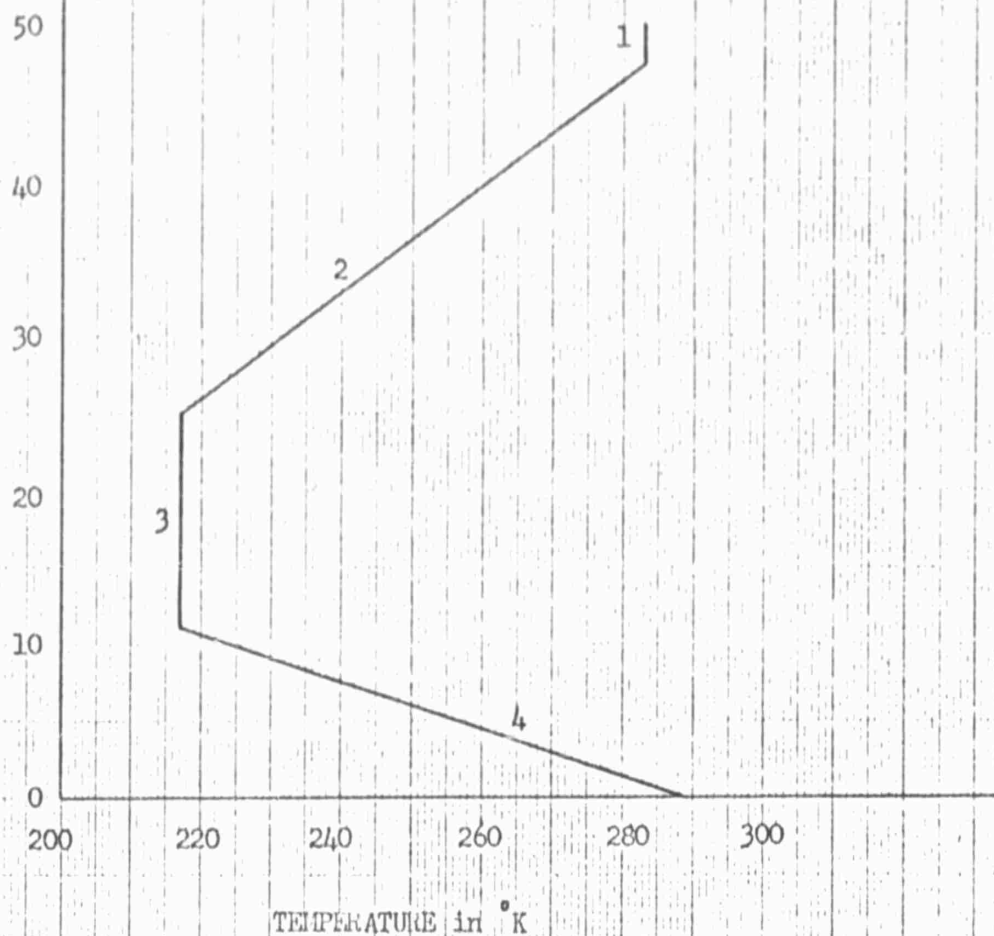
$$T_a = \sec \theta \int_0^{\infty} \alpha_h T_h \exp \left[ - \sec \theta \int_0^h \alpha_h dh \right] dh \quad (2)$$





1.  $T_h = 282.66 \text{ }^\circ\text{K}$  ( $47.4 < h < 53 \text{ Km}$ )
2.  $T_h = [216.78 + 2.941 (h - 25)] \text{ }^\circ\text{K}$  ( $25 < h < 47.4 \text{ Km}$ )
3.  $T_h = 216.78 \text{ }^\circ\text{K}$  ( $11 < h < 25 \text{ Km}$ )
4.  $T_h = [288.16 - 6.4891 h] \text{ }^\circ\text{K}$  ( $0 < h < 11 \text{ Km}$ )

ALTITUDE IN STANDARD GEOPOTENTIAL KILOMETERS



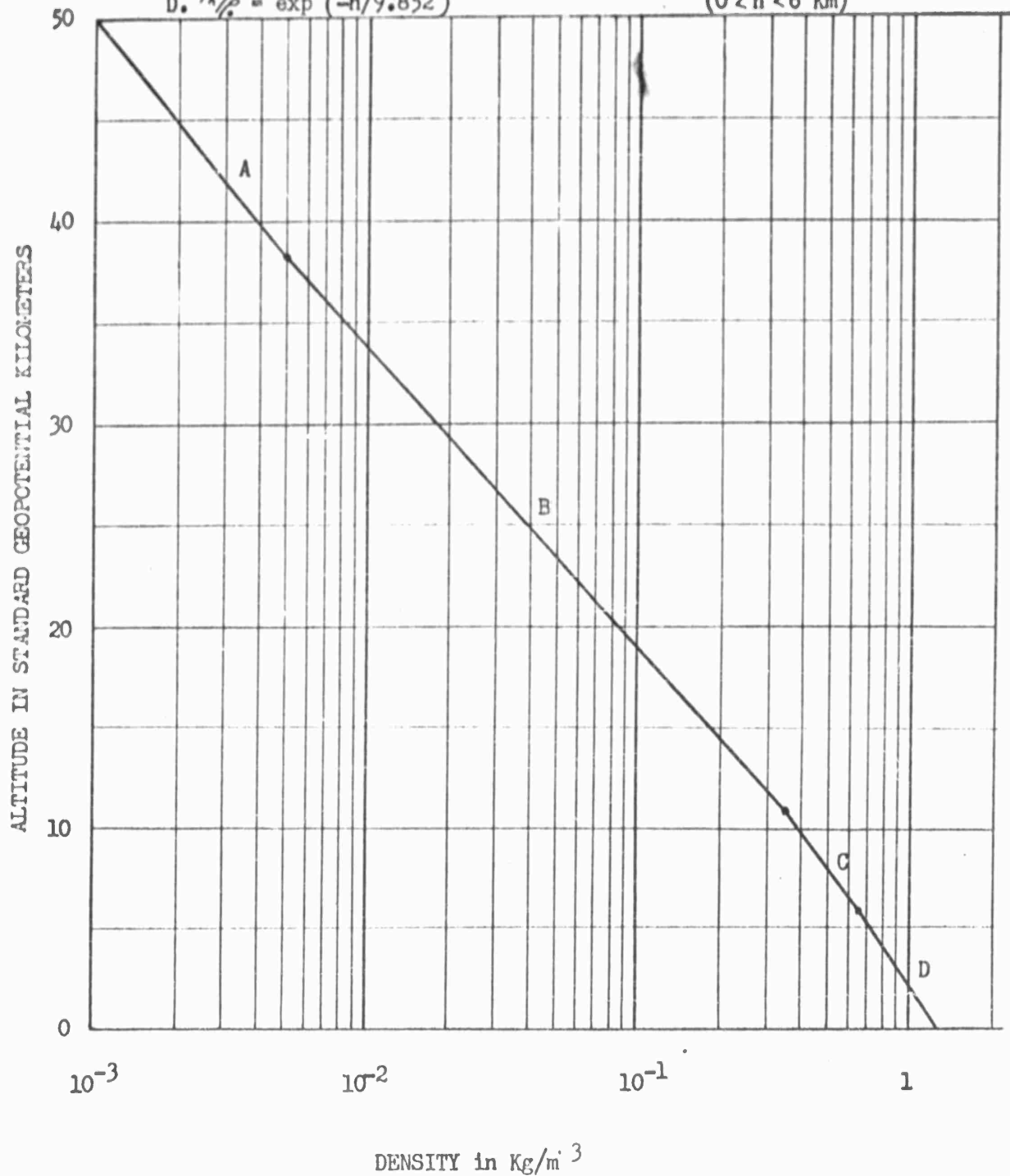
CALC			REVISED	DATE	VARIATION OF ATMOSPHERIC TEMPERATURE WITH ALTITUDE BOEING AIRPLANE COMPANY	Fig. C-1
CHECK						D6-7190
APR						PAGE 106
APR						

$$A. \rho_h/\rho_0 = 0.005321 \exp \left[ \frac{-(h - 38)}{7.6547} \right] \quad (38 < h < 50 \text{ Km})$$

$$B. \rho_h/\rho_0 = 0.300074 \exp \left[ \frac{-(h - 11)}{6.6948} \right] \quad (11 < h < 38 \text{ Km})$$

$$C. \rho_h/\rho_0 = 0.54406 \exp \left[ \frac{-(h - 6)}{8.3893} \right] \quad (6 < h < 11 \text{ Km})$$

$$D. \rho_h/\rho_0 = \exp (-h/9.852) \quad (0 < h < 6 \text{ Km})$$



CALC			REVISED	DATE	VARIATION OF ATMOSPHERIC DENSITY WITH ALTITUDE BOEING AIRPLANE COMPANY SEATTLE 24, WASHINGTON	Fig. C-2
CHECK						D6-7190
APPD						
APPD						PAGE 107

where:

$\alpha_h$  = the absorption coefficient at  $h$ ,

$h$  =  $r/\sec \theta$

$dh$  =  $dr/\sec \theta$

$T_h$  = temperature at the altitude,  $h$ .

Since the absorption coefficient,  $\alpha_h$ , is directly proportional to the density,

$\alpha_h = \alpha_0 \frac{\rho_h}{\rho_0}$ . At 8 kmc, the attenuation of the atmosphere at ground level is about

0.01 db/km, therefore,  $\alpha_0 = 0.002$ .

(1) Evaluation of the integral  $\int_0^h \alpha_h dh$ :

$$\int_0^h \alpha_h dh = \alpha_0 \int_0^h \frac{\rho_h}{\rho_0} dh \quad (3)$$

(a) For  $0 < h < 6$  km

$$\begin{aligned} \int_0^h \alpha_h dh &= 0.002 \int_0^h e^{-\frac{h}{9.852}} dh \\ &= 0.0197 \left[ 1 - e^{-\frac{h}{9.852}} \right] \end{aligned} \quad (4)$$

(b) For  $6 < h < 11$  km

$$\begin{aligned} \int_0^h \alpha_h dh &= \int_0^6 \alpha_h dh + \int_6^h \alpha_h dh \\ &= 0.008982 + 0.002 \int_6^h 0.54406 e^{-\frac{h-6}{8.3893}} dh \\ &= 0.01811 - 0.0091286 e^{-\frac{h-6}{8.3893}} \end{aligned} \quad (5)$$

(c) For  $11 < h < 38$  km

$$\begin{aligned}
 \int_0^h \alpha_h dh &= \int_0^{11} \alpha_h dh + \int_{11}^h \alpha_h dh \\
 &= 0.013075 + 0.002 \int_{11}^h 0.300074 e^{-\frac{h-11}{6.6948}} dh \\
 &= 0.013675 - 0.00060015 e^{-\frac{h-11}{6.6948}}
 \end{aligned} \tag{6}$$

(d) For  $38 < h < 50$  km

$$\begin{aligned}
 \int_0^h \alpha_h dh &= \int_0^{38} \alpha_h dh + \int_{38}^h \alpha_h dh \\
 &= 0.013661 + 0.002 \int_{38}^h 0.005321 e^{-\frac{h-38}{7.6547}} dh \\
 &= 0.013743 - 0.0008146 e^{-\frac{h-38}{7.6547}}
 \end{aligned} \tag{7}$$

(2) Evaluation of  $T_a$  at 20,000 feet (6.096 km)

The noise temperature at 20,000 feet is evaluated by first calculating the temperature  $\Delta T$ , contributed by the first 20,000 feet of the atmosphere.  $T_a$  at 20,000 feet is, then, the noise temperature at sea level minus the differential temperature  $\Delta T$  6.096.

(a) Calculations of  $\Delta T$  up to 6 kilometers:

$$\begin{aligned}
 \Delta T_6 &= \sec \theta \int_0^6 \alpha_h T_h \exp\left[-\sec \theta \int_0^h \alpha_h dh\right] dh \\
 &= \sec \theta \int_0^6 0.002 e^{-\frac{h}{9.852}} (288.16 - 6.4891 h) \cdot
 \end{aligned}$$

$$\exp\left\{-0.0197\left[1 - e^{-\frac{h}{9.852}}\right] \text{Sec } \theta\right\} dh$$

$$\Delta T_6 = \frac{0.57632 \text{Sec } \theta}{e^{0.0197 \text{Sec } \theta}} \int_0^6 e^{-\frac{h}{9.852}} \exp\left[0.0197 \text{Sec } \theta e^{-\frac{h}{9.852}}\right] dh$$

$$- \frac{0.0129782 \text{Sec } \theta}{e^{0.0197 \text{Sec } \theta}} \int_0^6 h e^{-\frac{h}{9.852}} \exp\left[0.0197 \text{Sec } \theta e^{-\frac{h}{9.852}}\right] dh$$

$$\text{Let } x = e^{-\frac{h}{9.852}}, \quad h = -9.852 \log x$$

$$dh = -9.852 \frac{dx}{x}$$

$$\text{At } h=0, x=1; \quad h=6, x=0.54406$$

Substituting the value of  $h$ ,

$$\Delta T_6 = - \frac{5.6779 \text{Sec } \theta}{e^{0.0197 \text{Sec } \theta}} \int_1^{0.54406} e^{0.0197 \text{Sec } \theta x} dx$$

$$- \frac{1.259689 \text{Sec } \theta}{e^{0.0197 \text{Sec } \theta}} \int_1^{0.54406} \log_e x e^{0.0197 \text{Sec } \theta x} dx$$

$$= \frac{-5.6779 \text{Sec } \theta}{e^{0.0197 \text{Sec } \theta}} \left[ \frac{e^{0.0197 \text{Sec } \theta x}}{0.0197 \text{Sec } \theta} \right]_1^{0.54406}$$

$$\begin{aligned}
& - \frac{1.259689 \text{ Sec } \theta}{e^{0.01975 \text{ Sec } \theta}} \left[ \frac{1}{0.01975 \text{ Sec } \theta} \right] \left\{ \left( \log_e x e^{0.01975 \text{ Sec } \theta x} \right)^{0.54406} \right. \\
& \left. - \left[ \log_e |x| + \sum_{n=1}^{\infty} \frac{(0.01975 \text{ Sec } \theta x)^n}{n \cdot n!} \right]^{0.54406} \right\} \\
\Delta T_6 &= \frac{288.218}{e^{0.01975 \text{ Sec } \theta}} \left[ e^{0.01975 \text{ Sec } \theta} - e^{0.010718 \text{ Sec } \theta} \right] \\
& + \frac{63.943594}{e^{0.01975 \text{ Sec } \theta}} \left[ 0.6090134 e^{0.010718 \text{ Sec } \theta} - 0.6090134 \right. \\
& - 0.009 \text{ Sec } \theta - 6.83 \times 10^{-5} \text{ Sec}^2 \theta - 3.5634 \times 10^{-7} \text{ Sec}^3 \theta \\
& \left. - 1.43142 \times 10^{-9} \text{ Sec}^4 \theta \right] \quad (8)
\end{aligned}$$

(b) Calculations of  $\Delta T$  up to 6.096 km (20,000 ft):

$$\begin{aligned}
\Delta T_{6.096} &= \Delta T_6 + \text{Sec } \theta \int_6^{6.096} \alpha_h T_h \exp \left[ -\text{Sec } \theta \int_6^h \alpha_h dh \right] dh \\
&= \Delta T_6 + \text{Sec } \theta \int_6^{6.096} 0.002 \times 0.54406 e^{-\frac{h-6}{8.3893}} \cdot \\
&\quad (288.16 - 6.4891h) \exp \left\{ -\text{Sec } \theta \left[ 0.01811 - \right. \right. \\
&\quad \left. \left. 0.0091286 e^{-\frac{h-6}{8.3893}} \right] \right\} dh \\
\Delta T_{6.096} &= \Delta T_6 + \frac{286.358297}{e^{0.01811 \text{ Sec } \theta}} \left[ e^{0.0091286 \text{ Sec } \theta} - e^{0.0088 \text{ Sec } \theta} \right]
\end{aligned}$$

$$\begin{aligned}
& + \frac{54.09751}{e^{0.01811 \sec \theta}} \left[ 0.72664 e^{0.0088 \sec \theta} - 0.715196 \cdot \right. \\
& e^{0.00919 \sec \theta} - 0.01145 + 3.86 \times 10^{-4} \sec \theta \\
& + 7.37 \times 10^{-7} \sec^2 \theta + 5.208 \times 10^{-9} \sec^3 \theta \\
& \left. + 1.1715 \times 10^{-11} \sec^4 \theta \right] \quad (9)
\end{aligned}$$

(3) Evaluation of  $T_a$  at 40,000 feet (12.192 km)

The procedure used to calculate the noise temperature,  $T_a$ , at 40,000 feet is similar to that used to calculate the noise temperature at 20,000 feet.  $T_a$  at 40,000 feet is, then, the noise temperature at sea level minus the differential temperature  $\Delta T_{12.192}$ . By substituting the equations in Figures C-1 and C-2 into Eq. (10),  $\Delta T$  at 40,000 feet can be calculated.

$$\begin{aligned}
\Delta T_{12.192} &= \sec \theta \int_0^6 \alpha_h T_h \exp \left[ -\sec \theta \int_0^h \alpha_n dn \right] dh \\
&+ \sec \theta \int_6^{12.192} \alpha_h T_h \exp \left[ -\sec \theta \int_0^h \alpha_n dn \right] dh \\
&+ \sec \theta \int_{12.192}^{12.192} \alpha_h T_h \exp \left[ -\sec \theta \int_0^h \alpha_n dn \right] dh \quad (10)
\end{aligned}$$

$$\begin{aligned}
\Delta T_{12.192} &= \sec \theta \int_0^6 0.002 e^{-\frac{h}{9.852}} (288.16 - 6.4891h) \cdot \\
&\exp \left\{ -0.0197 \left[ 1 - e^{-\frac{h}{9.852}} \right] \sec \theta \right\} dh \\
&+ \sec \theta \int_6^{12.192} 0.002 \times 0.54406 e^{-\frac{h-6}{8.3893}} \cdot
\end{aligned}$$

$$\begin{aligned}
& (288.16 - 6.4891h) \exp \left\{ -\sec \theta \left[ 0.01811 - 0.0091286 \cdot \right. \right. \\
& \left. \left. e^{-\frac{h-6}{8.3893}} \right] \right\} dh + \sec \theta \int_{12.192}^{12.192} 0.002 \times 0.54406 \cdot \\
& e^{-\frac{h-6}{8.3893}} (216.78) \exp \left\{ -\sec \theta (0.013765 - \right. \\
& \left. 0.0006 \exp \left[ -\frac{h-11}{6.6948} \right] \right\} dh
\end{aligned}$$

Because of the lengthy numerical computation involved, the calculations of  $\Delta T$  at 40,000 feet will not be included in this paper. The results are tabulated in Table C-1 and C-2.

#### (4) Evaluation of $T_0$ at Sea Level

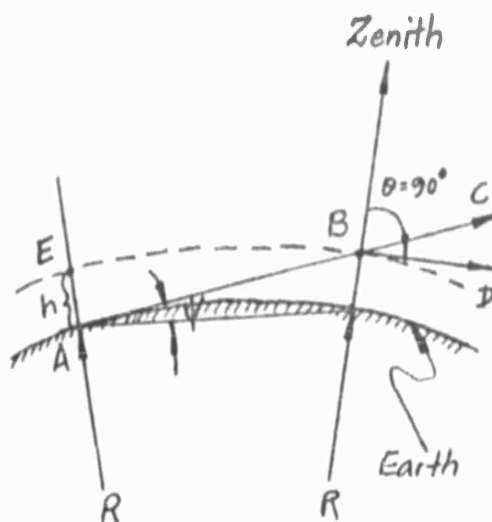
The noise temperature at sea level is evaluated by summing all the contribution of the atmosphere from the sea level to an altitude of 50 kilometers. Beyond this height, the noise contribution is negligibly small. Again, by substituting the equations in Figures C-1 and C-2 into the following equation, the temperature at sea level can be calculated.

$$\begin{aligned}
T_0 = & \sec \theta \int_0^6 \alpha_h T_h \exp \left[ -\sec \theta \int_0^h \alpha_h dh \right] dh \\
& + \sec \theta \int_6^{11} \alpha_h T_h \exp \left[ -\sec \theta \int_0^h \alpha_h dh \right] dh \\
& + \sec \theta \int_{11}^{25} \alpha_h T_h \exp \left[ -\sec \theta \int_0^h \alpha_h dh \right] dh \\
& + \sec \theta \int_{25}^{38} \alpha_h T_h \exp \left[ -\sec \theta \int_0^h \alpha_h dh \right] dh \\
& + \sec \theta \int_{38}^{47.4} \alpha_h T_h \exp \left[ -\sec \theta \int_0^h \alpha_h dh \right] dh \\
& + \sec \theta \int_{47.4}^{50} \alpha_h T_h \exp \left[ -\sec \theta \int_0^h \alpha_h dh \right] dh
\end{aligned} \tag{11}$$



- (5) Evaluation of  $T_a$  at any altitude when the antenna beam is pointing at  $\theta = 90^\circ$ .

When the antenna is pointing at  $\theta = 90^\circ$ ,  $\sec 90^\circ$  becomes infinity, and Equations (8) to (11) cannot be used to evaluate the noise temperature at this angle. However, by taking into account the curvature of the earth it can be shown that  $\sec \theta$  at  $\theta = 90^\circ$ , can be replaced by  $\csc \psi$ .



The figure at the left shows that when the antenna is pointing at the zenith, the noise temperature difference between a point at  $h$  altitude and a point at sea level is the noise contributed by the atmosphere from A to E. When the antenna is pointing at an angle  $\theta = 90^\circ$ , the noise temperature between points A and B is  $AC - BD$ . Since the radius of the earth,  $R$ , is much greater than the altitude,  $h$ , the angle  $CBD$  is very small. Therefore, the noise temperature difference between BC and BD can be neglected, and the noise difference between points at  $h$  altitude and at sea level when the antenna is pointing at  $\theta = 90^\circ$  is that portion of

the noise radiated into the antenna when the beam traverses the distance BA. Therefore, in Equation (2),  $h = r/\sec \theta$  can be replaced by  $h = r/\csc \psi$  without appreciable error when  $\theta = 90^\circ$ . From the geometry,  $\psi$  can be determined as:

$$AB \approx \sqrt{2Rh}$$

$$\csc \psi \approx \frac{AB}{h} \approx \sqrt{\frac{2R}{h}}$$

Substituting  $R = 3960 \times 5280$  feet and  $h = 20,000$  feet.

$$\csc \psi = 45.6, \quad \psi = 1.26^\circ$$

For  $\theta = 90^\circ$ , Equation (2) can be written as,

$$T_a = \csc \psi \int_0^\infty \alpha_n T_n \exp\left[-\csc \psi \int_0^h \alpha_n dh\right] dh \quad (12)$$

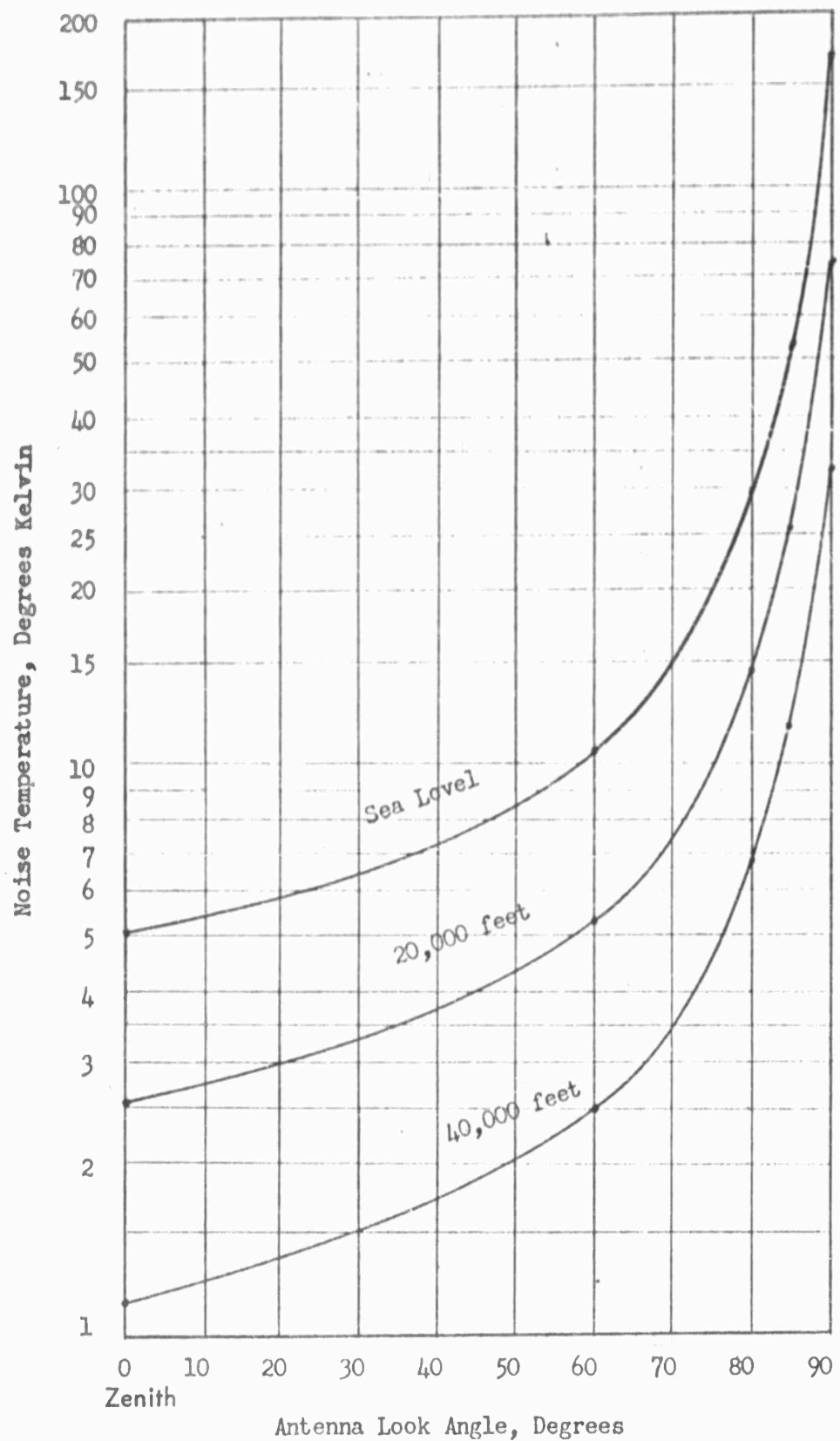
- (6) The results of Equations (8) to (12) for  $\Delta T$  at 6, 6.096 (20,000 ft.), 11, 12.192 (40,000 ft.), 20, 25, 30.48 (100,000 ft.), 38, 47.4 and 50 kilometers for antenna angles  $0^\circ$ ,  $60^\circ$ ,  $80^\circ$ ,  $85^\circ$  and  $90^\circ$  are tabulated in Table C-1. The noise temperature  $T_a$ , due to oxygen and water vapor in the atmosphere at sea level and at altitudes up to 50 km is tabulated in Table C-2 and plotted in Figure C-3.

Table C-1 NOISE TEMPERATURE DIFFERENCE,  $\Delta T$ , BETWEEN  
SEA LEVEL AND DIFFERENT ALTITUDES FOR  
SEVERAL ANTENNA LOOK ANGLES

ALTITUDE (KILOMETERS)	ANTENNA LOOK ANGLE				
	0° zenith	60°	80°	85°	90°
6	2.4165°K	4.7726	13.6232	26.2977	92.1717
6.096	2.5358	4.9891	14.3880	27.5022	93.4537
11	3.7957	7.4901	21.1593	40.3311	128.5322
12.192	3.9388	7.7725	21.9506	41.7736	131.6667
20	4.4175	8.7388	24.5944	46.6460	143.3437
25	4.5397	8.9799	25.2531	47.8616	146.4762
30.48	4.8311	9.7614	27.3402	50.8818	155.9789
38	5.0545	10.2272	28.5427	53.0937	165.2817
47.4	5.0674	10.2568	28.6150	53.2432	165.6197
50	5.0693	10.2607	28.6254	53.2625	165.6677

Table C-2 NOISE TEMPERATURE,  $T_a$ , DUE TO OXYGEN  
AND WATER VAPOR IN THE ATMOSPHERE

ALTITUDE (KILOMETERS)	ANTENNA LOOK ANGLE				
	0°	60°	80°	85°	90°
Sea Level	5.07°K	10.26	28.6	53.3	165.7
6	2.653	5.49	15.0	26.97	73.5
6.096	2.53	5.27	14.21	25.8	72.25
11	1.274	2.77	7.47	12.93	337.14
12.192	1.13	2.49	6.7	11.5	34.1
20	0.652	1.522	4.031	6.617	22.324
25	0.53	1.281	3.372	5.401	19.192
30.48	0.237	0.499	1.285	2.381	9.689
38	0.016	0.034	0.083	0.169	0.386
47.4	0.002	0.004	0.010	0.019	0.053



CALC			REVISED	DATE	NOISE TEMPERATURE, $T_a$ , DUE TO OXYGEN AND WATER VAPOR IN THE ATMOSPHERE	Fig. C-3
CHECK						
APPD						D6-7190
APPD						
					BOEING AIRPLANE COMPANY SEATTLE 24, WASHINGTON	PAGE 17

BAC 973 D-R3

2-7000

## APPENDIX D

### Calculation of Total Equivalent Antenna Temperature

The following equation,<sup>19</sup> was used to evaluate the antenna noise temperature due to atmospheric (oxygen and water vapor) and ground emissions:

$$T_A = \sum_i \bar{T}_i \left( \bar{G}_i \frac{\Delta\theta_i}{2\pi} \right) \quad (1)$$

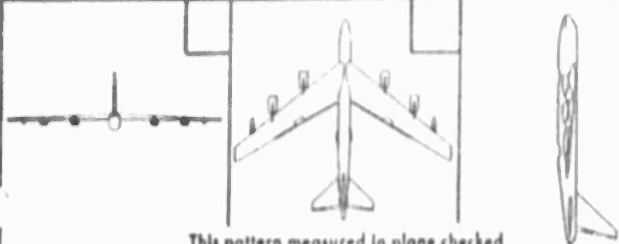
where

- $T_A$  = equivalent antenna temperature
- $T_i$  = directional effective temperature
- $G_i$  = directional gain function
- $\Delta\theta_i$  = Direction of interval angle

The noise temperature is calculated by determining the average temperature of the medium in which the antenna beam is pointing; the average is weighted by the gain function of the antenna.<sup>20</sup> A Cassegrain paraboloid antenna pattern was chosen for the calculation (Fig. D-1). The antenna gain is 30 db and the half-power beam-width is 5 degrees with sidelobes 25 db below the main lobe. The noise temperature contribution from the sidelobes and backlobes pointing toward the earth is greatly reduced because the airframe shields the antenna from ground emission. The reflection coefficient of the airframe is assumed to be 90%.

The percentage of the total power radiated by every five degrees of the antenna pattern in Figure D-1 is tabulated in Table D-1. The pattern is assumed to be symmetrical with respect to the beam angle  $\chi = 0^\circ$  axis;  $\chi = 0^\circ$  is the maximum position of the main beam.

Tables D-2 to D-10 show the incremental contribution of the antenna temperature due to atmospheric and ground emission at altitudes of 40,000 feet, 20,000 feet and sea level. The noise temperature was evaluated at antenna-look angles of  $0^\circ$ ,  $85^\circ$  and  $90^\circ$  respectively. A summary of the results is tabulated in Table D-11.

 <p>This pattern measured in plane checked</p>	FILE NO _____	SHEET _____ OF _____
	PLANE TYPE _____	MODEL SCALE _____
	ANTENNA TYPE <u>Cassegrain Paraboloid Antenna</u>	
	ANTENNA LOCATION _____	
	FREQUENCY FULL SCALE <u>8 kmc</u>	MODEL _____
MODEL SURFACE <u>Aluminum</u>		

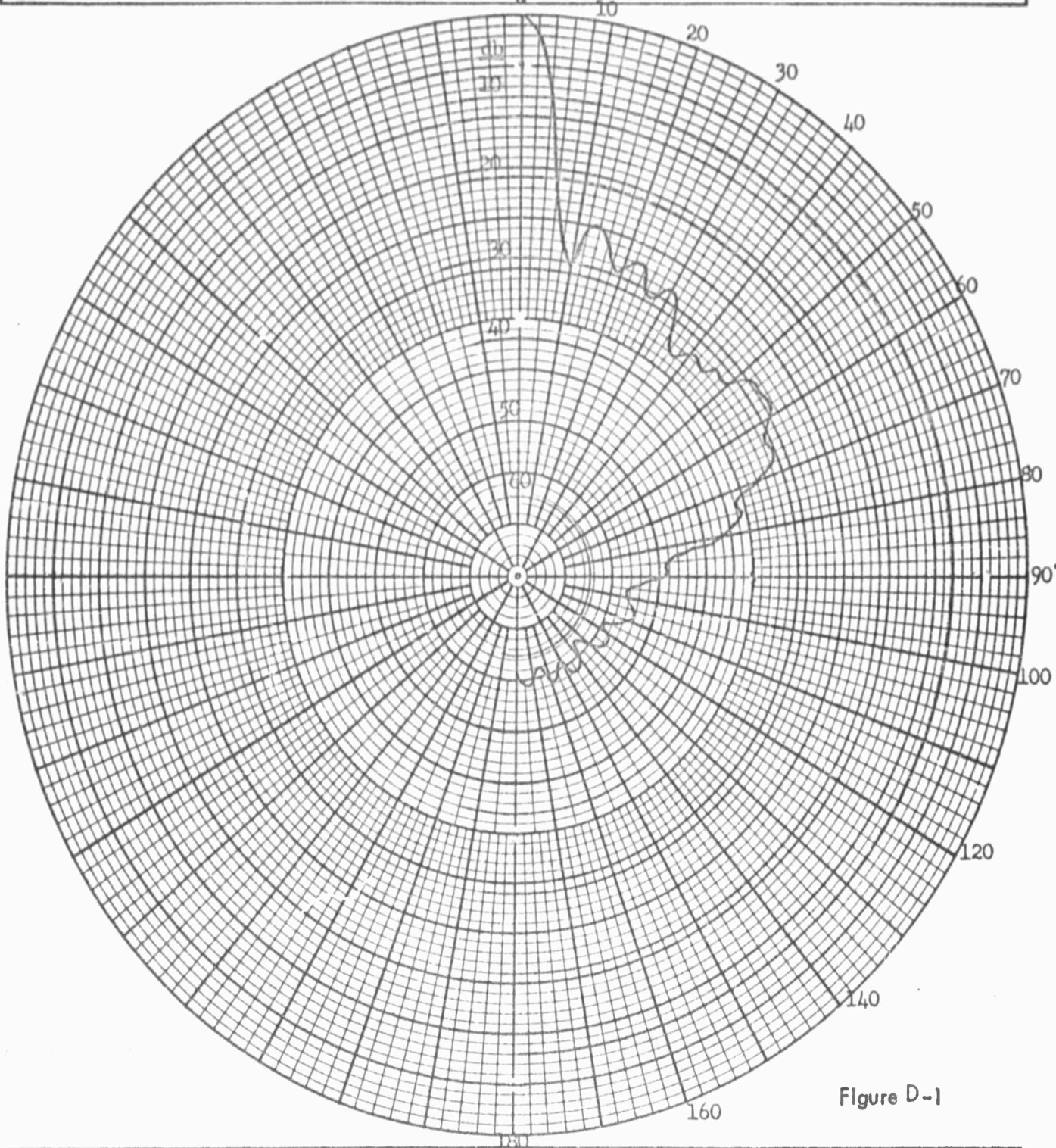


Figure D-1

BOEING AIRPLANE COMPANY	
REMARKS <u>2-Foot Cassegrain Paraboloid</u>	VARIABLE ANGLE $\phi$ ( ), $\theta$ ( )
<u>Antenna Pattern</u>	CONSTANT ANGLE $\phi$ = _____ $\theta$ = _____
OPERATOR _____ DATE _____	POLARIZATION $E_\phi$ ( ), $E_\theta$ ( ), _____
APPROVED _____ DATE _____	$\phi$ = Horizontal angle $\theta$ = Vertical angle
	CURVE PLOTTED IN: VOLTAGE ( ), POWER ( ), DECIBELS (X )

Table D-1 POWER DISTRIBUTION OF THE ANTENNA BEAM  
IN FIG. D-1

PORTION OF THE BEAM $\theta$ , DEGREES	$\bar{G}_1 \frac{\Delta \theta_1}{2\pi}$ PERCENT POWER
0 - 5°	48.316 %
5 - 10	0.2305
10 - 15	0.297
15 - 20	0.1785
20 - 25	0.1065
25 - 30	0.1285
30 - 35	0.0715
35 - 40	0.04225
40 - 45	0.05015
45 - 50	0.0630
50 - 55	0.1255
55 - 60	0.1255
60 - 65	0.0795
65 - 70	0.0630
70 - 75	0.0251
75 - 80	0.00125
80 - 85	0.0025
85 - 90	0.0016
90 - 180°	0.0009 *

\* Uniformly Distributed,  
or 0.0005% per 5°

D6-7190  
120

Table D-2 ANTENNA TEMPERATURE AT 40,000 ft. WHEN  
THE BEAM IS POINTING AT 0° (ZENITH)

$\gamma$ DEGREES	* $\bar{G}_1 \frac{\Delta \theta_1}{2\pi}$	** ATMOSPHERIC EMISSION	GROUND EMISSION	$\bar{G}_1 \bar{T}_1 \frac{\Delta \theta_1}{2\pi}$
0 - 5°	96.632%	1.14°K		1.10161°K
5 - 10	0.461	1.16		0.00535
10 - 15	0.594	1.20		0.00713
15 - 20	0.357	1.25		0.00446
20 - 25	0.373	1.30		0.00485
25 - 30	0.257	1.35		0.00347
30 - 35	0.143	1.40		0.00200
35 - 40	0.0845	1.50		0.00127
40 - 45	0.1003	1.65		0.00166
45 - 50	0.126	1.85		0.00233
50 - 55	0.251	2.10		0.00527
55 - 60	0.251	2.30		0.00577
60 - 65	0.159	3.00		0.00477
65 - 70	0.126	3.20		0.00403
70 - 75	0.0502	4.00		0.00201
75 - 80	0.025	5.50		0.00138
80 - 85	0.005	9.00		0.00045
85 - 90	0.0032	20.00		0.00064
TOTAL -----	99.9982	62.9		1.15845°K
90 - 180°	0.0018	(0.9) $\frac{62.9}{18}$	(0.1) 288	0.00058
	100.000%	$\sum \bar{G}_1 \bar{T}_1 \frac{\Delta \theta_1}{2\pi} = 1.15903°K$		

\* - Values from Table C-1 multiplied by 2 because of symmetry

\*\* - Values from Figure B-3

D6-7190  
121



Table D-3 ANTENNA TEMPERATURE AT 40,000 ft. WHEN  
THE BEAM IS POINTING AT 85°

$\theta$ DEGREES	$\bar{G}_1 \frac{\Delta \theta_1}{2\pi}$	ATMOSPHERIC EMISSION	$\bar{G}_1 \bar{T}_1 \frac{\Delta \theta_1}{2\pi}$
-5 - 0°	48.316 %	20.0°K	9.6632°K
0 - 5	48.316	9.0	4.134844
5 - 10	0.2305	5.5	0.0126775
10 - 15	0.297	4.0	0.01188
15 - 20	0.1785	3.2	0.005712
20 - 25	0.1865	3.0	0.005595
25 - 30	0.1285	2.3	0.002955
30 - 35	0.0715	2.1	0.0015015
35 - 40	0.04225	1.85	0.0007816
40 - 45	0.05015	1.65	0.0008275
45 - 50	0.0630	1.5	0.000915
50 - 55	0.1255	1.4	0.001757
55 - 60	0.1255	1.35	0.001694
60 - 65	0.0795	1.3	0.001036
65 - 70	0.0630	1.25	0.0007875
70 - 75	0.0251	1.2	0.0003012
75 - 80	0.0125	1.16	0.0001450
80 - 85	0.0025	1.14	0.0000285
85 - 90	0.0016	1.14	0.00001824
90 - 95	0.00005	1.16	
95 - 100		1.2	
100 - 105		1.25	
105 - 110		1.3	
110 - 115		1.35	
115 - 120		1.4	
120 - 125		1.5	
125 - 130		1.65	
130 - 135		1.85	
135 - 140		2.1	
140 - 145		2.3	
145 - 150		3.0	
150 - 155		3.2	
155 - 160		4.0	
160 - 165		5.5	
165 - 170		9.0	
170 - 175		20.0	
		61.76	0.00003088
	$\Sigma \bar{G}_1 \bar{T}_1 \frac{\Delta \theta_1}{2\pi} = 14.0573^\circ K$		

Table D-3 (cont'd)

$-\theta$ DEGREES	$\bar{G}_i \frac{\Delta \theta_i}{2\pi}$	ATMOSPHERIC EMISSION	$\bar{G}_i \bar{T}_i \frac{\Delta \theta_i}{2\pi}$
5 - 10°	0.2305 %	20.0°K	0.0461°K
10 - 15	0.2970	9.0	0.02673
15 - 20	0.1785	5.5	0.009818
20 - 25	0.1865	4.0	0.00746
25 - 30	0.1285	3.2	0.004112
30 - 35	0.0715	2.0	0.002145
35 - 40	0.04225	2.3	0.0009718
40 - 45	0.05015	2.1	0.0010532
45 - 50	0.0630	1.85	0.0011655
50 - 55	0.1255	1.65	0.0020708
55 - 60	0.1255	1.5	0.0018825
60 - 65	0.0795	1.4	0.001113
65 - 70	0.0630	1.35	0.0008505
70 - 75	0.0251	1.3	0.0003263
75 - 80	0.0125	1.25	0.0001563
80 - 85	0.0025	1.2	0.000030
85 - 90	0.0016	1.16	0.0000186
90 - 95	0.00005	1.14	
95 - 100		1.14	
100 - 105		1.16	
105 - 110		1.2	
110 - 115		1.25	
115 - 120		1.3	
120 - 125		1.35	
125 - 130		1.4	
130 - 135		1.5	0.00003205
135 - 140		1.65	
140 - 145		1.85	
145 - 150		2.1	
150 - 155		2.3	
155 - 160		3.0	
160 - 165		3.2	
165 - 170		4.0	
170 - 175		5.5	
175 - 180		9.0	
180 - 185		20.0	

1.68405 %

Noise Temperature from  
the Earth Direction for  
a shield of 100% refl. = 0.0993216°K

For:

$$90\% \text{ refl. } (0.9) 0.0993216 = 0.08939$$

$$10\% \text{ grd. } (0.1) 0.01684 \times 288 = 0.48500$$

$$\sum \bar{G}_i \bar{T}_i \frac{\Delta \theta_i}{2\pi} \text{ } -5^\circ \text{ to } -185^\circ = 0.57439^\circ\text{K}$$

Total Ant. Temperature:

$$\sum \bar{G}_i \bar{T}_i \frac{\Delta \theta_i}{2\pi} = 14.0573 + 0.57439 = \underline{\underline{14.6317^\circ\text{K}}}$$

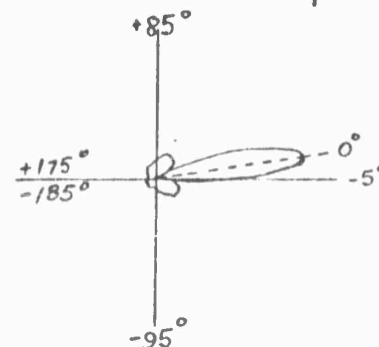


Table D-4 ANTENNA TEMPERATURE AT 40,000 ft. WHEN  
THE BEAM IS POINTING AT 90°

$\gamma$ DEGREES	$\bar{\alpha}_1 \frac{\Delta\theta_1}{2\pi}$	ATMOSPHERIC EMISSION	GROUND EMISSION	$\bar{\alpha}_1 \bar{T}_1 \frac{\Delta\theta_1}{2\pi}$
0 - 5°	48.316 %	20.0 °K		9.6632 °K
5 - 10	0.2305	9.0		0.020745
10 - 15	0.297	5.5		0.016335
15 - 20	0.1785	4.0		0.007140
20 - 25	0.1865	3.2		0.005968
25 - 30	0.1285	3.0		0.003855
30 - 35	0.0715	2.3		0.001645
35 - 40	0.04225	2.1		0.000887
40 - 45	0.05015	1.85		0.000928
45 - 50	0.06200	1.65		0.001039
50 - 55	0.1255	1.5		0.001883
55 - 60	0.1255	1.4		0.001757
60 - 65	0.0795	1.35		0.001073
65 - 70	0.063	1.3		0.000819
70 - 75	0.0251	1.25		0.000314
75 - 80	0.0125	1.2		0.000150
80 - 85	0.0025	1.16		0.000029
85 - 90	0.0016	1.14		0.000018
90 - 95	0.00005	1.14		
95 - 100		1.16		
100 - 105		1.2		
105 - 110		1.25		
110 - 115		1.3		
115 - 120		1.35		
120 - 125		1.4		
125 - 130		1.5		
130 - 135		1.65		
135 - 140		1.85		
140 - 145		2.1		
145 - 150		2.3		
150 - 155		3.0		
155 - 160		3.2		
160 - 165		4.0		
165 - 170		5.5		
170 - 175		9.0		
175 - 180		20.0		
		62.9		
TOTAL	50.00 %	125.8 °K		9.7278 °K
180 - 360°	50.00 %		(0.1)288	14.4000
		(0.9) 9.7278		8.7550
	100.00 %	$\sum \bar{\alpha}_1 \bar{T}_1 \frac{\Delta\theta_1}{2\pi} =$		32.883 °K

Table D-5 ANTENNA TEMPERATURE AT 20,000 ft. WHEN  
THE BEAM IS POINTING AT 0° (ZENITH)

$\theta$ DEGREES	* $\bar{G}_1 \frac{\Delta\theta_1}{2\pi}$	*** ATMOSPHERIC EMISSION °K	GROUND EMISSION	$G_1 T_1 \frac{\Delta\theta_1}{2\pi}$ °K
0 - 5°	96.632%	2.60		2.512432
5 - 10	0.461	2.70		0.012447
10 - 15	0.594	2.80		0.016632
15 - 20	0.357	2.85		0.010175
20 - 25	0.373	2.90		0.010817
25 - 30	0.257	3.10		0.007967
30 - 35	0.143	3.30		0.004719
35 - 40	0.0845	3.40		0.002873
40 - 45	0.1003	3.70		0.003711
45 - 50	0.126	4.00		0.005040
50 - 55	0.251	4.40		0.011044
55 - 60	0.251	5.00		0.012550
60 - 65	0.159	5.80		0.009222
65 - 70	0.126	7.00		0.008820
70 - 75	0.0502	9.00		0.004518
75 - 80	0.025	12.00		0.00300
80 - 85	0.005	20.00		0.00100
85 - 90	0.0032	50.00		0.00160
	99.9982%	144.55 °K		2.647566 °K
90 - 180°	0.00180	(0.9) $\frac{144.5}{18}$	(0.1) 288	0.00065
	100.000 %	$\sum \bar{G}_1 \bar{T}_1 \frac{\Delta\theta_1}{2\pi}$		= 2.648216 °K

\* - Values from Table C-1 multiplied by 2 because of symmetry

\*\*\* - Values from Figure B-3

Table D-6 ANTENNA TEMPERATURE AT 20,000 ft. WHEN  
THE BEAM IS POINTING AT 85°

$\gamma$ DEGREES	$\bar{G}_1 \frac{\Delta \theta_1}{2\pi}$	ATMOSPHERIC EMISSION	$\bar{G}_1 \bar{T}_1 \frac{\Delta \theta_1}{2\pi}$
-5 - 0	48.316%	50.0 °K	24.158 °K
0 - 5	48.316	20.0	9.6632
5 - 10	0.2305	12.0	0.02766
10 - 15	0.2970	9.0	0.02673
15 - 20	0.1785	7.0	0.012495
20 - 25	0.1865	5.8	0.010817
25 - 30	0.1285	5.0	0.006425
30 - 35	0.0715	4.4	0.003146
35 - 40	0.04225	4.0	0.0016896
40 - 45	0.05015	3.7	0.0018555
45 - 50	0.0630	3.4	0.002142
50 - 55	0.1255	3.3	0.0041415
55 - 60	0.1255	3.1	0.0038905
60 - 65	0.0795	2.9	0.0023055
65 - 70	0.0630	2.85	0.0017955
70 - 75	0.0251	2.8	0.0007028
75 - 80	0.0125	2.7	0.0003375
80 - 85	0.0025	2.6	0.000065
85 - 90	0.0016	2.6	0.0000416
90 - 95	0.00005	2.7	
95 - 100		2.8	
100 - 105		2.85	
105 - 110		2.9	
110 - 115		3.1	
115 - 120		3.3	
120 - 125		3.4	
125 - 130		3.7	
130 - 135		4.0	
135 - 140		4.4	
140 - 145		5.0	
145 - 150		5.8	
150 - 155		7.0	
155 - 160		9.0	
160 - 165		12.0	
165 - 170		20.0	
170 - 175		50.0	
	98.31595%	$\sum \bar{G}_1 \bar{T}_1 \frac{\Delta \theta_1}{2\pi} = 34.62674^\circ \text{K}$	

. Table D-6 Cont'd

$-\gamma$ DEGREES	$\bar{G}_1 \frac{\Delta \theta_1}{2 \pi}$	ATMOSPHERIC EMISSION	$\bar{G}_1 \bar{T}_1 \frac{\Delta \theta_1}{2}$
5 - 10	0.2305%	50.0 °K	0.11525 °K
10 - 15	0.2970	20.0	0.05940
15 - 20	0.1785	12.0	0.02142
20 - 25	0.1865	9.0	0.016785
25 - 30	0.1285	7.0	0.008995
30 - 35	0.0715	5.8	0.004147
35 - 40	0.04225	5.0	0.0021125
40 - 45	0.05015	4.4	0.0022066
45 - 50	0.0630	4.0	0.002520
50 - 55	0.1255	3.7	0.0046435
55 - 60	0.1255	3.4	0.004267
60 - 65	0.0795	3.3	0.0026235
65 - 70	0.0630	3.1	0.001953
70 - 75	0.0251	2.9	0.0007279
75 - 80	0.0125	2.85	0.00035625
80 - 85	0.0025	2.8	0.000070
85 - 90	0.0016	2.7	0.0000432
90 - 95	0.00005	2.6	0.0000013
95 - 100		2.6	
100 - 105		2.7	
105 - 110		2.8	
110 - 115		2.85	
115 - 120		2.9	
120 - 125		3.1	
125 - 130		3.3	
130 - 135		3.4	
135 - 140		3.7	
140 - 145		4.0	
145 - 150		4.4	
150 - 155		5.0	
155 - 160		5.8	
160 - 165		7.0	
165 - 170		9.0	
170 - 175		12.0	
175 - 180		20.0	
180 - 185		50.0	
	1.68405%	144.55	0.00007228
		Noise Temperature from the earth direction for a shield of 100% refl.	0.247594 °K

For:

$$90\% \text{ refl. } (0.9) 0.247594 = 0.22285$$

$$10\% \text{ grd. } (0.1) 0.01684 \times 288 = 0.48500$$

$$\sum \bar{G}_1 \bar{T}_1 \frac{-5^\circ \text{ to } -185^\circ}{2 \pi} = 0.70785 \text{ °K}$$

D6-7190

127

Total Ant. Temperature:

$$\sum \bar{G}_1 \bar{T}_1 \frac{\Delta \theta_1}{2 \pi} = 34.6267 + 0.7078 = 35.3345 \text{ °K}$$

Table D-7 ANTENNA TEMPERATURE AT 20,000 ft. WHEN  
THE BEAM IS POINTING AT 90°

DEGREES	$\bar{G}_1 \frac{\Delta \theta_1}{2\pi}$	ATMOSPHERIC EMISSION	GROUND EMISSION	$\bar{G}_1 \bar{T}_1 \frac{\Delta \theta_1}{2\pi}$
0 - 5°	48.316 %	50.0 °K		24.1580 °K
5 - 10	0.2305	20.0		0.0461
10 - 15	0.2970	12.0		0.03564
15 - 20	0.1785	9.0		0.016065
20 - 25	0.1865	7.0		0.013055
25 - 30	0.1285	5.8		0.007453
30 - 35	0.0715	5.0		0.003575
35 - 40	0.04225	4.4		0.001859
40 - 45	0.05015	4.0		0.002006
45 - 50	0.0630	3.7		0.002331
50 - 55	0.1255	3.4		0.004267
55 - 60	0.1255	3.3		0.004142
60 - 65	0.0795	3.1		0.002465
65 - 70	0.0630	2.9		0.001827
70 - 75	0.0251	2.85		0.0007154
75 - 80	0.0125	2.8		0.000350
80 - 85	0.0025	2.7		0.0000675
85 - 90	0.0016	2.6		0.0000416
90 - 95	0.00005	2.6		
95 - 100		2.7		
100 - 105		2.8		
105 - 110		2.85		
110 - 115		2.9		
115 - 120		3.1		
120 - 125		3.3		
125 - 130		3.4		
130 - 135		3.7		
135 - 140		4.0	144.55	0.00007228
140 - 145		4.4		
145 - 150		5.0		
150 - 155		5.8		
155 - 160		7.0		
160 - 165		9.0		
165 - 170		12.0		
170 - 175		20.0		
175 - 180		50.0		
	50.00 %			24.3 °K
180 - 360°	50.00 %		(0.1)288	14.400
		(0.9) 24.3		21.87
	100.00 %		$\sum \bar{G}_1 \bar{T}_1 \frac{\Delta \theta_1}{2\pi} =$	60.57 °K

Table D-8 ANTENNA TEMPERATURE AT SEA LEVEL WHEN  
THE BEAM IS POINTED AT 0° (ZENITH)

$\gamma$ DEGREES	* $\bar{\sigma}_1 \frac{\Delta \theta_1}{2\pi}$	** ATMOSPHERIC EMISSION	GROUND EMISSION	$\bar{\sigma}_1 \bar{T}_1 \frac{\Delta \theta_1}{2\pi}$
0 - 5°	96.632 %	5.2 °K		5.024864 °K
5 - 10	0.461	5.3		0.024433
10 - 15	0.594	5.4		0.032076
15 - 20	0.357	5.6		0.019992
20 - 25	0.373	5.9		0.022007
25 - 30	0.257	6.2		0.015934
30 - 35	0.143	6.5		0.009275
35 - 40	0.0845	7.0		0.005915
40 - 45	0.1003	7.5		0.0075225
45 - 50	0.126	8.0		0.010080
50 - 55	0.251	8.7		0.021837
55 - 60	0.251	9.7		0.024347
60 - 65	0.159	11.5		0.018285
65 - 70	0.126	13.0		0.016380
70 - 75	0.0502	16.5		0.008283
75 - 80	0.0250	23.0		0.005750
80 - 85	0.0050	40.0		0.00200
85 - 90	0.0032	110.0		0.00352
	<u>109.9982 %</u>	<u>295.0</u>		<u>5.27252</u>
90 - 180°	0.00180	(0.9) $\frac{295}{18}$	(0.1)288	0.00078
	<u>100.000 %</u>	$\sum \bar{\sigma}_1 \bar{T}_1 \frac{\Delta \theta_1}{2\pi} =$		<u>5.27330 °K</u>

\* - Values from Table C-1 multiplied by 2 because of symmetry

\*\* - Values from Figure B-3

D6-7190

129



Table D-9 ANTENNA TEMPERATURE AT SEA LEVEL WHEN  
THE BEAM IS POINTING AT 85°

$\gamma$ DEGREES	$\bar{\theta}_1 \frac{\Delta \theta_1}{2\pi}$	ATMOSPHERIC EMISSION	$\bar{\theta}_1 \bar{T}_1 \frac{\Delta \theta_1}{2\pi}$
-5 - 0°	48.316 %	110.0 °K	53.1476 °K
0 - 5	48.316	40.0	19.3264
5 - 10	0.2305	23.0	0.058015
10 - 15	0.297	16.5	0.049005
15 - 20	0.1785	13.0	0.023205
20 - 25	0.1865	11.5	0.0214475
25 - 30	0.1285	9.7	0.0124645
30 - 35	0.0715	8.7	0.0062205
35 - 40	0.04225	8.0	0.003380
40 - 45	0.05015	7.5	0.0037612
45 - 50	0.0630	7.0	0.004410
50 - 55	0.1255	6.5	0.0079625
55 - 60	0.1255	6.2	0.007595
60 - 65	0.0795	5.9	0.0046905
65 - 70	0.0630	5.6	0.003528
70 - 75	0.0251	5.4	0.001355.
75 - 80	0.0125	5.3	0.0006625
80 - 85	0.0025	5.2	0.000130
85 - 90	0.0016	5.2	0.0000832
90 - 95	0.00005	5.3	
95 - 100		5.4	
100 - 105		5.6	
105 - 110		5.9	
110 - 115		6.2	
115 - 120		6.5	
120 - 125		7.0	
125 - 130		7.5	
130 - 135		8.0	
135 - 140		8.7	
140 - 145		9.7	
145 - 150		11.5	
150 - 155		13.0	
155 - 160		16.5	
160 - 165		23.0	
165 - 170		40.0	
170 - 175		110.0	
	98.315957%	$\sum \bar{\theta}_1 \bar{T}_1 \frac{-5^\circ \text{ to } +175^\circ}{2\pi} = 289.8$	72.677061 °K

(D-9 cont'd)

$-\theta$ DEGREES	$\bar{G}_1 \frac{\Delta \theta_1}{2\pi}$	ATMOSPHERIC EMISSION	$\bar{G}_1 \bar{T}_1 \frac{\Delta \theta_1}{2\pi}$
5 - 10	0.2305%	110.0°K	0.25355°K
10 - 15	0.2970	40.0	0.11880
15 - 20	0.1785	23.0	0.041055
20 - 25	0.1865	16.5	0.0307725
25 - 30	0.1285	13.0	0.016705
30 - 35	0.0715	11.5	0.0082225
35 - 40	0.04225	9.7	0.0040982
40 - 45	0.05015	8.7	0.00436305
45 - 50	0.0630	8.0	0.005040
50 - 55	0.1255	7.5	0.0094125
55 - 60	0.1255	7.0	0.008785
60 - 65	0.0795	6.5	0.0051675
65 - 70	0.0630	6.2	0.003905
70 - 75	0.0251	5.9	0.0014809
75 - 80	0.0125	5.6	0.00070
80 - 85	0.0025	5.4	0.000135
85 - 90	0.0016	5.3	0.0000848
90 - 95	0.00005	5.2	0.0000026
95 - 100		5.2	
100 - 105		5.3	
105 - 110		5.4	
110 - 115		5.6	
115 - 120		5.9	
120 - 125		6.2	
125 - 130		6.5	
130 - 135		7.0	
135 - 140		7.5	0.0001475
140 - 145		8.0	
145 - 150		8.7	
150 - 155		9.7	
155 - 160		11.5	
160 - 165		13.0	
165 - 170		16.5	
170 - 175		23.0	
175 - 180		40.0	
180 - 185		110.0	
	1.68405 %		
Noise Temperature from the Earth Direction for a Shield of 100 % Reflectivity			= 0.512428°K

For:

$$\begin{aligned}
 90 \% \text{ refl.} & \quad (0.9) 0.512428 = 0.461185 \\
 10 \% \text{ grd.} & \quad (0.1) 0.01684 \times 288 = 0.485000
 \end{aligned}$$

$$\sum \bar{G}_1 \bar{T}_1 \frac{-5^\circ \text{ to } -185^\circ}{2\pi} = 0.946185^\circ\text{K}$$

D6-7190

131

Total Ant. Temperature:

$$\sum \bar{G}_1 \bar{T}_1 \frac{\Delta \theta_1}{2\pi} = 72.67706 + 0.94619 = \underline{\underline{73.62325^\circ\text{K}}}$$

Table D-10

ANTENNA TEMPERATURE AT SEA LEVEL, WHEN  
THE BEAM IS POINTING AT 90°

$\theta$ DEGREES	$\bar{G}_1 \frac{\Delta \theta_1}{2\pi}$	ATMOSPHERIC EMISSION	GROUND EMISSION	$\bar{G}_1 \bar{T}_1 \frac{\Delta \theta_1}{2\pi}$
0 - 5°	48.316 %	110.0 °K		53.1476 °K
5 - 10	0.2305	40.0		0.0922
10 - 15	0.2970	23.0		0.06831
15 - 20	0.1785	16.5		0.0294525
20 - 25	0.1865	13.0		0.024245
25 - 30	0.1285	11.5		0.0147775
30 - 35	0.0715	9.7		0.0069355
35 - 40	0.04225	8.7		0.0036575
40 - 45	0.05015	8.0		0.004012
45 - 50	0.0630	7.5		0.004725
50 - 55	0.1255	7.0		0.008785
55 - 60	0.1255	6.5		0.0081575
60 - 65	0.0795	6.2		0.004929
65 - 70	0.0630	5.9		0.003717
70 - 75	0.0251	5.6		0.0014050
75 - 80	0.0125	5.4		0.000675
80 - 85	0.0025	5.3		0.0001325
85 - 90	0.0016	5.2		0.0000832
90 - 95	0.00005	5.2		
95 - 100		5.3		
100 - 105		5.4		
105 - 110		5.6		
110 - 115		5.9		
115 - 120		6.2		
120 - 125		6.5		
125 - 130		7.0		
130 - 135		7.5	295	
135 - 140		8.0		0.0001475
140 - 145		8.7		
145 - 150		9.7		
150 - 155		11.5		
155 - 160		13.0		
160 - 165		16.5		
165 - 170		23.0		
170 - 175		40.0		
175 - 180		110.0		
	50.000 %			53.77515 °K
180 - 360°	50.000 %		(0.1)288	14.4000
		(0.9) 53.77515		48.39764
	100.000 %			
$\sum \bar{G}_1 \bar{T}_1 \frac{\Delta \theta_1}{2\pi} =$				116.573 °K

Table D-11 SUMMARY OF ANTENNA TEMPERATURE DUE TO  
ATMOSPHERIC AND GROUND EMISSIONS

ANTENNA LOOK ANGLE		SOURCE OF NOISE TEMPERATURE			TOTAL ANTENNA NOISE TEMPERATURE °K
		ATMOSPHERIC EMISSION °K	GROUND EMISSION		
			95% refl. °K	10% grd °K	
Sea Level {	0°	5.273	0.00055	0.00052	5.27 °K
	85°	72.677	0.4612	0.490	73.62
	90°	53.775	48.3976	14.40	116.57
20,000 Ft. {	0°	2.65	0.000539	0.00052	2.65
	85°	34.6	0.2230	0.490	35.30
	90°	24.3	21.870	14.40	60.57
40,000 Ft. {	0°	1.1585	0.00056	0.00052	1.16
	85°	14.060	0.0890	0.490	14.64
	90°	9.730	8.760	14.40	32.90

## APPENDIX E

### High-Power Testing of Microwave Components

The components in the airborne antenna system must withstand 10-kw cw power at 8.35 kmc. However, no such high power testing facility is available at either Boeing or at electronics firms offering the components. Varian Associates, makers of super-power klystrons, has offered to test some of these components but were unable to do so before the end of January 1961.

To simulate 10-kw cw-power in the microwave band, a traveling-wave circulator maybe used.<sup>32</sup> However, at X-band, the loss in a traveling-wave circulator severely limits the power multiplication. The multiplication factor in an existing RG-52/U T-W circulator was less than 6 under testing conditions. However, a power multiplication of 20 was needed to simulate 10-kw with the 500-watt klystron available at Boeing.

A standing-wave resonator with losses small compared to those in the device under test was built. A novel feature was the variable iris for controlling the resonator coupling, thus permitting maximum multiplication with minimum input VSWR. Power multiplications of up to 20 were achieved, depending on losses in the device under test. (Figs. E-1 and E-2).

The klystron operates at a fixed frequency of 9.5 kmc, with a peak power of 2. kw, and an average power of 600 watts. Components designed for the 9.-10.-kmc band (RG-52/U) were tested; from these results, the performance of similar designs scaled to the 8-kmc band (RG-51/U) can be inferred. Only low-loss components can be tested effectively since lossy components would lower the Q of the resonator and reduce its multiplication factor. Likewise, antennas and antenna feeds being two-terminal devices, can not be tested in this manner because they radiate power.

Some of the components tested are as follow:

1. TE-TEM-TE Rotary Joint (Teflon support)

This waveguide rotary joint was supplied by DeMornay-Bonardi. The transition between the RG-51/U waveguides is a coaxial section supported by Teflon. The joint was subjected to one kilowatt cw power at 9.5 kmc for a duration of three minutes. The heat generated in the center conductor and the surrounding teflon melted the conductor & charred the teflon. Figure E-3 is a photograph of the burn-down rotary joint.

2. TE-TEM-TE Rotary Joint (T-bar support)

This joint was manufactured by Western Electric Company and was obtained from military surplus. The transition between the RG-51/U waveguides is a coaxial section but the center conductor is supported by a T-bar located in one of the waveguides. It was subjected to six-kilowatt cw power at 9.5 kmc for a duration of one hour. The external surface of the joint was heated to approximately 220°F and the center conductor heated until its silver-soldered parts melted. This joint is better than the preceding

one because there is no dielectric heating involved. However, it fails to meet the 10-kw requirement. Center-conductor cooling would doubtless raise the power capacity of this joint, but is difficult to achieve by an external blower.

### 3. TE-TM-TE Rotary Joint

The joint tested was manufactured by Premier Microwave Corporation and was obtained from military surplus. The circular waveguide transition between the RG-52/U rectangular waveguides has a narrow bandwidth and is designed to operate at 9.3 to 9.4 kmc. It was subjected to five-kilowatt cw power for 15 minutes and then to ten kilowatts for another 15 minutes. The heat generated by the joint was dissipated with two blowers. Except for the heating, no effect on the electric characteristics was observed. Upon dismantling of the joint after the test, it was noticed that the rubber washer in the joint was melted but no other part was damaged or discolored (Fig. E-4a).

Upon request, Premier sent Boeing a compact, aluminum, TE-TM-TE mode, rotary joint for use with RG-51/U. The joint is designed to operate at a 9.3-9.4 kmc. It was subjected to about 10 kw cw power at 9.5 kmc for a period of 30 minutes. The heat generated by the joint was dissipated by a 150-watt air blower. The temperature rise was 120°F. No effect on the electrical or physical characteristics of the joint was observed after the test (Fig. E-4b). Therefore, it can be concluded that this type of rotary joint can withstand the required cw power because it does not suffer dielectric heating nor does it have highly concentrated currents within the joint.

### 4. Teflon Windows

Two Teflon windows of 0.03-inch and 0.06 inch thickness were tested. The window was placed in the transverse plane within a RG-52/U waveguide resonator, one-quarter guide wavelength from a shunting plunger. The 0.03-inch window was subjected to six-kilowatt cw power for about 20 minutes. Softening of the teflon was observed at the center portion of the window where the electric field is maximum. The 0.06-inch window was subjected to approximately 10-kilowatt cw power for 10 minutes. The center portion of the window was melted (Fig. E-5). Even in the larger RG-51/U waveguide, or in the 1-inch circular guide, the performance of a Teflon window would be marginal because of dielectric heating.

### 5. Teflon Cap

#### a. Voltage Breakdown

A .03-inch thick hemispherical teflon cap placed at the aperture of the circular antenna feed was tested for voltage breakdown in a vacuum chamber (Fig. E-6). The cap was under sea level pressure on one side and up to 90,000 feet altitude

air pressure on the other side. A peak power level of about 50-kw, two micro-second pulse at 8100 mc was applied to the cap for a period of five minutes at each 10,000 feet altitude interval and for a period of 30 minutes at 90,000 feet. No voltage breakdown or corona was observed.

b. Dielectric Heating

No X-band, 10-kw, cw-power is available for testing the dielectric heating of the Teflon cap. To simulate similar heating conditions, a 0.03-inch thick Tenite cap was used. Tenite has the same softening temperature as Teflon but is 200 times as lossy at X-band. The cap was subjected to 90 watts average power at 8100 mc for a duration of one hour. No deformation of the cap was observed. There was slight dielectric heating of the Tenite but the temperature rise in the material was well within the tolerable level. The degree of dielectric heating generated in the Tenite is approximately that of Teflon of the same thickness if subjected to 18-kw power. Related tests on various dielectric thicknesses (.06" -- .25") showed greater temperature rises with the thicker samples; therefore, Teflon caps no greater than .03" should be used.

c. Air Pressure

The .03-inch Teflon cap was pressure tested up to 30 psig without rupture or deformation. Thus, the cap will withstand the waveguide pressure of 15 psig or 15-30 psi at altitude.

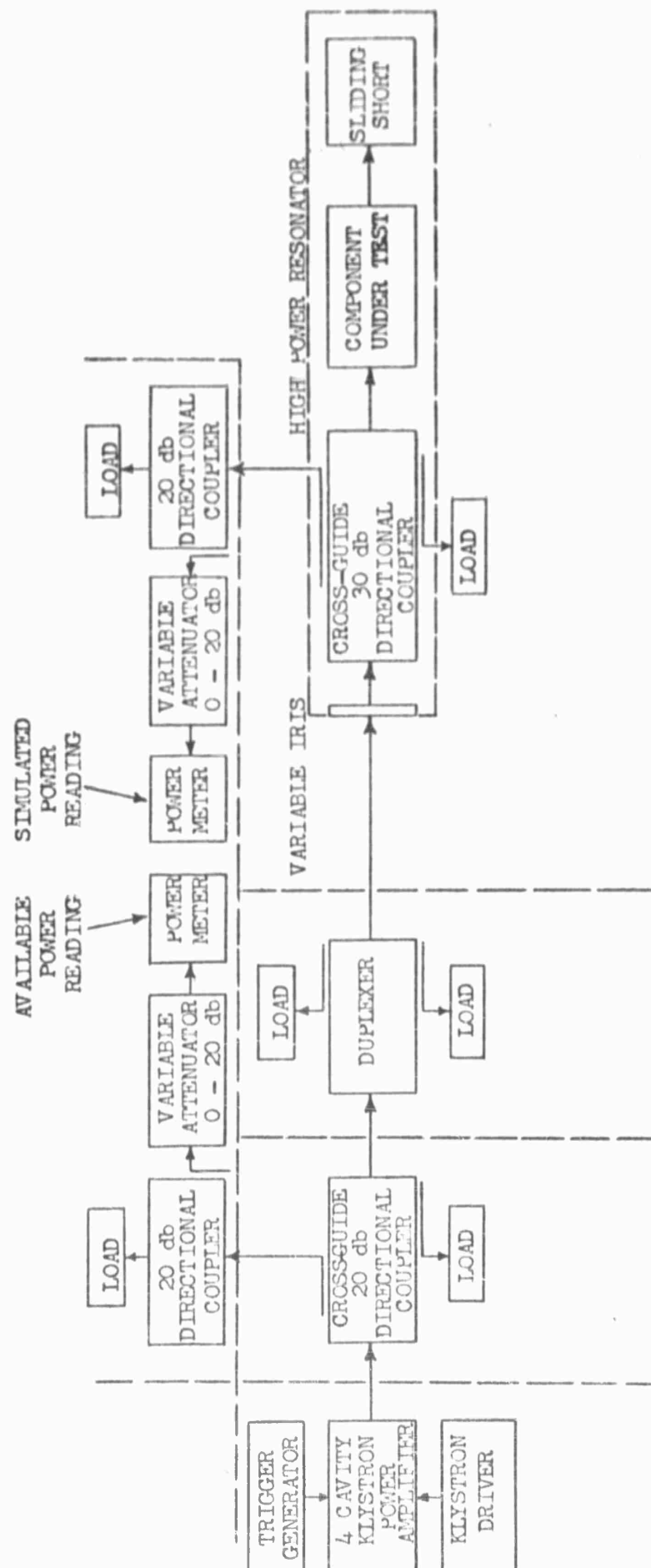


Fig. E-1 BLOCK DIAGRAM OF HIGH POWER TEST SET-UP



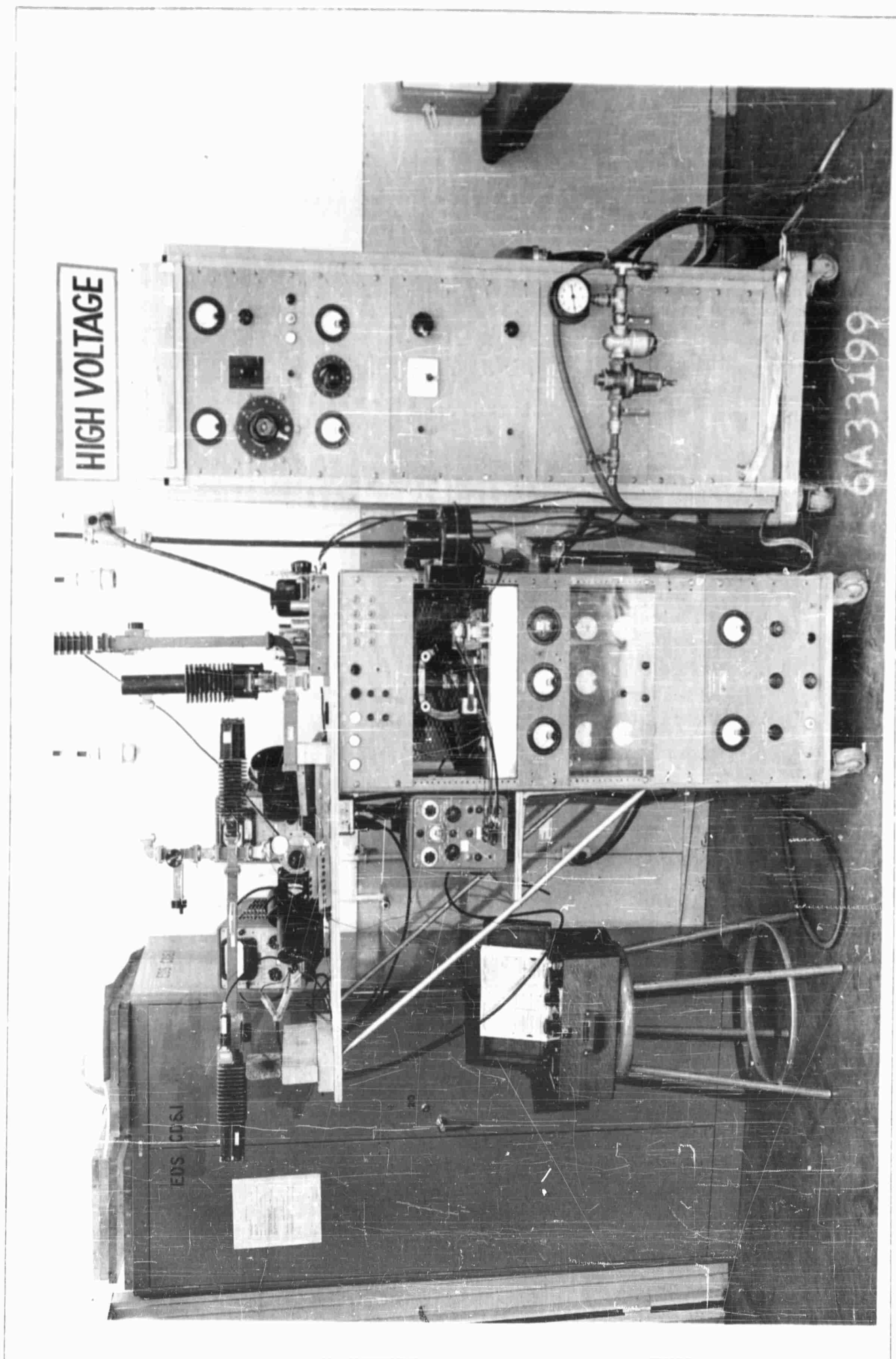


Fig. E-2 PHOTOGRAPH OF HIGH-POWER TEST SET-UP

BAC 1546 L-R3

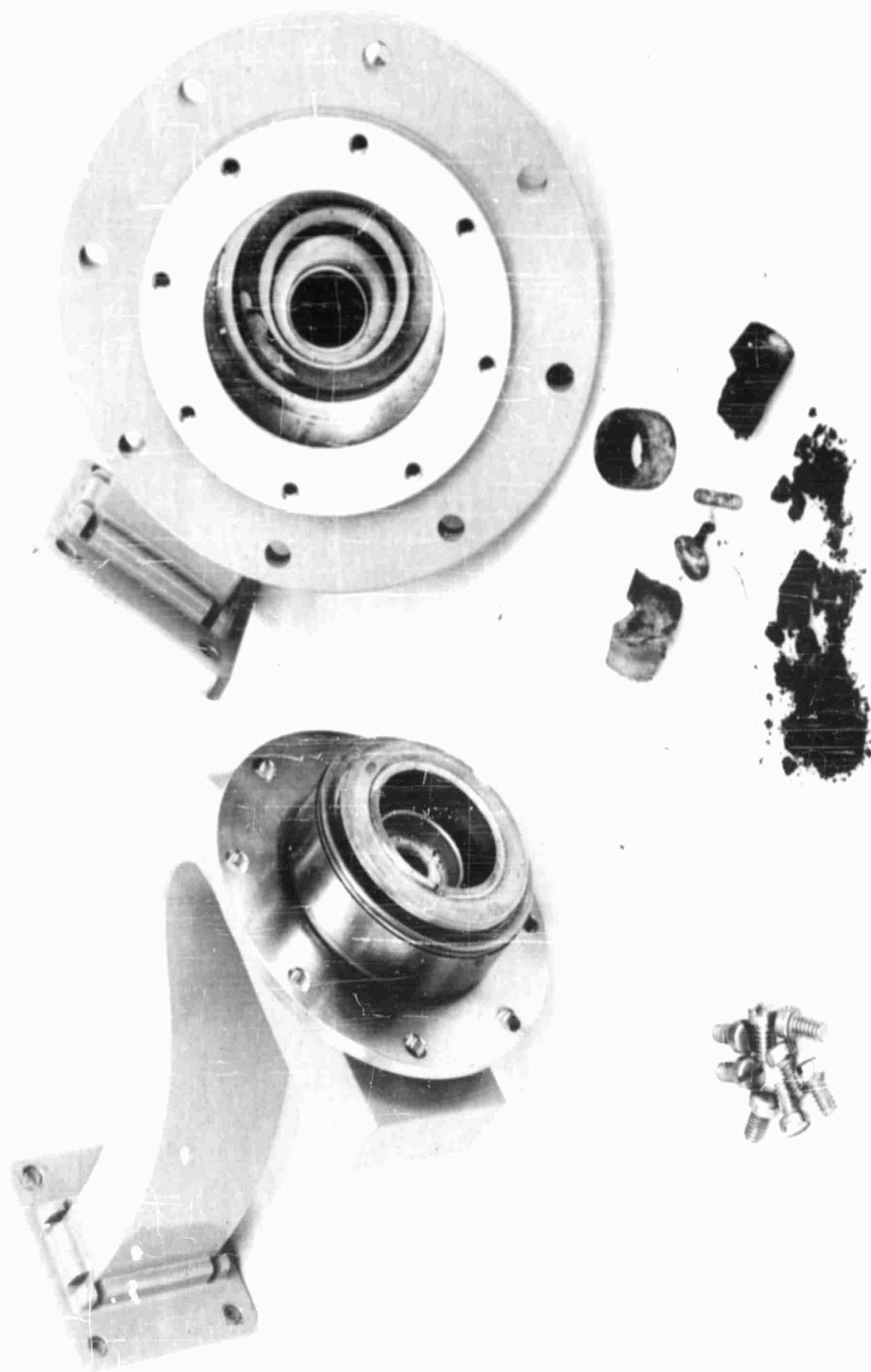


Figure E-3 TE-TEM-TE Rotary Joint with Teflon Support After Breakdown

CALC			REVISED	DATE		
CHECK						
APPD						D6-7190
APPD					BOEING AIRPLANE COMPANY SEATTLE 24, WASHINGTON	PAGE 139

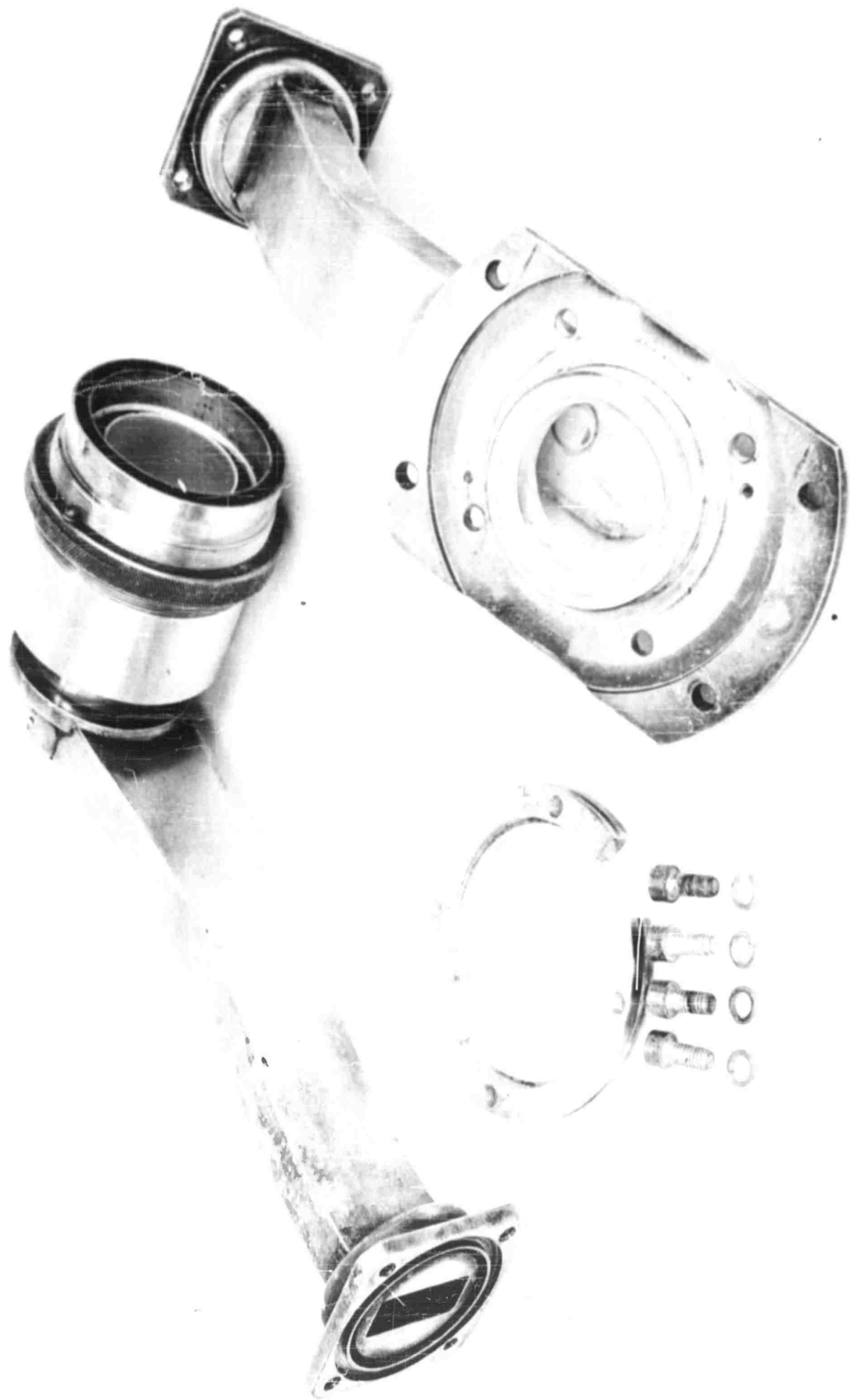


Figure E-4a TE-TM-TE Rotary Joint (For RG-52/U)

CALC			REVISED	DATE		
CHECK						
APPD						D6-7190
APPD						
					BOEING AIRPLANE COMPANY SEATTLE 24, WASHINGTON	PAGE 140

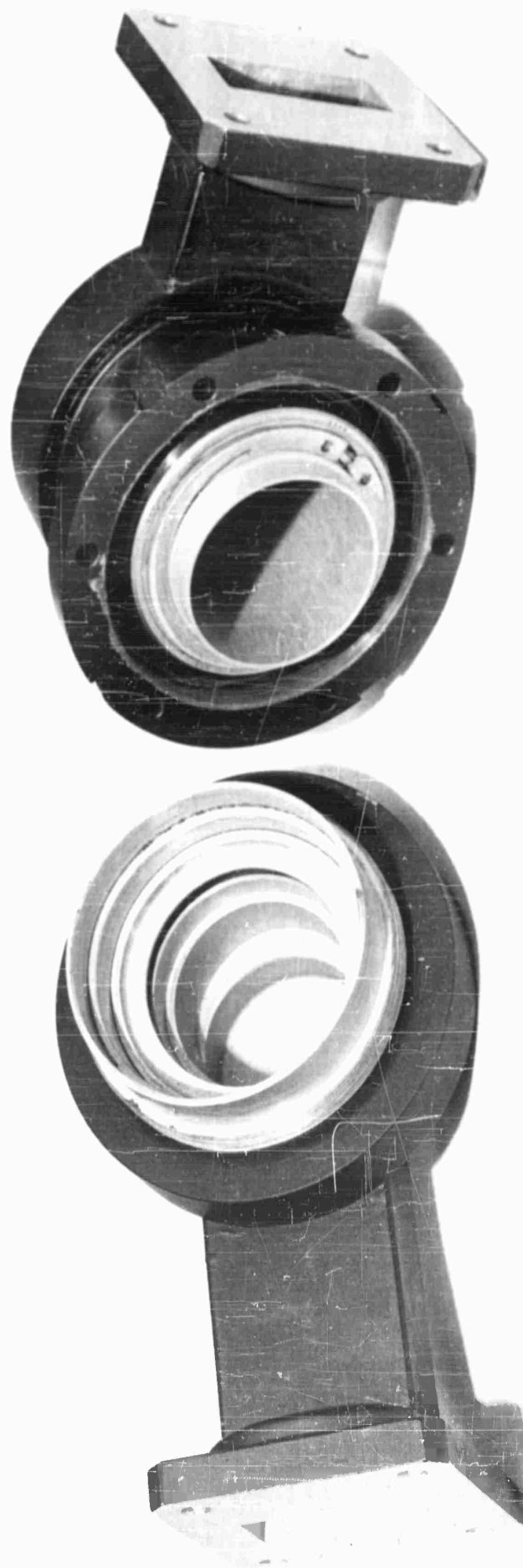


Figure E-4b TE-TM-TE Rotary Joint (For RG-51/U)

CALC			REVISED	DATE		
CHECK						
APPD						D6-7190
APPD					BOEING AIRPLANE COMPANY SEATTLE 24, WASHINGTON	PAGE 142

BAC 973 D R3

2-7000



BEFORE



AFTER

(a) 0.03-inch Thickness  
(6 KW CW, 20 minutes)



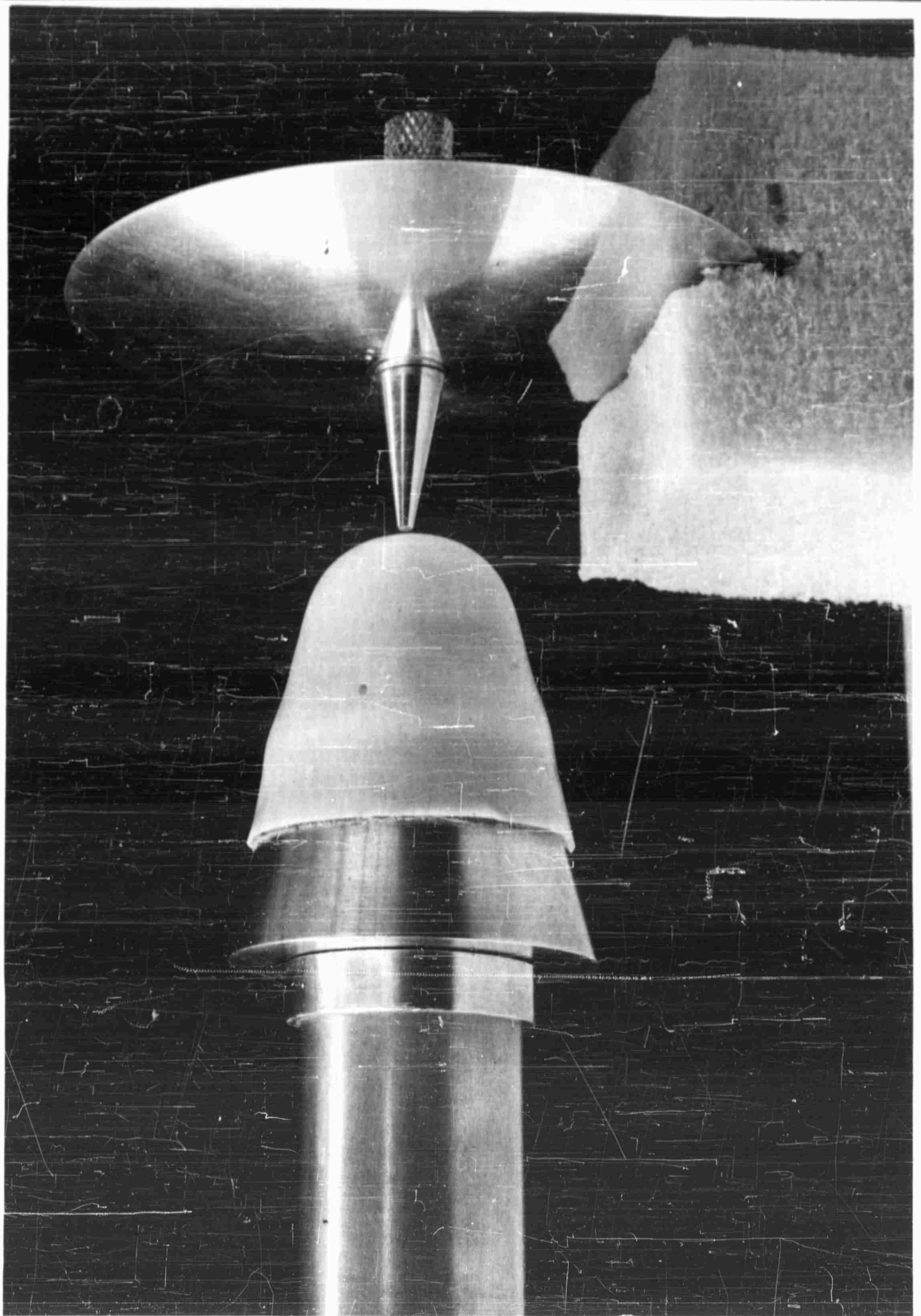
BEFORE



AFTER

(b) 0.06-inch thickness  
(10 KW CW, 10 minutes)

Figure E-5 - High-Power Test Results of Teflon Window



CALC			REVISED	DATE	Pressurizing Teflon Cap	Fig. E-6
CHECK						D6-7190
APPD						
APPD						PAGE 143
					BOEING AIRPLANE COMPANY SEATTLE 24, WASHINGTON	

## Appendix F

### Summary of "Project Needles" Techniques (Ref. 28)

"Orbital scatter communications," credited to W. E. Morrow and Harold Meyer of Thompson Ramo Woolridge Corporation, is a promising new technique that will use earth-circling belts of tiny hair-thin metallic whiskers. A pound of tiny dipole whiskers in orbit can provide as much effective signal reflecting area as approximately 1,000 pounds of material in the form of a conventional hollow-sphere passive communications satellite.

Millions of dipoles, less than 0.001 inches in diameter, 0.8 inches long, weighing 220 lb. per billion, will be ejected from a satellite as it circles the earth. A continuous belt of signal-reflecting surfaces in an equatorial orbit will result and will remain fixed with respect to earth stations except for small orbit perturbations. Two orbital belts, one in an equatorial orbit and the other in a polar orbit, can provide global coverage and should have a lifetime of several years before becoming dispersed enough to require replacement. A single belt of dipoles can provide a large number of simultaneous communication channels because of the large number of scattering locations available around the earth.

If the dipoles are ejected along a satellite velocity vector with a maximum velocity of plus and minus 10 fps., the belt will close upon itself in roughly one month and will assume a reasonable degree of uniformity in two months. If dipoles are ejected in all directions, the belt can be expected to spread about 20 mi. in thickness and about 5 mi. in width, with the bulk of the dipoles concentrated in a narrow portion of the belt. Average separation between individual dipoles in a 3,000 mile orbit would be about 1,000 ft.

The movement of the tiny dipoles in orbit through the beam of a fixed ground antenna will create some disadvantageous propagation characteristics. With a beam-filling belt multipath delays of 100-300 microseconds can be expected, and the motion of the dipoles will cause multipath delay to change 200-1000 times per second. This "doppler smear" characteristic suggests the use of non-coherent pulse code modulation techniques for the best results. The multipath delay is comparable to that due to ionospheric scatter but the fading rate is about 300 times higher. Digital transmission techniques, both for data and voice, may therefore be necessary.

Solar radiation pressure acting on the low-mass dipoles may cause annual orbital dispersion of about 20 mi. in a radial direction (thickness). If all dipoles had the same orientation in orbit, the effect on the belt would not affect its usefulness. Because of the random orientation the solar-caused perturbation will result in changes of dipole density within the belt. However, a cycle variation in orbit eccentricity, with a period of several months, is expected to cause substantially greater perturbations of the belt orbit. For a belt in polar orbit at an altitude of about 2,300 mi., the perigee is expected to be forced into the atmosphere after about 12 to 20 months. Longer lifetimes will be obtained at higher altitudes. Such a belt will be placed into orbit in the next few months as a "piggy-back" experiment aboard another satellite. In its final form, a belt produced

by a billion dipoles, weighing 220 lb., at an altitude of several hundred thousand ft. should provide communication data capacity of some tens of kilobits per second, over SHF circuits of up to 10,000 kilometers length, using 60 ft. diameter ground stations antennas, 10 kw transmitters, and low-noise maser receivers.



## APPENDIX G

### SATELLITE ORBIT COMPUTATIONS

#### 1. The Orbital Elements

Longitude and latitude of the subsatellite point on the earth and the height of the satellite above the earth will be predicted from the orbital elements (computation of an ephemeris).

A catalog of all satellites is maintained by the NORC (Naval Ordnance Research Computer), where orbital elements are determined from observations. For initial orbit determination and prediction, Cowell's method of numerical integration is used ; for large numbers of observations, the method of general oblateness perturbations is employed. (Refs. 33-35)

Six elements are needed to describe an elliptical orbit at some given time  $T_0$  (called the epoch)

Semimajor axis ( $a$ )

Eccentricity ( $e$ )

Inclination ( $i$ )

Right ascension of ascending node ( $\theta_0$ )

Argument of perigee ( $\omega_0$ )

Mean anomaly at epoch ( $M_0$ )

The epoch is given as the year, month, day, hour, minute, and second in universal time.

---

The semimajor axis of the ellipse is measured in earth's equatorial radii (equatorial radius is 3963.34 statute miles based on the international ellipsoid for the shape of the earth ). (Ref. 36)

The eccentricity is a ratio which is always less than unity for an ellipse and is equal to zero for a circle.

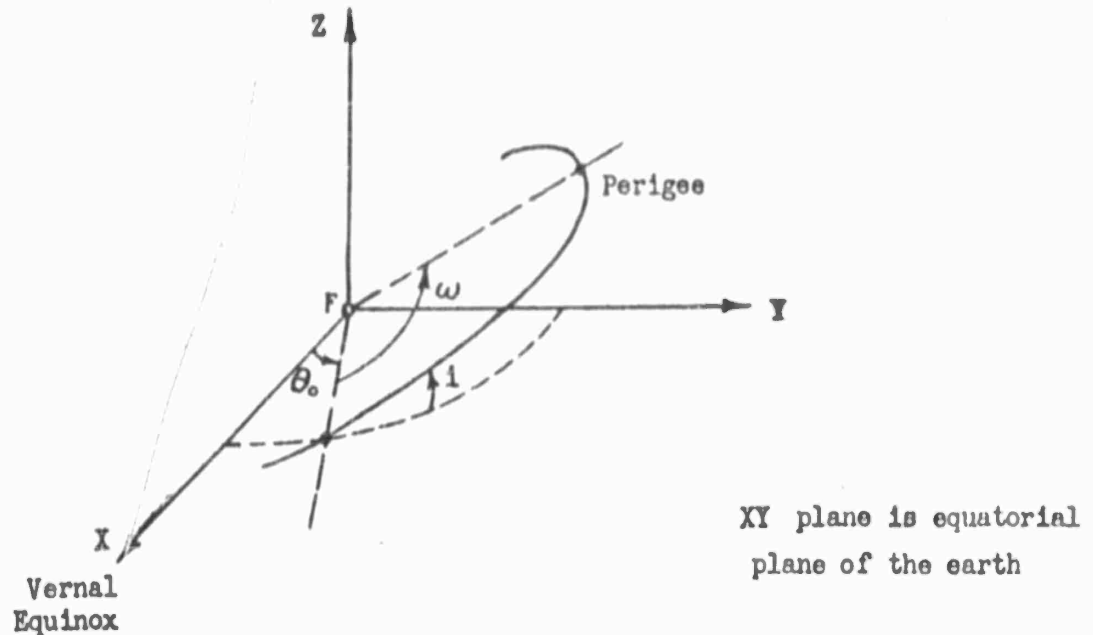


Fig. G.1 Coordinate Reference System

The inclination (Fig.G1.) is the angle measured in degrees from the equatorial plane of the earth to the orbital plane at the ascending node (that is, where the satellite crosses the equator in a northward direction).

The right ascension of the ascending node is measured in degrees eastward along the earth's equator from the vernal equinox to the ascending node.

The vernal equinox establishes the x-axis for the geocentric coordinate system, the z-axis passing through the earth's North pole, and the y-axis lying in the equatorial plane to form a right-handed coordinate system.

The argument of perigee (point of closest approach to the earth) is the angle in degrees measured in the orbital plane from the ascending node to the perigee.

The mean anomaly at epoch is given in degrees and represents the position of the satellite in the orbit with respect to the perigee.

Two major disturbing forces must be taken into account, one resulting from the shape of the earth (the equatorial bulge), and one resulting from the presence of the atmosphere. Because of the distribution of the mass of the earth, there is motion of the perigee in the orbital plane, and motion of the node in the equatorial plane. These perturbations are taken into account both in orbit determination and prediction.

The anomalistic period is the time for the satellite to make a complete revolution from perigee to perigee.

Depending on the orbital elements, the motion of node and perigee are a few degrees a day at most. For a polar orbit ( $i = 90^\circ$ ) there is no motion of the node; for an orbit having an inclination of  $63\frac{1}{2}^\circ$  there is no motion of the perigee. The perigee and apogee heights are measured from the surface of the earth, which is taken to correspond to the equatorial radius.

The vernal equinox is the intersection of the ecliptic and the celestial equator when the sun travels north in the spring, and is also called the "first point of Aries."

2. Secular and Periodic Motions of the Node of an Artificial Earth Satellite (Ref. 37)

$$\Delta \phi = \frac{2 \pi J R^2 \cos i}{a^2 (1-e^2)^2} \left\{ 1 - \frac{J R^2}{24 a^2 (1-e^2)^2} [4 (3-20 \sin^2 i) - e^2 (4+5 \sin^2 i)] \right. \\ \left. - \frac{J R^2}{12 a^2 (1-e^2)^2} [16 (2-5 \sin^2 i) e \cos w - (7-15 \sin^2 i) e^2 \cos 2 w] \right\} \\ + \frac{3 \pi D R^4 \cos i}{7 a^4 (1-e^2)^4} \left[ \left( 1 + \frac{3}{2} e^2 \right) (4-7 \sin^2 i) - (3-7 \sin^2 i) e^2 \cos 2 w \right]$$

$\Delta \phi$  = diff. in right ascension between two successive ascending nodes

J, D = coeffts. of 2nd and 4th order harmonics in the pot. fcn. for the oblate earth (ref. 38).

R = equatorial radius of earth

i = inclination of orbit to the equator

a, e = semi-major axis and eccentricity of osculating ellipse corresponding to the satellite at the node

w = argument of perigee (angular distance from the node to perigee).

node = point on celestial sphere where the satellite crosses the equator.

Example: - 1958B2 (Vanguard 1)  $\left(\frac{a}{R}\right) = 1.3603$ ;  $i = 34.26^\circ$ ;

$e = 0.1896$ ;  $J = 1.6232 \times 10^{-3}$ ;  $D = 0.885 \times 10^{-5}$

separate contributions of the J and D terms are

$$\Delta \phi (\text{deg/rev}) = (0.281 - 279 \times 10^{-6} \cos w + 1.79 \times 10^{-6} \cos 2 w) J + \\ (3.58 \times 10^{-4} - 5.37 \times 10^{-6} \cos 2 w) D$$

The linear (secular) terms in J is dominant.

## COMPUTER SUBSYSTEM

### Comparison Between Analog and Arithmetic or Incremental Digital Computers

Four factors determined the selection of digital instrumentation for the computer subsystem:

- (1) Accuracy - If a computing precision of better than one part in 1000 is required a digital computer should be used.
- (2) Flexibility - A digital computer is more easily adapted to using the same equipment for different tasks at different times; this type of flexibility is especially true of the arithmetic type of computer.
- (3) Compactness - In almost every case, digital computers are more compact than analog computers for the same application.
- (4) Reliability - Usually the only critical quantity in a digital computer is the basic clock frequency, whereas analog computers are dependent on stable voltages and careful balancing. Because more precise control can be effected over frequency than any other quantity, digital computers offer greater operational reliability.

### Arithmetic Digital Computers

The general configuration of the antenna platform positioning system with an arithmetic digital computer is shown in Figure H.1

At fixed time intervals,  $\Delta T$ , the readings from the aircraft instruments are encoded into whole numbers and gated into the computer memory. The computer then steps through its program solving the given equations. When the computer has executed the entire program, it reads the output data into buffer storage and stops. At time  $\Delta T$  later, fresh data are read in and the program is repeated. Whenever a new number appears in buffer storage, it is decoded into an analog signal for use by the antenna platform positioning system.

The encoders could be repeater servos and whole-number shaft-angle encoders. The computer will use a magnetic drum memory, the most compact storage medium available today when all required auxiliary equipment is considered. The main disadvantage of drum storage is that instructions and data must be carefully placed on the drum if waiting time for required words to appear under the readheads is to be minimized.

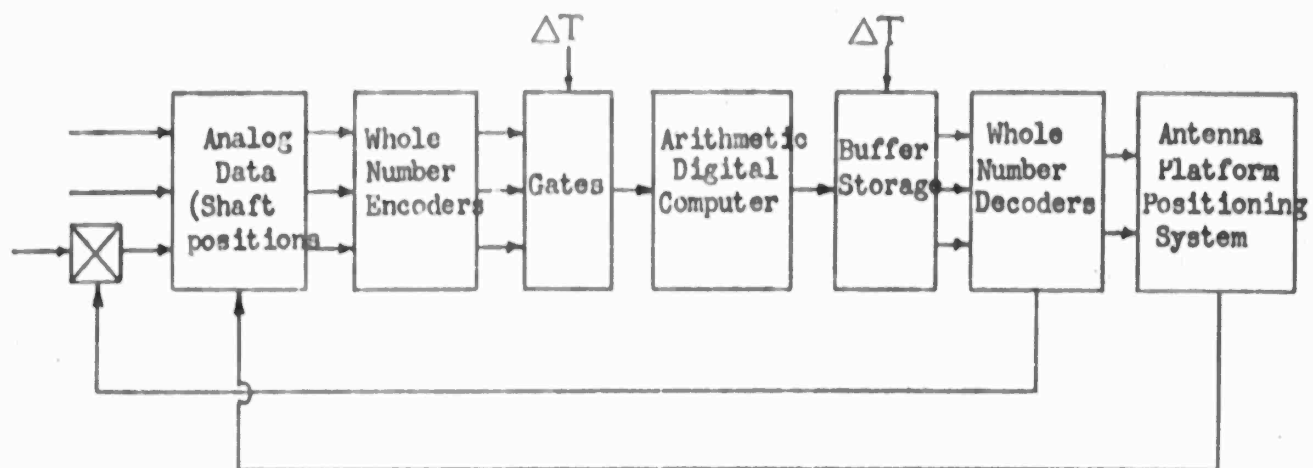


Fig. H-1 GENERAL SYSTEM CONFIGURATION USING AN ARITHMETIC DIGITAL COMPUTER

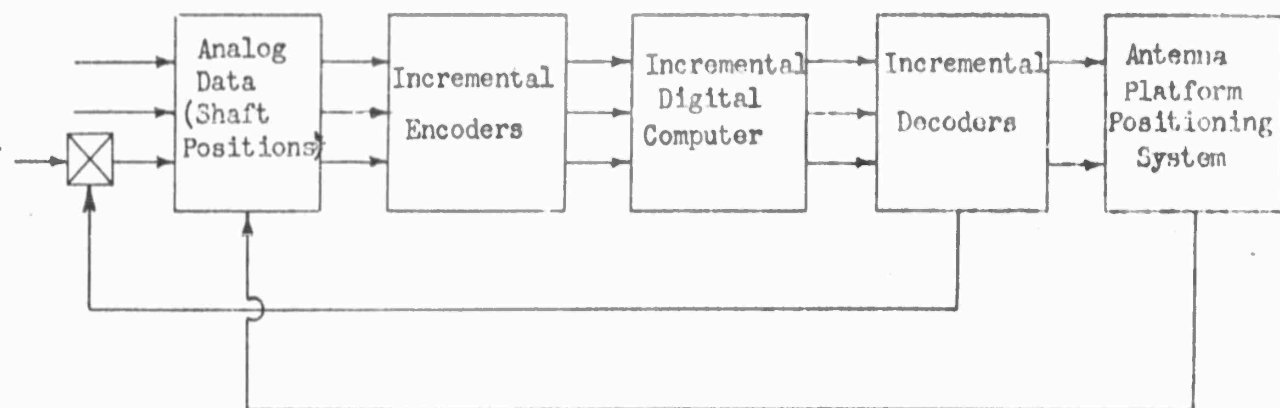


Fig. H-2 GENERAL SYSTEM CONFIGURATION USING AN INCREMENTAL DIGITAL COMPUTER

To minimize waiting time, the computer may use a two-address instruction code or a relative address system, and parallel arithmetic may be required. The buffer storage may be flip-flop registers, and the decoders may be servos with shaft-angle encoders used in feedback loops. Fundamentally, this machine adds numbers and performs certain logical comparisons. Integration and multiplication are performed numerically and trigonometric functions are evaluated using power series expressions.

This computer solves a stated problem by carrying out all basic operations under the control of the program which is a sequence of coded instructions. The instructions are stored in the computer memory together with the required data. Thus, the task which the computer performs can be changed by causing the computer to follow a different program which also is stored in the memory.

The arithmetic digital computer is therefore very flexible in its applications.

#### Incremental Digital Computers

The general system configuration using an incremental digital computer is shown in Figure H.2. In this case, the computer operates almost continuously, accepting input pulses whenever they occur and putting out output pulses whenever required. The incremental encoders may be incremental shaft-angle encoders which are considerably smaller than whole number encoders.

This computer may use a magnetic drum memory or, if the problem is too small to warrant the use of a drum, magnetic core shift registers may be used. The incremental decoder is smaller than a whole number decoder; it may be a stepping motor with an analog signal generator on the shaft, or in some cases, a simple smoothing of the output pulses yields the appropriate dc analog signal.

The incremental digital computer usually takes the form known as the digital differential analyzer or DDA, and processes incremental information. The basic element is the DDA integrator or increment multiplier, which yields an output pulse rate,  $\Delta Z$ , proportional to the product of a whole number  $Y$  and a pulse rate  $\Delta X$ . The accumulation of these  $\Delta Z$  pulses

then represents the integral of Y with respect to X. Products and trigonometric functions are determined by solving for the increment in the desired quantity in terms of known quantities and their increments. The computer processes all of the increment multipliers in a time known as the cycle time of the computer. Usually the cycle time and increment values are chosen in such a way that no variable changes by more than one increment in one cycle time. The problem which a DDA solves is defined by the interconnection of the increment multipliers; it is therefore not so flexible in the changing of its program as is the arithmetic computer.



## Appendix I

### ANTENNA DRIVE CONTROL SYSTEM (Refs. 39-42)

#### Z-Transform Method

A control system utilizing a digital computer is essentially a type of sampled-data control system in which the signals are in the form of a digital code (Figs. I.1 and I.4).

The digital computer interacts dynamically with other parts of the system, and its effect will be examined by the use of conventional servomechanism design techniques, namely, frequency analysis (Figs. I.5 and I.6).

If digital shaft encoders are attached to the output shafts and the system is connected as in Fig. I.1, then the computer can perform error detection and system compensation, and the stability and accuracy of the control system can be improved by designing a suitable program for the computer.

One of the most powerful tools for analyzing and designing digital and sampled-data feedback control systems is the Z-transform method which is reviewed briefly below.

The basic component of sampled-data control systems is the sampler which converts a continuous signal into a train of amplitude-modulated narrow pulses occurring at the sampling instants as shown in Figure I.2.

In the diagrams, an asterisk refers to sampled-data functions, small letters refer to functions of time, and capital letters written as functions of  $(s)$  are the Laplace transforms of the corresponding time functions.

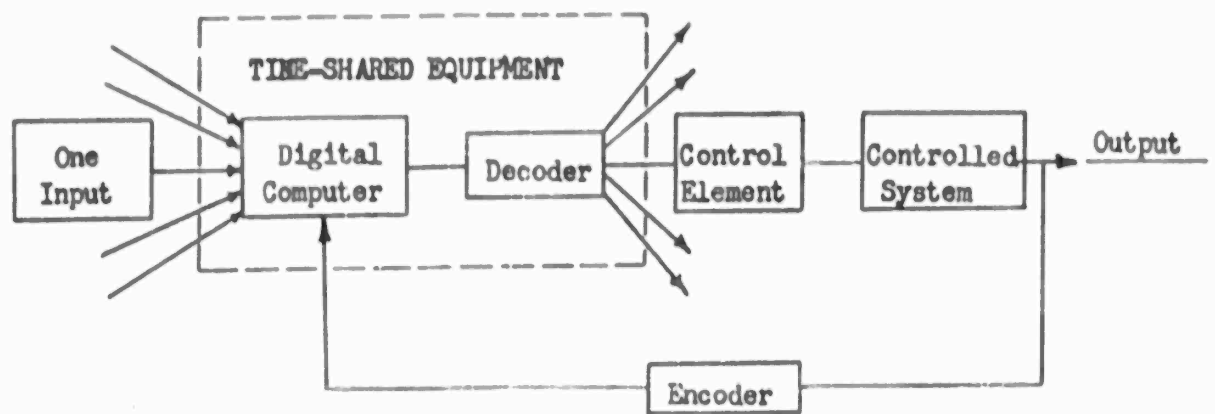


Fig. I-1 DIGITAL CONTROL SYSTEM

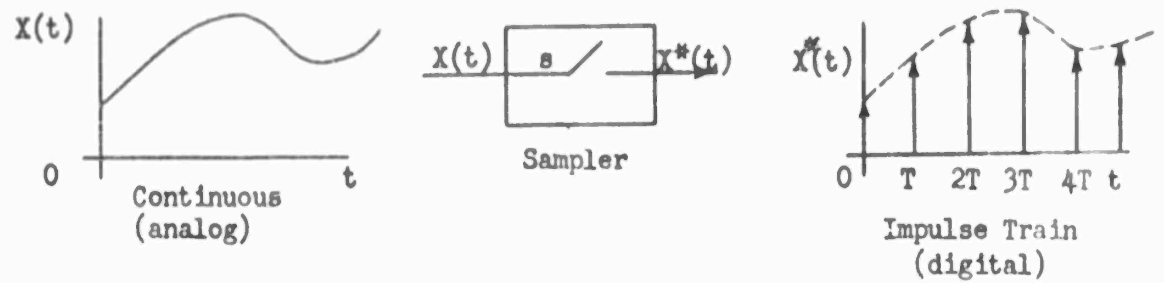


Fig. I-2 PROPERTIES OF AN IDEAL SAMPLER

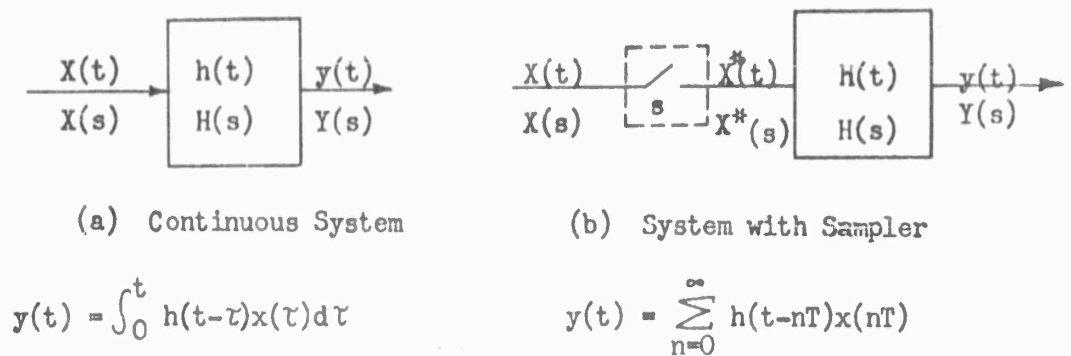


Fig. I-3 COMPARISON OF CONTINUOUS & SAMPLED-DATA SYSTEM

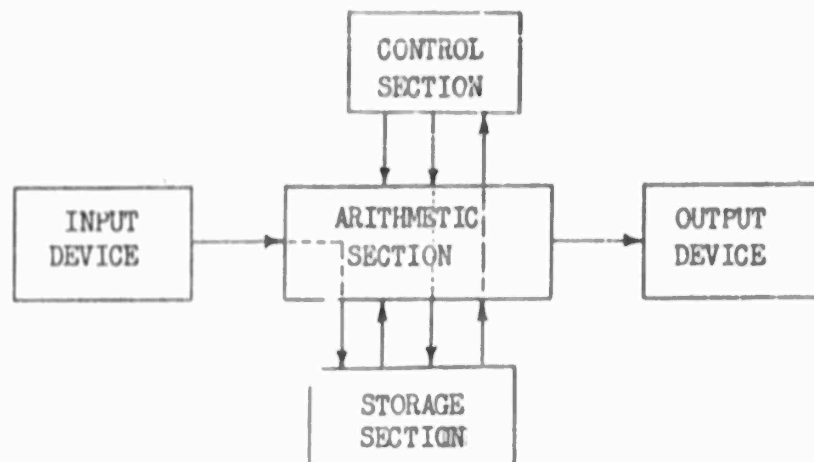
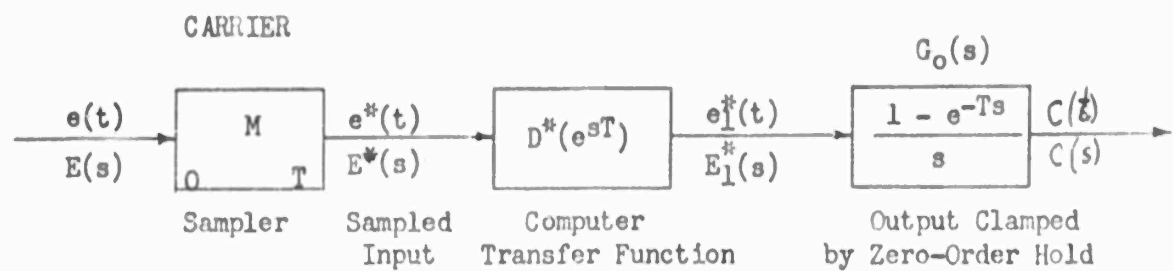


Fig. I-4 PROGRAM CONTROLLED DIGITAL COMPUTER



$$\begin{aligned}
 C(s) &= E(s)MD^*(e^sT) \times G_0(s) \\
 &= E^*(s) \times D^*(e^sT) \times G_0(s)
 \end{aligned}$$

Fig. I-5 BLOCK DIAGRAM OF OPEN LOOP DIGITAL COMPUTER CONTROL SYSTEM

Note: In the practical operation of a digital computer there exists a time delay in the computation  $e^{-ssT}$  which can be combined with  $G_0(s)$ .

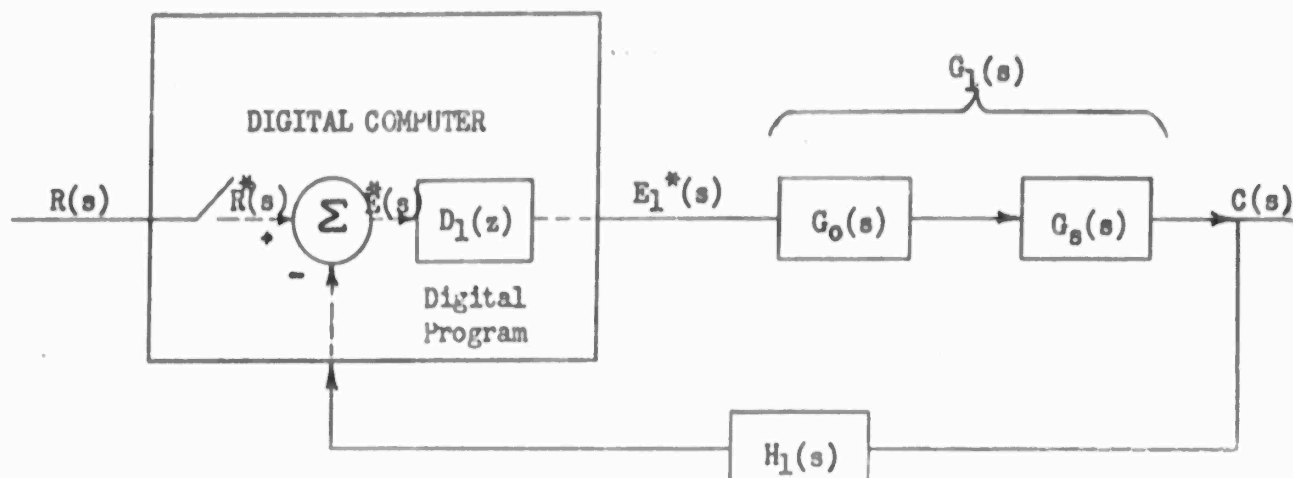


Fig. I-6 BLOCK DIAGRAM OF DIGITAL FEEDBACK CONTROL SYSTEM CHANNEL

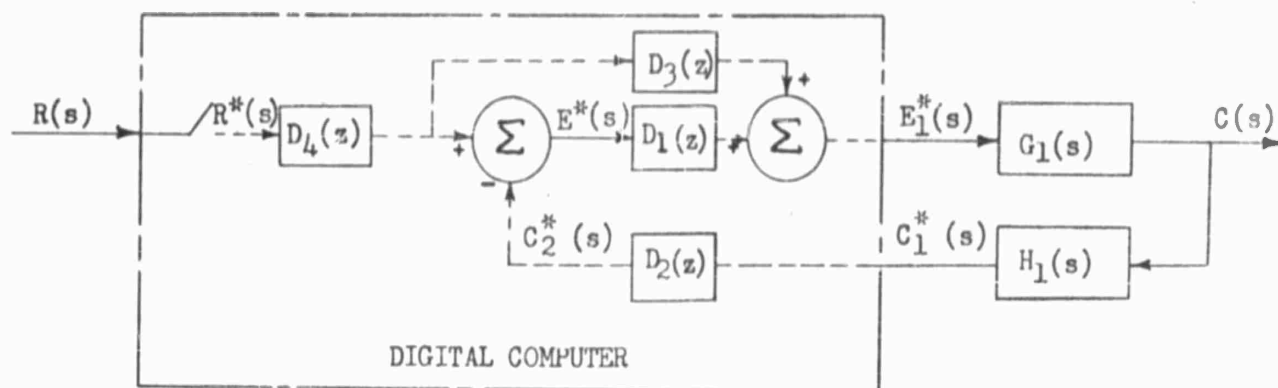


Fig. I-7 GENERALIZED DIGITAL COMPENSATION

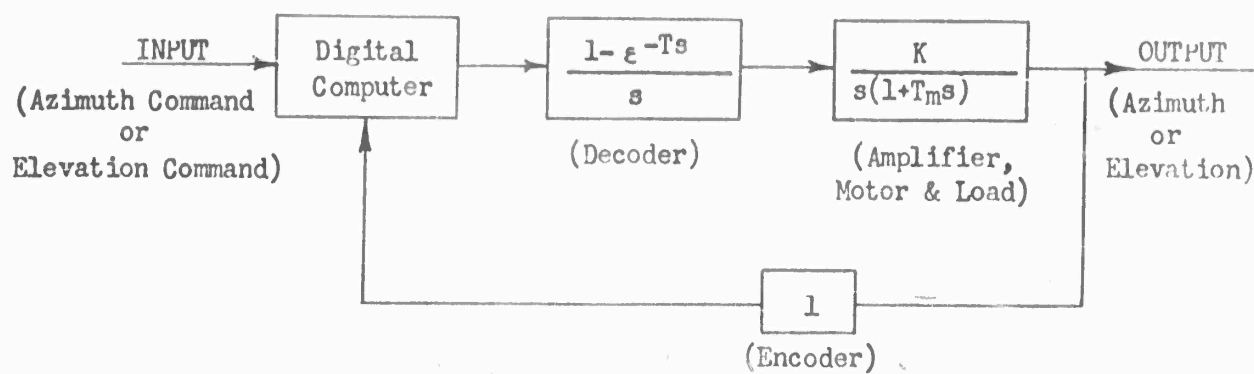


Fig. I-8 SINGLE CHANNEL OF ANTENNA DRIVE SYSTEM (SIMPLIFIED)

D6-7190

If the input to the sampler is  $x(t)$ , the output is given by:

$$x^*(t) = \sum_{n=-\infty}^{\infty} x(nT) \delta(t - nT).$$

Since

$$x(nT) = 0 \text{ for } n < 0,$$

$$x^*(t) = \sum_{n=0}^{\infty} x(nT) \delta(t - nT).$$

Taking the Laplace Transform,

$$X^*(s) = \sum_{n=0}^{\infty} x(nT) e^{-nTs}.$$

Substituting  $z$  for  $e^{Ts}$ ,

$$X^*(s) \Big|_{s = \frac{1}{T} \ln z} \triangleq X(z) = \sum_{n=0}^{\infty} x(nT) z^{-n}$$

where

$$X(z) = Z \{x^*(t)\} \text{ is the Z-transform of } x^*(t).$$

In a continuous system, Fig. I.3(a), the output is given by the convolution integral:

$$y(t) = \int_0^t h(t - \tau) x(\tau) d\tau$$

where  $y(t)$  is the output and  $h(t)$  is the impulse response function of the system. In terms of the complex variable  $s$

$$Y(s) = H(s)X(s)$$

where  $Y(s)$ ,  $H(s)$ , and  $X(s)$  are the Laplace transforms of  $y(t)$ ,  $h(t)$ , and  $x(t)$  respectively.

In the open-loop sampled-data system of Fig. 1.3(b), the output can be described by a convolution summation,

$$y(t) = \sum_{n=0}^{\infty} h(t - nT)x(nT).$$

At the sampling instant,  $mT$ ,

$$y(mT) = \sum_{n=0}^{\infty} h(mT - nT)x(nT).$$

Also, the L-transform of the output  $y(t)$  is  $Y(s) = \int_0^{\infty} y(t)e^{-st} dt$ .

Substituting and rearranging,

$$Y(s) = \sum_{n=0}^{\infty} x(nT) \mathcal{E}^{-nTs} \int_0^{\infty} h(t - nT) \mathcal{E}^{-(t - nT)s} dt.$$

Since

$$X^*(s) = \sum_{n=0}^{\infty} x(nT) \mathcal{E}^{-nTs} \quad \text{and} \quad H(s) = \int_0^{\infty} h(t) \mathcal{E}^{-st} dt,$$

it follows that

$$Y(s) = H(s)X^*(s).$$

The Z-transform

$$\begin{aligned} Y(z) &= Z \{y^*(t)\} = \sum_{m=0}^{\infty} y(mT)z^{-m} \\ &= \sum_{m=0}^{\infty} \sum_{n=0}^{\infty} h(mT - nT)x(nT)z^{-m} \\ &= \sum_{k=0}^{\infty} h(kT)z^{-k} \sum_{n=0}^{\infty} x(nT)z^{-n} \quad \text{where } m - n = k. \end{aligned}$$

Since

$$X(z) = \sum_{n=0}^{\infty} x(nT)z^{-n}$$

and

$$H(z) = \sum_{k=0}^{\infty} h(kT) z^{-k},$$

$$Y(z) = H(z) X(z)$$

where  $H(z)$  is called the pulsed transfer function.

By analogy with the L-transform, the inverse Z-transform of  $H(z)$  is given by:

$$h(kT) = \frac{1}{2\pi j} \oint_C H(z) z^{k-1} dz$$

where  $C$ , the contour of integration is a unit circle with center at the origin of the  $z$ -plane.

$$Z\{h^*(t - nT)\} = z^{-n} H(z)$$

describes the shifting theorem of the Z-transform.

### Error Compensation by Digital Programming

In Figure 17 the asterisk refers to sampled-data computation, and the functions of (s) are L transforms; for instance

$$R^*(s) = L \{ r^*(t) \}$$

The system performance will be derived from the system over-all transfer function which is defined as the ratio of system output to system input. The following symbols are used

$r^*(t)$  = sampled input

$c(t)$  = output

$e^*(t)$  = actuating error from the digital subtractor

$e_1^*(t)$  = processed error signal

$G_1(s)$  = transfer function of the decoder, the control elements and the controlled system

$H_1(s)$  = transfer function of the control elements in the feedback path and the encoder

$D_1(z)$  = required digital programming function for error compensation

Then

$$E^*(s) = R^*(s) - C_1^*(s) \quad (1)$$

$$E_1^*(s) = D_1^*(s) E^*(s) \quad (2)$$

$$C_1^*(s) = \overline{G_1 H_1}^*(s) E_1^*(s) \quad (3)$$

where

$$D_1^*(s) = D_1(z), \quad \overline{G_1 H_1}^*(s) = \overline{G_1 H_1}(z)$$

$$\overline{G_1 H_1}(z) = Z \text{ transform of } \overline{G_1(s) H_1(s)}$$

From (1) and (3)

$$E^*(s) = R^*(s) - \overline{G_1 H_1}^*(s) E_1^*(s) \quad (4)$$

From (2) and (4)

$$E_1^*(s) = \frac{D_1^*(s) R^*(s)}{1 + D_1^*(s) \overline{G_1 H_1}^*(s)} \quad (5)$$



$$C(s) = G_1(s) E_1^*(s) = \frac{D_1^*(s) G_1(s)}{1 + D_1^*(s) G_1 H_1^*(s)} R^*(s) \quad (6)$$

$$= G(s) R^*(s) \quad (7)$$

where

$$G(s) = \frac{D_1^*(s) G_1(s)}{1 + D_1^*(s) G_1 H_1^*(s)} \quad (8)$$

or

$$C(z) = G(z) R(z) \quad (9)$$

where

$$G(z) = Z \{G(s)\} = \frac{D_1(z) G_1(z)}{1 + D_1(z) G_1 H_1(z)} \quad (10)$$

is the over-all pulsed transfer function of the system.

The system error is  $e(t) = r(t) - c(t)$  and a system is said to be of high accuracy if

$$\left. \begin{aligned} c(t) &= r(t) \\ c(s) &= R(s) \\ c(z) &= R(z) \end{aligned} \right\} \quad (11)$$

i.e. the system over-all transfer function is equal to unity.

In conventional continuous-data servo systems this condition can hardly be realized, however in a digital or sampled-data feedback control system it is not difficult to make the output equal to the input at the sampling instants, so that the system error is made zero at the sampling instants. This can be done if the over-all pulsed transfer function of the system is made equal to unity by designing a suitable programming function, and if the sampling rate is kept high, an almost perfect control system can be obtained.

From equation (10) the system error at sampling instants is zero if

$$\frac{D_1(z) G_1(z)}{1 + D_1(z) G_1 H_1(z)} = 1 \quad (12)$$

From (12) it follows that

$$D_1(z) = \frac{1}{G_1(z) - G_1 H_1(z)} \quad (13)$$

is the desired digital programming function for system-error compensation. Since both  $G_1(z)$  and  $\overline{G_1 H_1}(z)$  are ratios of two polynomials in  $Z^{-1} = e^{-st}$  the programming function  $D_1(z)$  can be described by a ratio of two polynomials in  $Z^{-1}$  also.

In Figure 7

$$D_1(z) = \frac{E_1(z)}{E(z)} = \frac{\alpha_0 + \alpha_1 Z^{-1} + \alpha_2 Z^{-2} + \dots + \alpha_m Z^{-m}}{\beta_0 + \beta_1 Z^{-1} + \beta_2 Z^{-2} + \dots + \beta_n Z^{-n}} \quad (14)$$

where the processed signal  $e_1^*(t) = Z^{-1} \{E_1(z)\}$  is evaluated by the digital computer. Rearranging (14) and making use of the shifting theorem for Z-transforms.

$$\begin{aligned} & \alpha_0 e_1^*(t) + \alpha_1 e_1^*(t-T) + \alpha_2 e_1^*(t-2T) + \dots + \alpha_m e_1^*(t-mT) \\ &= \beta_0 e_1^*(t) + \beta_1 e_1^*(t-T) + \beta_2 e_1^*(t-2T) + \dots + \beta_n e_1^*(t-nT) \end{aligned} \quad (15)$$

where  $T$  = sampling period of the system.

Rearranging (15)

$$e_1^*(t) = \frac{1}{\beta_0} \left[ \sum_{k=0}^m \alpha_k e_1^*(t-kT) - \sum_{k=1}^n \beta_k e_1^*(t-kT) \right] \quad (16)$$

This is a form of numerical quadrature formula, and the computation involved can easily be performed by a digital computer. (Refs. 43 and 44)

### Generalized Digital Compensation

In a digital feedback control system, three quantities, the input, the error and the output - can be programmed in the digital computer as shown in Figure I-8,

In which

$$C(s) = G_1(s) E_1^*(s) \quad (17)$$

$$E(s) = R_1^*(s) - C_2^*(s) \quad (18)$$

$$C_2^*(s) = D_2^*(s) C_1^*(s) \quad (19)$$

$$C_1^*(s) = \overline{G_1 H_1}^*(s) E_1^*(s) \quad (20)$$

$$E_1^*(s) = D_1^*(s) E^*(s) + D_3^*(s) R_1^*(s) \quad (21)$$

Solving for  $E^*(s)$  from (18) (19) (20) and (21)

$$E^*(s) = \frac{1 - D_2^*(s) D_3^*(s) \overline{G_1 H_1}^*(s)}{1 + D_1^*(s) D_2^*(s) \overline{G_1 H_1}^*(s)} R_1^*(s) \quad (22)$$

Substitute (22) into (21) and simplifying

$$E_1^*(s) = \frac{D_1^*(s) + D_3^*(s)}{1 + D_1^*(s) D_2^*(s) \overline{G_1 H_1}^*(s)} R_1^*(s) \quad (23)$$

From (17) and (23)

$$C(s) = G(s) R_1^*(s) \quad (24)$$

where

$$G(s) = \frac{G_1(s) [D_1^*(s) + D_3^*(s)]}{1 + D_1^*(s) D_2^*(s) \overline{G_1 H_1}^*(s)} \quad (25)$$

Taking the Z transform of (24)

$$C(z) = G(z) R_1(z) \quad (26)$$

where

$$G(z) = Z \left\{ G(s) \right\} = \frac{G_1(z) [D_1(z) + D_3(z)]}{1 + D_1(z) D_2(z) \overline{G_1 H_1}(z)} \quad (27)$$

From (26), if the system transfer function  $G(z)$  is equal to unity,  $C(z) = R_1(z)$  and  $C^*(t) = r_1^*(t)$ . Thus, the system error at sampling instants is null if

$$G(z) = \frac{G_1(z) [D_1(z) + D_3(z)]}{1 + D_1(z) D_2(z) \overline{G_1 H_1}(z)} = 1 \quad (28)$$

Solving for  $D_3(z)$  from (28)

$$D_3(z) = \frac{1 + D_1(z) D_2(z) \overline{G_1 H_1}(z)}{G_1(z)} - D_1(z) \quad (29)$$

Therefore a quadrature formula for  $e_1^*(t)$  in terms of the past information of the output of  $D_3(z)$  and the present and past information of the input to  $D_3(z)$  can be derived for the necessary computation if  $D_3(z)$  is a physically realizable program.

A digital programming function,  $D_k(z)$  is physically realizable if the output of the network for the program does not depend upon the future information of the input signal and if the digital program can be written

$$D_k(z) = \frac{\sum_{i=0}^m \alpha_i z^{-i}}{\beta_0 + \sum_{i=1}^n \beta_i z^{-i}} \quad \text{where } \beta_0 \neq 0 \quad (30)$$

so that the expression of  $D_k(z)$  about the point at infinity contains no positive powers of  $z$ .

If the order of the numerator of  $G_1(z)$  is not equal to that of the denominator,  $D_3(z)$  may become unrealizable, but this difficulty can be overcome by choosing proper functions for  $D_1(z)$ ,  $D_2(z)$  and  $H_1(s)$  or by introducing a fourth programming function  $D_4(z)$  so as to make  $D_3(z)$  physically realizable.

The characteristic equation of the system is

$$1 + D_1(z) D_2(z) \overline{G_1 H_1}(z) = 0 \quad (31)$$

System stability will be achieved by designing  $D_1(z) D_2(z)$  so that all the roots of the characteristic equation lie inside the unit circle of the  $z$ -plane so that (31) satisfies the Schur-Cohn Criterion. (\*) The product  $D_1(z) D_2(z)$  can be considered as the system stabilizing function. After  $D_1(z)$  and  $D_2(z)$  are determined from system stability and transient performance considerations, the programming function  $D_3(z)$  is derived from (29) for zero system error. Since the feed-forward element  $D_3(z)$  is located outside the control loop it does not affect the stability of the system, and is the system-error reduction function.

This technique will be applied to the elevation and azimuth channels of the antenna drive system (Fig. 3.3 of main body of report). -

---

(\*) Refs. 45 and 46

## APPENDIX J

### Summary of Characteristics of Hughes M-252 Computer (designed in 1959, approximate cost \$80,000)

Class	General purpose
Circuitry	Solid State (silicon)
Type of operation	Serial
Number system	Binary
Arithmetic system	Fixed point
Timing	Synchronous
Clock Rate	250 kc
Word Length	22 bits total (19 plus sign and 2 spaces)

#### Operation Times (microseconds)

Add	88
Subtract	88
Multiply (per bit)	44
Divide (per bit)	88
Square Root	none
Transfer	88
Program Branching	88

#### Memory Data

Type	Drum rotating at 11,400 RPM
Capacity	5280 orders or 2640 numbers, 55,000 bits total (M-252 computer could use drum of MA-1 computer having capacity of 300,000 bits total)

#### Existing Input-Output Data - for use in the inertial guidance system of the SD-5 Surveillance Drone:

Conversion Accuracy: Input $\pm 0.3\%$ Output $\pm 1.0\%$	
Inputs:	2 ac : 0 to 8.88 V RMS
	3 dc : 0 to 8V
	6 digital : 0 or open (or + 15/+ 30 V)
	3 Incremental
Outputs:	11 dc : $\pm 8$ V
	10 digital : 0 or open (+)
	3 Incremental : 0 or open (+)
Functions:	(a) Preflight alignment and drift trim of the stable platform
	(b) Schuler tuning of the stable platform
	(c) Navigation and flight control of the entire mission
	(d) Selection of alternate flight profile segments as directed by data link
	(e) Conversion of polar coordinates to Universal Transverse Mercator (U.T.M., Army grid) coordinates.

## APPENDIX K

Digital Pointing Computer. (Sections 3.2.4 through 3.4.5.2 of Source Control Drawing D10-60603).

The numbers of figures and tables referred to in this appendix have been changed to refer to figures and tables in the main body of this report.

### 3.2.4 POWER SUPPLY

3.2.4.1 The computer shall be suitable for operation from the following aircraft power supplies:

- (a) Three phase alternating current supply, 380-420 cycles, 102-124 volts phase to neutral
- (b) Direct current supply 24-29 volts

3.2.4.2 The total power requirement of the computer shall not exceed 200 watts.

### 3.2.5 WEIGHT AND VOLUME

3.2.5.1 The weight of the computer, including input-output, and power supply units, shall not exceed 100 pounds.

3.2.5.2 The volume of the computer, including input-output and power supply units, shall not exceed 4 cubic ft.

### 3.2.6 INPUTS

3.2.6.1 The computer shall be capable of directly accepting some or all of the available analog inputs as listed in Table 4.1.2 of this report without any intermediate electro-mechanical conversion stage, and without drawing any appreciable current from the signal sources.

This is to be interpreted to mean that the input impedance of the computer circuit converting the input data into digital form shall not be less than that of a high quality voltmeter and shall not disturb the accuracy and normal operation of the autopilot, compass system, and doppler radar circuits being "tapped into".

3.2.6.2 The computer program shall be designed to utilize the most precise inputs available in computing any derived data, for instance the instantaneous aircraft position shall be computed from true heading and ground speed, rather than from the latitude and longitude indications which are derived from an electromechanical analog computer having 2-3% accuracy.

3.2.6.3 It shall be left to the discretion of the vendor whether or not all the available inputs will be utilized in the computer program. It is suggested that the redundant inputs should be utilized in suitable internal checks.

### 3.2.7 OUTPUTS

3.2.7.1 The computer shall be capable of directly supplying all required analog outputs without any intermediate electromechanical conversion stage.

3.2.7.2 The computer shall supply suitable clutch coil currents to the Lear type 3055 Dry Power Magnetic Clutch Servo Units employed for the azimuth and elevation channels of the antenna servo drive system.

3.2.7.3 If the computer cannot be readily adapted to supply output power adequate for operating these clutches directly, then the amplifier shown in Fig. 3.4 may be inserted to reduce the computer output power requirements.

3.2.7.4 There shall be an additional output voltage proportional to range rate (rate of change of length of the vector from aircraft to satellite). This will be a measure of doppler shift. (The most critical condition will exist when a 1500-mile high satellite rises "straight-up" near the horizon; its radial velocity will exceed 12,000 miles/hr., and its doppler shift at 8kmc will be about 150kc).

### 3.2.8 Special Modes of Operation

3.2.8.1 Polar Mode. There shall be provision for a special computer program to be used in polar regions to avoid the discontinuities of the geographic coordinates, and the mode of computation shall be determined by latitude. When the cosine of the present latitude becomes less than some predetermined constant, computation shall proceed in the polar mode in the next program cycle, with reference to either a pseudo-transverse pole located at the equator on the intersection of the true heading great circle arc at the instant of change to the polar mode, or with reference to a transverse pole located at the equator on the intersection of the greenwich meridian. All desired quantities are then to be transformed back to geographical coordinates.

#### 3.2.8.2 Satellite Near Zenith

3.2.8.2.1 When the satellite passes close to the zenith, provision shall be made in the computer program to slew the azimuth channel to the reciprocal relative bearing after the elevation reaches a predetermined value. (For instance, if  $89^\circ$  is chosen, a satellite passing overhead at  $1/5$  deg/sec angular rate allows 10 seconds to the Lear clutch servo motor rotating at 7300 RPM geared down 2270:1 to slew the azimuth drive through  $180^\circ$  before the satellite drops to below  $89^\circ$  on the reciprocal bearing.)



3.2.8.2.2 Special provision must be made to exclude the case where the elevation reaches or exceeds  $90^\circ$  due to suddenly applied bank angles. The antenna elevation look angle has a freedom of movement of " $25^\circ$  down to  $120^\circ$  up", measured from the horizontal plane, to make it possible to point the antenna at a satellite near the zenith when a  $30^\circ$  bank angle is applied to the aircraft without following the program branching outlined in 3.2.8.2.1.

### 3.2.9 Clock Synchronization

3.2.9.1 There shall be provision for synchronizing the airborne quartz crystal oscillator precision clock, possibly by means of listening to timing signals and punching a "bomb-release" type button.

3.2.9.2 The accuracy of synchronization shall not be inferior to that obtainable by means of a stop watch which can normally be manually punched correct to  $1/5$  second (equivalent to 1 mile of subsatellite position of a satellite orbiting at a speed of 5 miles/second).

3.2.10 Manual Controller: There shall be provision for controlling the operation of the computer by means of a manual controller having facilities for:

3.2.10.1 Manual resetting of the aircraft latitude and longitude in flight in accordance with the latest fix information, complete with memory feature so that no navigational information is lost during the period of resetting.

3.2.10.2 Controls for initiating functional tests (see 3.4.5.1).

3.2.10.3 Panel lights or other indications signifying

(a) malfunction (see 3.4.5.2)

(b) which of a number of selected satellites are above the horizon at a given time suitable for communications purposes, and control for selecting one of them.

(c) whether computer program branching into the polar mode has taken place.

### 3.2.11 Satellite Data

3.2.11.1 Satellite data will be available on request from Lincoln Laboratory in the form of IBM cards giving the orbital elements and their first derivatives predicted for hourly intervals up to one week ahead.

3.2.11.2 These data will be transferred to punched paper tape, and there must be provision for feeding the information into the digital pointing computer by means of a tape-reader to be stored there for periodic interpolation and updating of the satellite data.

- 3.2.12 **Memory Storage:** The capacity of the computer memory must be adequate for the intended functions with particular reference to the storing of satellite data and auxiliary navigational data, such as stored magnetic variation for all portions of the earth's surface where the magnetic compass can be used.
- 3.3 **Construction**
- 3.3.1 **Mounting**
- 3.3.1.1 The Manual Controller shall be built suitable for mounting on a desk type console.
- 3.3.1.2 The other units making up the complete computer assembly, shall be suitable for mounting, complete in their cases, within one or more of the modules making up the complete control console (See fig. K-1 and K-2) in a way ensuring easy removal for maintenance.
- 3.3.2 **Accessibility**
- 3.3.2.1 If electrical connection or mechanical adjustments of any portion of the system will be required for pre-flight or in-flight maintenance, then those portions of the system shall be designed to be easily accessible.

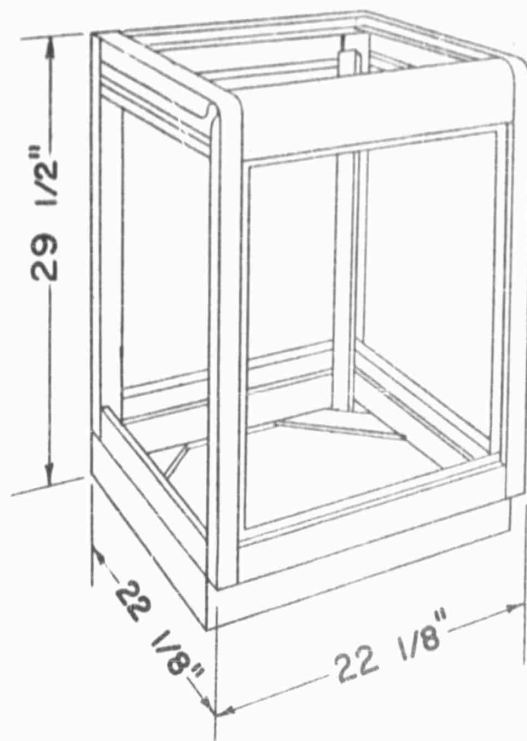


Fig. K-1 Desk Height Cabinet Rack

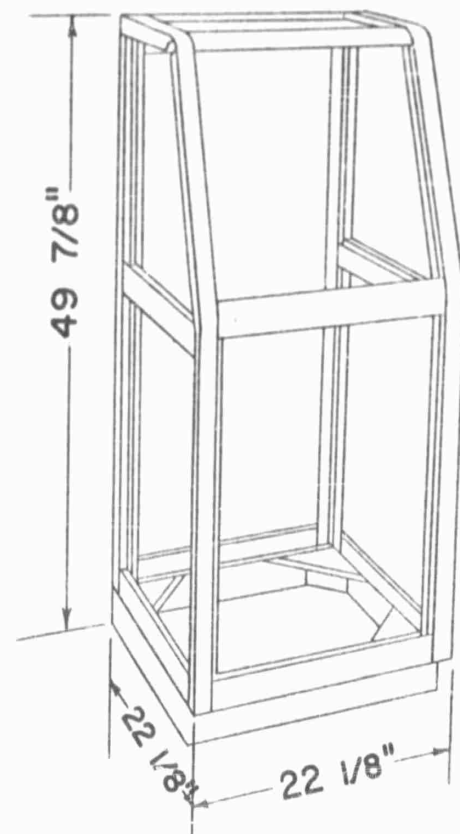


Fig. K-2 Sloping Front Console

### 3.4 Performance

- 3.4.1 Accuracy of computation. All data shall be handled to a sufficient number of digits, and all truncation errors kept sufficiently low, to ensure that the system accuracy is limited only by the accuracy of the existing aircraft sensors and stored satellite data.
- 3.4.1.1 This is to be interpreted to mean that:
- 3.4.1.1.1 Given correct inputs from the aircraft sensors the aircraft position shall be computed correct to 0.05% (1 mile in 2000 miles flown)
- 3.4.1.1.2 Given correct inputs from the stored satellite data the subsatellite position shall be computed correct to within  $\pm 3$  miles.
- 3.4.1.1.3 Given correct aircraft and subsatellite positions the antenna platform shall be positioned in azimuth and elevation correct to within the accuracy of the position feedback transducers employed (Kearfott Type R 982-004 three Minute Synchro Resolvers) at the sampling instants (i.e. within  $\pm$  three minutes of arc).
- 3.4.2 Environment. The unit shall be designed to operate within the limits of this specification under the following environmental conditions.
- 3.4.2.1 Temperature. All ambient temperatures between  $-65^{\circ}\text{F}$  and  $+160^{\circ}\text{F}$ .
- 3.4.2.2 Altitude. At any altitude between 0 and 10,000 feet.
- 3.4.2.3 Fungus. Fungus growth as encountered in tropical climates.
- 3.4.2.4 Vibration. Vibration as encountered in jet-powered aircraft.
- 3.4.2.5 Humidity. All conditions of relative humidity.
- 3.4.3 Explosion Proofing. The unit shall be designed to operate within an explosive atmosphere without igniting the atmosphere.
- 3.4.4 Life. The unit shall be designed for a minimum of 1,000 hours mean time between failures.
- 3.4.5 CORRECT FUNCTIONING
- 3.4.5.1 There shall be provision to check the correct functioning of the system in an easily demonstrable way, for instance with the compass and autopilot system operating, pressing test button A on the manual controller shall make the antenna point in the direction True North, elevation zero, and pressing test button B on the manual controller shall cause the antenna to point in a SW-ly direction, at an elevation of  $45^{\circ}$ . Alternate functional checks may be designed into the system at the discretion of the vendor.

3.4.5.2 At periodic intervals, before a new computation cycle begins, a check program is to be inserted which will test certain circuit properties. If an incorrect answer results, an indication of computer malfunction should be given, and the computer should switch to a standby mode.

## APPENDIX L SITE SURVEY PROFILES

After the vertical location of the antenna axis had been established on the centerline of the body, a survey was made to determine the effect of the body station location on the amount that the wing nacelles and tail surfaces obscured the beam.

It was assumed that normal operation of the system would occur during straight and level flight or in turning where a bank attitude only resulted. The latter condition produces obscuration of the celestial sphere varying in magnitude with the degree of bank of the aircraft. In level flight the only obscuration above the horizon would be by the fin and this is small regardless of the body station within the range considered. Wing deflection effects are not significant.

The centerline of the beam was used to determine the amount of obscuration. Previous investigations have shown that beam diffraction/reflection by wings and air-frame at X-band agrees rather well with the optical silhouette.<sup>49</sup> The shadow of the aircraft on the celestial sphere was viewed from a point at the intersection of the antenna axes. A shadow for a number of body stations within the probable range of locations was determined for various angles of bank. Conversion of these shadow graphs into areas which were then plotted permitted the determination of the amount of obscuration at all body stations within the range.

In any attitude of bank or level flight, the lower limit of the effective operating range was considered to be  $5^\circ$  above the local horizontal. The antenna drive mechanism directs the beam  $25^\circ$  below the horizontal reference plane of the aircraft. With a  $30^\circ$  bank the axis of the beam, when directed laterally, would thus be  $5^\circ$  above the local horizon at its lowest position. This lower limit of the operating range ( $5^\circ$  above the horizontal) has been used as a base point to plot the shadow graphs (Fig. L-2)

The areas within the shadows of the shadow graphs were plotted to obtain the graph figure L-1, which compares the amount of obscuration for any body station and any angle of bank up to  $30^\circ$ . This has been noted in three ways: "Percent Area Obscured", which is the ratio in percent of the area obscured to the total area contained in the  $85^\circ$  operation hemisphere, in square degrees, and in steradians.

Figure L-1 shows that at any angle of bank the obscuration increases as the antenna mount location is moved aft from body station 370 within the range of stations considered. Beyond the range of this graph the amount of obscuration would decrease and then increase again as the tail surfaces were approached.

CALC		REVISED	DATE
CHECK			
APR			
APR			

BOEING AIRPLANE COMPANY

D6-7190

PAGE 175

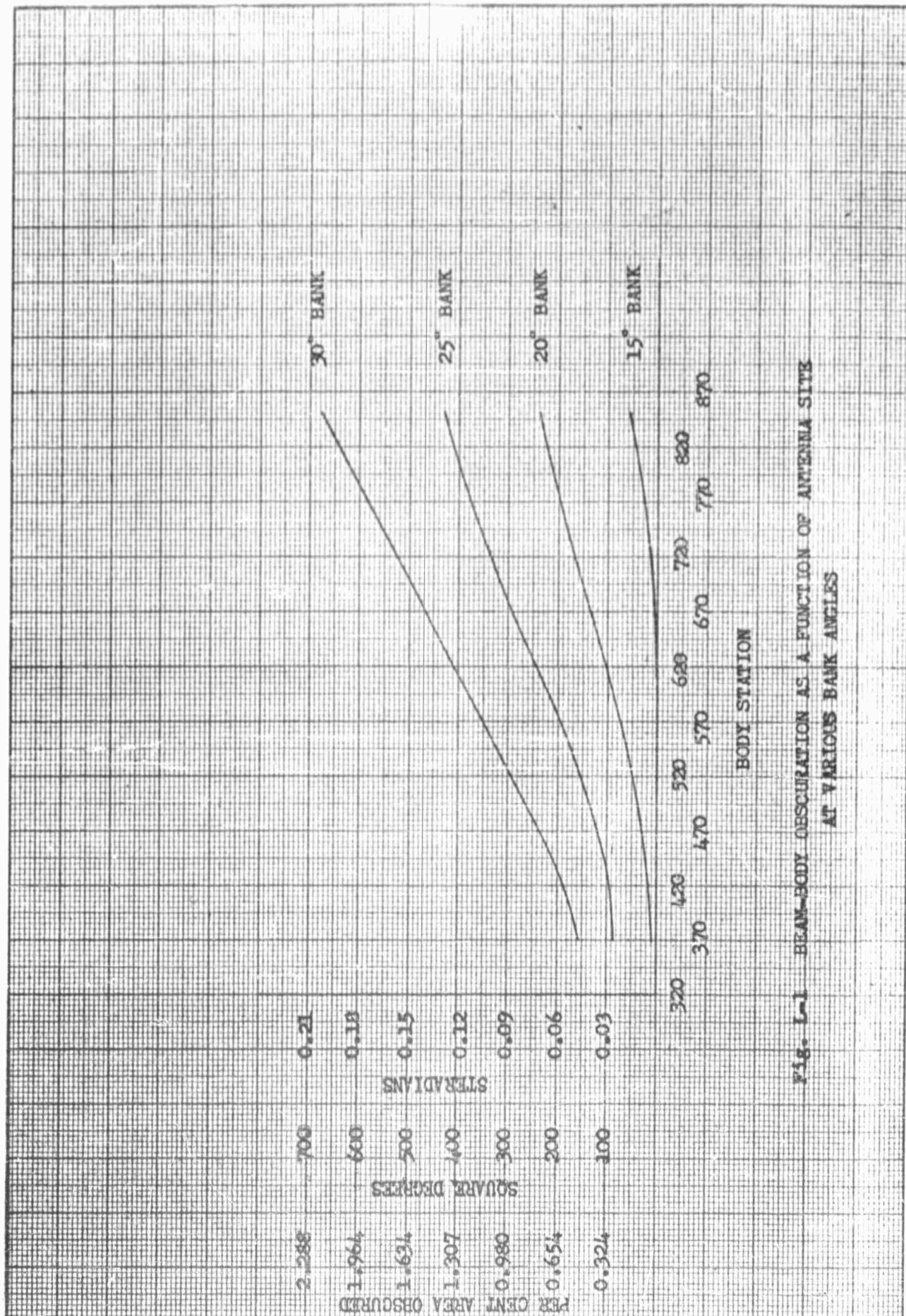


Fig. L-1 BEAM-BODY OBSCURATION AS A FUNCTION OF ANTENNA SITE AT VARIOUS BANK ANGLES



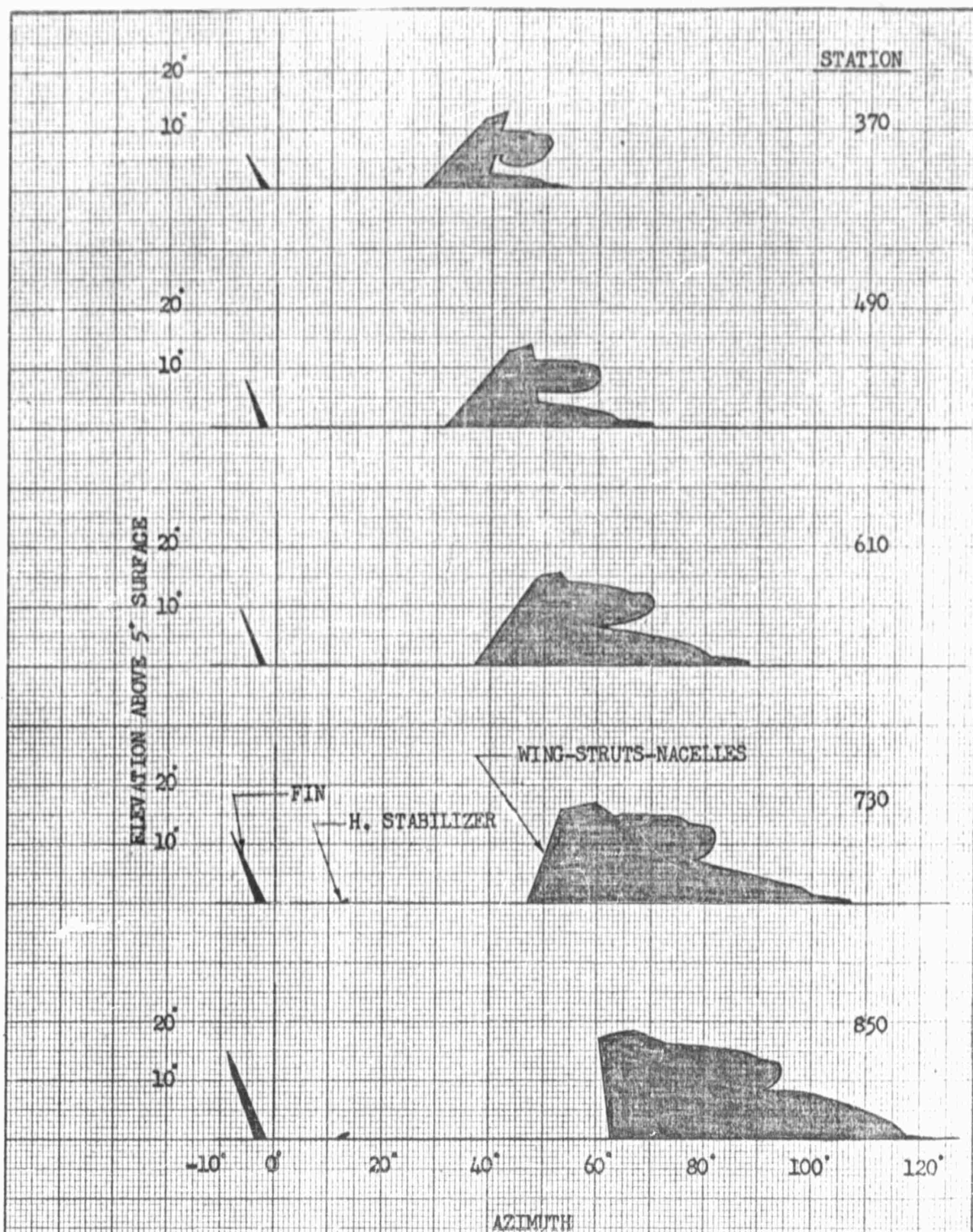





Fig. 1-2 BEAM-BODY OBSCURATION AT VARIOUS STATIONS  
FOR 30° BANK ANGLE



CALC		REVISED	DATE	BOEING AIRPLANE COMPANY	D6-7190
CHECK					
APR					
APR					
					PAGE 176

APPENDIX M

POWER REQUIREMENTS FOR  
MICROWAVE COMMUNICATION  
SYSTEM



PART NO.	DESCRIPTION	QTY	115 V A.C. LOAD (VA)											
			STAND-BY			RECEIVE			TRANSMIT					
			Ø A	Ø B	Ø C	Ø A	Ø B	Ø C	Ø A	Ø B	Ø C	Ø A	Ø B	Ø C
1C-2710-1	Antenna Drive	3	620	620	620	620	620	620	620	620	620	620	620	620
	Antenna Motor & Comp.	1	333	333	333	333	333	333	333	333	333	333	333	333
	Xmtr - Auxiliary	1	3333	3333	3333	3333	3333	3333	3333	3333	3333	3333	3333	3333
	Xmtr - Beam	1	-	-	-	-	-	-	-	-	13333	13333	13333	13333
M-252 	Computer	1	575*	-	-	575*	-	-	575*	-	-	575*	-	-
Hughes	Receiver	1	-	--	-	575*	-	-	575*	-	-	-	-	-
RD2642 	Recorder	1	60*	-	-	60*	-	-	60*	-	-	60*	-	-
DMQ36.0-0.43	Power Supply	2	230*	-	-	230*	-	--	230*	-	--	230*	-	-
RD5621-01	DC Amplifier	1	115*	-	-	115*	-	-	115*	-	-	115*	-	-
420744 	Remote Servo Assembly	3	345*	-	-	345*	-	-	345*	-	-	345*	-	-
RS911-6	Synchro Transmitter	3	8	-	-	8	-	-	8	-	-	8	-	-
Kearfott	Remote Indicators	3	8*	-	-	8*	-	-	8*	-	-	8*	-	-
8L32	Excitation Transformer	1	20*	-	-	20*	-	-	20*	-	-	20*	-	-
MSA-11000	RADOME BLOWER	1	200*	200*	200*	200*	200*	200*	200*	200*	200*	200*	200*	200*
TOTAL			5847*	4486*	4486*	6422*	4486*	4486*	4486*	19180*	17819*	17819*	17819*	17819*

PART NO.	DESCRIPTION	QTY.	DC LOAD (AMPS)		
			Stand-by	Receive	Transmit
10-888-5	Relay - Parallel Interlock	6	2.1	2.1	2.1
10-888-5	Relay - Control 1, 7, 8	3	1.04	1.04	1.04
10-888-5	Relay - Control 2 & 3	2	-	-	.7
10-888-5	Relay - Control 4	1	-	-	.35
10-888-5	Relay - Control 5 & 6	2	-	-	-
MS241440-2	Relay - Xmtr Aux. Pwr	1	-	-	.55
50084-002	Relay - Beam Power	1	-	-	Momentary
10-2710-1	Antenna Drive (Polarization)	1	-	.2	.2
91759	Wave Guide Switch	1	-	-	.5*
M-252 	Computer	1	5.*	5.*	5.*
Hughes	Receiver	1	-	5.*	-
	Transmitter	1	5.*	5.*	5.*
Lear Type	DC Amplifier	2	2.*	2.*	2.*
420744 	Remote Servo Assembly	3	3.*	3.*	3.*
TOTAL			18.50*	24.40*	20.80*

POWER REQUIREMENTS FOR MICROWAVE  
COMMUNICATION SYSTEM

(28 VOLT D.C. LOADS)  
TABLE M-2

 Modified

\* Estimated

REV

BOEING AIRPLANE COMPANY

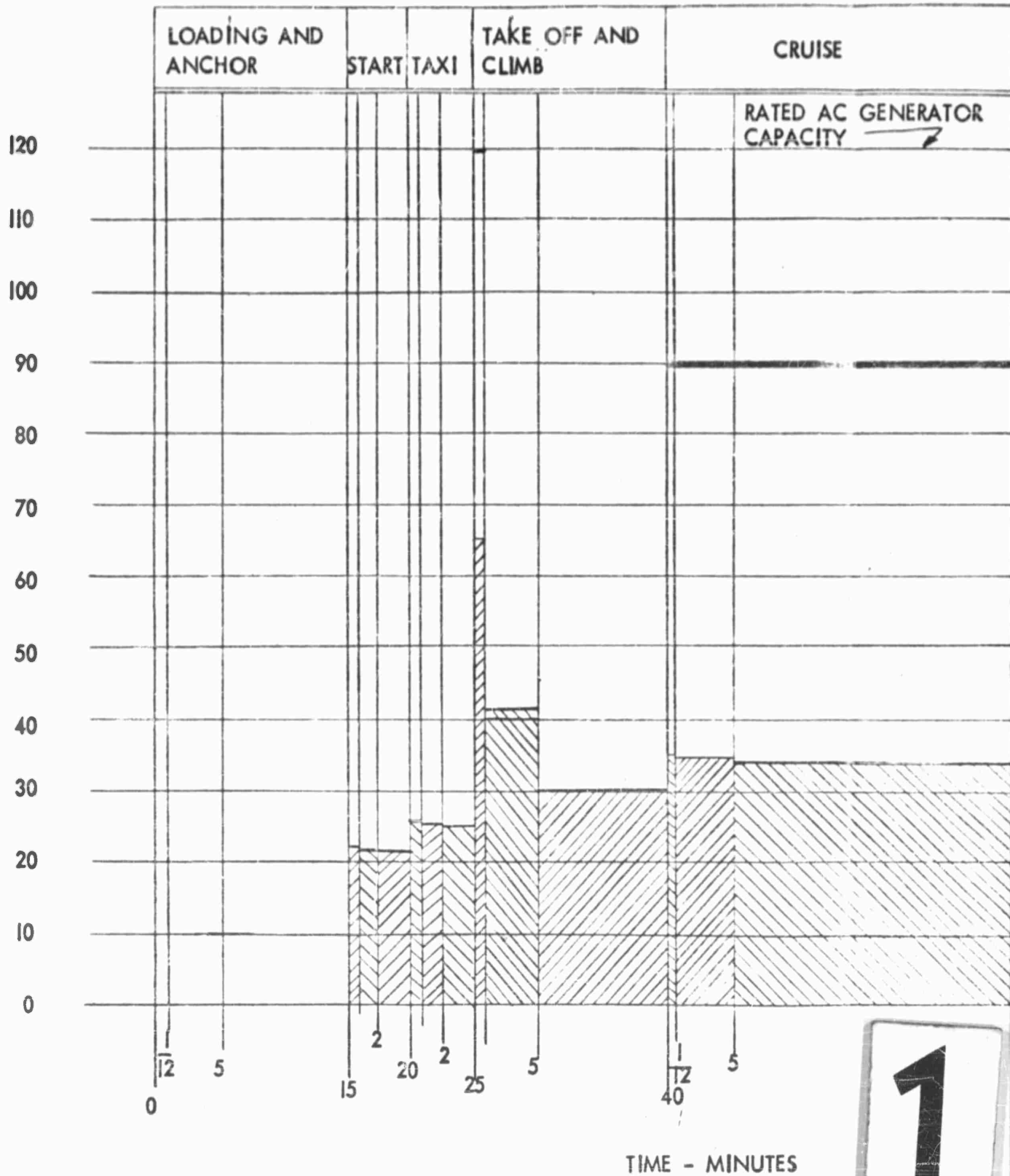
D6-7190

P NO. 179

		QTY.	28 V. A.C. LOAD $\phi$ 3 (VA)		
PART	DESCRIPTION		STAND-BY	RECEIVE	TRANSMIT
BAC-S16A-1 (AN3133-311)	Light - Upper Fuselage	2	84	84	84
10-2461 (A-7079-24)	Light - Upper Rendezvous	1	96	96	96
TOTAL			180	180	180
POWER REQUIREMENTS FOR MICROWAVE COMMUNICATION SYSTEM (28 VOLT A.C. LOADS) TABLE M-3					
D6-7190 P NO. 180		REV			

BUEING AIRPLANE COMPANY

KILOVOLT - AMPERES



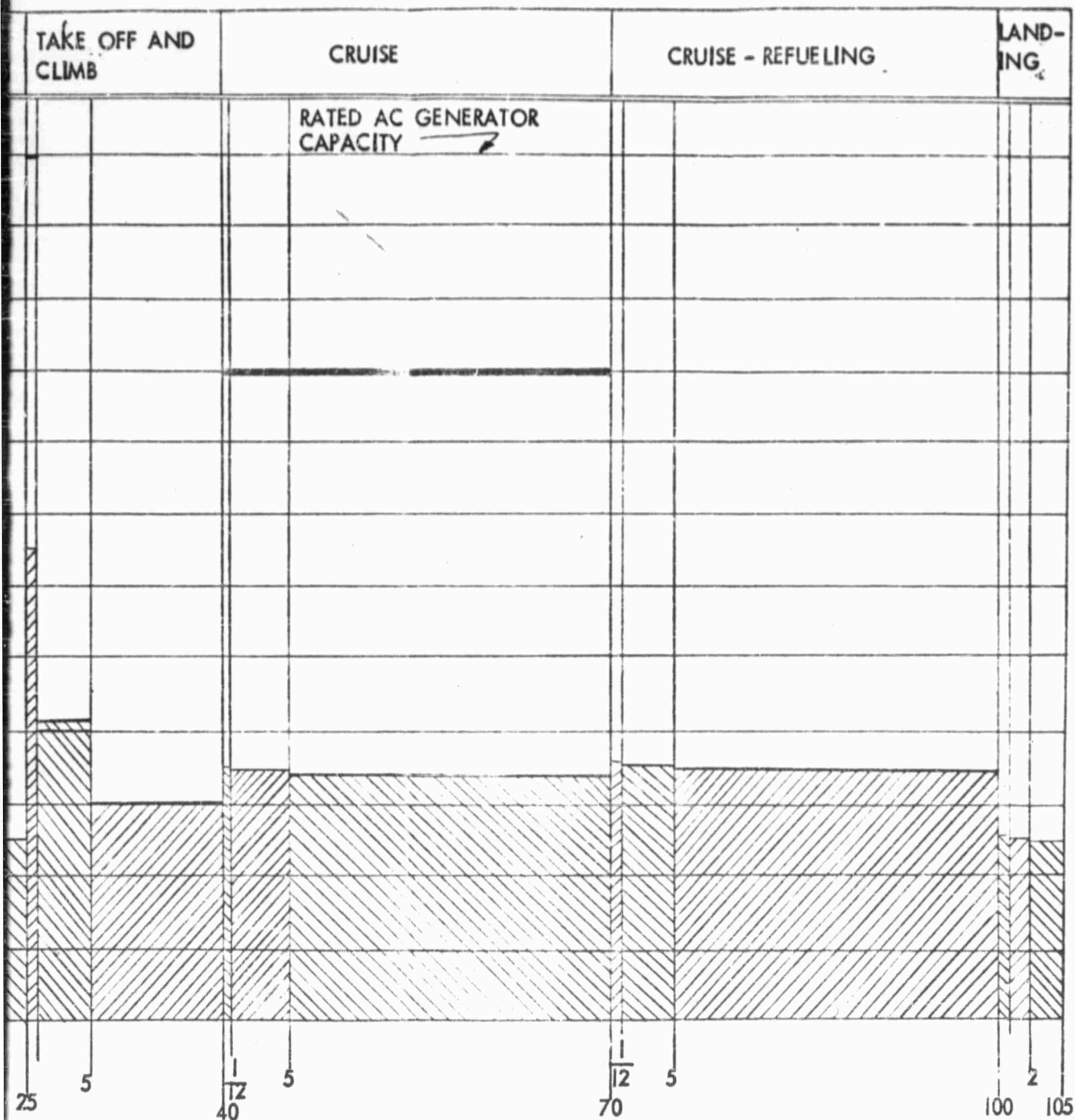
EXSISTING KC 135 LOAD - AC



ADDITIONAL MICRO WAVE SYSTEM LOAD - AC

1

CALC		
CHECK		
APR.		
APR.		



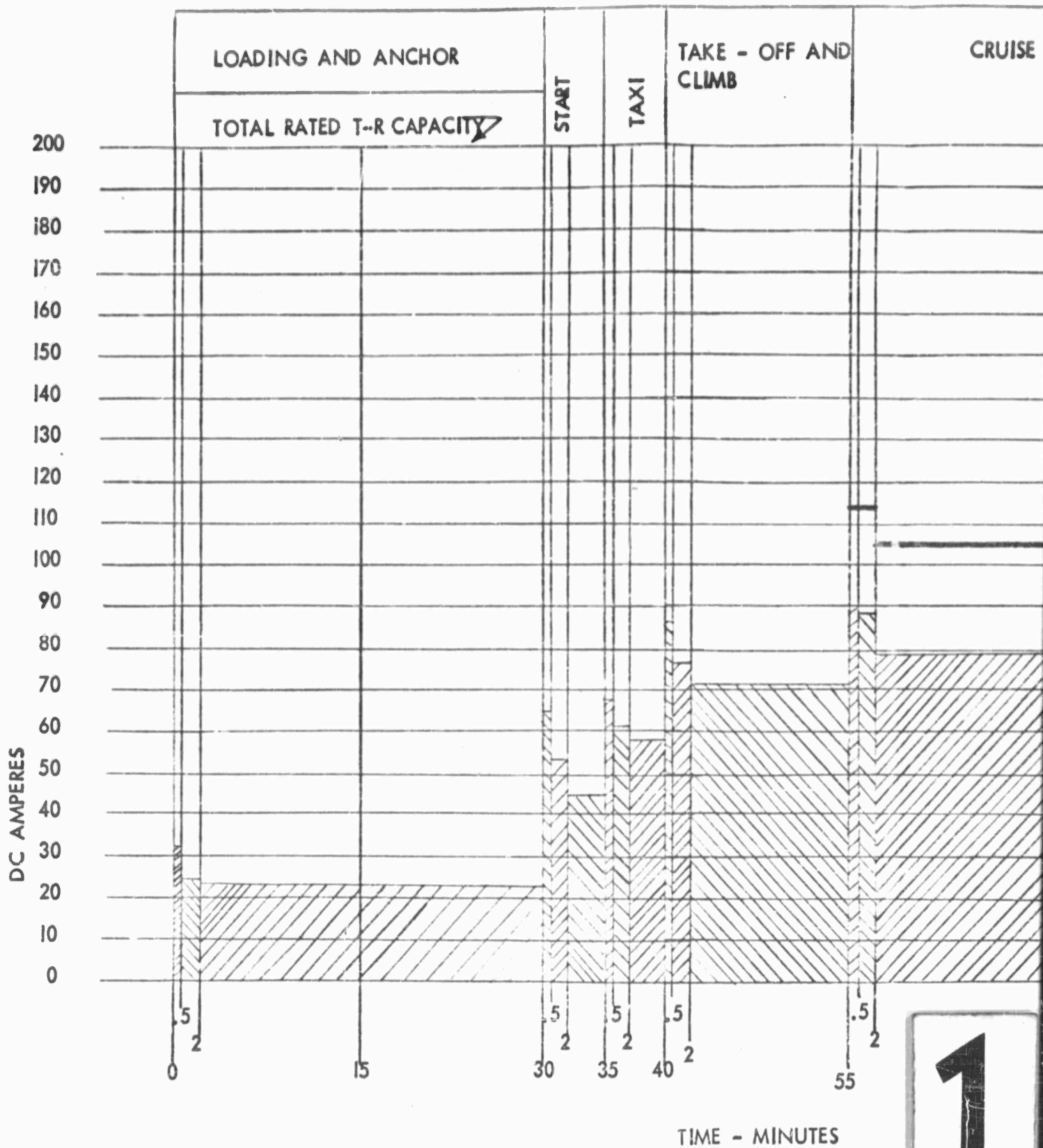
2

TABLE M-4

AD - AC

AVE SYSTEM LOAD - AC

CALC			REVISED	DATE	GRAPH - ELECTRICAL LOAD ANALYSIS AC BOEING AIRPLANE COMPANY RENTON, WASHINGTON	KC-135
CHECK						D6-7190
APR.						PAGE 181
APR.						

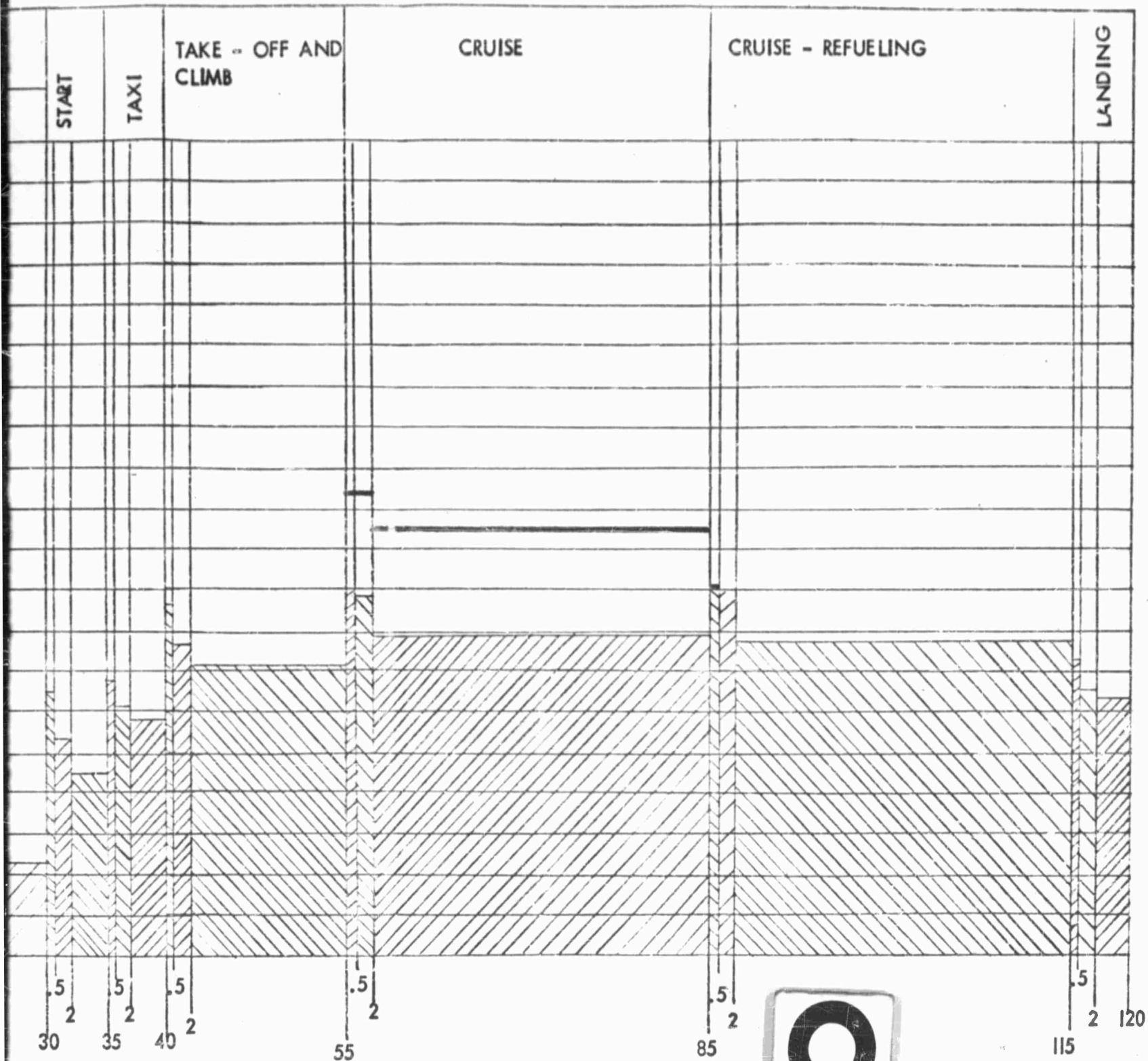


EXSISTING KC I35 LOAD - DC



ADDITIONAL MICRO WAVE SYSTEM LOAD - DC

CALC		
CHECK		
APR.		
APR.		



2

TABLE M-5

AD - DC

WAVE SYSTEM LOAD - DC

CALC			REVISED	DATE	GRAPH - ELECTRICAL LOAD ANALYSIS DC BOEING AIRPLANE COMPANY RENTON, WASHINGTON	KC 135
CHECK						D6-7190
APR.						PAGE 182
APR.						

APPENDIX N  
DRAWING INDEX

MICROWAVE ANTENNA INSTALLATION

- 65-17100 Equipment Instl - Microwave Antenna
  - 65-17102 Microwave Antenna Instl.
    - 65-17116 Framework, Assy of - Microwave Antenna
      - 69-13409 Pivot Shafts - Microwave Antenna
    - 65-17113 Dish Assy - Microwave Communications System
      - 65-17114 Feed Antenna
    - 65-17104 Gear Box - Assy. of - Elevation Drive - Microwave Antenna
      - 69-13400 Worm and Worm Wheel Set - Elevation Drive
      - 69-13406 Shafts - Elevation & Polarization Drives
      - 69-13413 Gear - Synchro, Elevation Drive
      - 69-13411 Housings, Bearing, Assy. of - Elevation Drive
      - 69-13412 Retainer - Synchro Gear, Elevation Drive
    - 65-17118 Cover - Assy of Lower Platform
    - 65-17119 Housing - Assy. of Lower Platform
    - 65-17121 Details - Lower Platform
    - 69-13401 Gear - Polarization Drive
    - 69-13402 Gear - Azimuth Drive
    - 69-13403 Gear - Idler Drive
    - 69-13404 Gear - Pinion, Azimuth Drive
    - 69-13407 Housing - Assy. of - Polarization Drive
      - 69-13405 Housing - Shaft, Polarization Drive
      - 66-11375 Gear - Idler, Polarization Drive
      - 69-13406 Shafts - Elevation and Polarization Drive
      - 66-11376 Gear - Pinion, Polarization Drive

BOEING



Drawing Index - Microwave Antenna Installation (Contd.)

65-17102 (Contd.)

69-13408	Bearing Retainer - Assy. of
69-13409	Pivot Shafts
69-13410	Support - Bracket
69-13414	Tuner - Assy. of
10-60602	Slip Ring Assy.
10-60600	Wave Guide
65-17105	Duct Instl - Radome Air Conditioning
66-2955	Washer
65-17106	Duct Instl - Overhead Distribution - Rework
65-23068	Joint Assy - Overhead Distribution Duct
65-23066	Channels - Overhead Distribution Duct Joint
65-23067	Bearing Plates - Overhead Distribution Duct Joint
69-11053	Corner Angle - Overhead Distribution Duct Joint
69-11063	Gasket - Overhead Distribution Duct Joint
65-17110	Support Instl - Antenna Housing Sta. 660-680
69-13418	Doubler
66-11929	Splice Bar
65-17117	Power Distribution - Forward
10-888-5	Relay
65-17120	Power Distribution - Aft
65-39093	Bracket Support
10-888-5	Relay
66-11922	Panel Instl - Switched DC Bus
66-11921	Panel Instl - Circuit Breaker Kit
69-13416	Power Switch Instl.

Drawing Index - Microwave Antenna Installation (Contd.)

65-17122 Light Inntl - Sta. 507

69-10591 Fairing - Assy. of

9-66041 Placard

50-3347 Structure Inntl - Beacon Light

60-5774 Fitting - Beacon Light Drain, Assy. of

30-3582 Clip - Attach.

60-3196 Support Bracket-Beacon Light

60-3256 Retainer Ring - Beacon Light

10-2461 Rendezvous Light - Assy. of

10-60603 Computer

65-17157 Microwave System Wiring Diagram

65-17148 Radome Inntl - Microwave Antenna

69-13417 Latch - Radome Support

69-13415 Fitting - Radome Support

D10-60601 Radome

65-17147 Radome - Assy. of Microwave Antenna

65-16150 Lines - Radome (REF)

65-10276 Vent Inntl - Fwd. Body Fuel Tank

63-10400 Scupper-Cavity Vent Fwd. Body Fuel Tanks

66-1434 Cushion Assy - Sliding Clamp Tube Support

60-2042 Support Inntl - Clamp Vent

30-1527 Clip

30-1584 Strip - Rubbing Fuel Tank Vent Line

66-2918 Bracket Assy - Vent Line Body Fuel Tanks

65-12151 Junction Box Inntl - Fwd. Body Fuel Tank Vent

**BOEING**

Drawing Index - Microwave Antenna Installation (Contd.)

9-64034 Flange - 3 Inch OD Tube Gravity Feed

66-1434 Cusion Assy - Sliding Clamp Tube Support

69-1422 Clamp - Sliding - 4 Inch A/R Line, Assy. of

66-1435 Angle - Sliding Clamp Tube Support

66-4625 Strap Assy - Sliding Clamp Tube Support

66-1195 Strap Assy - Sliding Clamp Tube Support

69-1422 Clamp - Sliding - 4 Inch A/R Line, Assy. of

66-1435 Angle - Sliding Clamp Tube Support

66-4625 Strap Assy - Sliding Clamp Tube Support

66-1195 Strap Assy - Sliding Clamp Tube Support

65-12148 Doubler Instl - Fwd. Body Tank Vent Outlet

65-10275 Outlet Installation Vent - Fwd, Body Fuel Tank

65-12151 Junction Box Instl - Fwd. Body Fuel Tank Vent

9-64034 Flange - 3 Inch OD Tube Gravity Feed

90-3225 Cover - Fuel Tank Vent Outlet, Assy. of

69-5013 Scoop - Vent Outlet, Body Fuel Tanks

50-3138 Tube Assy.

69-1768 Tube Assy - Water Drain - Vent Outlet Body Fuel Tanks

65-12150 Tube Assy. of - Fwd. Body Fuel Tank Vent

69-10594 Bracket - Vent Tube Support

65-12151 Junction Box Instl - Fwd. Body Tank Vent Outlet

9-64034 Flange

10-1650-39 Tube Coupling

50-6214 Diagram - Lining Thickness and Materials

66-11932 Refurbishment - Microwave Antenna Instl.

65-17123 Refurbishment Structure - Microwave Antenna Instl.

D6-7129 Functional Test Requirements - Microwave Communication System

BOEING

## APPENDIX O

### Peripheral Microwave Investigations

Several microwave techniques not anticipated or called out in the Request for Proposal have been encountered by this study, and are mentioned here for discussion:

1. Noise Generator: mounted behind the antenna feed and coupled through a directional coupler, a gas-tube noise generator could be used to measure receiver noise figure. Mounted on the leading edge of the vertical fin, it could be used to measure system noise figure and antenna gain in flight.
2. Radiometer: no provisions were made for a switching Dicke-type radiometer as used in radioastronomy. This could be incorporated into the present design with some plumbing change.
3. Monopulse pattern:  $\Sigma$  and  $\Delta$  antenna patterns might be useful in determining antenna pointing system errors, and in angle-of-arrival measurements. The additional losses in a hybrid junction and dual (or quadruple) feeds was considered excessive for the present design.
4. Polarimeters SO commonly employ phase-shifters in the main line, but these would introduce front end losses intolerable in the present system. This led to the choice of the "old-fashioned" but low-loss method of rotating the receiver and antenna around the beam axis. Rapid polarization shifts cannot thus be measured with the chosen polarization-shifter.
5. Waveguide Cooling: the high (10-kw) transmitter power will result in waveguide heating (100 watt per foot) plus additional hot-spots at rotary joints, bends, etc. Because of the difficulty of passing liquid coolant through rotating waveguide joints, a forced air scheme was tried. Measurements were made of the temperature rise of a section of RG-51/U heated to 100 watts/ft by a 1000-amp 60 cps current and cooled by an internal air stream. This work was stopped when it became apparent that other means of cooling would be adequate (Section II-80). However, the technique was deemed to be of sufficient general interest that the measurements were completed under Company sponsorship. A report is under preparation.
6. Doppler Shift: due to the nature of the scatterer, the doppler shift of some signals to be received by this antenna system may not be readily "captured" by ordinary phase-lock receivers. However, by a simple extension of the pointing computer program, range rate - and therefore doppler shift - can be desired. Some thought should be devoted to the form in which the computed doppler shift should appear for best utilization by the receiver (or transmitter).